MIMO MC-CDMA Systems over Indoor Optical Wireless Communication Channels

By

FUAD EID S ALSAADI

Submitted in accordance with the requirements for the degree of

Doctor of Philosophy

UNIVERSITY OF LEEDS

School of Electrical & Electronic Engineering

March, 2011

Declaration

The candidate confirms that the work submitted is his own and that appropriate credit has been given where reference has been made to the work of others

Signed ..... (Candidate)

Date .....

STATEMENT 1

This copy has been supplied on the understanding that it is copyright material and that no quotation from the thesis may be published without proper acknowledgement

Signed ..... (Candidate)

Date .....

STATEMENT 2

The right of FUAD EID S ALSAADI to be identified as Author of this work has been asserted by him in accordance with the Copyright, Designs and Patents Act 1988

Signed ..... (Candidate)

Date .....

Acknowledgments

First and foremost I thank and praise Allah Subhana Wa Tallah who granted me health and knowledge to complete this work. This research project would not have been possible without the support of many people. I wish to express my gratitude to my resourceful supervisor, Professor Jaafar Elmirghani for his abundant help, and his invaluable support and guidance throughout my research. I would also like to present all respect, gratitude and appreciation to my parents for their continued prayer, love and support throughout my entire life, and my wife for her care, love and understanding. This research project has been supported by the Government of the kingdom of Saudi Arabia; their support is fully appreciated.

Abstract

Optical wireless communication systems offer a number of advantages over their radio frequency counterparts. The advantages include freedom from fading, freedom from spectrum regulations and abundant bandwidth. The main limitations of optical wireless systems include background noise attributed to natural and artificial light sources and multipath propagation. The former degrades the signal to noise ratio while the latter limits the maximum achievable data rate.

This thesis investigates the use of transmit power adaptation in the design of optical wireless spot-diffusing systems to increase the power associated with the main impulse response components, resulting in a compact impulse response and a system that is able to achieve higher data rates. The work also investigates the use of imaging diversity receivers that can reject the background noise components received in directions not associated with the signal. The two techniques help improve the optical wireless system performance. The multibeam transmitter and the multi-detector angle diversity receiver or imaging receiver form a multiple input multiple output (MIMO) system. The work also investigates additional methods that can improve the performance such as transmitter beam angle adaptation, and improved modulation and coding in the form of multi-carrier code division multiple access (MC-CDMA). Furthermore, the work investigates the robustness of a link design that adopts the combination of these methods in a realistic environment with full mobility.

Table of Contents

List of Figures

List of Tables

List of Abbreviations

AEL.....	Accessible emission limit
ABCM.....	Adaptive beam clustering method
ALSMS.....	Adaptive line strip multibeam system
AWGN.....	Additive white Gaussian noise
ATM.....	Asynchronous transfer mode
APD.....	Avalanche photodiode
BN.....	Background noise
BCM.....	Beam clustering method
BPSK.....	Binary Phase Shift Keying
BJT.....	Bipolar-junction transistor
BEF.....	Bit rate enhancement factor
BER.....	Bit-error-rate
CDMA.....	Code division multiple access
CF.....	Communication floor
CPC.....	Compound parabolic concentrator
CGH.....	Computer-generated hologram
CBR.....	Constant bit rate
CDS.....	Conventional diffuse system
CHS.....	Conventional hybrid system
DFE.....	Decision-feedback equalizer
DPIM.....	Digital pulse interval modulation
DSP.....	Digital signal processor

DFT.....	Discrete Fourier transform
EMAP.....	Embedded Meta-data format for Affixing on Picture
EGC.....	Equal gain combining
FFT.....	Fast Fourier transform
FET.....	Field-effect transistor
FOV.....	Field-of-view
FLCB.....	Fluorescent lights with conventional ballast
FLEB.....	Fluorescent lights with electronic ballast
FDMA.....	Frequency division multiple access
Ir.....	Infrared
IrDA.....	Infrared Data Association
IrLAP.....	Infrared Link Access Protocol
IrLMP.....	Infrared Link Management Protocol
IM/DD.....	Intensity modulation and direct detection
IEC.....	International Electro-technical Commission
ISI.....	Intersymbol interference
IFFT.....	Inverse fast Fourier transform
LD.....	Laser diode
LED.....	Light emitting diode
LSMS.....	Line strip multibeam system
LOS.....	Line-of-sight
LAN.....	Local area network
LPF.....	Lowpass filter
MPE.....	Maximum Permissible Exposure

MRC.....	Maximum ratio combining
MC-DS-CDMA.....	MC-Direct Sequence-CDMA
MAC.....	Medium access control
MBAAS.....	Multibeam angle adaptive system
MBPAAS.....	Multibeam power and angle adaptive system
MC-CDMA.....	Multicarrier code division multiple access
MC-SS.....	Multicarrier spread spectrum
MAI.....	Multiple access interference
MIMO.....	multiple input multiple output
MSM.....	Multiple subcarrier modulation
NRZ-OOK.....	Non-return-to-zero OOK
OOK.....	On-off keying
OOC.....	Optical orthogonal code
OW.....	Optical wireless
OFDM.....	Orthogonal frequency division multiplexing
PRC.....	Peak reduction carrier
PAPR.....	Peak to average power ratio
PCs.....	Personal computers
PDAs.....	Personal digital assistants
PAR38.....	Philips PAR 38 Economic
PIN.....	Positive-intrinsic negative
PSD.....	Power spectral density
PPM.....	Pulse position modulation
PFDR.....	Pyramidal fly-eye diversity receiver

RF.....	Radio frequency
RZ-OOK.....	Return-to-zero OOK
SB.....	Select best
SIr.....	Serial Infrared
SNR.....	Signal-to-noise ratio
SNIR.....	Signal-to-noise-interference-ratio
SSM.....	Single subcarrier modulation
SDMA.....	Space division multiple access
TDMA.....	Time division multiple access
TCM.....	Trellis-coded modulation
2DABCM.....	Two-dimensional adaptive beam clustering method
2DBCM.....	Two-dimensional beam clustering method
VBR.....	Variable bit rate
VFIr.....	Very Fast Infrared
WDMA.....	Wavelength division multiple access
ZF.....	Zero forcing

Glossary of Symbols

ϑ ..... Incidence angle

ϑ_d ..... Incident angle of the direct ray with respect to the transmitter normal

δ ..... Reception angle

ψ_C ..... Concentrator's acceptance semi-angle

ϕ ..... Angle of the incident ray with respect to the surface element normal (first-order reflection)

ϕ_b ..... Angle between adjacent beams

φ_1 ..... Angle of the reflected ray towards the receiver with respect to the normal of dA_1

φ_2 ..... Angle of the reflected ray towards the receiver with respect to the normal of dA_2

γ_1 ..... Angle of the reflected ray (from the surface element dA_1 to dA_2) with respect to the normal of dA_1

γ_2 ..... Angle of the reflected ray (from the surface element dA_1 to dA_2) with respect to the normal of dA_2

α_i ..... Transmission beam angles with respect to the transmitter normal

α_x ..... Reception angle associated with a pixel with respect to the receiver's normal along the *x* line

α_y ..... Reception angle associated with a pixel with respect to the receiver's normal along the *y* line

θ_x	Transmission angle in the *x*-axis
θ_y	Transmission angle in the *y*-axis
ζ	Quantum efficiency of the device
λ	Wavelength
ρ	Reflection coefficient
Δt	Bin width
μ	The mean delay
σ_{pr}	Standard deviation of the preamplifier shot noise
σ_{bn}	Standard deviation of background light-induced shot noise
σ_{s0}	Shot noise component associated with P_{s0}
σ_{s1}	Shot noise component associated with P_{s1}
σ_0	Standard deviation of the shot noise associated with logic 0
σ_1	Standard deviation of the shot noise associated with logic 1
σ_t^2	Total noise variance
σ_η^2	Variance of the noise component
$\sigma_{I_1}^2$	Variance of the same subcarrier interference from the other users
$\sigma_{I_2}^2$	Variance of the other subcarrier interference component from the other users
η_c	A fixed capacitance per unit area
$\tau_{\max}$	Duration of the impulse response
τ_γ^k	The time delay associated with the γ^{th} ray of the k^{th} user

Γ	FET channel noise factor
Γ_{rays}	The number of received rays
A	Entrance area of the concentrator
A'	Exit area of the concentrator
A_d	Photodetector area
$A_{eff}(\delta)$.....	Effective light-collection area
A_R	Collection area
Az	Azimuth angle
B	Bit rate
b_m^k	The m^{th} data bit of user k
BW.....	Receiver bandwidth
c	Speed of light
C_d	Detector capacitance
C_g	FET gate capacitance
c_n^k	The n^{th} chip of the spreading code
D	Root mean square delay spread
dA	Reflection surface element area
dP	Power radiated into a solid angle element
d_x	The *x*-axis horizontal separations between the receiver's normal and the reception area centre
d_y	The *y*-axis horizontal separations between the receiver's normal and the reception area centre
El	Elevation angle

f_c	Subcarrier frequency
G	The open-loop voltage gain
g_m	FET transconductance
h	Reception area height
$h(t)$	Impulse response of the channel
$h^{(k)}(t)$	Impulse response due to the k^{th} reflection
$h_{conf}(t)$	Channel response of the particular OW configuration
h_p	Planck's constant
I_1	The same subcarrier interference from the other users
I_2	Other subcarrier interference component from the other users
$I(t)$	Received instantaneous current at the output of the photodetector at a certain position
I_p	Average photocurrent
J	Total number of photodetectors
k	Boltzmann's constant
K	Total number of active users
L	Length of the room
L_{Lamp}	Total number of the lamps
$M_{element}$	Total number of reflecting elements
N	Total number of subcarriers
N_C	Concentrator's internal refractive index
N_{code}	Length of the spreading code

N_s	Total number of spots
n	Mode number of the radiation beam that describes the beam shape
$n(t)$.....	Background noise
$\hat{\mathbf{n}}_R$	Unit-length orientation vector of the receiver
$\hat{\mathbf{n}}_T$	Unit-length orientation vector of the transmitter
P	Electrical transmitted power of the data bit
P_{bn}	Total background noise
P_{dA}	Optical power radiated by a surface element dA in Lambertain pattern with $n=1$
P_e	Probability of error
P_i	Incident optical power
$P_{LOS}^{(0)}$	Direct received power (LOS component)
P_{n_d}	Direct path component of the BN
$P_{n_{reflection}}$	Total noise power received through the reflecting elements
$P_{reflection}^{(1)}$	Power received by a surface element with an area dA_1 and a reflection coefficient ρ_1 in the first-order reflection
$P_{reflection}^{(2)}$	Total power received by a second-order reflection
P_R	Total power received at the receiver
P_{s0}	The power associated with logic 0
P_{s1}	The power associated with logic 1
P_{spot}	The power assigned to the spot

P_T	Transmit power
q	Electronic charge
R	Photodetector responsivity
R_1	Distance between the transmitter and the surface element dA_1
R_2	Distance between the surface element dA_1 and the receiver
R_3	Distance between the two surface elements dA_1 and dA_2
R_4	Distance between the surface element dA_2 and the receiver
$R(\vartheta)$	Radiation intensity pattern
R_d	Direct distance between the transmitter (source) and the receiver
r_{det}	Radius of the Photodetector
$rect(\ )$	Step function
R_F	Feedback resistance
r_{hc}	Radius of a hemispheric concentrator
$\mathbf{r}_R$	Position vector of the receiver
$\mathbf{r}_T$	Position vector of the transmitter
S	The desired signal component from the desired user ($k = 0$)
$s^k(t)$	The transmitted optical power
t	Absolute time
T	Absolute temperature
T_b	Bit duration
T_c	Chip duration

$T_C(\delta)$	Concentrator transmission factor
$T_F(\delta)$	Filter transmission factor
T_s	The MC-CDMA symbol duration
v	Optical frequency
v_0	The decision variable of the m^{th} data bit of the first user
W_i	Spot's weight directly proportional to the SNR it produces
W_T	Total of the spot's weight
$x(t)$	Instantaneous optical power
$X[k]$	The discrete Fourier transform (DFT) of $x[n]$
x_r	Horizontal separation distance between the imaging receiver and the *y*-*z* wall
y_r	Horizontal separation distance between the imaging receiver and the *x*-*z* wall
z_{CF}	Height of the communication floor
z_x	The height of the centre of a reception area above the communication floor on the *y*-*z* wall
z_y	The height of the centre of a reception area above the communication floor on the *x*-*z* wall

1. INTRODUCTION

1.1. Why Optical Wireless?

Communication played a critical role in the evolution of human civilisation. The development of communication technology has been motivated by the human desire to communicate over distances. In the early days of human civilisation, natural phenomena were employed to get messages across. Notices of important events, such as enemy invasions or royal births, would be transmitted through the sounding of horns or the lighting of fires.

The history of modern-day communications technology coincided with the invention of the wireline telegraph in 1832 by Samuel Morse, who created the first wired "near instantaneous" long distance communication links. However, Bell's telephone, which allowed one of the most efficient forms of telecommunication through the use of our voices, led to the development of our present day communications technology. A degree of flexibility was added through the invention of wireless telegraph (now referred to as radio) in 1896 by Guillermo Marconi when wireless communication became useable for voice transmission. Twentieth century inventions such as television, facsimile, video and computers have provided a wider range of communication capabilities. However, great demands have been placed on the links that convey their respective data.

The large increase in personal computers and personal digital assistants in indoor environments have resulted in the need for flexible interconnection through distributed or centralised data communication systems. The traditional fashion to facilitate this requirement is to use wired physical connections. However, these physical connections introduce difficulties in installation, rewiring, maintenance, as

well as further expansion. Wireless communication systems offer an attractive alternative providing users with mobility and flexibility. Both, radio frequency (RF) and infrared (Ir) radiation are possible methods that can be used to implement wireless systems. RF is the basis of most of the current wireless communication systems. This has led to high congestion in the RF spectrum and has limited its ability to accommodate new high bit rate services [1-2]. The desire for substantial bandwidth, high-speed links and inexpensive components, which are small and consume little power, has motivated recent interest in infrared wireless communications [3-54]. The dawn of the modern era of optical communications coincided with the 1960's invention of the laser [55].

Carriers within the radio range of the electromagnetic spectrum can provide limited bandwidths, typically up to tens of MHz, whereas Ir signals are able to extend this by several orders of magnitude. Moreover, the radio spectrum available for communication purposes is regulated by government organisations whereas the infrared spectrum is free from such restrictions. Ir transmission is confined to the environment, for example, a room in which it originates as Ir signals, cannot penetrate opaque objects such as walls. This signal confinement allows Ir links to offer immunity to interference caused by other RF wireless devices, with the possibility of frequency reuse in different parts of the same building. The Ir medium also offers security at the physical layer, hence reducing the need for data encryption. In addition, Ir links provide freedom from multipath fading [30], which simplifies their design, and typically have a large bandwidth which can directly reflect on the achievable data rate. These combined favourable features coupled with the prospective substantial increase in bandwidth may mean that, in time, optical wireless (OW) communication links could rival their radio counterparts.

OW communication links have several drawbacks. Optical signals are subjected to attenuation and dispersion due to multipath propagation. Light does not penetrate walls but walls are able to reflect incoming light rays. Indoor reflective surfaces have a diffuse nature, which implies that the transmitted signal reaches the receiver through various paths and different lengths. This makes the transmitted pulse spread, multipath dispersion, which results in intersymbol interference (ISI) [3]. OW links are impaired by intense ambient light sources which emit a substantial amount of power within the wavelength range of silicon photodetectors, resulting in an optical signal corrupted by background noise (BN) [20-21]. Furthermore, the maximum allowed optical power is restricted by eye and skin safety regulations [56-58]. OW receivers require photodetectors with a large photosensitive area in order to collect sufficient signal power and to achieve an acceptable performance, (typically a bit-error-rate (BER) of 10^{-9}). However, the photodetector capacitance is directly proportional to its area, i.e., a large photosensitive area results in large capacitance, hence limiting the achievable receiver bandwidth [22].

Various techniques have been proposed to combat the limitations of the OW systems and larger bit rates have been achieved. Although, significant research has been done, much more work is needed before even a fraction of the potential bandwidth is achieved in practical systems. The research presented in this thesis aims to address the impairments of optical wireless systems and provides practical solutions, hence increasing the system data rate and/or enabling high data rate multi-user communications where the increased channel rate is shared among users. Optical wireless can be viewed as a valuable complement to wireless radio, rather than being a competitor in a number of applications since mobility in optical wireless is typically achieved in an efficient manner indoors only. Radio is a cost-effective

medium in wide-range applications in which user mobility must be maximised, or transmission through walls is required. Infrared is the preferred choice in short-range high-speed multimedia applications, which require very high bandwidth with mobility. A comparison between optical wireless and radio frequency systems is given in Table 1.1.

TABLE 1-1: COMPARISON BETWEEN OPTICAL WIRELESS AND RADIO SYSTEMS IN INDOOR WIRELESS COMMUNICATION

	Optical wireless systems	**Radio systems**
Advantages	▪ Unregulated large bandwidth. ▪ Possibility of frequency reuse in different parts of the same building. ▪ Immunity to interference between links operating in different rooms. ▪ Security and freedom from spectrum regulation and licensing. ▪ Freedom from fading. ▪ Inexpensive components, which are small and consume little power.	▪ Possibility of transmission through walls. ▪ High mobility. ▪ The omni directional portable antenna is relatively insensitive to rotation.
Disadvantages	▪ Shot noise induced by intense ambient light. ▪ Intersymbol interference due to multipath dispersion. ▪ The need for a backbone network to interconnect OW access points in different rooms. ▪ Transmit optical power is restricted by eye safety regulations.	▪ Regulated bandwidth. ▪ Multipath fading. ▪ Interference from other users ▪ Expensive for the moment without guarantee of high bit rates. ▪ Low security.

1.2. Research Objectives

The objectives of the study was

- To investigate the viability of designing low complexity indoor optical wireless systems that address the OW environment impairments. This aim would cover designing and modelling proper transmitter and receiver configurations for high-speed OW applications.
- To investigate the use of transmit power adaptation to increase the power associated with the main impulse response components, resulting in a compact impulse response and a system that is able to achieve higher data rates.
- To investigate the use of imaging diversity receivers to reject the background noise components, received in directions not associated with signal.
- To investigate additional adaptation methods that can improve the optical wireless system performance such as transmitter beam angle adaptation, and improved modulation and coding in the form of multi-carrier code division multiple access (MC-CDMA).
- To investigate the robustness of a link design that adopts the combination of these methods in a realistic indoor environment with full mobility.

1.3. Original Contributions

The author has:

1. Further developed an existing ray-tracing method to model the characteristics of the optical wireless channel. This adapted ray-tracing method includes channel impulse response, multipath dispersion, and the optical power

induced by ambient light in diversity emission/detection configurations. He developed a simulation tool and a mathematical model for diversity reception, which accounts for the detector directivity, location, elevation and azimuth angle, and used it to evaluate the performance of OW diffuse/spot-diffusing systems.

2. Introduced a novel beam power adaptation method to the design of OW systems to improve the system performance in the presence of BN, multipath dispersion and mobility. The main goal is to reduce the effect of intersymbol interference, and to enhance the SNR thus enabling the system to achieve mobility while operating at high bit rates. The work has shown that assigning high power levels to spots nearest to the receiver can improve the received optical signal as well as maximise the receiver SNR.
3. Designed, investigated and evaluated the performance of a mobile OW system that employs an adaptive beam clustering method (ABCM) in conjunction with diversity detection. The ABCM system improves the SNR and increases the channel bandwidth compared to the non-adaptive OW systems, which reflects on the achievable data rate. The increase in SNR and channel bandwidth were used to achieve higher data rates: 2.5 Gbit/s and 5 Gbit/s, where previous OW systems used to operate at hundred's of Mbit/s. The rates achieved are world record data rates.
4. Introduced a mobile adaptive line strip multibeam system (ALSMS) with an angle diversity receiver and assessed its performance under the constraints of ambient light noise and multipath propagation. It is shown that the performance of ALSMS and ABCM are similar as the adaptive algorithm distributes the power among the spots according to the receiver position. The

author has evaluated the performance of the angle diversity ALSMS in the presence of very directive noise, in addition to impaired propagation where shadowing exists with transmitter/receiver mobility. The channel characteristics of these infrared links have been evaluated under a highly impaired environment, in the presence of mini cubical offices, partitions and furniture. The shadowed ALSMS link was compared with the non-adaptive shadowed LSMS, demonstrating the significant improvements offered by employing the beam power adaptation method. Based on the modelling results, it is shown that a spot-diffusing geometry with beam power adaptation, in conjunction with diversity detection, is a suitable candidate to combat OW shadowing.

5. Proposed for the first time, an optical wireless system that combines orthogonal frequency division multiplexing (OFDM) signalling with code division multiple access (CDMA) multi-user capabilities. Multi-carrier CDMA (MC-CDMA) combines some of the desirable features of OFDM and CDMA in that it offers multi-user capabilities at a reduced channel rate. BER analysis for the MC-CDMA system with multiple active users in an indoor OW channel was performed and reported. A performance improvement was achieved by using an OW MC-CDMA system, compared to the conventional OW on-off keying (OOK) system and OW CDMA system. The effect of all the parameters such as the symbol rate, delay spread, receiver structure, and positions of transmitter and receiver were considered.
6. Presented a mobile adaptive spot-diffusing OW MC-CDMA system, as a method that can provide multiple access facilities, suited to the limited bandwidth in OW systems under the impairments of ambient light noise and

multipath propagation. A zero forcing (ZF) equalisation technique was employed to reduce multiple access interference and improve the BER performance. The results show that, while the OW MC-CDMA system utilising CDS or LSMS geometries benefits, the equalisation scheme, which increases receiver complexity, is not necessary when the ALSMS replaces CDS or LSMS at the data rate considered. Furthermore, an adaptive LSMS system was proposed, studied and shown to be a desirable means for improving the performance of mobile OW MC-CDMA systems, in a highly impaired environment where shadowing exists.

7. Proposed a novel two-dimensional adaptive beam clustering method (2DABCM) combined with new imaging diversity receivers (diversity in imaging receivers has not been previously proposed/investigated), and evaluated its performance through channel and noise modelling. The 2DABCM analysed, employs three two-dimensional clusters of spots distributed in different directions. The imaging diversity receiver introduced, is built of photodetector arrays on each side of the receiver, to facilitate capturing reflections from the sides and different angles. 2DABCM multipath dispersion, ambient light interference, and imaging diversity receiver design were considered.
8. Analysed antenna imaging diversity combining schemes including: select best (SB) and maximum ratio combining (MRC) for the imaging 2DABCM system and evaluated their performance. The results showed that MRC offers further improvement when implemented to combine the signals at the outputs of the imaging pixels. Previous indoor mobile optical wireless systems operated typically at 30 Mbit/s to 100 Mbit/s and here, the author reported

systems that operate at 2.5 Gbit/s and 5 Gbit/s. The author was able to achieve these improvements through the introduction of three new approaches: transmit beam power adaptation, a 2D beam clustering, and MRC diversity imaging. The author investigated the effect of transmitter/receiver mobility on the performance of OW links employing a beam power adaptation method, spot-diffusing and imaging diversity receivers in the presence of intense background ambient light noise, multipath propagation, and shadowing. A significant SNR improvement was achieved compared with the other geometries considered (imaging CDS and imaging LSMS). This improvement is due to the presence of direct path components, made possible through the use of the spot-diffusing transmitter configuration. Furthermore, the beam power adaptation method introduced was shown to enhance those direct path components and reduce the influence of reflections. Imaging receivers were shown to help mitigate the BN effect by selecting (or MRC combining) those pixels that observe lower BN, and by minimising the preamplifier thermal noise through the use of small sized pixels (with lower per pixel capacitance allowing a high resistance (with lower noise) to be employed for the same bandwidth). This SNR improvement, coupled with the additional bandwidth obtained, was shown to enable a fully mobile 5 Gbit/s optical wireless system while achieving acceptable performance (BER of 10^{-9}).

9. Introduced a novel beam angle adaptation method to the design of multibeam optical wireless systems to effectively reduce the impact of mobility as well as improve link performance in the presence of shadowing. The angle adaptation method introduces a degree of freedom allowing the spatial distribution of the spots to be adjusted (to positions near the receiver)

regardless of the transmitter position. The main goal is to spatially optimise the spots' distribution in an area (ceiling and/or walls) using a multibeam transmitter whose beam angles can be adapted and controlled by a digital signal processor (DSP). The ultimate goal is to maximise the SNR at a given receiver location. Further SNR improvements can be achieved when the power is re-distributed to unobstructed spots. The trade-off between complexity and performance enhancement was investigated. The system robustness against shadowing and signal blockage was also considered.

10. Evaluated the performance of a link design that utilises a new multibeam power and angle adaptation system (MBPAAS) under the impairments of BN, multipath propagation, mobility, shadowing and signal blockage. Two different detection techniques: angle diversity receivers and imaging receivers were employed. The results indicate that the SNR is independent of the transmitter position in this system, and can be maximised at all receiver locations when the new methods (beam angle and beam power adaptation) are implemented, either with a diversity receiver or with an imaging receiver. The SNR performance achieved using the imaging receiver is superior to that obtained with a diversity receiver. Mobile multibeam 2.5 Gbit/s and 5 Gbit/s OW systems were shown to be feasible, which are useful results for wireless communications, through the introduction of three approaches: beam angle and beam power adaptation, spot-diffusing, and imaging receivers. Higher data rates are possible using these systems.

These original contributions are supported by the following publications:

Journals

[1] Alsaadi, F. E. and Elmirghani, J. M. H.,'High-Speed Spot Diffusing Mobile Optical Wireless System Employing Beam Angle and Power Adaptation and Imaging Receivers,' Lightwave Technology, Journal of, vol. 28, pp. 2191-2206, 2010.

[2] Alsaadi, F., Nikkar, M. and Elmirghani, J. M. H.,'Adaptive mobile optical wireless systems employing a beam clustering method, diversity detection, and relay nodes,' Communications, IEEE Transactions on, vol. 58, pp. 869-879, 2010.

[3] Alsaadi, F. E. and Elmirghani, J. M. H.,'Beam power and angle adaptation in multibeam 2.5 Gbit/s spot diffusing mobile optical wireless system,' Selected Areas in Communications, IEEE Journal on, vol. 28, pp. 913-927, 2010.

[4] Alsaadi, F. E. and Elmirghani, J. M. H.,'Adaptive mobile multicarrier code division multiple access optical wireless systems employing a beam clustering method and diversity detection,' Optoelectronics, IET, vol. 4, pp. 95-112, 2010.

[5] Alsaadi, F. and Elmirghani, J. M. H.,'Adaptive mobile spot diffusing angle diversity MC-CDMA optical wireless system in a real indoor environment,' Wireless Communications, IEEE Transactions on, vol. 8, pp. 2187-2192, 2009.

[6] Alsaadi, F. and Elmirghani, J.,'Performance evaluation of 2.5 Gbit/s and 5 Gbit/s optical wireless systems employing a two dimensional adaptive beam clustering method and imaging diversity detection,' Selected Areas in Communications, IEEE Journal on, vol. 27, pp. 1507-1519, 2009.

[7] Alsaadi, F. and Elmirghani, J.,'Adaptive mobile line strip multibeam MC-CDMA optical wireless system employing imaging detection in a real indoor environment,' Selected Areas in Communications, IEEE Journal on, vol. 27, pp. 1663-1675, 2009.

[8] Alsaadi, F. E. and Elmirghani, J. M. H.,'Spot diffusing angle diversity MC-CDMA optical wireless system,' Optoelectronics, IET, vol. 3, pp. 131-141, 2009.

[9] Alsaadi, F. and Elmirghani, J.,'Mobile Multigigabit Indoor Optical Wireless Systems Employing Multibeam Power Adaptation and Imaging Diversity Receivers,' Optical Communications and Networking, IEEE/OSA Journal of, vol. 3, pp. 27-39, 2010.

Conference papers

[10] Alsaadi, F. E. and Elmirghani, J. M. H., "Mobile Multi-Gigabit Spot-Diffusing Optical Wireless System Employing Beam Angle and Power Adaptation and Imaging Reception," in GLOBECOM 2010, 2010 IEEE Global Telecommunications Conference, 2010, pp. 1-6.

[11] Alsaadi, F. E. and Elmirghani, J. M. H., "Multibeam 2.5 Gbit/s Mobile Optical Wireless Systems Employing Beam Power and Angle Adaptation

Method," in Communications (ICC), 2010 IEEE International Conference on, 2010, pp. 1-6.
[12] Alsaadi, F. E. and Elmirghani, J. M. H., "Adaptive multibeam clustering angle diversity optical wireless system," in Optical Network Design and Modeling (ONDM), 2010 14th Conference on, 2010, pp. 1-6.
[13] Alsaadi, F. E. and Elmirghani, J. M. H., "Adaptive 2.5 Gbit/s Optical Wireless Systems Employing a Two Dimensional Beam Clustering Method and Imaging Diversity Receivers," in Communications, 2009. ICC '09. IEEE International Conference on, 2009, pp. 1-8.
[14] Alsaadi, F. E. and Elmirghani, J. M. H., "Mobile MC-CDMA Optical wireless System Employing an Adaptive Multibeam Transmitter and Diversity Receivers in a Real Indoor Environment," in Communications, 2008. ICC '08. IEEE International Conference on, 2008, pp. 5196-5203.
[15] Alsaadi, F. E. and Elmirghani, J. M. H., "MC-CDMA Indoor Optical Wireless System," in Global Telecommunications Conference, 2007. GLOBECOM '07. IEEE, 2007, pp. 2455-2460.

1.4. Thesis Outline

Chapter 2 gives a general overview of optical wireless communication systems. The chapter outlines the merits and impairments of this type of communication, previous advances made, and where the contributions of this study are situated.

Chapter 3 outlines the OW environment used in all communication scenarios examined in this work. The simulation method adopted to model the communication channel and induced background noise is detailed. Furthermore, spot-diffusing geometries such as LSMS and BCM, which are some of the attractive configurations considered in the literature, are discussed and used as baselines in order to evaluate the novel configurations proposed in this study.

A novel transmit power adaptation method is introduced in Chapter 4. The spot-diffusing configurations (LSMS and BCM) drawn in Chapter 3 are developed in this chapter (where beam power adaptation is introduced), and the results indicate significant performance improvements in terms of delay spread, channel bandwidth, and SNR, compared to the non-adaptive systems.

MC-CDMA is a transmission scheme that combines the robustness of orthogonal modulation with the flexibility of multi-user CDMA schemes. It can lower the symbol rate and is therefore suited to the bandwidth limited optical wireless indoor channel. The merits of an OW MC-CDMA system including modelling and performance analysis are the subject of Chapter 5. The chapter demonstrates the BER performance improvement achieved through the use of an MC-CDMA scheme, compared to the conventional OW OOK system and the OW CDMA system. A comparison of the adaptive and non-adaptive OW MC-CDMA systems is also considered showing the effect of delay spread, receiver structure, transmitter and receiver positions, and SNR on their BER performance. Furthermore, an adaptive LSMS geometry with diversity detection is proposed, studied and shown as a desirable means for improving the performance of mobile OW systems in a harsh environment. Such an environment is typically encountered in real office configurations, where optical signal blockage (owing to cubicles), windows, doors, furniture, ambient light noise, and multipath propagation, all exist.

Chapter 6 presents high-speed indoor OW communication systems employing a novel 2DABCM and a new imaging diversity reception. The design of both 2DABCM transmitter and imaging diversity receiver is discussed. The performance of imaging OW systems utilising selection and combining techniques, including SB and MRC, is investigated and evaluated under the impairments of ambient light noise and multipath propagation. At a BER of 10^{-9}, 2.5 Gbit/s and 5 Gbit/s indoor OW communication systems are shown to be feasible when the transmitter is stationary at the room centre and the receiver is mobile.

Mobile multi-gigabit indoor OW communication systems adopting three methods: spot-diffusing, beam power adaptation, and imaging diversity are proposed in

Chapter 7. The focus of the chapter, however, is on attaining a low-complexity high-speed mobile indoor OW link based on the combination of these methods. An LSMS system is developed and evaluated here for the first time with imaging diversity receivers, and used to facilitate comparison with the proposed systems. The system's performance based on a conventional diffuse transmitter with different detection schemes: a single non-imaging receiver with a field-of-view (FOV) of 65^{o}, a single imaging receiver and an imaging diversity receiver, are also evaluated and compared. The high SNR achieved through the use of an adaptive spot-diffusing transmitter with imaging diversity receivers employing MRC, can be used to reduce the transmit power which helps meet eye safety requirements. This SNR, coupled with the increase in channel bandwidth, can enable the OW system to achieve mobility while operating at high bit rates (5 Gbit/s). Alternatively these improvements can be used to enable multi-user communication through the introduction of an MC-CDMA scheme. Furthermore, the effectiveness of the proposed link design against shadowing and signal blockage is considered.

Chapter 8 introduces a novel beam angle adaptation method, which helps target the spots at the optimum location yielding the best SNR at the receiver. The chapter gives a link design that is less sensitive to the room geometry (than CDS and LSMS), as the diffusing spots can be targeted at the optimum location that maximises the receiver SNR. The power can also be re-distributed among the spots to further improve the receiver SNR. The link design adapts the beam angles and beam powers, thus enabling the system to adapt to the room geometry and to transmitter and receiver mobility; to maximise the SNR and reduce the delay spread hence increasing the channel bandwidth. The performance of a link design employing spot-diffusing, beam angle and beam power adaptation, in conjunction with a 12^{o} FOV

angle diversity receiver is assessed in the presence of BN, multipath dispersion, mobility, shadowing and signal blockage. The results show that through the use of these methods the OW system is able to achieve the required performance (BER of 10^{-9}) while operating at high bit rates (2.5 Gbit/s and 5 Gbit/s). This is achieved with full mobility at 2.5 Gbit/s and 5 Gbit/s which is a useful result for wireless communications. Furthermore, the trade-off between the power penalty and the computational saving (introduced as a result of sub-optimum beam angle adaptation) is investigated.

In Chapter 9, a high-speed spot diffusing mobile optical wireless system utilising beam angle adaptation, beam power adaptation and imaging receivers is presented. The chapter also investigates eye safety, by introducing a limitation in the beam angle and power adaptation algorithm, so that no spot power exceeds the typically quoted 1 mW eye safe limit at the near infrared wavelengths, and a good performance is observed. Robustness to shadowing and signal obstruction is also considered, and it is confirmed that their effects can be sufficiently mitigated through the use of these methods (spot-diffusing, imaging reception, beam angle and beam power adaptation).

A summary of the contributions of the present study and the thesis conclusions are given in Chapter 10.

Proposals towards further research are drawn in Chapter 11.

2. LITERATURE REVIEW

2.1. Introduction

Infrared (Ir) wireless local area network (LAN) systems have attracted attention due to their potential in high-speed transmission, electromagnetic interference avoidance and low-cost sub-systems. The use of infrared radiation for indoor applications has been widely studied. The first indoor optical wireless (OW) system was proposed by Gfeller and Bapst in 1979 [3]. Much more research has since been carried out [3-49, 59]. Perhaps the most promising feature of the Ir transmission is its extended bandwidth. Ir light is characterised by THz frequencies that can support a bandwidth of hundreds of GHz, which is substantially greater than that associated with radio wireless. Although large bandwidth is important, it is not the only feature that has made optical wireless technology especially attractive for indoor wireless communication systems. To achieve wider understanding, both advantages and disadvantages, in indoor OW systems, need to be carefully weighed.

Besides an extended bandwidth, OW links offer several other advantages over their radio counterparts. Due to the nature of light, optical signals cannot propagate through opaque objects such as walls which limits or eliminates interference between Ir systems in adjacent rooms. Furthermore, an OW link provides immunity to interference caused by other radio frequency wireless devices, and offers wavelength reuse in adjacent rooms. It also offers a degree of security at the physical layer and prevents interference between links operating in different rooms. Furthermore, an OW system allows the use of inexpensive optoelectronic devices. Typical optical transceiver components include light emitting diodes (LEDs), laser diodes (LDs), positive-intrinsic negative (PIN) photodiodes and avalanche photodiodes (APDs),

and are low-cost compared to similar components used in radio. Optical transceiver components enable simple intensity modulation and direct detection (IM/DD) techniques. Intensity modulation (direct modulation) is performed by varying the drive current of LEDs or laser diodes. Direct detection is performed by producing an electric current, proportional to the incident optical power, through the use of PIN photodiodes or APDs. When an infrared link employs IM/DD, the short optical wavelength and large photosensitive reception area result in efficient spatial diversity which prevents multipath fading. Freedom from multipath fading greatly simplifies the infrared links' design. In addition, OW links offer freedom from spectrum regulation and licensing.

OW links offer the opportunity for high-speed communications as well as the potential to achieve data rates well beyond 2.5 Gbit/s with full mobility, although these have not been experimentally demonstrated to date. Typical data rates ranging from 10 Mbit/s for diffuse systems, to 155 Mbit/s for cellular OW systems to 1-10 Gbit/s for line-of-sight (LOS) OW have been experimentally demonstrated [8, 28, 32, 36]. This work reports systems that operate at 2.5 Gbit/s and 5 Gbit/s with full mobility. Infrared wireless LANs can be used to connect portable devices to base stations, which are interconnected by a wired backbone network, and then communicate with different users and even a computer server. The network backbone can feed OW transceivers that act as access points throughout the environment as shown in Fig. 2.1, in which the mobile users have access to all the available services on high-speed wired networks. Hardware and software based multiple access techniques are desirable [34, 60-64].

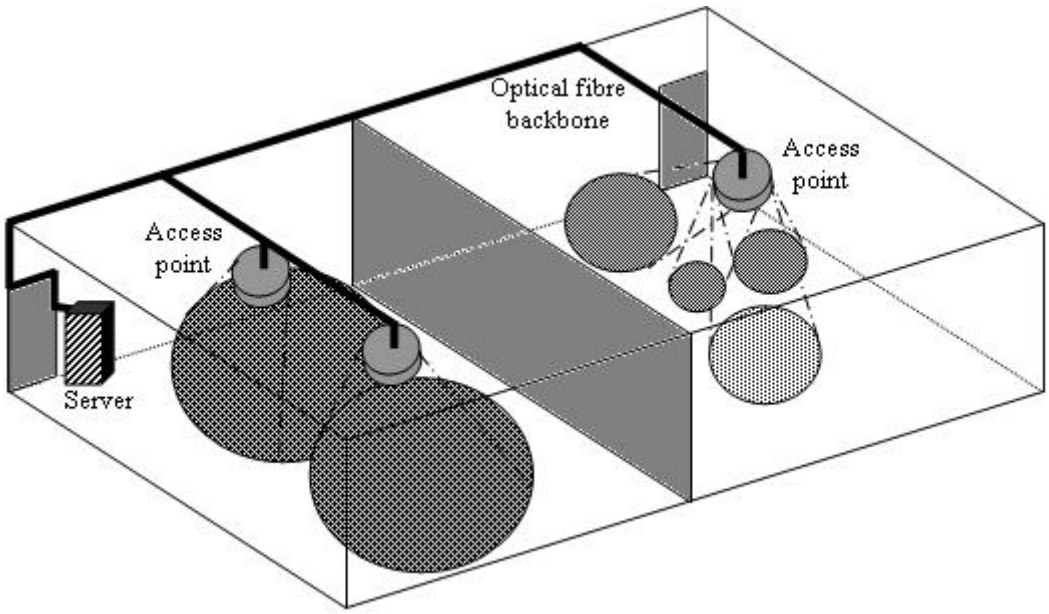

Figure 2-1: Access points in a local area network for connecting OW devices with a wired network

Despite these advantages, there are two major impairments associated with optical wireless systems when employing intensity modulation with direct detection. The first is additive shot noise due to sunlight and artificial light, which degrades the signal-to-noise (SNR). The second is multipath dispersion associated with non-directed LOS infrared systems, which results in significant intersymbol interference (ISI). In addition to these two main drawbacks, OW networks rely on a fibre distribution network that feeds access points as optical signals are blocked by walls and opaque objects. Furthermore, the maximum allowed optical power is constrained by eye and skin safety regulations [56-58]. Consequently, the detector photosensitive area should be sufficiently large in order to collect sufficient optical power hence achieving an acceptable performance, which is typically a probability of error of 10^{-9} in digital optical communications. However, a large photosensitive area means a high capacitance, which limits the available bandwidth. Further details of indoor optical wireless limitation are given later in this Section.

Over the past decade, various techniques have been proposed to mitigate the impairments imposed by OW channels, and to overcome the high capacitance associated with large photosensitive areas. Novel methods such as computer generated holograms and optical leaky feeders were examined [11-12]. Performance improvements were achieved through the use of different lens and filter structures [41]. Several of the novel cellular OW systems, operated typically at a bit rate of up to 155 Mbit/s, were demonstrated [14-17, 24, 29, 43]. A data rate of up to 1 Gbit/s in a line of sight asynchronous transfer mode (ATM) network was also reported [25]. OW systems have been traditionally used in many indoor applications, such as remote controls, headphones, conferencing systems and video transmission systems [4, 18]. Short-range low-speed OW data links for computer applications such as mice, printers, organizers, and palm top personal computers (PCs) have also been found [19]. An overview of the research, which has been carried out in the literature of the OW systems, is given in this chapter.

This chapter gives brief details of the OW communication links. The limitations of the indoor optical wireless communication system are presented. The transmission and reception of optical signals are described. Modulation schemes and multiple-access techniques used in optical wireless systems are then discussed. The chapter concludes with a description of the currently used indoor OW systems.

2.2. Optical Wireless Communication Scenarios

Optical wireless communication Scenarios can be classified according to two criteria: (i) the existence of a direct path between the transmitter and receiver and (ii) the degree of transmitter and receiver directionality [30]. This classification scheme is shown in Fig. 2.2. LOS and non-LOS propagation systems represent the two most

common configurations of indoor OW links. LOS links rely upon a direct path between the transmitter and receiver, regardless of their beam angles, while non-LOS links generally rely upon light reflections from walls, ceilings and other diffuse reflecting surfaces. LOS links improve power efficiency and minimise multipath dispersion, but can suffer from shadowing. Non-LOS systems offer robust links and reduce the effect of shadowing through the use of signals reflected from walls, ceiling, and other reflectors. On the other hand, they are affected by multipath dispersion, which causes pulse spread and significant ISI, in addition to higher path losses compared with LOS links.

Both LOS and non-LOS links can further be classified into directed, hybrid and non-directed, based on the transmission radiation pattern and the receiver field-of-view (FOV). Directed links employ directional transmitter and receiver i.e. have a narrow beam/FOV. They inherently require transmitter-receiver alignment in order to establish communication, which makes directed systems less convenient to use in certain applications [6-7, 65-68]. A non-directed link employs a wide-angle transmitter and receiver, which alleviates the need for such alignment. Directed link scenarios minimise path losses and reduce the impact of ambient light noise, hence maximising power efficiency. Unfortunately, directed systems are not suitable for portable devices as they require aiming of the transmitter and receiver, and may suffer from shadowing. Although tracking satellite transmitters can offer the possibility of terminal mobility, they do not overcome shadowing [25, 29]. Non-directed link designs do not offer such power efficiency but allow an excellent degree of mobility within the covered zone, where mobile users can simply roam without losing connection. Furthermore, a hybrid link can be established by employing transmitters and receivers with different degrees of directionality.

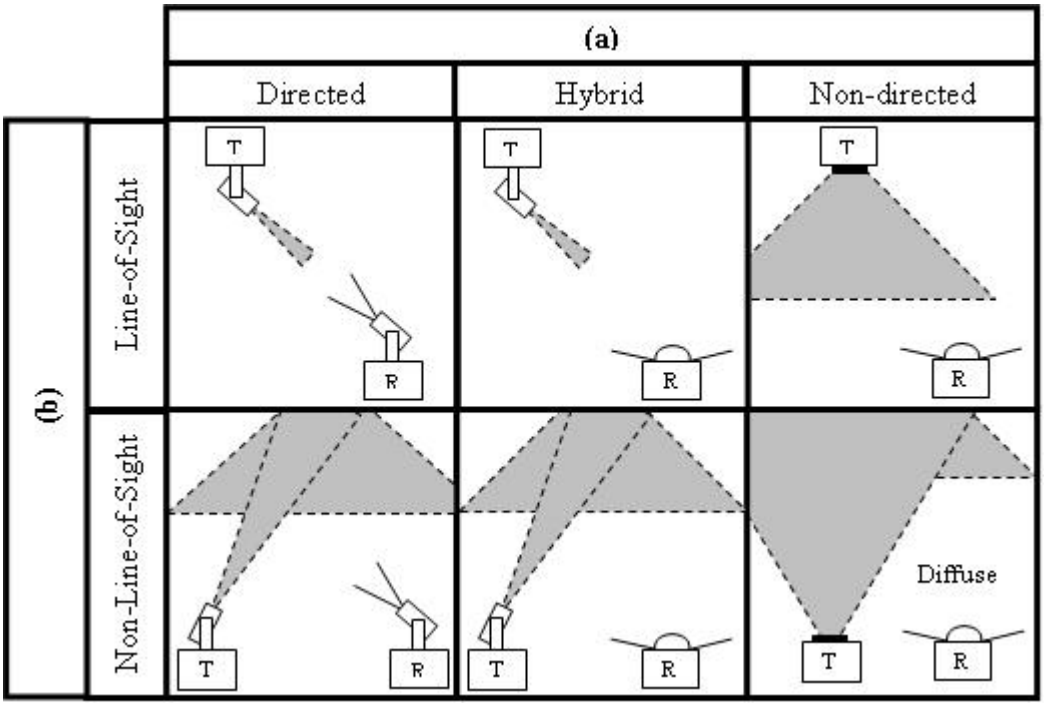

Figure 2-2: Classification of OW links based on: (a) the degree of transmitter and receiver directionality and (b) the existence of a direct path between the transmitter and receiver [30]

A non-directed non-LOS link scenario which is often referred to as a diffuse link is the most desirable approach (among the approaches described) for indoor mobile applications. Diffuse systems also play a very important role in environments where shadowing exists. This is due to the fact that diffuse propagation systems do not require transmitter-receiver alignment or line-of-sight and instead make use of reflections from walls, ceiling, and other reflectors. However, systems adopting this technique have poor power efficiency and a much-reduced data rate compared with a directed LOS. A conventional diffuse system (CDS) employs a wide beam transmitter and a wide FOV receiver, both pointing up towards the ceiling, where the transmitted signal reaches the receiver through multiple diffuse reflections (ceiling and walls). Diffuse systems provide robustness against signal blockage and shadowing enabling mobile users to instantly connect and collaborate in a wireless

environment. However, diffuse systems are subject to multipath dispersion which results in signal spread and intersymbol interference. The effects of multipath propagation can be reduced through the use of diversity and/or equalization.

2.3. Indoor Optical Wireless Limitations

Indoor optical wireless environments are free from atmospheric impacts, which normally affect outdoor OW systems. However, data transmission in indoor OW systems is limited by four impairments: background noise (BN), multipath dispersion, high photodetector capacitance and eye safety.

2.3.1. Background Noise

Unlike optical fibre receivers, OW receivers are distorted by ambient light noise. The major sources of ambient light noise in indoor OW environments are; direct sunlight, fluorescent lamps, and incandescent lamps, which corrupt the signal and represent background noise (BN). These sources emit a substantial amount of power within the wavelength range of silicon photodetectors, as well as introducing shot noise, and can saturate the photodetector when their intensity is high [20, 69]. Although ambient light can be much stronger than the transmitted data signal, its influence can be minimised by using optical filters [70]. Inexpensive daylight filters, which are commonly used in OW links, are normally placed in front of the photodetector to eliminate visible optical radiation. Typical daylight filters remove radiation of wavelength < 760 nm [20]. The optical power spectra of the three common ambient light noise sources are illustrated in Fig. 2.3 (a) [30]. A combined silicon photodiode-daylight filter is shown in Fig. 2.3 (b) [30].

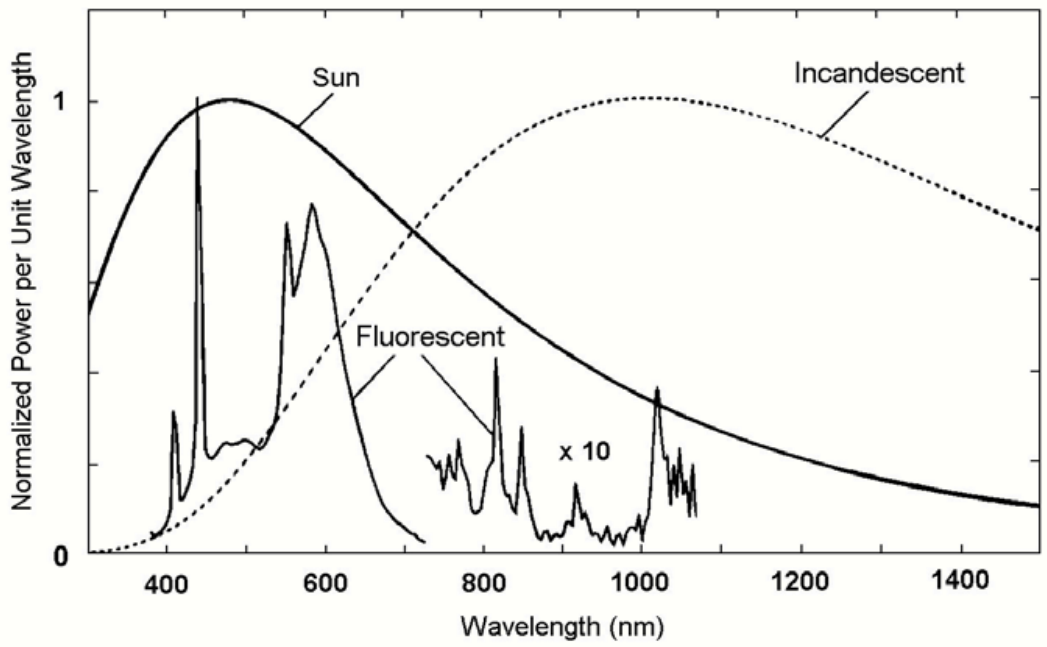

(a)

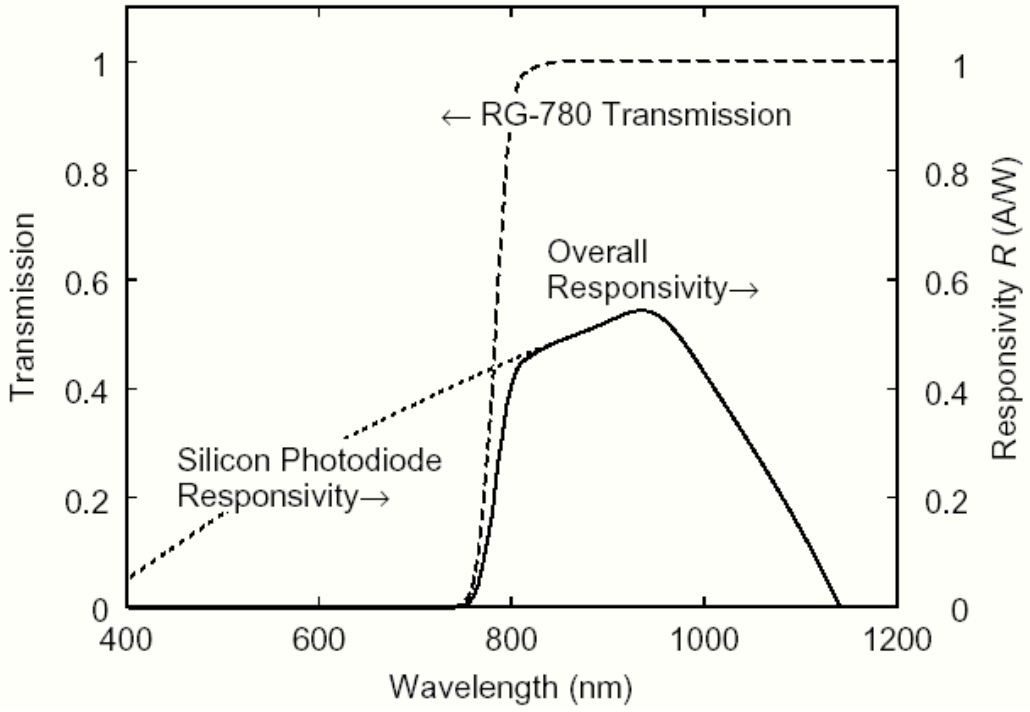

(b)

Figure 2-3: (a) Optical power spectra of the three common ambient noise sources [30]. (b) Transmission of a silicon photodiode employing a daylight filter [30]

The characteristics and the effect of the ambient light sources have been widely studied [67-75]. It was found that fluorescent light produces a small amount of BN, while sunlight and incandescent light (for example, halogen and tungsten filament lamps) produce the highest noise level, tungsten being the worst BN source. Sunlight is not subject to fast unexpected changes, therefore its influence can be considered as a stationary photon stream. This steady photon stream is then converted by the photodetector into a photocurrent that consists of two different noises: a DC component and a Gaussian shot noise component. The DC current noise component can be easily removed by using simple AC-coupling.

Artificial light sources induce interference due to cyclic variation of light intensity. The interference produced by an incandescent lamp is an almost perfect sinusoid with a frequency double the power-line frequency [69]. This double line frequency is a consequence of the fact that positive and negative alternations of the electrical line power are converted into a positive optical power. This interfering signal and the DC component of the BN can be effectively removed by using an electrical high-pass filter. Despite the use of such a filter the background shot noise current produced by incandescent lights is much higher in level than that produced by low- and high-frequency fluorescent lights [20], as shown in Fig. 2.3. This is due to the fact that the spectrum of the incandescent lights, such as halogen and tungsten filament lamps, falls within the passband of the daylight filter [73]. Furthermore, incandescent lights are highly directive sources that cause a burn-out effect of the received signal, particularly underneath the light source. Narrow bandpass optical filters can only be used if accompanied by laser transmitters (not LEDs) [76]. Such filters (typically interference filters) are also limited in the range of angles at which they accept the radiation.

Fluorescent lights are classified into two categories: fluorescent lights with conventional ballast (FLCB) and fluorescent lights with electronic ballast (FLEB). Fluorescent lights produce most of their optical power outside the passband of a daylight filter [67-75]. Therefore, fluorescent lights can have a lower impact in indoor OW environments as they have a lower power density at the wavelengths associated with optical photodetectors, compared with the other light sources. However, the electrical interference, produced by a fluorescent lamp, is a distorted sinusoid and its spectrum is much broader than that of an incandescent lamp.

Fluorescent light flickers at a constant rate, determined by the lamp drive frequency, and induces interference at harmonics of the power-line frequency. The electrical spectrum of the photocurrent, generated by conventional ballast fluorescent light, extends to about 50 kHz [71, 77]. This interference can significantly impair the signal. Its impact can be eliminated through the use of high-pass filters and through careful choice of the modulation scheme [75]. FLEBs use switching transistors to modulate the power at a frequency (typically within the range of 20 – 50 kHz), in order to improve the efficiency of the lamp-ballast assembly and reduce its size. The interference spectrum induced by electronic ballast fluorescent light reaches frequencies of up to a few MHz due to the high frequency of the switches [68]. Although, an electrical high-pass filter is used, this interference could induce high power penalties, resulting in ISI when the data rate is above 10 Mbit/s [75]. The impact of this interference can be reduced through the employment of detectors with common-mode rejection as proposed by Barry [78]. A modification of this technique was analysed by Moreira et al. demonstrating its ability to significantly reduce the influence of artificial light, and its suitability for systems operating at high data rates

[72]. Furthermore, it has been shown that interference induced by fluorescent lights can be reduced by using spread spectrum techniques [79].

Various techniques have been considered to mitigate the impact of ambient light noise [44-45, 56-58, 80-92]. A narrow beam optical source coupled with a narrow FOV receiver can be employed to reduce the background noise. Diversity reception techniques can also be used to significantly reduce the influence of ambient light noise [26, 44-46, 81-82]. The angle diversity receiver utilises multiple non-imaging receiving elements that are aimed at different directions. These receiving elements can help reduce the effect of ambient light noise by eliminating/reducing the unwanted signals received from a direction other than that of the desired signal. They can also reduce the multipath dispersion by employing narrow FOV receivers that combine the received signals optimally. An improvement in performance is achieved by using non-imaging diversity detection, however cost and complexity have to be considered where each receiving element requires the use of a separate optical concentrator. Diversity receivers have been considered in this study.

An appropriate technique that can help combat background noise, significantly reduce ISI, and improve system performances, is an imaging receiver. Yun and Kavehrad proposed the fly-eye receiver [40], which consists of a single imaging optical concentrator (e.g., a lens) that forms an image of the received light on a collection of photodetectors. Performance comparison of LOS links has been presented in [93] which compares imaging receivers and non-imaging receivers. Djahani and Kahn reported that in non-LOS links, imaging receivers and multibeam transmitters can reduce the required transmitter power by more than 20 dB [94]. Compared to the non-imaging angle diversity receiver, an imaging receiver provides two advantages. Firstly, all photodetectors share a common imaging concentrator,

reducing the receiver's size and cost. Secondly, all the photodetectors can be laid out in a single planar array which facilitates the use of a large number of photodetector pixels, leading to enhanced performance. In order to combine the advantages of imaging receivers and diversity schemes (hence providing robustness to ambient light noise and multipath dispersion), this work introduces novel imaging diversity receivers.

2.3.2. Multipath Dispersion

Channel dispersion associated with multipath propagation is an important concern in designing indoor optical wireless systems. Multipath dispersion occurs when the transmitted signal reaches the receiver through different paths at different times due to reflections by walls, ceiling and other reflector objects. Multipath dispersion causes the received pulse to spread, resulting in ISI. The severity of ISI induced by multipath propagation can be measured by using the channel root-mean square delay spread. In directed LOS links, the transmitted signal reaches the receiver directly where a narrow beam transmitter and a narrow FOV receiver, aligned with one another, are employed. Therefore, directed LOS links provide almost negligible multipath dispersion. In contrast, diffuse systems suffer from multipath dispersion due to the wide beam/FOV transceivers used. The intersymbol interference induced by multipath dispersion can be a major degrading factor when the data rate exceeds 10 Mbit/s in a typical room size [30].

Channel characteristics of indoor OW links have attracted great attention in order to devise techniques that can help mitigate multipath dispersion. Various techniques have been proposed to combat multipath propagation as well as reduce the effect of ISI. An angle diversity receiver employing uncorrelated narrow FOV detectors,

which are oriented in different directions, can be used to reduce the impact of multipath propagation due to the limited range of rays captured [26, 53, 95]. A significant reduction in the multipath dispersion can be achieved through careful design of the detecting elements orientation and directionality. The pyramidal fly-eye diversity receiver (PFDR) has been proposed as a receiver structure that can significantly reduce multipath dispersion [33, 38, 44-45, 96-97]. An optimisation of the PFDR has also been proposed to reduce the effect of multipath propagation and to improve the link performance [44, 50]. The main drawbacks of this approach are the potentially large size and high cost of the multiple receiving elements associated with angle diversity receivers. As an alternative, imaging receivers have been proposed as a method that can be implemented to combat the limitations (multipath dispersion and ambient light) of the non-directed LOS OW communications [43, 93-94, 98]. In this thesis, new imaging diversity receivers are proposed to provide link robustness against these two major limitations as well as improve the system's performance. Imaging diversity receivers are discussed in Chapter 6 and Chapter 7.

Furthermore, Transmitter beam diversity has been proposed as a method that can be implemented to enhance the performance of OW systems [39, 42, 51-52, 96-97, 99]. Multibeam transmitters were first proposed by Yun and Kavehrad [40] to create multiple diffusing spots that point in different directions towards reflecting surfaces. Systems that adopt this approach possess the advantages of the direct LOS systems and overcome the drawbacks of diffuse links. Significant performance improvements can be achieved by using a line strip multibeam system (LSMS) in conjunction with an angle diversity receiver [95-97, 100]. These methods (spot-diffusing and diversity) were evaluated within complicated room designs (cubical office partitions, windows, doors, furniture, ambient light noise, and multipath propagation) in the

case of a static transmitter [99, 101]. Although an improvement in performance was achieved, the need for mobility, which results in significant performance degradation especially when shadowing exists, is a challenge in practical systems. In addition, a beam clustering method (BCM) was presented and shown to be a promising means for improving the performance of OW communication links [102-103].

In this thesis, a mobile OW system, based on a new adaptive multibeam system with diversity detection is proposed in order to mitigate the mobility induced impairments, and to improve the system's performance [104-105] (Chapter 4). Beam power adaptation and diversity techniques have been widely used in radio wireless communication [106-109]. The effectiveness of the proposed system (angle diversity adaptive LSMS) in a harsh indoor environment is also studied [110-111] (Chapter 5). Furthermore, a novel design that uses a two-dimensional adaptive beam clustering method (2DABCM), in conjunction with a new imaging diversity receiver, is proposed and evaluated under the constraint of multipath dispersion and ambient light noise [112-113] (Chapter 6). Higher bit rate OW systems (2.5 Gbit/s and 5 Gbit/s) are shown to be feasible with full mobility through the combination of beam power adaptation, spot-diffusing and imaging reception [114-115] (Chapter 7). Regardless of the transmitter position, the SNR of an angle diversity multibeam system can be maximised, at a given receiver location through the implementation of two novel methods: beam angle and beam power adaptation. The proposed system; multibeam power and angle adaptive system (MBPAAS) can achieve a significant SNR improvement when coupled with either diversity receivers or imaging receivers. Higher data rate mobile OW systems (2.5 Gbit/s and 5 Gbit/s) are reported [116-119] (Chapter 8 and Chapter 9).

2.3.3. Photodetector High Capacitance

Virtually all indoor optical wireless systems employ IM/DD modulation techniques. The SNR of a direct-detection receiver is proportional to the square of the received optical power. Furthermore, the optical transmitter power is limited by eye safety concerns and power consumption. These constraints imply that a photodetector with a large photosensitive area should be employed in order to maximise the optical power collected. Unfortunately, the capacitance of the photodetector is directly proportional to its area, i.e. a large photosensitive area equates to a large capacitance which restricts the attainable bandwidth. The large capacitance at the input of an amplifier acts as a lowpass filter (LPF) which attenuates the high frequency components of the received signal. However, the dominant white thermal noise, which is observed after the input stage, will not be attenuated. This noise may degrade the SNR at higher signal frequencies. When a white noise process following a LPF is referred back to the input of the filter, its power spectral density becomes quadratic in frequency, and therefore it is often called f^2 noise. Since the f^2 noise variance in an amplifier is proportional to the square of the capacitance (hence the square of the photodetector area), its effect can be reduced by employing a photodetector array instead of a single photodetector [120]. In a well-designed receiver, this noise will be insignificant compared with the background shot noise [120]. Therefore, it is ignored in this work.

In order to maximise the signal power collected without using a large photodetector area (hence avoiding the photodetector high capacitance), the photodetector's effective range of reception angles should be increased. The effective area of the photodetector array can be increased by using a custom-built lens as in [94], or by using a hemispherical lens when non-imaging diversity receivers are used as in [30].

Furthermore, the effect of the high photodetector capacitance can be reduced through the use of circuit design techniques, such as bootstrapping [22].

2.3.4. Optical Safety

The maximum allowed optical power is restricted by eye and skin safety regulations [56-58], which place limitations on indoor OW systems. This is due to the fact that the best wavelength band for most applications of infrared wireless links is typically (780-980 nm) where optical transceivers are available at low cost [57]. However, radiation in this wavelength can pass through the human cornea and can be focused by the eye lens onto the retina, where it can potentially induce thermal damage and may cause retinal burn [56-58]. The degree of this radiation hazard depends on a number of factors such as exposure level, exposure time, beam characteristics and the operating wavelength.

In general, laser diodes and high-radiance LEDs emit an optical power in the 700-1550 nm wavelength band, which may cause eye damage if absorbed by the retina. The energy density of an incident light can be focused by the human eye onto the retina by factors 100,000 or more [121]. Therefore, the Maximum Permissible Exposure (MPE) levels are quite small. The optical wavelengths beyond 1400 nm have much less effect due to the fact that the cornea is opaque at these wavelengths. It has been suggested that the 1550 nm band may be better suited for infrared links. However, photodiodes in this band, which are made of germanium or InGaAs, have a much higher cost and capacitance per unit area compared with their silicon counterparts [30].

The eye safety standards of infrared transmitters are regulated by the International Electro-technical Commission (IEC) [122]. LDs are classified into Class 1, 2, 3A and

3B, as shown in Table 2.1 based on the accessible emission limit (AEL). The AEL depends on the wavelength, diameter and emission semi-angle of the optical source. IEC command that all transmitters must be Class 1 eye safe under all circumstances of use. Table 2.1 shows that launch power must not exceed 0.5 mW for systems employing point laser sources at the wavelength regions where most low-cost devices operate.

TABLE 2-1: SAFETY CLASSIFICATION FOR A POINT SOURCE EMITTER

	Wavelength			
	1550 nm Infrared	**1310 nm Infrared**	**880 nm Infrared**	**650 nm Visible**
Class 1	< 10 mW	< 8.8 mW	< 0.5 mW	< 0.2 mW
Class 2	N/A	N/A	N/A	0.2 – 1 mW
Class 3A	10 – 50 mW	8.8 – 45 mW	0.5 – 2.5 mW	1 – 5 mW
Class 3B	50 – 500 mW	45 – 500 mW	2.5 – 500 mW	5 – 500 mW

Various techniques were proposed in order to mitigate the laser hazard at high emitted power. The risk of eye damage can be significantly reduced by using wide beam sources. Furthermore, LDs operating inside the Class 3B region can be made Class 1 eye safe through the use of diffusers to spread their radiation over a wide emission angle. An almost 70% efficiency can be achieved by using such types of diffusers. A computer-generated hologram (CGH) was proposed as a beam-splitting element with a diffraction efficiency close to 100% [40, 123-125]. This hologram breaks up the optical beam in a fabricated pattern diffusing the image of the laser-spot efficiently on the retina. However, a so called hot spot can be produced in the

middle of the diffuser pattern. The intensity of the hot spot, which is usually higher than the rest of the pattern, can be reduced by careful optimisation and manufacture. The presence of hot spots may result in a reduction in the maximum permitted transmit power [123]. This effect can be overcome by using an integrating-sphere diffuser, proposed by Pohl et al, offering an eye-safe emission power in the range of 100 mW – 1 W [126].

2.4. Reception of Optical Wireless Data

A key component in an OW receiver is the photodetector where the optical signal is converted into an electrical signal suitable for further processing. The block diagram of a typical OW receiver is shown in Fig. 2.4.

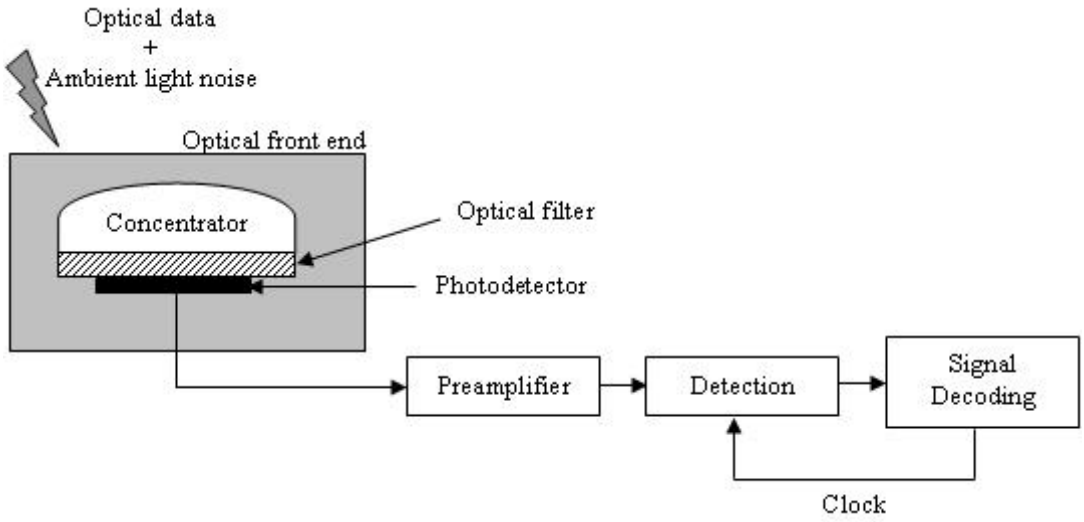

Figure 2-4: Block diagram of a typical OW receiver

The photodetector is placed behind a front end that consists of a concentrator and an optical filter. The concentrator can enhance the amount of signal power that reaches the photodetector area, while the optical filter is used to reduce ambient light noise. The photodetector is followed by a preamplifier and a detection circuit that is

controlled by a clock extracted by a clock recovery circuit. The latter is part of a signal decoder following the detection circuit. The main components of the OW receiver are discussed next.

2.4.1. Concentrator

An optical concentrator can be used to increase the effective light-collection area hence allowing the use of photodetectors with a smaller photosensitive area and hence a lower capacitance. Such a device can transform the incident light rays over a wide area into a set of light rays emerging from a smaller area, which matches the photodetector area. Although, a higher level of signal power can be collected by employing such a concentrator, more ambient light noise can also be received. However, the BN influence can be reduced by using optical filters.

OW systems may employ imaging or non-imaging concentrators. Most short-distance infrared systems use non-imaging concentrators. An idealised non-imaging concentrator [127] having an internal refractive index N_C can achieve a transmission factor

$$T_C(\delta) = \begin{cases} \dfrac{N_C^2}{\sin^2(\psi_C)}, & 0 \le \delta \le \psi_C \\ 0, & \delta > \psi_C \end{cases}, \tag{2.1}$$

where ψ_C and δ are the concentrator's acceptance semi-angle and the reception angle respectively, so that when the reception angle δ exceeds ψ_C, the concentrator transmission factor, $T_C(\delta)$ rapidly approaches zero. Usually $\psi_C \le 90^o$. Observing (2.1), non-imaging concentrators exhibit a trade-off between transmission factor and acceptance semi-angle, such that $T_C(\delta)$ increases when ψ_C decreases.

The non-directional hemispheric concentrator is a common non-imaging concentrator that can achieve an acceptance semi-angle of 90^o and a transmission factor of N_C^2 [78]. This transmission factor can be achieved if the radius r_{hc} of the hemispheric concentrator meets the condition [128]

$$r_{hc} \geq N_C \times r_{\mathbf{det}}, \tag{2.2}$$

where r_{det} is the photodetector radius. The compound parabolic concentrator (CPC) is another common non-imaging concentrator having $\psi_C < 90^o$ [11, 127-129]. The CPC can achieve a much higher transmission factor than the hemispheric concentrator at the cost of a narrow ψ_C. This makes CPC suitable for directed links. A CPC with $\psi_C < 90^o$ can achieve a transmission factor close to that given by (2.1). An optical filter can be placed on the front surface of the CPC, as shown in Fig. 2.5. An angle diversity receiver employing narrow CPCs can be used to reduce the influence of ambient light noise and improve the SNR [129]. In this thesis, a CPC is employed as a non-imaging concentrator, while the imaging concentrator used is a lens [94].

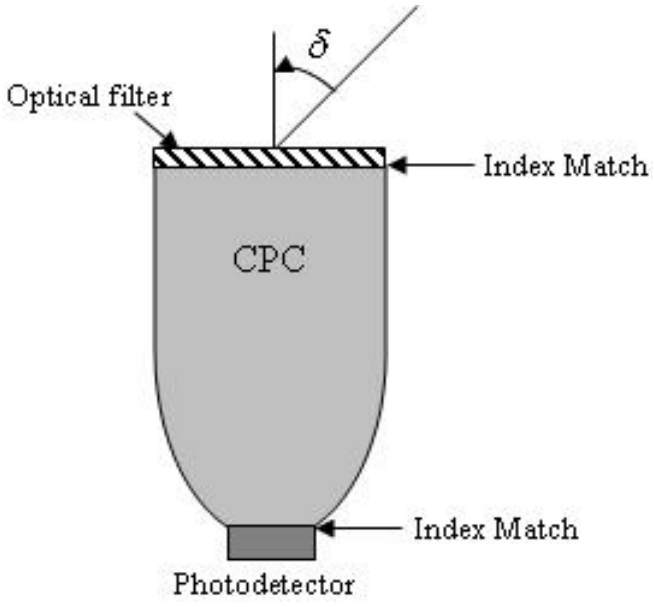

Figure 2-5: Compound parabolic concentrator (CPC) with planar optical filter

2.4.2. Optical Filter

Ambient light represents the dominant noise source in an indoor OW system, and it is characterised by a broad optical spectrum as shown in Fig. 2.3 (a). The influence of the ambient light noise can be significantly reduced by limiting the optical receiver optical bandwidth through the use of optical filters. Optical filters, either high pass filters or band pass filters, are used in front of the photodetector to eliminate ambient light noise. High pass filters essentially pass light at wavelengths beyond the cut-off wavelength, which is set near 700 nm in order to stop visible light. They are usually constructed of coloured glass or plastic, and therefore their transmission characteristics are inherently independent of the incident angle. This makes them the most commonly used optical filters in commercial infrared systems.

On the other hand, a band pass filter is the other alternative that can be used to attenuate ambient light noise. Such a filter can be realised by using multiple thin dielectric layers, and relies upon optical interference in the Fabry-Perot cavities formed [30, 83]. Band pass filters can achieve narrow bandwidths, resulting in significant rejection of the ambient light noise. However, their transmission characteristics highly depend on the incident angle. This drawback can be reduced through placing the thin-film optical filter on the hemispherical concentrator surface [78].

2.4.3. Photodetector

A photodetector is an opto-electronic device that represents the heart of an optical wireless receiver. It converts the incident light into an electrical signal. Due to the

very low intensity of the received light, the detector should possess the following desirable characteristics:

- High conversion efficiency (responsivity) at the operating wavelength
- Efficient detection process to avoid introducing additional noise
- Low-bias-voltage requirements are usual in portable devices together with tolerance to temperature fluctuations

Additional attractive characteristics can be defined in most practical applications. The photodetector should be small, lightweight, rugged, reliable, and cost-effective, and its characteristics should be insensitive to age and environment. Furthermore, the 780 - 950 nm wavelengths are typically used in most infrared link applications compared with the band beyond 1400 nm. This is due to the availability of low-cost, low-capacitance and large-area silicon photodiodes operating at that wavelength region (780 - 950 nm) as mentioned earlier. Two types of silicon photodiodes are widely used: an APD and a PIN. Both are available with large detection areas, resulting in an enhanced collected optical power.

APDs provide an improvement in link budget due to the avalanche multiplication process, through which an internal gain can amplify the photocurrent [130]. This also helps overcome the influence of the front-end noise hence improving the receiver SNR. However, the noise typically increases and is manifest as multiplicative noise, which can limit the performance. For this reason, APDs should be used when the preamplifier noise is the major source of noise and the ambient-induced shot noise is weak, whereas when the ambient-induced shot noise is dominant, a PIN photodiode is the better choice. In addition, PINs are cheaper, simpler to manufacture and require less complex biasing than APDs.

The basic steady-state operation of a photodiode can be characterised by the photocurrent it produces in response to an input optical power. The photocurrent is given by

$$I_p = q\zeta \frac{P_i}{h_p v}, \tag{2.3}$$

where I_p is the average photocurrent, q is the electron charge, ζ is the quantum efficiency of the device, P_i is incident optical power, h_p is the planck's constant, v is the optical frequency and $h_p v$ is the photon energy. The internal quantum efficiency ζ represents the probability that an incident photon creates an electron-hole pair. The responsivity of the photodiode can be expressed as

$$R = \frac{I_p}{P_i} = \frac{q\zeta\lambda}{h_p c}, \tag{2.4}$$

where c and λ are the speed of light and the wavelength respectively. The photodetector responsivity R (A/W) represents the optoelectronic conversion factor, and it is a key parameter in link modelling. Responsivities of silicon photodiodes are typically in the range of 0.5-0.75 A/W. Furthermore, the photodiode should have a high responsivity and a large bandwidth. The latter is limited by the transmit-time of carriers through the PN junction.

2.4.4. Preamplifier

Based on their configuration, optical receiver preamplifiers can be classified into three types: low impedance, high impedance and transimpedance preamplifiers. The high impedance preamplifiers provide high sensitivity, but they inherently require an equalizer due to the limitation imposed on their frequency response by the front end

RC time constant. They also have a limited dynamic range due to their high input load resistance. In contrast, transimpedance amplifiers offer a large dynamic range and a wide bandwidth due to their negative feedback, and therefore they are suitable in most infrared link applications [131]. However, their preamplifier noise level is higher and their sensitivity is lower compared to that of high impedance amplifiers. The low impedance preamplifiers offer a large bandwidth, but are limited by their high noise and therefore have a poor sensitivity. As such they are not suited to the power limited optical wireless link. Lower noise levels can be achieved when a field-effect transistor (FET) is used as a front-end device, instead of a bipolar-junction transistor (BJT) [131-132]. However, in relation to power consumption, a BJT may achieve superior results [132]. In this thesis, both transimpedance amplifiers (FET and BJT) are used.

2.5. Transmission of Optical Wireless Data

Optical transmitters mainly convert the electrical signal into optical form and then launch the resulting optical signal into the optical link. LDs and LEDs are the two commonly used optical sources for infrared transmission. LEDs are extremely low cost and they are generally considered eye-safe due to their sufficiently large surface area emitting light over a relatively wide spectral range. Typical LEDs emit light into semi-angles (at half power) in range of almost 10^{o} - 30^{o}, which make them suitable for most indoor applications. However, LEDs suffer several potential drawbacks such as:

- In typical low-cost devices, modulation bandwidths are limited to tens of MHz.

- Poor electro-optic power conversion efficiency (typically 10 – 20%), however new devices have efficiencies as high as 40%.
- Poor elimination of ambient light noise due to the use of a wide receiver optical passband, which is required due to the LEDs' broad spectral width (typically 25 – 100 nm).

On the other hand, LDs are much more expensive than LEDs and they require a more complex drive circuit, but offer many advantages including:

- Wide modulation bandwidths ranging from hundreds of MHz to more than 10 GHz.
- Electro-optic power conversion efficiencies of 30 – 70 %.
- Very narrow spectral widths, which range from several nm to below 1 nm.

Furthermore, LDs require a diffuser to destroy their spatial coherence and to spread the radiation over a sufficiently extended emission aperture and emission angle when used in diffuse OW links. A computer-generated hologram can act as a diffuser that achieves almost 100% efficiency. It also gives the designer the freedom to tailor the radiation pattern [51].

2.6. Modulation Schemes

In optical wireless communication systems, modulation takes place in two steps. The transmitted information is first coded as waveforms and then these waveforms are modulated onto the instantaneous power of the carrier. Direct amplitude modulation of the optical carrier is complex to implement, as optical wireless links suffer from

extensive amplitude fluctuations, and therefore it is not preferred. A much simpler modulation technique that conveys data on an optical carrier is intensity modulation. This section initially defines an IM/DD channel, and then discusses the most common modulation schemes used over this channel: on-off keying (OOK), pulse position modulation (PPM) and sub-carrier modulation.

2.6.1. Intensity Modulation and Direct Detection (IM/DD)

In OW communication links, intensity modulation with direct detection is the preferred choice [30], whereby the intensity of the light wave is modulated based on the information signal. The simplicity of this technique is due to the fact that intensity modulation (IM) can be achieved through the variation of the bias current of a LD or LED. In contrast to RF where the information is contained in the amplitude, phase or frequency of the carrier, it is contained in the intensity of the optical carrier in an OW system. It should be noted that the transmitted signal must be positive as the intensity can never be negative. Direct detection (DD) is the simplest configuration that can be used to detect an intensity modulated signal. In a DD receiver, a photodetector generates a photocurrent that is proportional to the instantaneously received optical power. The modelling of an OW channel employing IM/DD is illustrated in Fig. 2.6. It involves an infrared emitter as the transmitter and a photodetector as the receiver.

At the transmitter, the input data stream is converted into a time-variant photocurrent, which can drive the light source to produce an optical radiation. The optical signal diffusely propagates to the receiver through various reflecting objects within a room.

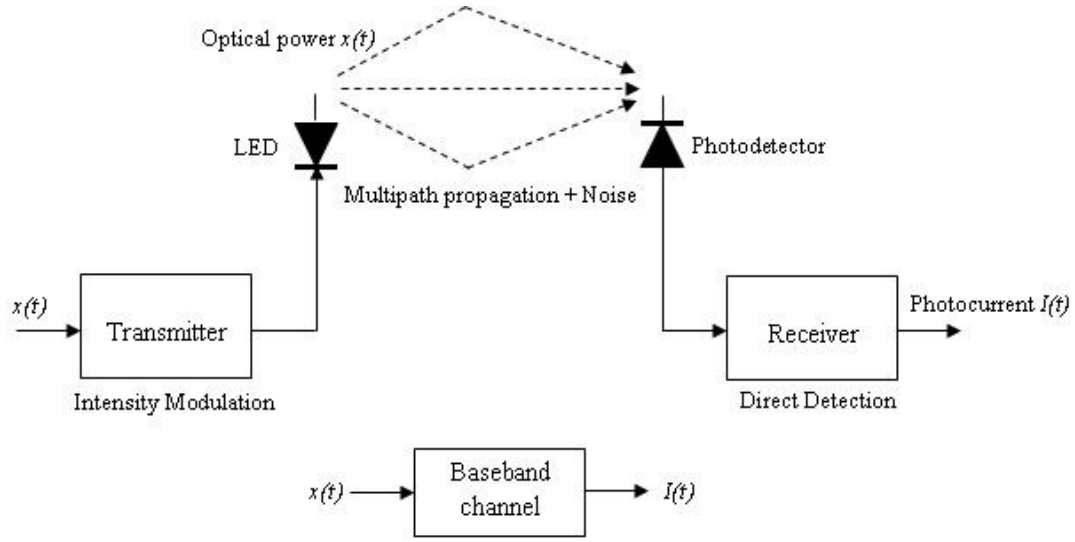

Figure 2-6: Channel model of an OW link

At the receiver, the amplitude of the received electric signal is squared and then integrated to find its intensity through the use of a square law detector. The square law detector produces a photocurrent proportional to the received instantaneous power, i.e. proportional to the square of the received electric signal. The photodetector is also illuminated by ambient light sources inducing shot noise. The IM/DD channel can be modelled as a baseband linear system, with instantaneous optical power $x(t)$, received instantaneous current $I(t)$ at the output of the photodetector at a certain position, and an impulse response $h(t)$, which is fixed for a certain transmitter and receiver configuration and set of locations. The IM/DD channel can be characterised by [30]

$$I(t) = R\,x(t) \otimes h(t) + n(t), \tag{2.5}$$

where t is the absolute time, R is the photodetector responsivity, $\otimes$ denotes convolution, and $n(t)$ is the background noise (BN), which is modelled as white and Gaussian, and independent of the received signal.

In the following sections, modulation techniques, which are suitable for indoor optical wireless, are compared in terms of power and bandwidth efficiency.

2.6.2. On-Off Keying (OOK)

OOK is the simplest modulation scheme to implement in optical wireless systems. In OOK, during a fixed time slot, a pulse of light is sent if the bit is '1' and no light is transmitted in the event of a '0' bit. OOK can be classified into two categories: non-return-to-zero OOK (NRZ-OOK) and return-to-zero OOK (RZ-OOK), which are depicted in Fig. 2.7, with a 50% duty cycle for RZ. With NRT-OOK, the pulse duration T_P is equal to the bit duration, T_{bit}, while it is lower than the bit duration in RZ-OOK.

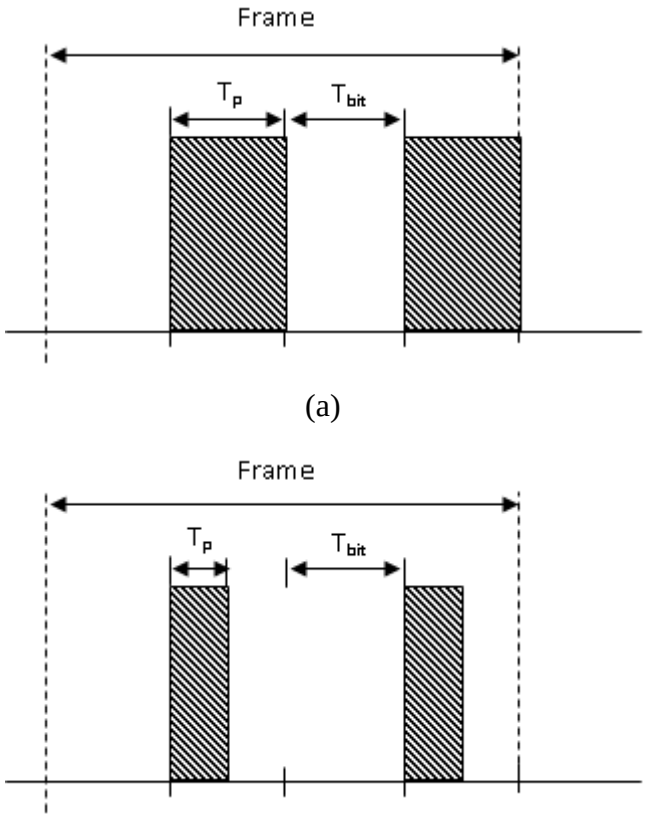

Figure 2-7: Basic OOK signal

NRZ-OOK provides higher bandwidth efficiency than RZ-OOK, but requires higher average power. OOK is an appropriate modulation scheme for high bit rate OW systems [14, 16-17, 24] due to its simplicity and the ability of LD/LED to switch on and off at rates into Gbit/s. However, ISI can be significantly increased. ISI can be effectively reduced by utilising an equalisation technique [14, 24, 133-134].

2.6.3. Pulse Position Modulation (PPM)

In OW systems, the maximum transmit power may be limited by eye safety and power consumption concerns, especially in mobile transmitters. Therefore, OW systems require high average power efficiency in order to combat these limitations. High average power efficiency can be achieved by employing pulse position modulation at the cost of relatively poor bandwidth efficiency [67]. This makes the PPM scheme more susceptible to multipath-induced ISI than NRZ-OOK. PPM is an orthogonal modulation scheme in which M data bits are conveyed by a single pulse in one of L possible positions. The L positions are represented as slots, and L-PPM has L slots in a single symbol time (frame). Each frame contains a pulse occupying one slot and $L-1$ empty slots. The pulse is located at a slot that is proportional to the binary value of the original digital symbol. Each frame can be concluded by a guard interval in order to avoid interframe interference and for timing extraction purposes. However, the inclusion of guard interval may call for larger bandwidth. A 16-PPM scheme with a guard interval is shown in Fig. 2.8.

PPM has been widely used in a number of low data rate commercial products [57-58, 60, 63, 135-138]. An improved PPM, in which the pulses have a raised-cosine shape, has been proposed by Pérez-Jiménez et al. [139]. It was reported that this scheme provides 30% more bandwidth efficiency than the basic PPM.

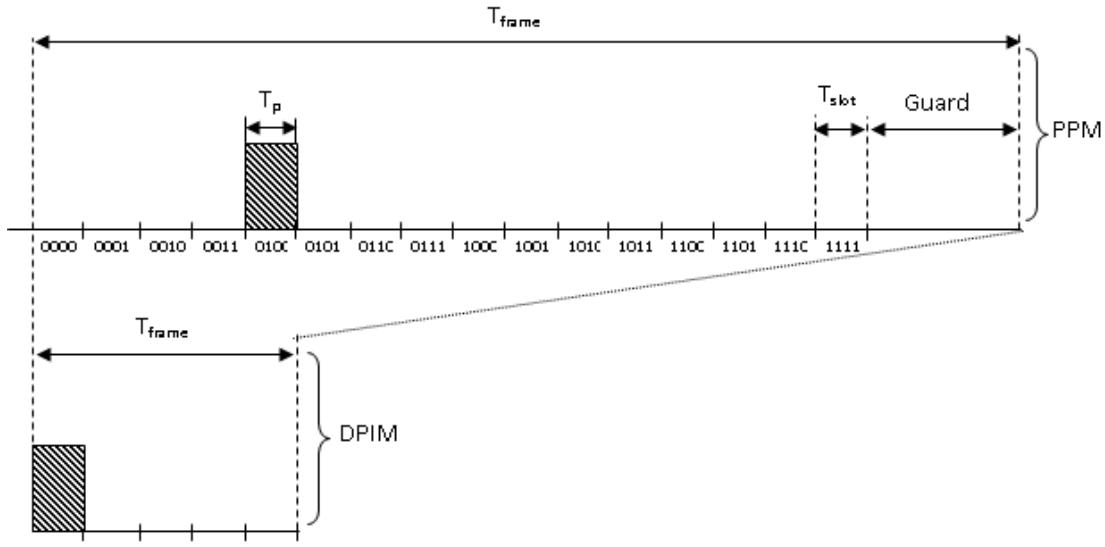

Figure 2-8: Transmission signal for 4 bits in 16 time slots 16-PPM and DPIM

It has also been demonstrated that adopting trellis-coded modulation (TCM), which is used to maximise the minimum Euclidean distance between allowed signal sequences, can improve the PPM performance [140]. Although PPM offers higher average power efficiency than OOK, it increases the system complexity due to the stringent synchronization requirements in the receiver, where the pulse position in time conveys the information. A digital pulse interval modulation (DPIM) scheme has been proposed by Kaluarachi et al. in [141] as a potential alternative to PPM, a technique where pulses can be transmitted in a variable length frame in contrast to transmitting PPM pulses within a fixed frame. In DPIM, each frame is initiated with a pulse followed by a number of slots according to the binary value of the data word as illustrated in Fig. 2.8. In effect, the data in DPIM can be encoded as a number of slots between adjacent pulses. An additional guard slot can be added to each frame following the pulse in order to avoid frames where the time between adjacent pulses is zero. DPIM can provide higher transmission capacity than PPM due to the elimination of all the unused slots within each frame, and requires no frame

synchronization since each frame is initiated with a pulse. However, it may lead to group generated errors when a pulse is wrongly detected.

2.6.4. Subcarrier Modulation

High-speed single carrier modulation schemes such as OOK and PPM are affected by ISI due to multipath dispersion at high data rates. Single subcarrier modulation (SSM) is a scheme whereby a bit stream is modulated onto a single radio frequency carrier that is used to modulate an optical carrier. Binary phase shift keying (BPSK) can be used, for example, as subcarrier modulation. Such a BPSK subcarrier requires twice the bandwidth of an OOK signal. Since the subcarrier is typically a sinusoid that takes positive and negative values, a dc bias must be added to avoid negative values which leads to, an increase in power requirements.

In multiple subcarrier modulation (MSM), multiple bit streams are modulated onto subcarriers at different radio frequencies with multiplexing in the frequency domain. The composite signal then modulates the intensity of an optical source. In effect, each subcarrier symbol rate can be reduced in comparison to the rate of a single carrier if both systems operate at the same total bit rate. Each subcarrier can be realised as a separate narrowband signal. MSM experiences reduced distortion and therefore equalization is not required at the receiver [89]. Furthermore, MSM has a higher bandwidth efficiency than single carrier modulation schemes and it can provide multi-access facilities while making use of the simplicity of IM/DD. However, it has poor optical average power efficiency compared with single carrier schemes. Furthermore, MSM can offer higher immunity to the low frequency noise caused by fluorescent lights compared to OOK. Much effort has been done to improve the power efficiency of MSM systems. Two simple and effective methods

have been proposed by You and Kahn [142]. In the first approach, block coding can be employed between the information bits and the subcarrier amplitudes in order to increase the minimum value of the multiple subcarrier waveforms. The fixed DC bias, which increases power requirements, can be replaced by a signal varying on a symbol-by-symbol basis as shown in the second approach. Furthermore, the power efficiency in MSM systems can be improved by transmitting a suboptimum set of peak reduction carrier (PRC) among N subcarriers yielding a reduction in the DC bias [143].

Orthogonal frequency division multiplexing (OFDM) is a particularly attractive technique that utilises multiple subcarriers overlapped in the frequency domain [144-146]. OFDM is a parallel data transmission scheme in which high data rates can be achieved by transmitting N orthogonal subcarriers. Both modulation and multiplexing can be digitally achieved by using an inverse fast Fourier transform (IFFT). At the receiver, the individual subcarriers can be demodulated without interference due to their orthogonality, and can then be recovered by using analogue filtering techniques. Demodulation and demultiplexing can also be performed using a fast Fourier transform (FFT). OFDM provides higher bandwidth efficiency than single carrier modulation schemes and it has little distortion. In most OFDM implementations any residual ISI can be removed through the use of a guard interval known as a cyclic prefix. On the other hand, OFDM has several disadvantages in the form of sensitivity to frequency offset estimation, the need for accurate subcarrier synchronisation and a high peak to average power ratio (PAPR).

2.7. Multi-Access Techniques

Multiple access techniques refer to the way in which multiple users can share the infrared medium simultaneously. The techniques of interest here are those that are based on physical layer concepts, and therefore they are based on some of the infrared medium characteristics including [30]:

- The possibility of reuse of the same infrared bandwidth in each room within a building as infrared radiation cannot penetrate walls or other opaque objects.
- Intensity modulation can use a short duty cycle pulse to improve power efficiency making time division multiple access (TDMA) suitable in comparison to other techniques [30].
- The possibility of achieving high angular resolution in an angle diversity receiver due to the short wavelength of infrared signals [30], which is important for space division multiplexing.
- Unwanted wavelengths can be attenuated through the use of optical filters which pass the relevant wavelength only.

Multiple access techniques can be classified into two categories: optical multiplexing techniques and electrical multiplexing techniques.

2.7.1. Optical Multiplexing Techniques

Optical multiplexing refers to techniques where the infrared medium can be shared by multiple users by making use of its optical features. Optical multiplexing

techniques can be categorised into two groups: wavelength division multiple access (WDMA) and space division multiple access (SDMA) [30].

2.7.1.1. WDMA

In WDMA multiple users simultaneously transmit information sharing the same physical space through the use of narrow-band emitters operating at different wavelengths. A WDMA receiver employs a bandpass optical filter to select the desired wavelength before the detection process. The transmitter needs to be tuneable so that it is able to transmit at different wavelengths. However, tuneable LDs are expensive and require complex techniques to achieve accurate tuning to a given wavelength. Furthermore, large area tuneable bandpass filters such as single- or multiple-stage Fabry-Perot filters are costly and may prove difficult to couple with the desired optical concentrator.

2.7.1.2. SDMA

SDMA relies on the use of an angle diversity receiver, which employs multiple receiving elements aimed in different directions, in order to discriminate signals based on their directions. As an example of SDMA, a hub may be able to simultaneously establish LOS links with several mobile transceivers. This hub can employ an angle diversity receiver to mitigate co-channel interference in the same cell. Furthermore, SDMA can be implemented by using quasi-diffuse transmitters coupled with angle diversity receivers [30].

2.7.2. Electrical Multiplexing Techniques

Electrical multiplexing techniques can offer reliable transmission for multiple users sharing the same optical channel. Electrical multiplexing techniques can be divided into three methods: time division multiple access (TDMA), frequency division multiple access (FDMA) and code division multiple access (CDMA).

2.7.2.1. TDMA

TDMA allows multiple users to share the same optical channel by dividing the time into different time slots. The transmitters emit a signal based on their allocated time slots without overlapping. TDMA can provide high power efficiency due to its low duty cycle, which makes TDMA popular in applications involving portable users where power consumption is critical [30]. However, high coordination is required in order to avoid loss of synchronisation resulting in high complexity.

2.7.2.2. FDMA

In FDMA, the bandwidth is split into frequency bands where each channel occupies a certain band. FDMA has lower power efficiency than TDMA, and its power efficiency gets poorer when the number of users increases [147].

2.7.2.3. CDMA

CDMA relies on the assignment of orthogonal codes as an address for each user, which substantially increases the bandwidth occupied by the transmitted signal. In the CDMA receiver, the information can be recovered through the correlation of the incoming CDMA sequences with the code sequence assigned to the user. There are

two types of optical address codes that have widely been studied, namely, optical orthogonal codes (OOCs) [148-150] and prime codes [151-152]. OOCs belong to the family (0, 1) which have good auto- and cross-correlation properties (i.e. a maximum cross-correlation of 1). Although, prime codes have a maximum cross-correlation of 2, they can help increase the number of users in the network. OOCs have better auto- and cross-correlation properties than prime codes, but they require much more complex algorithms in terms of production [153]. In addition, they may violate the correlation properties if used in a variable bit rate (VBR) application. A new code, namely, extended prime code, which has been proposed by Yang and Kwong [154], can reduce the cross-correlation from 2 to 1, and therefore outperforms OOCs and prime codes in terms of number of user, bit rate and error probability. Alternatively, strict-OOCs, proposed by Zhang [155], can guarantee the minimum value for the correlation constrains in both VBR and constant bit rate (CBR) applications. This improvement can be achieved without expanding the bandwidth and increasing the system complexity.

Compared to the other schemes, CDMA offers several advantages including easy frequency planning, flexibility of user allocation and high immunity to interference if a high processing gain is used. However, these advantages are achieved at the cost of reduced data throughput due to the bandwidth limitation of diffuse optical wireless systems. It has been reported that in a diffuse optical wireless system, PPM-CDMA offers higher power efficiency than OOK-CDMA [156-157], but it has a lower bit rate enhancement factor (BEF) [157]. However, Elmirghani et. al have demonstrated that hybrid PPM-CDMA (hPPM-CDMA) provides higher BEF in comparison with OOK-CDMA [61, 157]. Further improvement can be achieved by employing an alternative hybrid scheme based on PIM-CDMA (hPIM-CDMA) [158]. Both hPPM-

CDMA and hPIM-CDMA schemes can improve data throughput through data compression achieved by utilising a shorter symbol length than OOK-CDMA. Poor power efficiency, however, can be observed.

2.8. Multi-Carrier CDMA (MC-CDMA)

A high data rate in multi-user wireless access is needed to support multimedia applications, which require very high bandwidth with mobility [144-145, 159-160]. CDMA is a potential candidate to support multimedia services because it has the ability to cope with the asynchronous nature of multimedia traffic. Previous work has presented the benefits of wireless infrared CDMA based schemes [161]. In [162], it was shown that PPM-CDMA significantly increases the bit rate at a given number of users. Yamaguchi et al have assessed the performance of indoor wireless Ir CDMA systems using OOC's and a decision-feedback equalizer (DFE) in diffuse channels [163]. Griner and Arnon have examined the use of an adaptive multilevel serial composite decision feedback and feedforward equalizer to mitigate multi-user distortion [164]. Optical wireless CDMA networks have been the subject of extensive research, but the schemes introduced provided multiple access features at the cost of reduced data throughput under limited bandwidth, and supported a limited number of simultaneous users, as a result of using OOC's. A potential solution is to combine the multiple access features of CDMA with the bandwidth efficient features of OFDM resulting in MC-CDMA. OFDM can support high data rates with little or no need for channel equalization as the aggregate throughput is distributed over the set of subcarriers and the symbol rate is reduced. The application of OFDM over an indoor optical wireless channel has been investigated in [165-167]. As mentioned earlier, OFDM is more bandwidth efficient than single carrier modulation schemes

and it experiences little distortion. However, it faces the difficulty of subcarrier synchronisation and sensitivity to frequency offset estimation. CDMA offers multi-user capabilities but expands the bandwidth. Therefore, techniques for reducing the symbol and chip rate are essential. Combining OFDM and CDMA has one major advantage. It can lower the symbol rate in each subcarrier compared to OFDM where a longer symbol duration makes it easier to synchronise and reduces the impact of channel dispersion. However, the major drawback of the multicarrier transmission schemes is an increased PAPR, yielding an increased signal dynamic range and hence the need to maintain linearity in components (for example LEDs) over a larger signal range, compared with the single carrier schemes. MC-CDMA systems offer significant reduction in the PAPR and in the dynamic range [168]. This is because all carriers in MC-CDMA systems convey the same information stream in contrast with OFDM systems, and therefore they can be adequately manipulated to obtain a reduced PAPR. A modification of the MC-CDMA system, called multicarrier spread spectrum (MC-SS) system, has been proposed [169] to achieve a reduced dynamic range for all users in the system.

This work proposes, for the first time, an optical wireless system that combines OFDM signalling with CDMA multi-user capabilities. The application of MC-CDMA in optical wireless is mainly motivated by the need to support high data rate services in a multi-user wireless environment characterised by harsh indoor optical channels. MC-CDMA signals can be efficiently generated and demodulated using FFT devices without substantially increasing the receiver's complexity [170]. MC-CDMA systems combine the robustness of orthogonal modulation with the flexibility of CDMA schemes [160, 170]. MC-CDMA schemes are categorised into two groups; MC-Direct Sequence-CDMA (MC-DS-CDMA) which spread the signal in the time

domain and MC-CDMA which performs the operation in the frequency domain. In both schemes, the different users share the same bandwidth at the same time and separate the data by applying different user specific spreading codes, i.e., the separation of the user's signals is carried out in the code domain. Moreover, both schemes apply multicarrier modulation to reduce the symbol rate and, thus, the amount of ISI per subchannel. This ISI reduction is significant in spread spectrum systems where high chip rates occur. In [160], Hara and Prasad have shown that MC-CDMA outperforms MC-DS-CDMA in terms of downlink BER performance. Therefore, the high spectral efficiency and the low receiver complexity of MC-CDMA make it a good candidate for the downlink of a wireless system. Modelling and performance analysis of the OW MC-CDMA system is carried out in [111, 171-173] (Chapter 5).

2.9. OW Applications

The commercial importance of the infrared technology is best demonstrated by its widespread use in devices that incorporate Infrared Data Association (IrDA) ports. IrDA was established in 1993 as a non-profit organization to develop and promote hardware and software standards that create infrared communication links. IrDA standards support a broad range of appliances, computing, and communications devices. Directed OW beams are commonly used in remote control devices and are also used in serial links for operating computer peripherals. IrDA technology involves over 300 million electronic devices including desktop, notebook, palm PCs, printers, digital cameras, public phones, mobile phones, pagers, personal digital assistants (PDAs), electronic wallets, toys, watches, and other mobile devices [57-58]. Over the last decade, the IrDA has produced standards for the following signal

rates: 2.4 kbit/s, 9.6 kbit/s, 19.2 kbit/s, 38.4 kbit/s, 57.6 kbit/s, 115.2 kbit/s, 0.576 Mbit/s, 1.152 Mbit/s, 4 Mbit/s, and 16 Mbit/s [57-58, 85, 92]. Bit rates up to 115.2 kbit/s employ RZ-OOK modulation with a duty cycle of 0.1875, whereas links that operate at 0.576 Mbit/s and 1.152 Mbit/s employ RZ-OOK with a duty cycle of 0.25. Links operating at 4 Mbit/s employ 4-PPM with pulse duration of 125 ns [57]. A standard called Very Fast Infrared (VFIr) was promoted by the IrDA for data rate of 16 Mbit/s [92]. With this standardisation, infrared can be extended to applications requiring connectivity beyond 4 Mbit/s [85], hence playing a significant role in future high-capacity indoor wireless systems. IrDA is currently investigating ways to standardise even faster standard interfaces that offer data rates above 100 Mbit/s, and has in 2009 issued a standard for 1 Gbit/s OW communication [174]. Some of the IrDA achievements are given in Table 2.2. The main IrDA markets include data networking in the indoor environment, broadband multimedia services to mobile users within such an environment, together with general connectivity to base networks. Several companies have introduced data communication products using optical wireless technology and many other computer communications products are entering the market [135-137].

TABLE 2-2: IrDA ACHIEVEMENTS [174]

Date	Achievements
1993	▪ IrDA Charter meeting of 50 companies ▪ IrDA Serial Infrared (SIr) Physical Layer Link Specification
1994	▪ Infrared Link Access Protocol (IrLAP) and Link Management Protocol (IrLMP)
1995	▪ Extensions to SIr standard (including 4 Mbit/s) ▪ Microsoft support for IrDA connectivity to Windows 95,

	establishing wireless connectivity between PCs using Windows 95 and peripheral devices
1996	▪ Established consumer infrared bi-directional standards initiative
1997	▪ Established standards and agreements between IrDA and the most popular IT companies in the world such as NEC, Ericsson, Nokia, for transferring data over short distances using IrDA infrared data communication ports on wireless communication devices
1998	▪ New standard specification for cordless human input devices such as joysticks, mice, and keyboards.
1999	▪ Released Advanced Infrared Wireless (Air) medium access control (MAC) specification.
2000	▪ Established standards for MP3 players to use it with computers.
2001	▪ IrDA convened a new special interest group to support infrared burst transmission for high speed multimedia content delivery
2002	▪ Established cooperative arrangements with allied associations such as the association for Retail Transaction Standards.
2004	▪ Established technology standards for infrared communication. IrDA communication standards have been broadly deployed in mobile devices including mobile phones, PDAs, printers and digital still cameras.
2005	▪ A high-speed infrared communications protocol is adopted by IrDA as a global standard. IrSimple transfer rates of 16 Mbit/s were reported
2007	▪ IrSimple application notes including Embedded Meta-data format for Affixing on Picture (EMAP) and IrSimple broadcasting were available to members and public
2009	▪ Giga-Ir specification that enables a data rate of 1 Gbit/s was approved and available to members

2.10. Summary

This chapter has provided a literature review of the main issues associated with the physical layer of an OW communication system. Special attention was given to the impairments associated with OW systems (ambient light noise, multipath dispersion, high photodetector capacitance and eye safety) and the methods that have been proposed to reduce their effects. This chapter has also addressed the various communication scenarios, the most common modulation schemes and multiple-access techniques in OW communication systems. The chapter concluded with an overview of the current commercial infrared wireless systems and associated standards.

3. OPTICAL WIRELESS CHANNEL MODELLING

3.1. Introduction

OW links have to provide high-quality access, high data rates, and reliable performance, and therefore the characterisation of the OW channel is essential to address the system performance limits and design issues. This chapter investigates models for the indoor optical wireless channel, through the use of simulation tools based on geometrical modelling of indoor environments, together with an iterative technique for calculating multiple reflections. Simulations and calculations reported in this thesis were carried out using MATLAB. Indoor optical wireless links are subjected to two major impairments, background noise and multipath propagation, which can introduce significant distortion in the received optical power and can significantly degrade the system performance. Based on the directionality of the transmitter and receiver, OW communication links can be categorised as either directed LOS or diffuse. In directed LOS links, the transmitted signal reaches the receiver directly, while in diffuse systems, the transmitted signal reaches the receiver through multiple diffuse reflections (ceiling and walls). Directed LOS links provide high power efficiency and minimise multipath dispersion, but suffer from shadowing due to possible obstruction of the direct path by moving objects. Diffuse systems offer links that are robust in the presence of shadowing. These links do not require transmitter-receiver alignment or line-of-sight and, instead, make use of reflections from walls, ceiling, and other reflectors. However, diffuse transmission links are affected by multipath dispersion, (which causes pulse spread and significant ISI), in addition to a poor power efficiency. Multibeam transmitters can replace the diffuse transmitter leading to significant SNR improvement, reduced multipath dispersion,

and shadowing mitigation. A multibeam transmitter is used to create multiple beams pointed in different directions, hence, forming a lattice of diffusing spots. Several methods have been used to create multiple diffusing spots. A computer generated hologram can be used as a beam splitting element as in [39, 51], or a number of transmitters can be used to produce a certain number of beams as in [26]. Significant performance improvements can be achieved by using an LSMS [95, 97, 100]. However, performance degradation can be induced when mobility is introduced [175]. A beam clustering method (BCM) was shown to improve the performance of OW communication links [102-103]. In addition, multipath dispersion and ambient light noise can be reduced by using receiver diversity [33, 38, 44-47]. Within this study, the performance of spot-diffusing OW systems (LSMS and BCM), in conjunction with an angle diversity receiver is evaluated in the presence of ambient light noise, multipath propagation, and mobility, and simulation results are presented. These two attractive configurations (LSMS and BCM) will be considered as two baselines to facilitate comparison with new systems presented later in the thesis. The impact of shadowing and signal blockage is not taken into account in this chapter, and will be discussed in Chapter 5. A comparison of a CDS with a single wide FOV receiver is also considered.

3.2. Channel Characteristics

In OW communication links, intensity modulation with direct detection is the preferred choice [30]. Multipath propagation in an indoor OW channel using IM/DD can be fully characterised by the impulse response $h(t)$ of the channel [100]

$$I(t, Az, El) = \sum_{m=1}^{M_{element}} R\, x(t) \otimes h_m(t, Az, El) + \sum_{m=1}^{M_{element}} n_m(t, Az, El) \qquad (3.1)$$

where $I(t, Az, El)$ is the received instantaneous current at the output of the photodetector at a certain position due to $M_{element}$ reflecting elements, t is the absolute time, Az and El are the directions of arrival in azimuth and elevation (angle), $M_{element}$ is the total number of reflecting elements, $x(t)$ is the transmitted instantaneous optical power, $\otimes$ denotes convolution, $R = 0.5\,A/W$ is the photodetector responsivity. $n_m(t, Az, El)$ represents the received background noise due to the m^{th} reflecting element at a receiver whose position is given by Az and El . Each reflecting element (depending on its location in the room and location of noise sources) contributes differently to the noise at the receiver. The background noise is modelled as white and Gaussian, and independent of the received signal.

The OW channel differs from the conventional Gaussian-noise channel, since $x(t)$ represents power rather than amplitude. This leads to two constraints on the transmitted signal. Firstly, $x(t)$ must be non-negative, i.e. $x(t) \geq 0 \ \ \forall t$. Secondly, the average value of $x(t)$ must not exceed a specified value dictated by the eye safety standards for laser systems.

3.3. Simulation Model

In order to investigate the effects of diffuse transmission on indoor OW systems, a propagation simulator was developed in an empty room with floor dimensions of 8 m × 4 m (length × width), and ceiling height of 3 m. Previous work has shown that plaster walls reflect a light ray in a form close to a Lambertian function [3]. Therefore the walls (including ceiling) and floor were modelled as Lambertian reflectors with reflectivity coefficients of 0.8 and 0.3 respectively. Reflections from doors and windows are considered to be identical to reflections from walls. The

transmitted signal propagates to the receiver through multiple reflections from the room reflecting surfaces (walls and ceiling) which were divided into a number of equal-size, square-shaped reflection elements with area dA and reflection coefficient ρ. Signals are assumed fully blocked underneath the CF, 1 m above the floor, i.e. no ground reflections are considered. The reflection elements acted as secondary emitters that diffuse the received signals from their centres in the form of a Lambertian pattern. The reflections are termed first order reflections when surface elements, illuminated by a transmitter, reflect the optical signal partly towards the receiver. Such a surface element not only reflects the signal towards the receiver, but also towards other surface elements (on the walls and ceiling) that then, in turn, reflect the signal towards the receiver (second-order reflections). Reflections can continue beyond this second order, however it is noted that third-order reflections and higher do not produce a significant change in the received optical power [3, 10, 17, 27]. Therefore reflections up to second-order are considered. The size of the surface element determines the spatial resolution of the computation. The accuracy of the received impulse response shape, and the received optical signal power, are controlled by the size of the surface element dA. Throughout this thesis surface elements of 5 cm × 5 cm for first-order reflections, and 20 cm × 20 cm for second-order reflections were used for all the configurations considered. These dA values have been selected in order to keep the computation within reasonable time and measure (the computation time increases drastically when the surface element size is decreased). Propagation models including line-of-sight, first-order reflections, and second-order reflections are described in the next section.

In order to simulate the proposed systems (CDS with a single wide FOV receiver, LSMS and BCM systems both with an angle diversity receiver) under mobility, the

transmitter was placed at three different locations on the CF: (2m, 4m, 1m)[1], (1m, 1m, 1m) and (2m, 7m, 1m), pointed upwards, and emitted 1 W total optical power in an ideal Lambertian radiation pattern. Computer generated holographic beam-splitters are assumed to be mounted on the emitter, resulting in multiple narrow beams, which illuminate multiple small areas forming a lattice of diffusing spots on the ceiling (LSMS configuration), and on the ceiling and two end walls (BCM configuration). Computer generated holograms can be used to produce static beam intensities [39, 51]. To facilitate the characterisation of the received signal, the receiver was placed at different locations on the CF with a photosensitive area of 1 cm^2.

The room illumination was provided by eight spotlight lamps, which represent ambient background interference for our purpose, equidistantly placed on the ceiling and point straight downward. Spotlight lamps were deliberately assumed as they are very directive noise sources that cause signal burn-out effects underneath (such a noise source). Modelling of ambient light noise is given in Section 3.5. Furthermore, in order to combat background noise as well as multipath dispersion, a diversity receiver is an appropriate choice, where significant performance improvements can be achieved by receiving the signal from different spatial orientations and by using appropriate combining techniques. An angle diversity receiver is considered in Section 3.6.

[1] Parameters between brackets represent (width, length, height) which corresponding to (*x*, *y*, *z*) Cartesian coordinates. This format is used throughout this thesis.

3.4. Propagation Model

An optical signal emitted by a transmitter reaches a receiver through various paths of different length. These propagation paths change with the transmitter-receiver movement, and/or the movement of the surrounding objects. However, the paths are fixed for a given fixed configuration. Multipath propagation in an indoor OW channel using IM/DD can be fully characterised by the impulse response $h(t)$ of the channel. The channel impulse response $h(t)$ can be represented approximately as a scaled and delayed Dirac delta function [30]. In order to compute the impulse response at the entire CF, a simulation package based on a ray-tracing algorithm was developed for arbitrary transmitter-receiver configurations in an arbitrary room size that comprises diffuse reflectors. An OW signal theoretically undergoes an infinite number of reflections, the channel impulse response can be given as

$$h(t) = \sum_{k=o}^{\infty} h^{(k)}(t), \tag{3.1}$$

where $h^{(k)}(t)$ is the impulse response due to the k^{th} reflection. Third- and higher-order reflections are ignored due to their small contribution [10]. It is also noted that the largest contribution to the received optical power is associated with the first- and second-order reflections [10]. Within this work as previously mentioned, up to second-order reflections are considered, and therefore k takes values of 0, 1, and 2. The models for the transmitter, receiver, and reflectors are defined next.

3.4.1. Transmitter and Receiver Models

A wide-beam optical transmitter can be represented by a position vector $\mathbf{r}_T$, a unit-length orientation vector (transmitter normal vector that is perpendicular to the plane

where the transmitter is placed on) $\hat{\mathbf{n}}_T$, a power P_T, and a radiation intensity pattern $R(\vartheta)$. The radiation intensity pattern $R(\vartheta)$ can be defined as the optical power per unit solid angle emitted from the transmitter at angle ϑ with respect to $\hat{\mathbf{n}}_T$. Following Gfeller [3], a diffuse transmitter with a generalized Lambertain radiation pattern can be modelled as

$$R(\vartheta) = \frac{n+1}{2\pi} P_T \cos^n(\vartheta), \qquad -\frac{\pi}{2} \le \vartheta \le \frac{\pi}{2}, \tag{3.1}$$

where n is the mode number of the radiation beam that describes the beam shape, where the higher the n the narrower the light beam. The mode n is related to the half-power semi-angle and can be represented as

$$n = \frac{-ln(2)}{ln(cos(hps))}. \tag{3.2}$$

An ideal Lambertian transmitter source has a half-power semi-angle equal to 60°, corresponding to $n = 1$. The coefficient $((n+1)/2\pi)$ ensures that integrating $R(\vartheta)$ over the surface of a hemisphere results in the total average transmitted optical power P_T.

Similarly, a single element receiver can be represented by a position vector $\mathbf{r}_R$, orientation vector $\hat{\mathbf{n}}_R$, collection area A_R, and FOV. The angle FOV is defined such that only a light ray whose angle of incidence with respect to the receiver normal $\hat{\mathbf{n}}_R$ is less than FOV can be received. Therefore, the receiver can have control over the range of incident rays detected through the control of FOV. The latter may be limited and used to reduce unwanted reflections or noise. Furthermore, a detector receives an optical power P that is proportional to its effective light-collection area $A_{eff}(\delta)$, which can be expressed as [30]

$$A_{eff}(\delta) = A_R \cos(\delta) rect(\delta / FOV), \tag{3.3}$$

where δ is the angle of reception with respect to the receiver normal $\hat{\mathbf{n}}_R$. The step function is given by

$$rect(\delta/FOV) = \begin{cases} 1 & for \quad (\delta/FOV) \le 1 \\ 0 & for \quad (\delta/FOV) > 1 \end{cases}. \tag{3.4}$$

Increasing the detector area can help increase the effective signal-collection area, but it is expensive and leads to a limit in the receiver bandwidth and an increase in the receiver noise. However, the effective area can be increased by employing an optical concentrator coupled with an optical filter (to eliminate background noise) in front of the detector, and can be given as

$$A_{eff}(\delta) = T_F(\delta) T_C(\delta) A_R \cos(\delta) rect(\delta/\psi_C), \tag{3.5}$$

where $T_F(\delta)$ is the filter transmission factor, $T_C(\delta)$ is the concentrator transmission factor, and ψ_C is the concentrator FOV (semi-angle).

3.4.2. Reflector Model

Experimental measurements have shown that most building materials including plaster walls (with the exception of glass) are approximately Lambertain reflectors [3]. In this study, it is assumed that all reflection surfaces in the set-up room are approximated as Lambertain reflectors. Therefore, the reflecting surface elements are modelled as ideal diffuse reflectors with $n_{element} = 1$, i.e., the radiation intensity pattern $R(\vartheta)$ emitted by a differential reflecting element is independent of the angle of incidence. Due to this fact, a reflection can be decomposed into two sequential steps: firstly, the element is considered as a receiver with area dA that receives a power dP, which can be given as

$$dP = R(\vartheta)\frac{dA}{R^2}\cos(\phi), \tag{3.6}$$

where R is the distance between the transmitter and the surface element dA and ϕ is the angle of the incident ray with respect to the surface element normal. Secondly, the surface element is treated as a diffuse transmitter with total power $P_{dA} = \rho\, dP$ and an ideal Lambertain radiation intensity pattern, as given by (3.1) with $n_{element} = 1$.

3.4.3. Line-of-Sight and First-Order Reflection Analysis

The ray-tracing set-up for first- and second-order reflections, in the case of a fully diffuse configuration (where both transmitter and receiver are placed on the CF pointing straight upward), is shown in Fig. 3.1.

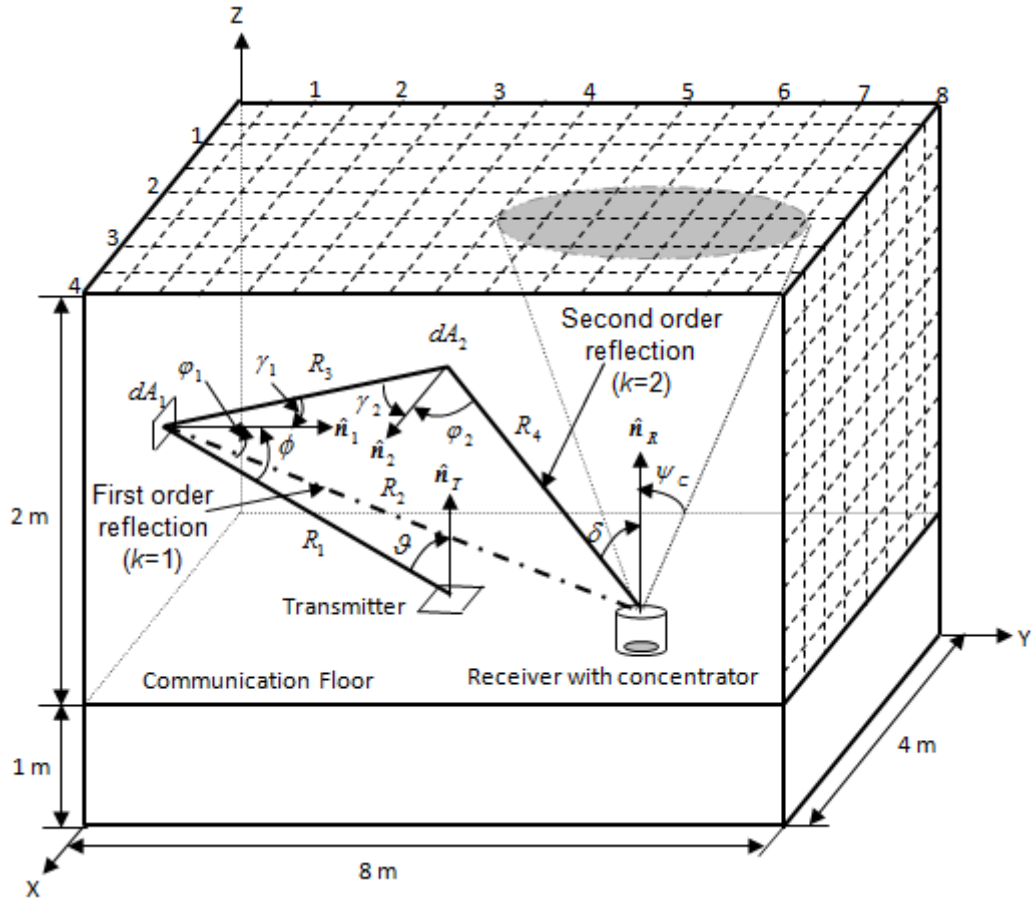

Figure 3-1: OW channel

The channel impulse response can be produced by tracing all possible rays captured by the receiver through reflections. For each particular light ray, the associated optical power and the time spent on the journey (from the transmitter to the receiver), have to be evaluated to determine $h(t)$. The corresponding time can be calculated by dividing the path length (the corresponding distance) by the velocity of light in free space. Following the two sequential steps mentioned above, the power received by a surface element with an area dA_1 and a reflection coefficient ρ_1 in the first-order reflection can be calculated by observing Fig. 3.1,

$$P_{reflection}^{(1)} = \frac{n_{element}+1}{2\pi R_2^2} P_{dA_1} \cos^{n_{element}}(\varphi_1) A_{eff}(\delta), \tag{3.7}$$

where φ_1 is the angle of the reflected ray towards the receiver with respect to the normal of dA_1 and R_2 is the distance between the surface element dA_1 and the receiver. P_{dA_1} is the optical power radiated by the surface element dA_1 in Lambertain pattern with $n=1$, and can be calculated as

$$P_{dA_1} = \rho_1 dP_{dA_1} = \frac{n+1}{2\pi R_1^2} P_T dA_1 \rho_1 \cos^n(\vartheta)\cos(\phi), \tag{3.8}$$

where R_1 is the distance between the transmitter and the surface element dA_1. Upon substituting equations (3.5), and (3.8) into equation (3.7), $P_{reflection}^{(1)}$ can be rewritten as

$$P_{reflection}^{(1)} = \frac{(n+1)(n_{element}+1)}{4\pi^2 R_1^2 R_2^2} T_F(\delta) T_C(\delta) P_T dA_1 \rho_1 A_R \cos^n(\vartheta) \cos(\phi)\cos^{n_{element}}(\varphi_1)\cos(\delta) rect(\delta/\psi_C), \tag{3.9}$$

The LOS component can be calculated similarly as

$$P_{LOS}^{(0)} = \frac{n+1}{2\pi R_d^2} T_F(\delta) T_C(\delta) P_T A_R \cos^n(\vartheta_d)\cos(\delta) rect(\delta/\psi_C), \tag{3.10}$$

where R_d is the direct distance between the transmitter (source) and the receiver and ϑ_d is the angle of incidence of the direct ray with respect to the transmitter normal.

3.4.4. Second-Order Reflection Analysis

Following the reflections analysis given in the previous section, the optical power, which is reflected by the surface element dA_1 and is received at a surface element with an area dA_2 and a reflection coefficient ρ_2, can be calculated, by observing Fig. 3.1, as

$$dP_{dA_2} = \frac{n_{element}+1}{2\pi R_3^2} P_{dA_1} dA_2 \cos^{n_{element}}(\gamma_1)\cos(\gamma_2). \tag{3.11}$$

Here, γ_1 and γ_2 are the angles of the reflected ray (from the surface element dA_1 to dA_2) with respect to the normal of dA_1 and dA_2 respectively, and R_3 is the distance between the two surface elements dA_1 and dA_2. The reflecting surface element dA_2 acts as a secondary Lambertain diffuse transmitter with $n_{element}=1$ and with a total power $P_{dA_2} = \rho_2\, dP_{dA_2}$. Therefore, the total power received by a second-order reflection is given as

$$P_{reflection}^{(2)} = \frac{n_{element}+1}{2\pi\, R_4^2} \rho_2 dP_{dA_2} \cos^{n_{element}}(\varphi_2) A_{eff}(\delta), \tag{3.12}$$

where φ_2 is angle of the reflected ray towards the receiver with respect to the normal of dA_2 and R_4 is the distance between the surface element dA_2 and the receiver. Upon substituting equations (3.5), (3.8), and (3.11) into equation (3.12), $P_{reflection}^{(2)}$ can be rewritten as

$$P_{reflection}^{(2)} = \frac{(n+1)(n_{element}+1)^2}{8\pi^3 R_1^2 R_3^2 R_4^2} T_F(\delta) T_C(\delta) P_T A_R dA_1 dA_2 \rho_1 \rho_2 \cos^n(\vartheta) \cos^{n_{element}}(\gamma_1)\cos(\gamma_2)\cos^{n_{element}}(\varphi_2)\cos(\delta) rect(\delta/\psi_C). \tag{3.13}$$

Taking LOS, first- and second-order reflections into account, the total power received at the receiver can be calculated, from the summation over all reflecting surface elements, as

$$P_R = P_{LOS}^{(0)} + \sum_{m=1}^{M_{element}} \left(P_{reflection}^{(1)} \right)_m + \sum_{m=1}^{M_{element}} \left(P_{reflection}^{(2)} \right)_m , \quad (3.14)$$

where $M_{element}$ is the total number of reflecting elements. The parameters R_1, R_2, R_3, R_4, R_d, ϑ, ϕ, γ_1, φ_1, γ_2, φ_2, ϑ_d and δ are calculated in Appendix A. The impulse response in a practical OW system is continuous, however the simulator subdivides the reflecting surfaces into discrete elements. The effect of discretisation can be reduced by subdividing time into bins of widths Δt and grouping the powers received within each bin into a single received power. This accounts for the smoothness seen in the resulting impulse responses presented in this thesis. A good choice for the bin width is $\Delta t = \sqrt{dA}/c$, which is roughly the time light takes to travel between neighbouring elements. Identical histogram to the actual $h^{(k)}(t)$ is achieved as dA approaches zero. It should be noted that reducing dA leads to improved resolution in impulse response evaluation together with an increase in the computation time. Therefore, the surface element size dA has to be chosen in order to keep the computation time within reasonable limits [3, 10, 26-27].

3.5. Ambient Light Modelling

The dominant source of noise in indoor optical wireless systems is artificial ambient light such as, incandescent lamps and fluorescent lamps. Ambient light, which hits the receiver and falls within its optical passband, is converted into an electrical current that corrupts the signal as background noise. Certain measures, such as optical filters, can be used to reduce the influence of ambient light noise. The background noise level produced from daylight filtered fluorescent light is an order of magnitude smaller than the corresponding BN of incandescent and halogen lights.

This is due to the fact that fluorescent lamps, driven either by an electronic ballast (FLEB) or a coil (FLCB), produce most of their optical power outside the passband of a daylight filter [20]. The room illumination was provided by eight halogen spotlights ('Philips PAR 38 Economic' (PAR38)), which cause high optical spectral corruption levels to the received data stream. PAR38 emits a power P_l of 65 W in a narrow beamwidth which is modelled as a generalized Lambertain radiant intensity with order $n_{Lamp} = 33.1$ (based on experimental measurements [73]), which corresponds to a semi-angle of 11.7^o. The eight spotlights were placed 2 m above the CF at (1, 1, 3), (1, 3, 3), (1, 5, 3), (1, 7, 3), (3, 1, 3), (3, 3, 3), (3, 5, 3), and (3, 7, 3), see Fig. 3.2.

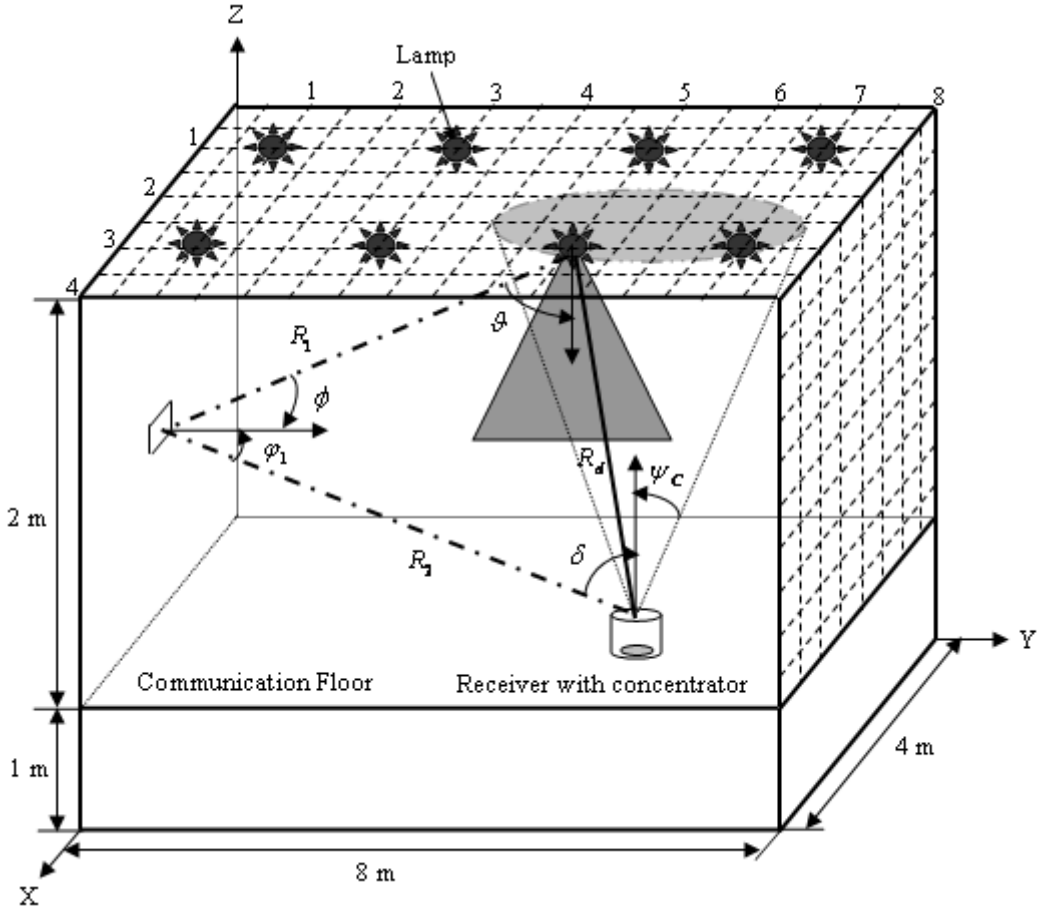

Figure 3-2: Modelling of the ambient light

These lamps produced a well-illuminated environment. Interference from daylight through windows and doors was not considered in this work. It has been shown that ambient light (such as a halogen lamp illumination) can be modelled as a Lambertian source [73]. Therefore, the total background noise power, which is produced by a specific source, l, and is received at a detector, can be given as

$$P_{n,l} = \left(P_{n_d} + P_{n_{reflection}}\right)_l, \tag{3.15}$$

where P_{n_d} is the direct path component of the BN and $P_{n_{reflection}}$ is the total noise power received through the reflecting elements. Following the reflection analysis previously given, P_{n_d} and $P_{n_{reflection}}$ can be calculated, by observing Fig. 3.2, as

$$P_{n_d} = \frac{n_{Lamp}+1}{2\pi R_d^2} T_F(\delta) T_C(\delta) P_l A_R \cos^{n_{Lamp}}(\vartheta) \cos(\delta) rect(\delta/\psi_C), \tag{3.16}$$

$$P_{n_{reflection}} = \frac{(n_{Lamp}+1)(n_{element}+1)}{4\pi^2 R_1^2 R_2^2} T_F(\delta) T_C(\delta) P_l dA_1 \rho_1 A_R \cos^{n_{Lamp}}(\vartheta) \cos(\phi) \cos^{n_{element}}(\varphi_1) \cos(\delta) rect(\delta/\psi_C). \tag{3.17}$$

The total background noise P_{bn}, collected at a receiver at a certain location, can be calculated through the summation of the noise power received at the detector from all light sources, and is given as

$$P_{bn} = \sum_{l=1}^{L_{Lamp}} \left(P_{n_d}\right)_l + \sum_{l=1}^{L_{Lamp}} \sum_{m=1}^{M_{element}} \left(P_{n_{reflection},m}\right)_l, \tag{3.18}$$

where L_{Lamp} is the total number of the lamps (eight spotlight lamps in our case).

3.6. Angle Diversity Receiver

In contrast to the single wide FOV receiver, an angle diversity receiver is a collection of narrow-FOV detectors oriented in different directions. These detectors can spatially eliminate undesired signals hence significantly reducing the effect of

ambient light noise and multipath dispersion. Employing diversity techniques in OW environments was studied by several researchers [33, 38, 40, 42, 44-47, 51, 95-96, 100, 103, 125]. It has been shown that employing such a configuration (diversity reception) gives an additional degree of freedom that can be used to eliminate some of the background interference. Furthermore, narrower FOVs can be used to limit the range of incident rays accepted and hence reduce the signal spread, at the possible expense of power loss. Due to the nature of the noise sources and their directivity together with the transmitter diversity used, the desired optical signal reaches the receiver from all directions unlike the undesired interference signals. Therefore, reducing the diversity receiver FOV can reduce the noise at a rate more significant than the rate at which the signal is reduced. However, beyond a certain FOV, the reduction in noise power is not significant while the signal power is continuously reduced and hence an optimum FOV has to be identified.

In order to achieve a high SNR, the photocurrents received in the various elements are amplified separately, and the resulting electrical signals are processed in an approach that maximises the power efficiency of the system. Several possible diversity schemes such as, select-best (SB), equal gain combining (EGC), and maximum ratio combining (MRC) can be considered. It has shown that EGC produces SNR results poorer than those associated with SB and MRC [96]. Therefore, within this work, two approaches: SB and MRC are considered to process the received diversity signals. In SB the receiver simply selects the detector with the best SNR. In contrast to the SB approach, where the multiple signals resulting from the individual detectors are not fully used, in MRC the output signals of all the detectors are combined through an adder circuit, where each input to the circuit is summed with a weight directly proportional to its SNR. In this chapter, we consider

SB which represents a simple form of diversity. MRC is employed in Chapter 6, Chapter 7, and Chapter 9.

The receiver diversity system considered consists of seven photodetector branches as shown in Fig. 3.3. Each face bears a certain direction that can be defined by two angles: azimuth Az and elevation El. While the El of six photodetectors remains at 20^o, the seventh one faces up with El of 90^o, and the Az for the seven branches of the receiver are fixed at 0^o, 55^o, 90^o, 125^o, 235^o, 270^o, and 305^o. The corresponding FOVs were restricted to 12^o, 30^o, 25^o, 30^o, 30^o, 25^o, and 30^o respectively. The Az, El, and FOVs were chosen through an optimisation similar to that in [44, 46] to achieve the best SNR, considering the transmitter locations as well as the system motion.

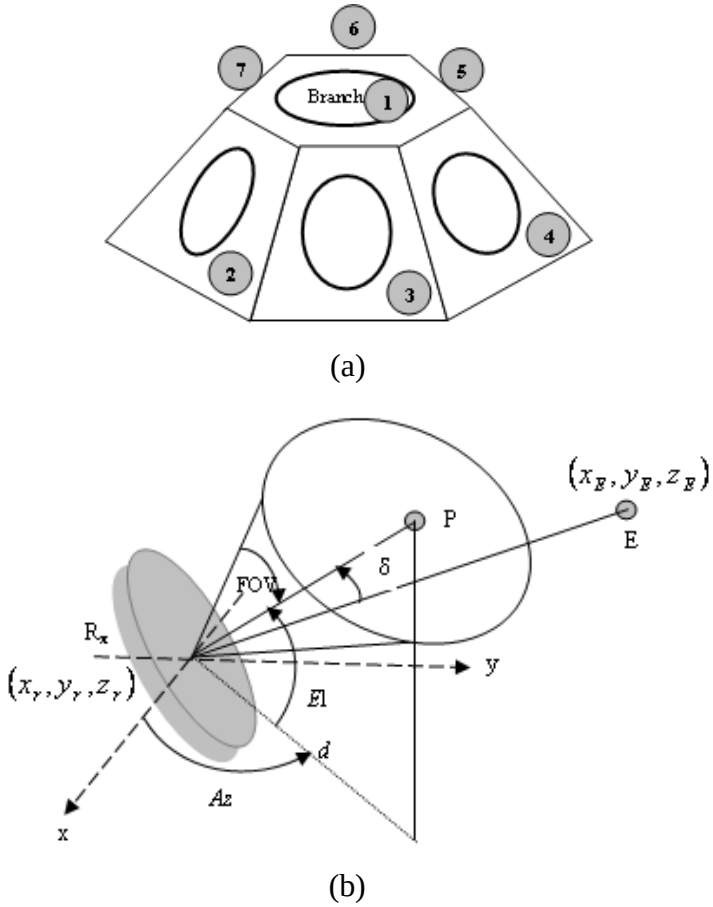

Figure 3-3: Angle diversity detection technique: (a) Physical structure of angle diversity receiver with seven branches and (b) Azimuth and elevation analysis for diversity detection model

Moreover, the angle diversity receiver is designed so that at least five diffusing spots are always positioned within the receiver FOV (for a typical ceiling height of 3 m), providing a robust link against diffusing spot blockage. The photosensitive area of each photodetector was set to 1 cm^2 with a responsivity of $0.5\,\text{A/W}$. The angle diversity receiver was always placed on the CF, a plane 1 m above the floor. The faces of the diversity receiver are inclined, hence, the conventional diffuse system analysis, given in Section 3.4 (which assumes a single upwards-facing detector), has to be modified. Therefore, for each photodetector, the reception angle δ (the angle between the detector's normal and the incident ray) can be calculated by employing the geometrical analysis in [44] with respect to the receiver location, the detector's *El* and *Az* angles, and the reflection element. Observing Fig. 3.3 (b), the reception angle of the incident ray from the surface element E at coordinates of (x_E, y_E, z_E) on a ceiling or wall onto a photodetector of an angle diversity receiver located at (x_r, y_r, z_r) is given by [44]

$$\cos(\delta) = \frac{\left|\overrightarrow{PR_x}\right|^2 + \left|\overrightarrow{ER_x}\right|^2 - \left|\overrightarrow{EP}\right|^2}{2\left|\overrightarrow{PR_x}\right|^2\left|\overrightarrow{ER_x}\right|^2}, \tag{3.19}$$

where the distances $\left|\overrightarrow{PR_x}\right|$, $\left|\overrightarrow{ER_x}\right|$ and $\left|\overrightarrow{EP}\right|$ are shown in Fig. 3.3 (b) and represent distances between the receiver, a general point P, which is located on the detector's normal 1 m above the CF, and the surface element E, and are given by [44]

$$\left|\overrightarrow{PR_x}\right|^2 = 1 + \left(\frac{1}{\tan(El)}\right)^2. \tag{3.20}$$

$$\left|\overrightarrow{ER_x}\right|^2 = (x_r - x_E)^2 + (y_r - y_E)^2 + (z_r - z_E)^2. \tag{3.21}$$

$$\left|\overrightarrow{EP}\right|^2 = \left[\left(\left(\frac{\cos(Az)}{\tan(El)}\right) + x_r\right) - x_E\right]^2 + \left[\left(\left(\frac{\sin(Az)}{\tan(El)}\right) + y_r\right) - y_E\right]^2 + \left[(z_r + 1) - z_E\right]^2. \tag{3.22}$$

The power received by each photodetector is limited by its FOV where each photodetector receive the rays whose angles of incidence lie within its FOV.

3.7. Mobile System Configurations

LSMS and BCM are two attractive configurations [95-97, 100, 102-103, 175], therefore, they are studied and evaluated (in this chapter) under the constraint of BN, multipath dispersion, and mobility, and used for comparison purposes in order to evaluate the novel configurations proposed in this thesis in later chapters. The two multibeam systems (LSMS and BCM in conjunction with an angle diversity receiver) were simulated and compared with the CDS.

3.7.1. Conventional Diffuse System (CDS)

This is the basic configuration and it has been widely investigated [3, 10, 17, 26-27, 53, 121]. The conventional diffuse system employs a single beam transmitter, typically, with a Lambertian radiation pattern and a single wide FOV receiver. In CDS as shown in Fig. 3.4, both the transmitter and the receiver are pointed upwards and their normals are perpendicular to the CF. Therefore, there is no LOS component between the transmitter and receiver, and the total optical power is collected at the detector through reflections from walls and ceiling. For comparison purposes, a diffuse transmitter has been simulated with a single wide FOV receiver to generate channel impulse responses.

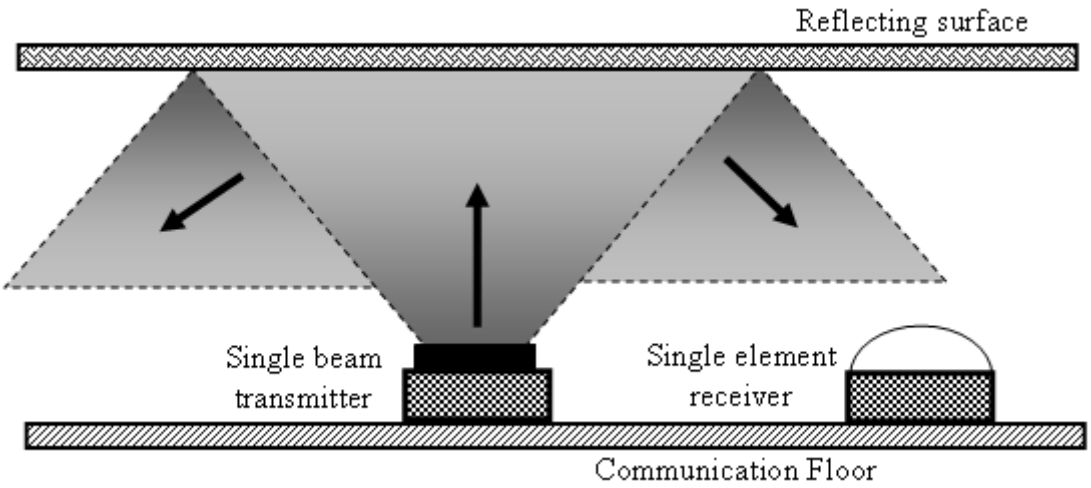

Figure 3-4: A conventional diffuse link with a single transmitter and a single receiver

3.7.2. Line Strip Multibeam System (LSMS)

A simple structure of diffusing spots in a line strip multibeam system (LSMS) was examined in [95-97, 100, 175] and shown to produce SNR improvement compared to CDS and compared to the uniform multibeam transmitter. The LSMS multibeam transmitter is assumed to produce 80×1 beams aimed at the ceiling and pointed straight down with equal intensities. The total optical power (1 W total transmit power) emitted by the transmitter remains unchanged (for comparison purposes) as in CDS, therefore each spot is allocated 12.5 mW. The LSMS multibeam transmitter forms a line of diffusing spots in the middle of the ceiling at x = 2 m and along the y-axis when the transmitter is at the centre of the room, as shown in Fig. 3.5 (a). The difference in distance between adjacent spots is 10 cm. These spots act as secondary distributed emitters which emit Lambertian radiation [39, 42, 51-52, 54, 95-97, 100, 123, 175]. The positions of the spots are affected by the transmitter movement. Fig. 3.5 (b) shows the mobile LSMS configurations at two different transmitter positions on the CF (1m, 1m, 1m), and (2m, 7m, 1m).

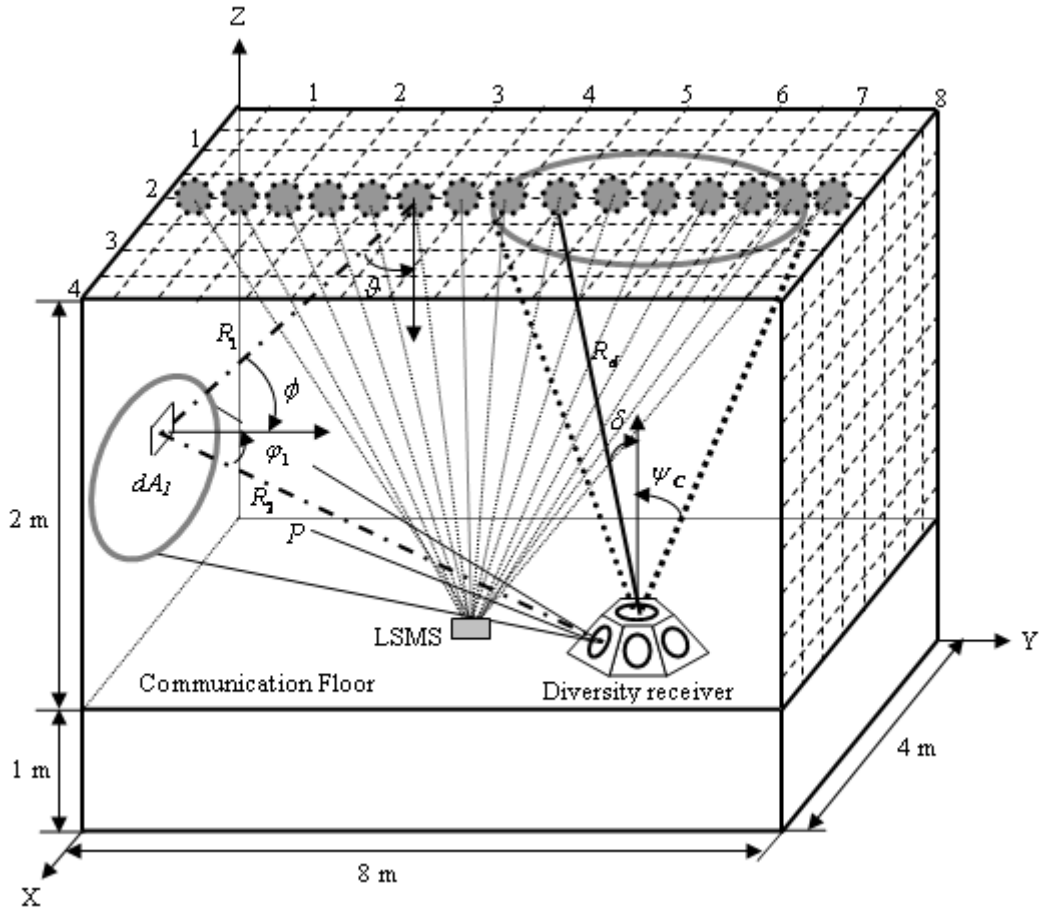

(a)

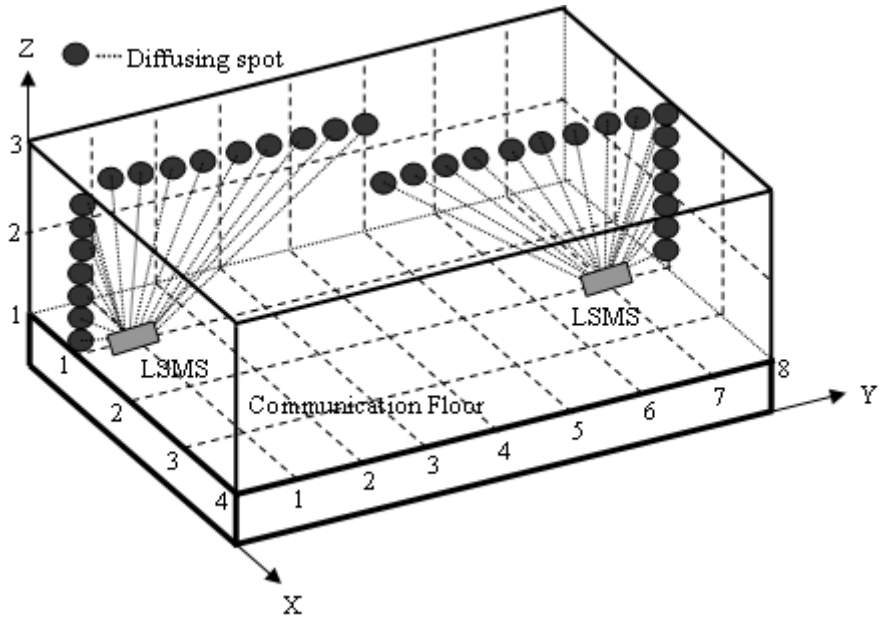

(b)

Figure 3-5: Line strip configuration: (a) propagation model for LSMS with an angle diversity receiver and (b) mobile LSMS configuration at two transmitter positions (1m, 1m, 1m) and (2m, 7m, 1m)

To be able to consider transmitter mobility, a transmitter at the room centre $(x_T, y_T, z_T) = (2m, 4m, 1m))$ is used to compute the transmission beam angle associated with each diffusing spot at coordinates (x_i, y_i, z_i). The transmission beam angles α_i (with respect to the transmitter normal as shown in Fig. 3.6) can be calculated as

$$\alpha_i = \tan^{-1}\left(\frac{(y_T - y_i)}{(z_i - z_{CF})}\right), \qquad 1 \le i \le N_s, \tag{3.23}$$

where $z_{CF} = 1\,\text{m}$ is the height of the communication floor and N_s is the total number of spots. These transmission beam angles have been considered as reference points for the LSMS (since in the LSMS scenario, transmission beam angles are unchangeable angles at all transmitter locations). As the transmitter starts moving, the spot positions and heights change accordingly. At certain locations on the CF, some of the spots on the ceiling start to appear on one of the walls, for instance, at locations close to the corner (transmitter in the corner of the room $(x_T, y_T, z_T) = (1\text{m}, 1\text{m}, 1\text{m}))$, some of the ceiling spots appear on the wall as shown in Fig. 3.6.

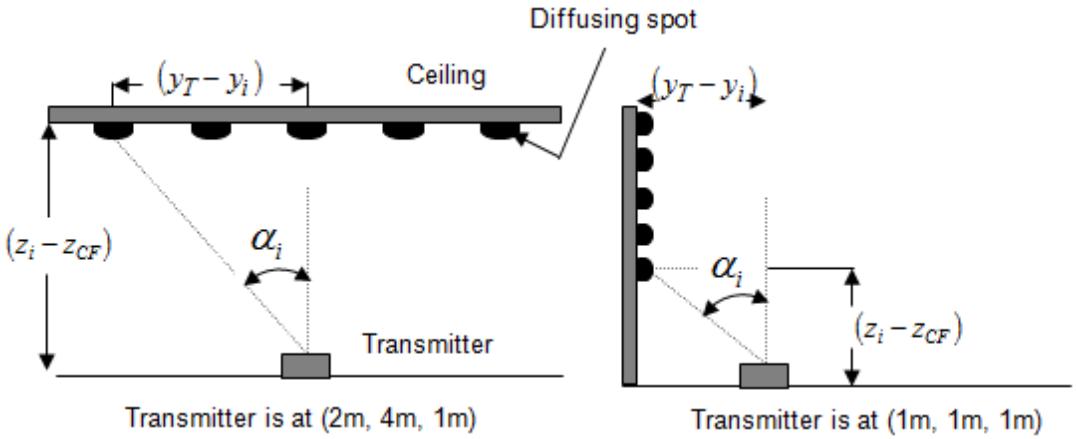

Figure 3-6: Two cases of spots distribution on ceiling and wall for two different transmitter positions

The spots height z_i on the wall can be calculated, by observing Fig. 3.6, as

$$z_i = \frac{(y_T - y_i)}{\tan \alpha_i} + z_{CF} \,. \tag{3.24}$$

Throughout this thesis, computations are carried out to define the new spots' positions (on the ceiling and/or walls) based on the reference points and the transmitter location following the process illustrated in a flowchart form in Fig. 3.7.

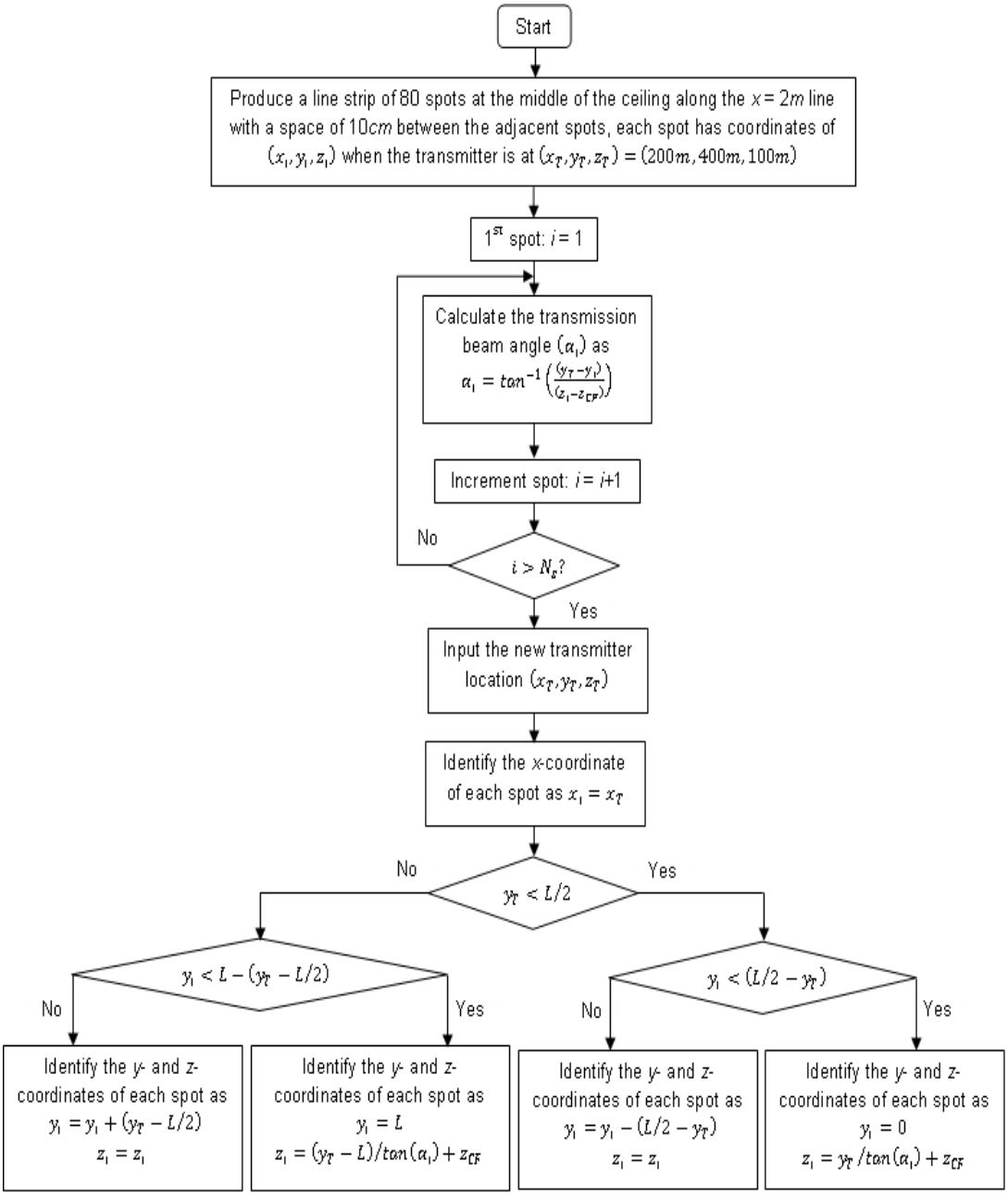

Figure 3-7: Flowchart illustrating the mobility analysis in the LSMS

The multibeam transmitter and the multi-detector angle diversity receiver form a multiple input multiple output (MIMO) system. LSMS performs better than conventional diffuse systems in terms of SNR, however SNR degradation can be induced due to the impact of transmitter motion, i.e. the impact of having some non-illuminated regions in the ceiling and having some of the spots appear on the side walls. To reduce the performance degradation due to transmitter mobility, beam clustering can be employed where, for example, three clusters of beams are aimed at the ceiling and the two end walls when the transmitter is placed at the room centre. As the transmitter moves, beam clustering maintains a better distribution of spots in the room.

3.7.3. Beam Clustering Method (BCM)

The spot distribution pattern based on a beam clustering method was proposed and examined in [102-103]. Our system here employs 100 diffusing spots with total power of 1 W and each spot is allocated 10 mW and operates as a secondary emitter. The multibeam clustering transmitter is assumed to produce 100 × 1 beams that form three groups of spots aimed at the three main surfaces ceiling and two end walls. The BCM transmitter employs three clusters of spots distributed as follows: 80 diffusing spots on the ceiling and 10 spots on each wall when the transmitter is in the centre of the room. The difference in distance between the adjacent spots in the ceiling and walls is 10 cm and 20 cm respectively. The number of spots used in BCM was chosen to achieve high SNR and low delay spread on the CF based on an optimisation similar to that in [102-103]. The proof of the absolute optimality of the number of beams and the angle between the beams warrants further study. The structure has the ability to view and cover its surroundings through the three clusters

of diffusing spots, which gives the receiver an option to collect the signals through the nearest diffusing spots and the shortest paths. In our system the position of the spots on the ceiling and side walls varies as the transmitter moves. To help visualise the mobile BCM configuration, Figs. 3.8 (a) and (b) illustrate a limited number of diffusing spots in an optical wireless communication system at two transmitter positions (2m, 4m, 1m) and (1m, 1m, 1m) respectively.

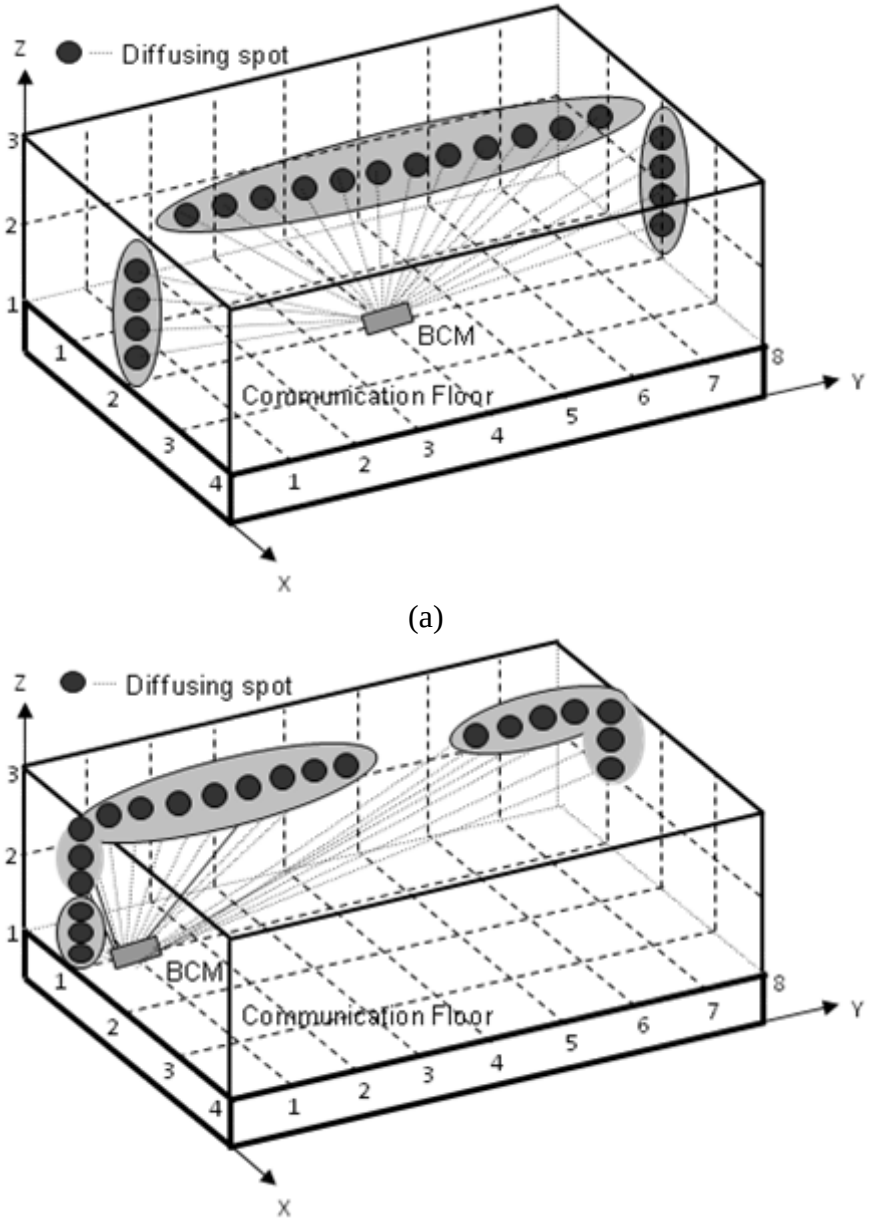

Figure 3-8: Beam clustering mobile configuration when the transmitter is placed at two locations: (a) the centre of the room (2m, 4m, 1m) and (b) the corner of the room (1m, 1m, 1m)

Calculations similar to those in LSMS were carried out to identify the new spot locations based on transmitter position and the beam angles associated with the BCM system.

3.8. Performance Analysis and Simulation Results

In this section, we investigate and evaluate the performance of the spot-diffusing geometries (LSMS and BCM), in conjunction with an angle diversity receiver, in the presence of ambient light noise, multipath dispersion and mobility. To facilitate comparison, a diffuse transmitter combined with a wide FOV receiver is also considered. Under transmitter and receiver mobility a simulation tool, similar to the one developed for a simple diffuse system by Barry et al. [10], was developed and used to calculate the received optical power (using equation (3.14)) and produce the impulse response. An optical filter and/or optical concentrator were not used in this chapter. The use of these components can further improve the systems' performance, but their relative performances remain generally unchanged. In this case, the received optical power including LOS components, first- and second-order reflections were computed using equations (3.10), (3.9) and (3.13) respectively, while omitting both filter and concentrator transmission factors. In the case of the spot-diffusing geometry, we assume that the journey of the beam, from the transmitter (on the CF) to the spot (on the ceiling or walls), is an ideal journey where no power is lost and the pulse width does not increase. This is reasonable since the beams forming the spots are highly confined, (beam blockage by furniture and other objects is considered in Chapter 5). Therefore, the spot-diffusing structure is able to offer LOS components (between the diffusing spots and the receiver), where a number of light spots on the ceiling and/or the walls can concurrently illuminate the receiver directly.

Several parameters are of interest and can be derived from the simulated impulse response such as SNR and root mean square delay spread (D). Because of the diffuse transmission, an indoor OW link is subjected to multipath dispersion, which can cause pulse spread in time, and hence ISI in the received signal. D is a good measure of signal spread due to temporal dispersion, and is discussed in Section 3.8.2.

For each transmitter movement, in all the configurations studied, computations were carried out at 14 different receiver positions (at constants x = 1 m and x = 2 m and along the y-axis) on the CF. Due to the room symmetry, the results produced at constants x = 1 m and x = 3 m are similar.

3.8.1. Impulse Response

The channel impulse response specifies the received optical power that results from multipath propagation. In order to simulate the channel impulse response, based on spot-diffusing geometry coupled with diversity reception, the received multipath profiles due to each spot were computed at each photodetector, based on the detector's FOV and the area (on the ceiling and/or walls) the detector observes at each set of transmitter and receiver locations. The resultant power profile at each photodetector is the sum of the powers due to the total number of diffusing spots considered. The impulse response of the three configurations (CDS with a wide FOV receiver, LSMS and BCM with an angle diversity receiver) is depicted in Fig. 3.9 at transmitter and receiver locations of (2m, 4m, 1m) and (1m, 1m, 1m). Fig. 3.9 compares the received power levels (μW) as a function of time (ns) between the three configurations considered. It is clearly seen that the spot-diffusing structure is significantly better than the CDS.

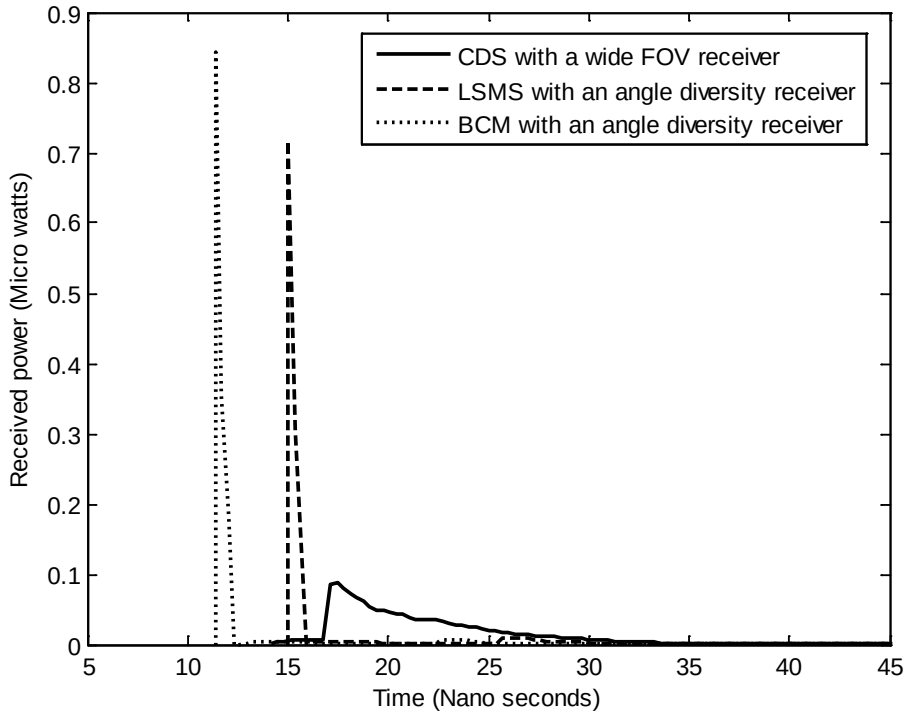

Figure 3-9: Impulse response of three configurations: CDS with a wide FOV receiver, LSMS and BCM with an angle diversity receiver at transmitter and receiver locations of (2m, 4m, 1m) and (1m, 1m, 1m) respectively

This is attributed to the introduction of secondary transmitters (spots) and the presence of LOS components between the diffusing spots and the receiver. The impulse response generated by a spot-diffusing geometry consists of direct path components, where the received power is at its maximum level, and reflection components (first- and second-order components). It can be observed that the direct ray reaches the receiver through the shortest path, (between the diffusing spots and the receiver) which delivers the highest power level, whereas, first- and second-order reflections start arriving at the receiver after a certain time with lower power levels, compared to that attributed to the direct path component. When a diversity receiver is employed, the strong initial part of the impulse response curve is not affected, where the high power due to the direct path component is preserved, while the contribution

of reflections is reduced. This is manifest in the confined impulse response of the spot-diffusing configuration with the diversity receiver compared to that associated with CDS (where no direct path component is established). CDS produces 1.46 μW received optical powers with much more signal delay, a spread of almost 2.65 ns (over a large time period) due to the diffuse transmission and wide receiver FOV (FOV = 90^o). A significant reduction in the signal spread from 2.65 ns to 0.46 ns can be achieved when an angle diversity LSMS replaces the CDS with wide FOV receiver. However, a reduction in the received optical power from 1.46 μW (CDS with wide FOV receiver) to 1.23 μW can be induced. This is due to the limited range of rays captured by narrow FOV diversity receivers. However, it has to be observed that LSMS, with an angle diversity receiver, offers a better overall SNR performance than CDS due to the significant reduction in the collected background noise, see Fig. 3.11. Furthermore, an improvement in the received optical power, from 1.23 μW to 1.51 μW , together with a reduction in the signal spread, from 0.46 ns to 0.37 ns, is achieved in the BCM link over the LSMS when both systems employ an angle diversity receiver. This illustrates the improvement achieved through clustering and distributing the spots on different surfaces, which gives the receiver an option to collect the signals through the nearest diffusing spots and the shortest paths. In addition, the impulse responses for all cases studied are analysed to compare the effect of transmitter mobility on the received optical power and its spread, and the results are presented in terms of delay spread and SNR, see Fig. 3.10 and Fig. 3.11.

3.8.2. Delay Spread

Due to diffuse transmission, indoor OW links are subjected to multipath dispersion, which results in ISI. The root mean square delay spread is a good measure of signal spread due to temporal dispersion. The delay spread of an impulse response is given by [100]

$$D = \sqrt{\frac{\sum_i (t_i - \mu)^2 h^2(t_i)}{\sum_i h^2(t_i)}}, \quad where\ \mu = \frac{\sum_i t_i h^2(t_i)}{\sum_i h^2(t_i)}, \tag{3.25}$$

where t is the time delay associated with the received optical power $h(t)$ and μ is the mean delay. The discretisation is the result of dividing the reflecting surfaces into small elements. Since the positions of the transmitter, receiver, and the reflecting elements are fixed, the received optical power and the delay spread can be considered deterministic for given transmitter and receiver locations.

Figs. 3.10 (a) and (b) compare the delay spread of the three configurations when the receiver moves along the x = 1 m and x = 2 m lines respectively, at three transmitter locations: (1m, 1m, 1m), (2m, 4m, 1m) and (2m, 7m, 1m). The figures give a better perspective on how delay spread varies with transmitter/receiver position within a room. The results show a significant delay spread reduction along the *y*-axis for both spot-diffusing configurations (LSMS and BCM with an angle diversity receiver), compared to the CDS link, when the transmitter is stationary at the room centre. For example when the receiver is located 3 m away from the transmitter (i.e. the transmitter is placed at the centre of the room (2m, 4m, 1m) and the receiver is at one of the edges of the room (2m, 1m, 1m)), the delay spread can be reduced by a factor of 15, when the LSMS with an angle diversity receiver is employed instead of the CDS with a wide FOV receiver.

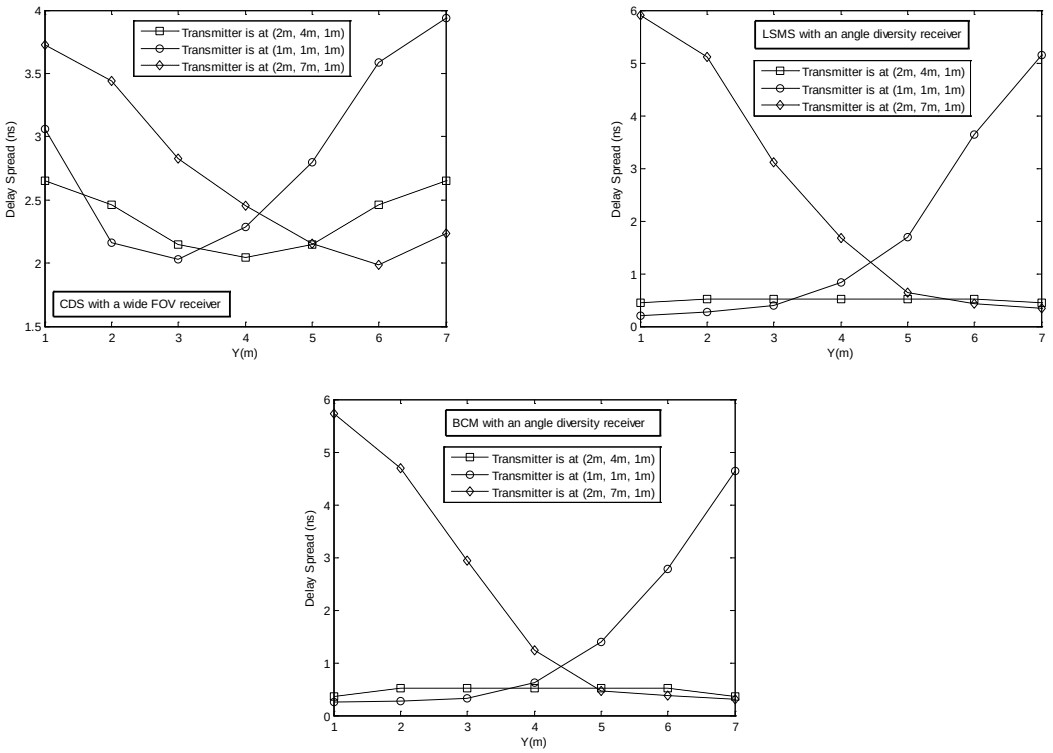

(a)

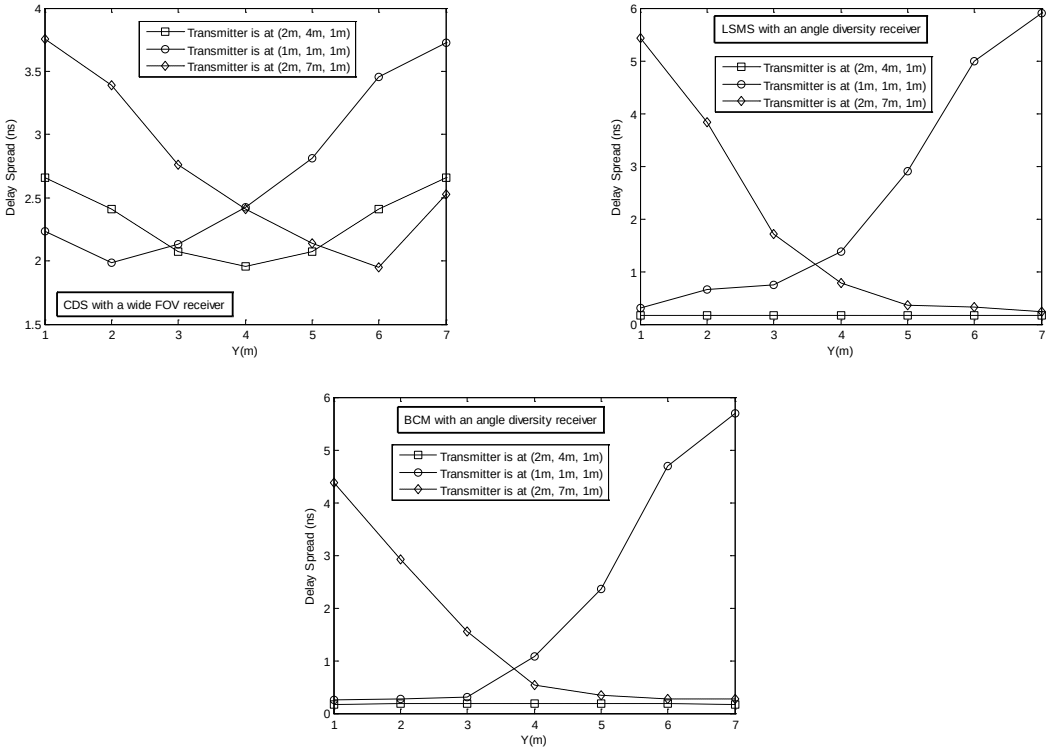

(b)

Figure 3-10: Delay spread for the three proposed configurations at three transmitter positions: (1m, 1m, 1m), (2m, 4m, 1m) and (2m, 7m, 1m), when the receiver moves along the: (a) x = 1 m line and (b) x = 2 m line

This is due to the ability of the spot-diffusing configuration (when the transmitter is placed at the centre of the room) to more uniformly cover its surrounding through the diffusing spots, which gives the receiver an option to collect the signals through the nearest diffusing spots and the shortest paths, and due to the limited range of rays captured, corresponding to the limited FOV associated with the diversity receivers. At that transmitter position, the delay spread of both LSMS and BCM increases towards the room centre, which is completely different from the CDS. This is due to the presence of "spot transmitting points" near the edges of the room and due to the lower contribution of the far spot. Transmitter mobility increases the delay spread of LSMS, as might be expected, at receiver locations away from the transmitter. For example when the transmitter is placed in the corner of the room (1m, 1m, 1m) and the receiver moves at constant x = 2 m and along the y-axis (i.e. from y = 1 m to y = 7 m) the LSMS delay spread has a clear decaying trend ranging from 0.3 ns to about 6 ns. An opposite trend is observed when the transmitter is placed at (2m, 7m, 1m) and the receiver moves along the x = 1 m line. This is a result of having non-illuminated regions in the ceiling when the LSMS transmitter moves towards the side wall. This effect can be reduced if the spots are clustered and distributed on different surfaces so that the mobile BCM transmitter can provide higher diffusing spots illumination than that associated with LSMS, resulting in performance improvement, see Figs. 3.11(a) and (b).

3.8.3. SNR Performance Analysis

Indoor mobile OW communication systems are strongly impaired by the shot noise induced by ambient light noise. The probability of error P_e in an indoor mobile OW communication system can be written as

$$P_e = Q\left(\sqrt{SNR}\right), \tag{3.26}$$

where $Q(x) = \left(1/\sqrt{2\pi}\right)\int_x^\infty e^{-\left(z/\sqrt{2}\right)^2} dz$ is the Gaussian function which assumes a value of 6 at a probability of error $P_e = 10^{-9}$, and an SNR of 15.6 dB. Detailed derivation of the *Q* factor is presented in Appendix B. The assumption of Gaussian noise statistics holds in our case, since thermal and shot noise can be accurately modelled as Gaussian processes. Considering the impact of pulse spread caused by ISI where $P_{s1} - P_{s0}$ accounts for the eye opening at the sampling instant, the SNR is given by [131, 176]

$$SNR = \left(\frac{R \times \left(P_{s1} - P_{s0}\right)}{\sigma_t}\right)^2, \tag{3.27}$$

where $R = 0.5\,\mathrm{A/W}$ is the photodetector responsivity, P_{s0} and P_{s1} are the powers associated with logic 0 and 1 respectively, and $\sigma_t^{\,2}$ is the total noise variance and is made up of three components. Firstly, the noise associated with the pre-amplifier components σ_{pr}, which is a function of the receiver topology adopted. To enable comparison to previous work [175], we used a bit rate of 50 Mbit/s. The pre-amplifier used in this study for the OOK system is the PIN-BJT design proposed by Elmirghani et al. [22]. This pre-amplifier has a noise current density of $2.7\ \mathrm{pA}/\sqrt{\mathrm{Hz}}$ and a bandwidth of $70\ \mathrm{MHz}$. The pulse response was found through convolution of the impulse response with a rectangular transmitted pulse of 20 ns duration. This corresponds to a 50 Mbit/s bit rate, and the receiver used had a bandwidth of 70 MHz [22], which ensures that it does not cause significant additional dispersion at the bit rate chosen. The preamplifier noise is given by

$$\sigma_{pr} = 2.7 \times 10^{-12} \times \sqrt{70 \times 10^6} = 0.023\ \mu A. \tag{3.28}$$

The pre-amplifier bandwidth can be limited through the use of a pre-detection filter. A pre-detection filter can be used to reduce the effect of receiver noise at the price of pulse spread. Within this work, the effect of such filters on the received signal has not been taken into account.

Secondly, background light-induced shot noise σ_{bn}, can be evaluated by computing the corresponding shot noise current. It can be calculated from its respective associated power level P_{bn} using

$$\sigma_{bn} = \sqrt{2 \times q \times P_{bn} \times R \times BW}\ , \tag{3.29}$$

where q, P_{bn} and BW are the electron charge, the received background optical power and receiver bandwidth respectively. Finally, the noise induced by the received signal power, consists of two components; shot noise component σ_{s0}, associated with P_{s0} and shot noise component σ_{s1}, associated with P_{s1}. This signal-dependent noise σ_{si} is very small (in non-optically pre-amplified systems) and can be neglected. The noises σ_0 and σ_1 associated with logic 0 and 1 respectively are given as

$$\sigma_0 = \sqrt{\sigma_{pr}^2 + \sigma_{bn}^2 + \sigma_{s0}^2} \quad \textit{and} \quad \sigma_1 = \sqrt{\sigma_{pr}^2 + \sigma_{bn}^2 + \sigma_{s1}^2}\ . \tag{3.30}$$

Substituting (3.30) into (3.27) with $\sigma_t = \sigma_0 + \sigma_1$ [176], the SNR can be given as

$$SNR = \left(\frac{R \times \left(P_{s1} - P_{s0} \right)}{\sqrt{\sigma_{pr}^2 + \sigma_{bn}^2 + \sigma_{s0}^2} + \sqrt{\sigma_{pr}^2 + \sigma_{bn}^2 + \sigma_{s1}^2}} \right)^2 . \tag{3.31}$$

For simplicity, in the case of angle diversity, we consider one way of processing the resulting electrical signal from the different photodetectors, namely, SB, selection of the photodetector with the best SNR. Therefore, equation (3.31) can be rewritten as

$$SNR_{SB} = \underset{j}{MAX}\left(\frac{R \times \left(P_{s1} - P_{s0}\right)}{\sqrt{\sigma_{pr}^2 + \sigma_{bn}^2 + \sigma_{s0}^2} + \sqrt{\sigma_{pr}^2 + \sigma_{bn}^2 + \sigma_{s1}^2}} \right)_j^2, \quad 1 \le j \le J, \tag{3.32}$$

where J is the number of photodetectors.

Figs. 3.11(a) and (b) illustrate the SNR of the previous three mobile OW systems operating at 50 Mbit/s under the constraints of background noise and multipath dispersion, when the receiver moves along the x = 1 m and x = 2 m lines respectively, at three transmitter positions: (1m, 1m, 1m), (2m, 4m, 1m) and (2m, 7m, 1m). In a CDS system, when the transmitter is at the room centre, the SNR is maximum at the room centre, which is attributed to two effects. Firstly, the distance between the transmitter and the receiver is minimum (at this receiver location) compared to other locations. Secondly, the noise distribution is very low, as a result of the receiver not being underneath a spotlight. The results also show that background noise has a significant effect on the CDS performance (where a single wide FOV receiver is used). The impact is more evident when the receiver is underneath a spotlight as depicted at $y = 1, 3, 5, 7\ m$. This can easily be seen as peaks and troughs in the CDS SNR curves. The effect of BN can be reduced through the use of a diversity receiver, due to its ability to choose the reception direction and select the branch that observes minimum BN (selection diversity is used here). The combination of spot-diffusing (LSMS) and diversity reception can achieve a uniform SNR over the entire CF when the transmitter is placed at the room centre as a result of the good spots' distribution on the ceiling. LSMS with an angle diversity receiver offers a significant SNR improvement over the CDS with a single wide FOV receiver. For example an SNR improvement of 21 dB can be achieved when the LSMS replaces the CDS at transmitter and receiver locations of (2m, 4m, 1m) and (1m, 1m, 1m).

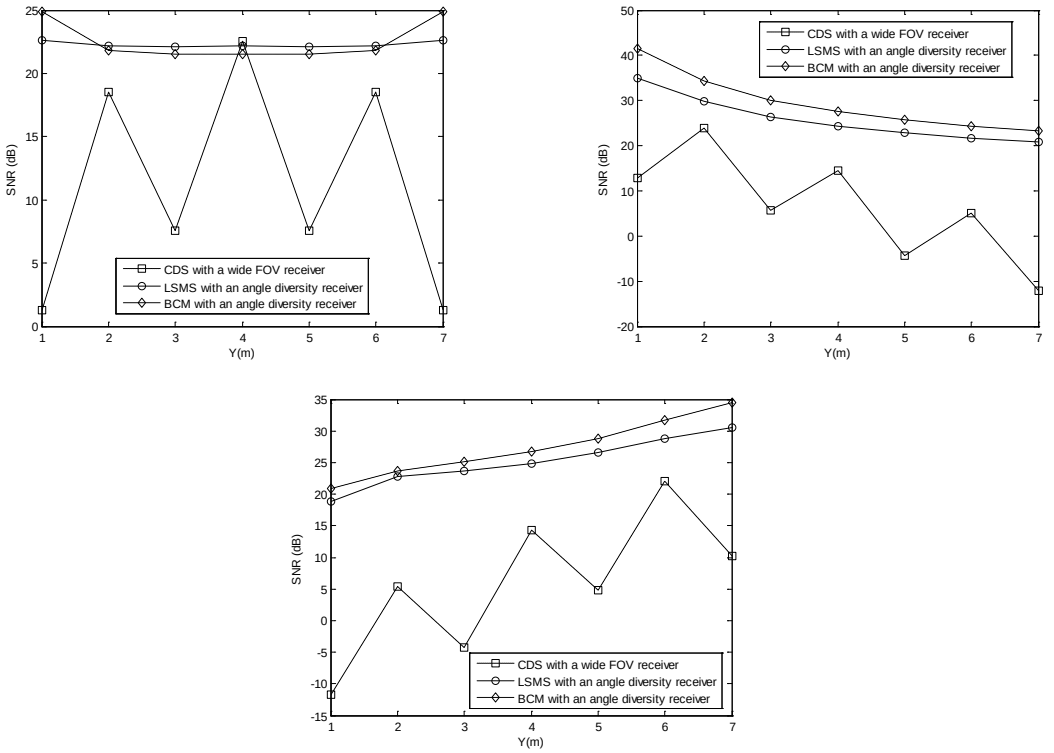

(a)

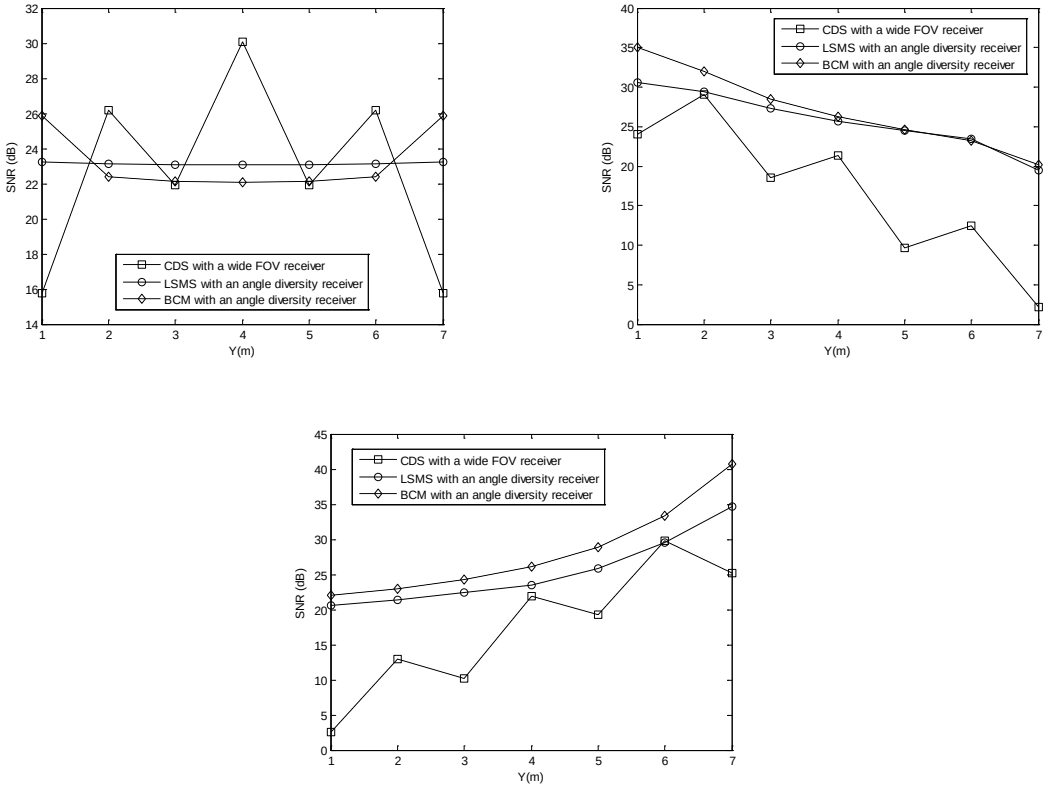

(b)

Figure 3-11: SNR of the three proposed configurations at three transmitter position: (1m, 1m, 1m), (2m, 4m, 1m) and (2m, 7m, 1m), when the receiver moves along the: (a) x = 1 m line and (b) x = 2 m line

A further SNR improvement of 2 dB can be obtained when the spots are clustered on the ceiling and two end walls (i.e. BCM is employed). The BCM configuration helps the receiver (when it is located near the room sides and corners) to collect stronger received power through shorter paths compared to that associated with LSMS (where the spots are distributed on the ceiling). Mobility can induce significant SNR performance degradation in optical wireless systems based on diffuse as well as spot-diffusing configurations. An SNR degradation of 16 dB can be observed in the LSMS performance when the receiver is placed in the corner of the room (1m, 1m, 1m) and the transmitter moves from (1m, 1m, 1m) to (2m, 7m, 1m); while in the CDS performance impairment it is about 24 dB. In spite of transmitter motion, the improvement in SNR, when LSMS with diversity receivers is employed, is clearly visible over the given receiver locations (14 different locations) on the CF compared to the CDS with a wide FOV receiver. At the worst communication path considered, the LSMS improves the SNR performance by more than 30 dB over the conventional diffuse system in agreement with the results presented in [175]. Furthermore, among all the systems considered, it is to be noted that the best SNR levels are obtained by the BCM with an angle diversity receiver.

3.9. Summary

In this chapter, an OW channel propagation model was introduced and used to evaluate the characteristics of an OW communication link. The effects of background noise and multipath propagation in indoor OW systems were discussed and evaluated. Furthermore, to facilitate comparison as well as establish base lines, indoor optical wireless systems based on spot-diffusing configurations, LSMS and BCM were studied, and their performance was evaluated and compared with the

CDS. It was shown that the CDS with a wide FOV receiver is very sensitive to ambient light noise and multipath dispersion. In contrast, LSMS with an angle diversity receiver provides robust communication links tolerant to background noise and multipath distortion, which yields a significant SNR improvement. The diversity receiver selectively confines the range of reception angles, while still able to collect significant power from the diffusing spots, where each spot is very compact spatially on the ceiling with significant power, e.g. 12.5 mW in our case of LSMS. It was also shown that in an LSMS system with an angle diversity receiver, the receiver SNR is almost independent of the receiver-transmitter separation when the transmitter is placed at the room centre. However, a significant SNR degradation can be induced when the transmitter is mobile. Furthermore, the beam clustering method was shown to be a promising means of improving the performance of mobile optical wireless links. The BCM system with an angle diversity receiver improves the SNR by almost 33 dB at the worst communication path and produces improvements at other locations compared to the CDS with a single wide FOV receiver. It is expected that the performance of BCM will improve if a photodetector array (imaging receiver) with MRC is used. In addition, an optical concentrator coupled with an optical filter in front of the detector can offer even further improvements.

4. ANALYSIS OF MULTIBEAM OPTICAL WIRELESS SYSTEMS EMPLOYING A BEAM POWER ADAPTATION METHOD AND DIVERSITY DETECTION

4.1. Introduction

The need for mobile computing and mobile multimedia communication, in general, has focused interest on optical wireless where a large bandwidth is potentially available [102, 175]. Mobile users experience a time varying channel which results in weak coverage in certain zones/parts of the room as the user moves. In order to take into consideration the system performance degradation due to user mobility, the most important issue that an OW spot-diffusing system designer must take into account is the amount of received power, which varies with the distance between the diffusing spots and the receiver (the dispersion is lower in these systems due to receiver proximity to a diffusing spot at most locations and directional noise can be reduced through diversity detection). Due to this fact, an adaptive technique is employed to increase the received optical power at a given receiver location, as well as reduce the performance degradation due to user motion. In effect the transmitter in an adaptive multibeam system assigns higher powers to beams nearest to the receiver, so as to maximise the receiver SNR. It is to be noted that the goal of our new adaptive algorithm is different from conventional transmit power control in systems, such as CDMA where, for example, the goal may be the reduction of the near-far problem. Our goal here is to optimise the optical spot power distribution on the ceiling and/or walls of a room to enhance signal reception at a given receiver location which is essential even in the presence of a single transmitter and a single receiver. Furthermore, when multiple transmitters/receivers are present in the

environment, opportunistic scheduling [177] can be used to maximise the overall throughput of the system in the presence of interference and time varying channels. This merits further study. It should also be noted that optical multibeam power adaptation shares some common features with radio beam-forming in that both attempt to direct the transmit power to a given spatial location so as to maximise the receiver SNR for example. There are however some distinct differences. Radio beam-forming typically uses the interference between multiple antenna beams to form a new transmit beam that has certain spatial distribution properties. Optical multibeam power adaptation is a scalar process as the control of the phase of an optical carrier is a difficult task to achieve in a simple low cost LAN wireless system. Here multiple beams are generated, each with a different spatial orientation, and the power is simply redistributed among the beams (spatial power redistribution) in order to achieve the best SNR at the receiver. This results in a simple implementation and produces significant performance improvements as this chapter demonstrates.

In this chapter, we propose and evaluate a new OW configuration that employs an adaptive beam clustering method (ABCM) in conjunction with diversity detection. Our goal is to increase the received optical power, reduce the effect of ISI, and improve the SNR when the system operates under the constraints of background noise, multipath dispersion and mobility. The proposed system (adaptive beam clustering transmitter with a diversity receiver) is evaluated at 50 Mbit/s to enable comparison with previous work, and is also assessed at higher bit rates: 2.5 Gbit/s and 5 Gbit/s. Simulation results show that at a bit rate of 50 Mbit/s, a significant SNR improvement of 22 dB is achieved when an ABCM system replaces LSMS at a 6 m transmitter-receiver horizontal separation, when both systems employ an 8^{o} angle diversity receiver. This SNR improvement can be used to reduce the transmit

power at this bit rate (50 Mbit/s). The results also show that the 8^o angle diversity ABCM system increases the channel bandwidth from 37.6 MHz (a conventional diffuse system) to 10.2 GHz. The increase in SNR and channel bandwidth is used to achieve higher data rates: 2.5 Gbit/s and 5 Gbit/s.

4.2. Simulation Environment

The characteristics of the mobile channel formed by the combination of an adaptive multibeam transmitter and an angle diversity receiver are investigated. Simulation was conducted in an environment similar to that described in the previous chapter, where an empty room, with dimensions of 8 m × 4 m × 3 m, was considered. The ceiling, walls and floor of the room were modelled as ideal Lambertian reflectors with a reflectivity of 0.8 for the walls and ceiling and 0.3 for the floor. Reflections from doors and windows are considered completely the same as reflections from walls. To model the reflections, the room reflecting surfaces (ceiling and walls) were divided into a number of equal-size, square-shaped reflection elements. These elements were treated as small emitters and were modelled as Lambertian reflectors. Up to second-order reflections were taken into account. Surface elements of 5 cm × 5 cm for first-order reflections, and 20 cm × 20 cm for second-order reflections were used.

To quantify the proposed system's performance under mobility, four configurations were considered: ALSMS, ABCM, LSMS, and BCM with an angle diversity receiver of seven branches. The multibeam transmitter was positioned at three locations on the CF: (2m, 4m, 1m), (1m, 1m, 1m), and (2m, 7m, 1m), pointed upwards, and emitted 1 W total optical power with an ideal Lambertian radiation pattern. The multibeam transmitter is assumed to produce $N_s \times 1$ beams that form N_s spots (on the

ceiling for LSMS configuration, and on the ceiling and two side walls for BCM configuration) with equal total power. Computer generated holograms can be used to produce static beam intensities and we have highlighted the relevant work in the literature [39, 51]. Power adaptation among the beams can be achieved at low complexity by using a liquid crystal device to generate dynamically varying holographic elements, hence adapting the beam powers as required. These devices have μs to ms response times [178], which are adequate given that beam power adaptation has to be carried out at the rate at which the environment changes (for example human motion), and not at the data rate. A feedback channel from the receiver to the transmitter can inform the transmitter of the SNR associated with a given power distribution among the spots. This channel can be provided by a low data rate diffuse channel, or by using one of the beams or an additional beam (spot) at a low data rate as a feedback channel. At low data rate, the power associated with such a beam can be maintained at a fixed level. It should be noted that our system makes use of commercially available components and can therefore be implemented at relatively low cost.

In order to examine our new adaptive multibeam transmitter configurations, the same previously described eight halogen spotlights (Philips PAR 38 Economic), which result in one of the most stringent optical spectral corruptions to the received data stream, have been chosen. The eight spotlights were equidistantly placed on the ceiling as shown in Fig. 3.2. Furthermore, in order to combat background noise as well as multipath dispersion, a diversity receiver is an appropriate choice, where significant performance improvements can be achieved by receiving the signal from different spatial orientations and by using appropriate combining techniques. The angle diversity receiver described in Chapter 3, Section 3.6 (where seven

photodetector branches with a photosensitive area of 1 cm^2 each and a responsivity of 0.5 A/W, are used) is employed here. As previously mentioned, the direction of each photodetector is characterised by two main parameters: azimuth (*Az*) and elevation (*El*) angles. The *El* of six photodetectors remains at 20^o, while the seventh one faces up with *El* of 90^o. The *Az* for the seven branches of the diversity receiver are fixed at 0^o, 55^o, 90^o, 125^o, 235^o, 270^o, and 305^o respectively. The corresponding FOVs were restricted to 12^o, 30^o, 25^o, 30^o, 30^o, 25^o, and 30^o respectively. The optical signals received in the various photodetectors can be treated separately, and can be processed using the selection/combining methods mentioned. SB, which represents a simple form of diversity, is considered in this chapter. The receiver simply picks the photodetector with the largest SNR among all photodetectors. The diversity receiver is always placed on the CF along the $x = 1$ m and $x = 2$ m lines.

Furthermore, in order to investigate the effect of the FOV on the received signals, an 8^o FOV angle diversity receiver is also considered. In this case, the *El* of the seven photodetectors are set at 90^o, 40^o, 40^o, 40^o, 40^o, 40^o, and 40^o, and the *Az* for the seven branches of the receiver are fixed at 0^o, 65^o, 90^o, 120^o, 245^o, 270^o, and 295^o. Additional simulation parameters are given in Table 4.1. LSMS and BCM are two attractive configurations [95-97, 100, 102-103, 175]. Therefore, they are used for comparison purposes in order to evaluate the proposed novel configurations. Furthermore, Section 4.3 introduces and evaluates our new adaptive configurations (ALSMS and ABCM).

TABLE 4-1: PARAMETERS USED IN SIMULATION

Parameter	**Configuration Uplink Transmission**						
Room							
Length	8 m						
Width	4 m						
Height	3 m						
ρ _x_z Wall	0.8						
ρ _y_z Wall	0.8						
ρ _x_z op. Wall	0.8						
ρ _y_z op. Wall	0.8						
ρ _Floor	0.3						
Transmitter							
Number of transmitter	1						
Location (x, y, z)	(1,1,1)		(2,4,1)		(2,7,1)		
Elevation	90^o		90^o		90^o		
Azimuth	0^o		0^o		0^o		
Diversity Receiver							
Number of branches	7						
Photodetector's area	1 cm^2	1 cm^2	1 cm^2	1 cm^2	1 cm^2	1 cm^2	1 cm^2
FOV	8^o	8^o	8^o	8^o	8^o	8^o	8^o
Location (x, y, z)	(1,1,1), (1,2,1), (1,3,1), (1,4,1), (1,5,1), (1,6,1), (1,7,1) (2,1,1), (2,2,1), (2,3,1), (2,4,1), (2,5,1), (2,6,1), (2,7,1)						
Elevation	90^o	40^o	40^o	40^o	40^o	40^o	40^o
Azimuth	0^o	65^o	90^o	120^o	245^o	270^o	295^o
Time bin duration	0.3 ns						
Bounces	1				2		
Number of elements	32000				2000		
dA	5 cm × 5 cm				20 cm × 20 cm		
Spot lamps							
Number of spot lamps	8						
Locations (x, y, z)	(1,1,3), (1,3,3), (1,5,3), (1,7,3) (3,1,3), (3,3,3), (3,5,3), (3,7,3)						
Modulation Technique	OOK				OOK		
Wavelength	850 nm				850 nm		
Preamplifier design	PIN-BJT				PIN-FET		
Bandwidth	70 MHz				2.5 GHz		5 GHz
Bit rate	50 Mbit/s				2.5 Gbit/s		5 Gbit/s

4.3. Mobile Adaptive System Configurations

4.3.1. Adaptive Algorithm

The received power in an OW spot-diffusing system varies with the distance between the diffusing spot and the receiver. Therefore, a possible technique that can enhance the received power, reduce multipath dispersion, and mitigate the performance degradation due to mobility as well as improve the system performance is an adaptive technique introduced here for adjusting the spot powers. Unlike the previous work in [102, 175], where the total power is equally distributed among the spots, the adaptive multibeam transmitter presented here distributes the total power so as to optimise the receiver SNR. In effect the spots nearest to the receiver are allocated the highest power level, whilst the farthest spot is assigned the lowest power level so as to maximise the receiver SNR. A flowchart that illustrates the operation of our adaptive algorithm is given in Fig. 4.1. For a single transmitter and a single receiver at a given set of coordinates, the new adaptive algorithm adjusts the transmit powers of the individual beams as follows:

1. It distributes the total power, 1 W, on the spots in equal intensities.
2. It computes the power received at the diversity receiver as well as calculates SNR. In a practical implementation, circuits can be designed with an appropriate medium access control (MAC) protocol to facilitate the computation of the SNR. Here, periodic silences are introduced to estimate the noise, when this is coupled with signal plus noise (and interference) measurements (at other times), the SNR can be estimated.

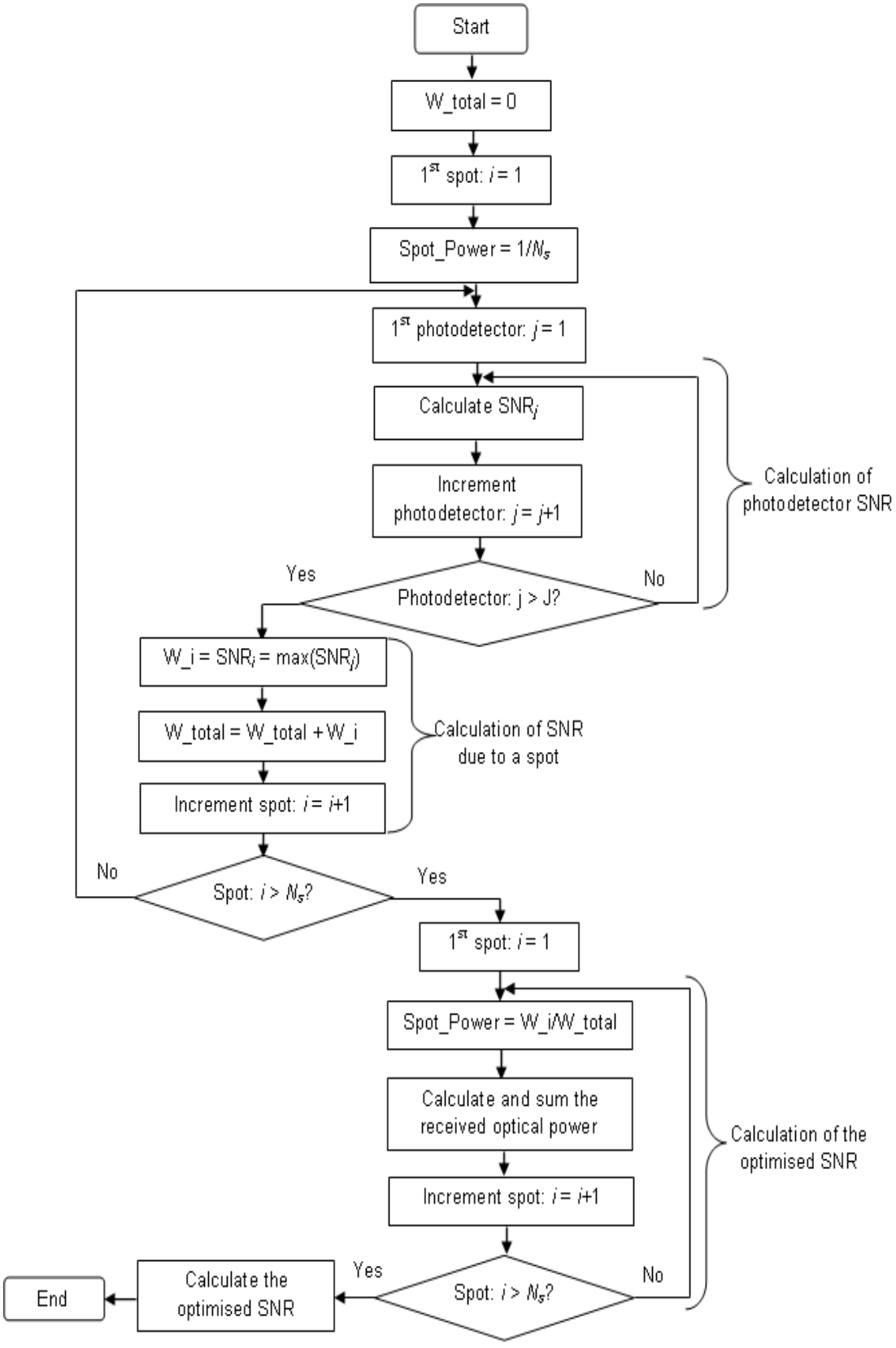

Figure 4-1: Flowchart of the adaptive algorithm

3. It selects the best link (the photodetector with the best SNR) to use as a desired communication link (desired photodetector), in essence the diversity receiver implements "select best" combining.
4. It switches on each spot individually, computes the power received at the desired photodetector as well as calculates the SNR.
5. It sends a feedback signal, at a low rate, to inform the transmitter of the SNR associated with the beam (spot). This feedback channel can be implemented using a CDS or by modulating an additional beam whose power is kept fixed (as the data rate is low).
6. It repeats steps 4 and 5 for all the spots.
7. It re-distributes the total power among the spots, according to the SNR they produce at that photodetector, where a spot that produces maximum SNR gets the highest power level assignment.

The algorithm described above applies to the single user case where the beam powers are adapted so as to maximise the SNR at one given receiver location. In a multi-user scenario, the optimum beam power distribution that maximises the receiver SNR may be different among the users. Several approaches can be used to handle this situation. For example opportunistic communication techniques with scheduling [177] can be employed where the beam powers are chosen to maximise the SNR in a given region for a given time period, or effectively allocate more power to users who experience a better channel (lower background noise and multipath dispersion) at a given time period. Also note that, beam power adaptation has to be carried out at the rate at which the environment changes (human motion). This is a low rate which relaxes the requirements on the feedback channel and on the adaptation process, even

in the presence of multiple users. The power is redistributed among the beams by modulating the liquid crystal holographic element. Assigning optical beam powers to spots according to the SNR they produce at the receiver mimics maximum ratio combining techniques although this is a transmitter approach. The proof of the absolute optimality of this transmit power adaptation approach under different scenarios (e.g. co-user interference and noise), warrants further study. In this work we show the significant performance improvement it produces. A line strip spot-diffusing system is an attractive OW transmitter configuration [95-97, 100, 175]. Therefore, it is evaluated making use of the beam power adaptation method introduced.

4.3.2. Mobile Adaptive LSMS (ALSMS)

In this section we extend the treatment proposed and examined in [175] (and presented in Section 3.7.2) by introducing transmit power adaptation implemented on the beam (spot) powers. The results demonstrate that significant performance (SNR) improvement can be obtained. The adaptive multibeam transmitter produces 80 × 1 beams aimed at the ceiling with different intensities. A line of diffusing spots with a distance of 10 cm between adjacent spots is formed in the middle of the ceiling along the x = 2 m line when the transmitter is placed at the centre of the room. These spots become secondary distributed emitters which emit Lambertian radiation. The spot distribution structure in ALSMS is similar to that in LSMS (see Fig. 3.5), but the total power is adaptively distributed among the beams in ALSMS. In our system the positions of the spots on the ceiling vary as the transmitter moves, and the locations of the spots can be determined in the room following the procedure given in Fig. 3.7

(flowchart illustrating the mobility analysis in the LSMS). The transmit powers associated with the beams are adjusted according to the algorithm given earlier in this section.

4.3.3. Mobile Adaptive BCM (ABCM)

A structure of spot distribution based on the beam clustering method proposed and examined in the previous chapter, is extended here (by introducing beam power adaptation) and the results indicate a significant SNR improvement can be achieved. The system arrangement in ABCM is similar to that explained in BCM (Section 3.7.3) and shown in Fig. 3.8, where a multibeam transmitter positioned at the centre of the room, produces 100 × 1 spots aimed at the ceiling and two end walls. The main difference in the new system (ABCM) is that the powers associated with the beam are optimised with the aim of maximising the SNR at the receiver. Three clusters of spots with different intensities are created in the middle of the ceiling and two end walls at x = 2 m (80 diffusing spots on the ceiling and 10 spots on each wall) when the transmitter is placed at the centre of the room. In a similar fashion, the new spot locations based on transmitter position and the beam angles associated with the ABCM transmitter can be identified. Different power levels are assigned to the spots according to the adaptive algorithm introduced.

4.4. Simulation Results

The performance of all the configurations considered (LSMS, BCM, ALSMS, and ABCM systems, in conjunction with an angle diversity receiver) was investigated in terms of impulse response, delay spread, channel bandwidth and SNR. The

performance was evaluated when the systems operated under the constraints of BN (eight directional spotlights n_{Lamp} = 33.1) and multipath dispersion with transmitter and receiver mobility. A significant performance improvement is achieved when our power adaptation method is implemented; however, there is a moderate increase in receiver complexity. This is associated with the training phase when the SNRs, due to each beam, are computed at the receiver and the optimum spot powers are selected at the transmitter. The transmitter computations are simple and the receiver operations are comparable to those needed when implementing receiver diversity, and as such the complexity increase is moderate.

At each set of transmitter and receiver locations, a simulation algorithm, similar to that adopted in Chapter 3 for the spot-diffuse system, was developed here by introducing a beam power adaptation method, and used to calculate the impulse response and the received optical power at the diversity receiver. The inclination associated with the faces of the diversity receiver was also considered. Several parameters can be obtained from the simulated impulse response such as SNR, delay spread and 3 dB channel bandwidth.

4.4.1. Impulse Responses

The impulse responses of the two configurations (LSMS, and ALSMS) with angle diversity receivers, when the transmitter is placed in the corner of the room (1m, 1m, 1m), and the receivers are located at (1m, 1m, 1m) and (2m, 7m, 1m), are depicted in Fig. 4.2. These two receiver locations were selected in order to consider the best and the worst links respectively (based on the transmitter and receiver separation), hence the impact of mobility. Fig. 4.2 compares the power levels (μW) as a function of

time (ns) in LSMS and ALSMS. It is clearly seen that the adaptive multibeam transmitter structure significantly increases the power levels as well as markedly reducing the signal spread. This is due to assigning higher power levels to spots nearest to the receiver, yielding high direct path components, almost $1\,\mu\mathrm{W}$ associated with ALSMS at the least successful position when the receiver is placed at (2m, 7m, 1m). However, equally distributing the power levels among the spots, results in low direct path components approximately $0.1\,\mu\mathrm{W}$ in the LSMS system. The results also show that a drop in the received power levels, attributed to the large distance between the transmitter and the receiver (e.g. the least successful position studied in Fig. 4.2), is significantly enhanced by a factor more than 10 when the beam power adaptation method is implemented.

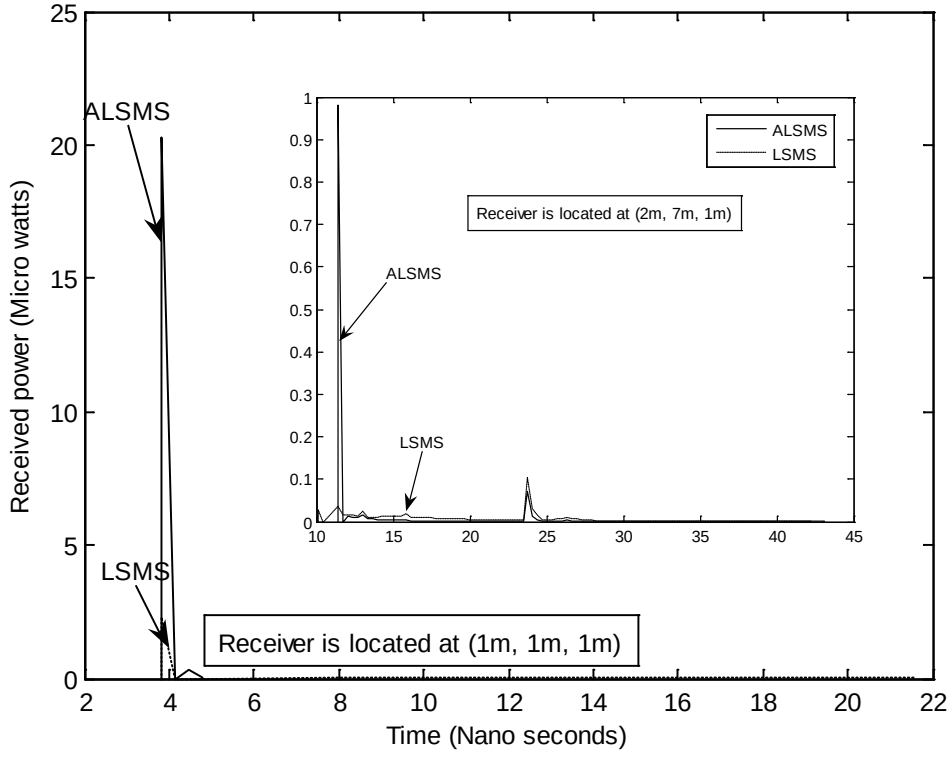

Figure 4-2: Impulse response of two configurations; LSMS and ALSMS when the transmitter is placed in the corner of the room (1m, 1m, 1m) and the receivers at (1m, 1m, 1m) and (2m, 7m, 1m)

Furthermore, an improvement in the received optical power is clearly visible when the adaptive spot-diffusing transmitter is employed instead of a spot-diffusing transmitter, and when the transmitter and receiver are co-located in the corner of the room, as shown in Fig. 4.2. The impulse responses associated with ABCM and BCM systems can be explained in a similar manner. In addition, impulse responses for all the cases studied are analysed to compare the impact of transmitter/receiver mobility on the received optical power, and to examine the extent to which multibeam power adaptation mitigates this effect.

4.4.2. Delay Spread Evaluation

Fig. 4.3 (a) compares the delay spread of three configurations: LSMS, ALSMS, and ABCM when the transmitter is placed in two different positions (1m, 1m, 1m) and (2m, 4m, 1m), and the receiver moves at constant x = 2 m, and along the y-axis over the CF. It can be seen that the adaptive LSMS has a lower delay spread compared with the LSMS at all transmitter positions. This is attributed to re-distribution of the total power to the spots nearest to the receiver, resulting in very high level direct path components and limited low level first and second order reflection components. The delay spread of the mobile LSMS increases as the receiver moves away from the transmitter, and reaches almost 6 ns at one of the least successful locations when the transmitter is placed at (1m, 1m, 1m) and the receiver is at (2m, 7m, 1m). Degradation in the delay spread of the mobile OW system is improved by employing the adaptive multibeam transmitter configuration in conjunction with diversity detection at all transmitter and receiver locations.

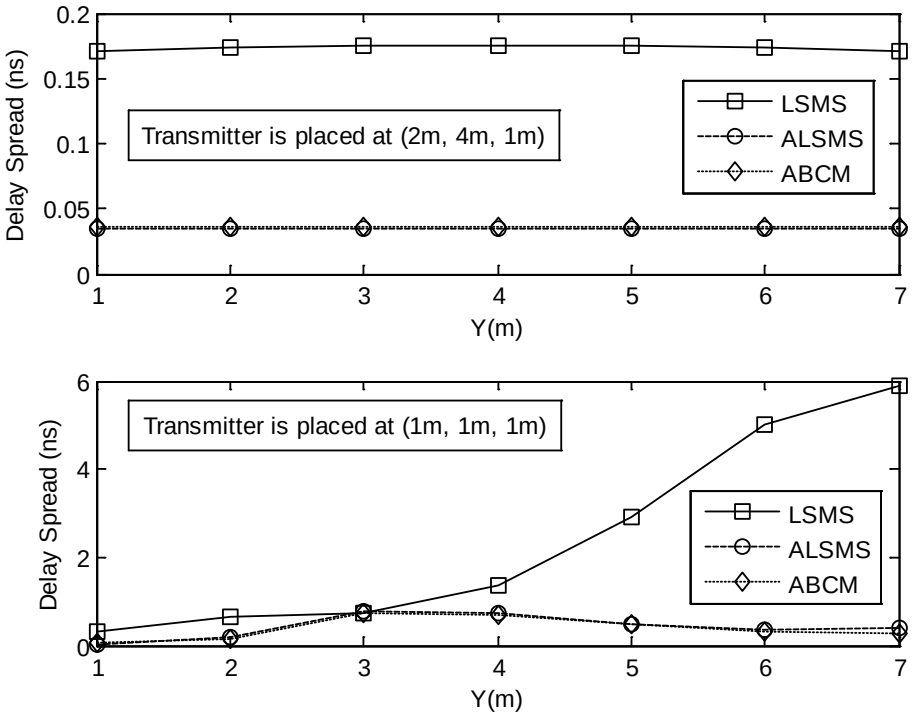

(a)

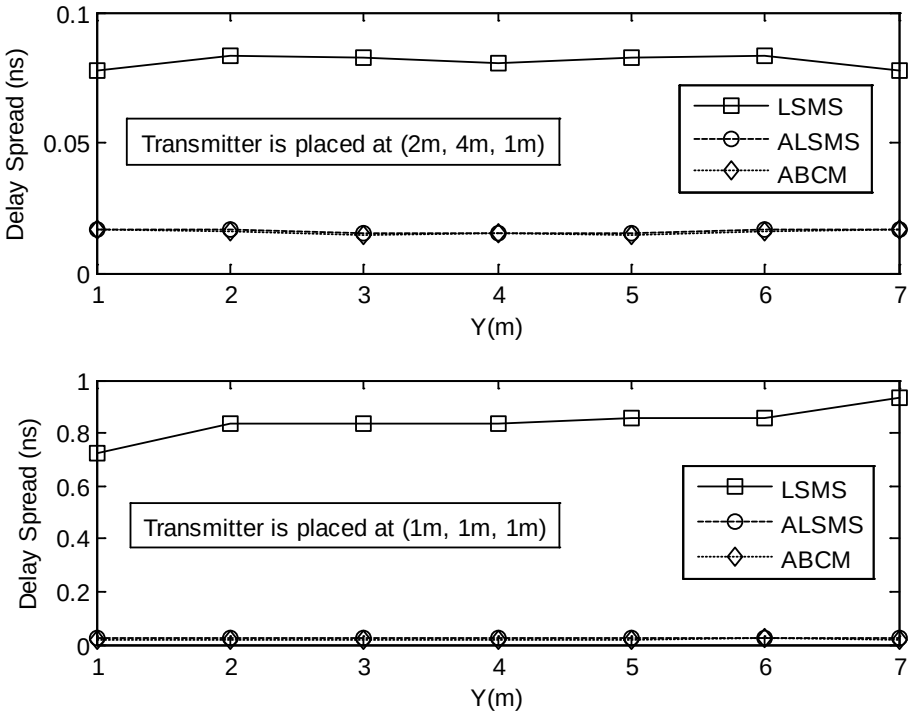

(b)

Figure 4-3: Delay spread distribution of three mobile OW systems: LSMS, ALSMS and ABCM when the transmitter is placed at (1m, 1m, 1m) and (2m, 4m, 1m) and the receiver moves along the x = 2 m line; (a) 12^{o} FOV angle diversity receiver and (b) 8^{o} FOV angle diversity receiver

For example at the least successful locations, when the transmitter is placed at (1m, 1m, 1m) and the receiver is at (2m, 7m, 1m), a significant reduction in the delay spread is achieved, a factor of 20, when our new ABCM replaces LSMS. Furthermore, almost similar delay spread performance in both mobile adaptive OW systems; ALSMS and ABCM are observed. Previous work [102] showed that the BCM is better than LSMS since its geometry results in spot clusters (higher powers) nearer to most receiver positions as the transmitter moves. However, with spot power adaptation the performance of ALSMS and ABCM are similar as the adaptive algorithm distributes the power among the spots according to receiver position.

A comparison of the delay spread of the three configurations (LSMS, ALSMS, and ABCM) employing an 8^o diversity receiver is shown in Fig. 4.3 (b). A reduction in the delay spread in all the configurations considered is observed when an 8^o diversity receiver is implemented, due to the limited range of rays captured. This improvement in the delay spread, which is reflected as an increase in the channel bandwidth as shown in Figs. 4.4 (a) and (b), comes with a reduction in power efficiency; see Figs. 4.7 (a) and (b).

4.4.3. Channel Bandwidth

The 3 dB channel bandwidth of three configurations: CDS with a single wide FOV receiver, BCM and ABCM systems with an angle diversity receiver is depicted in Fig. 4.4 (a) when the transmitter is placed at (1m, 1m, 1m) and (2m, 4m, 1m), and the receiver moves along the x = 2 m line. Fig. 4.4 (b) shows the 3 dB channel bandwidth of the BCM and ABCM configurations that employ an 8^o diversity receiver.

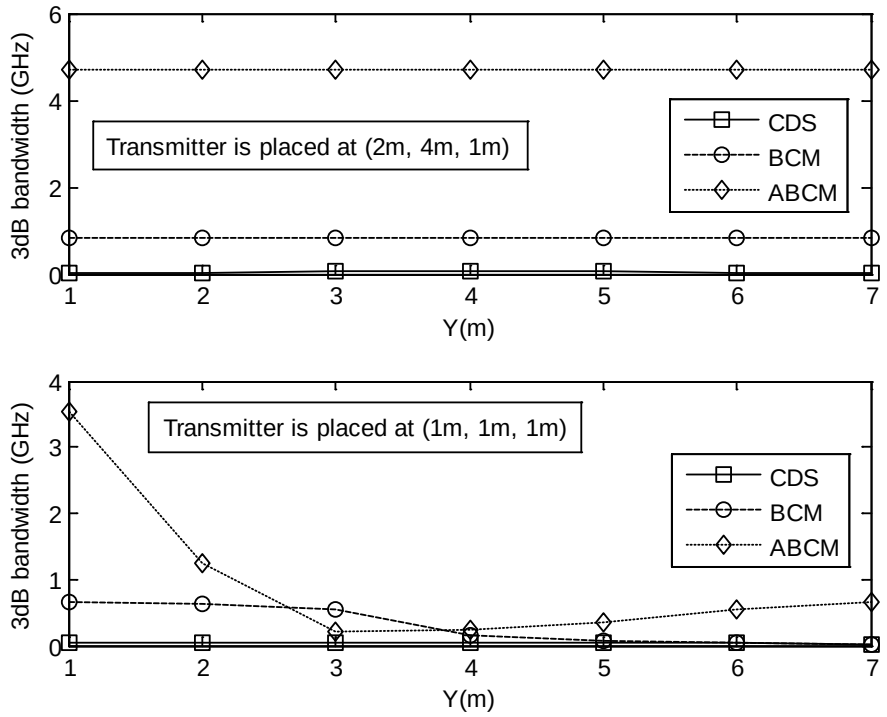

(a)

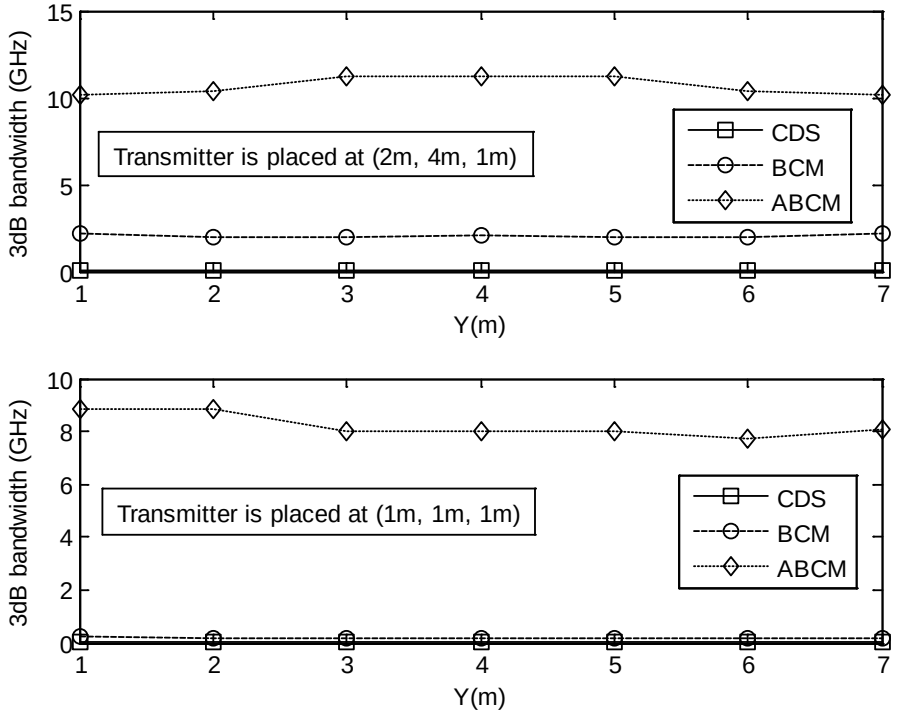

(b)

Figure 4-4: 3 dB channel bandwidth of three mobile OW systems: CDS, BCM and ABCM when the transmitter is placed at (1m, 1m, 1m) and (2m, 4m, 1m) and the receiver moves along the x = 2 m line; (a) 12^{o} FOV angle diversity receiver and (b) 8^{o} FOV angle diversity receiver

The CDS is the baseline against which most researchers in OW compare their results. This system was first investigated as early as 1979 [3]. We have compared our results to published OW simulation and experimental work (simpler systems: CDS; spot diffusing with angle diversity giving 2 GHz bandwidth [10, 39-40, 179] respectively) to validate our simulator and calculation methods and good agreement is observed. The increase in bandwidth from 37.6 MHz channel bandwidth to about 10.2 GHz took place over an extended period of three decades. The results show that a diffuse link employing a single wide FOV receiver can achieve a channel bandwidth of approximately 38 MHz in good agreement with that reported in [10]. The diffuse channel bandwidth can be increased from 38 MHz to 220 MHz when a 12^o FOV receiver replaces the wide FOV receiver, see Fig. 4.5. However, a reduction in the received power from 1.56 μW to 24.18 nW is observed. This power reduction can be reduced with the received power increasing from 24.18 nW to 1.29 μW when a multi-spot-diffusing transmitter (such as that reported in [40] and [39] in 1992 and 1999 respectively) is employed instead of the diffuse transmitter, see Fig. 4.4 (a). The spot-diffusing geometry gives the narrow FOV receiver an option to collect significant power from the diffusing spots (each spot is very compact spatially on the ceiling, but has significant power, e.g. 12.5 mW in our case). This power enhancement comes with an increase in the channel bandwidth from 220 MHz to 647 MHz. Previous work [179] has shown that link designs adopting a multibeam transmitter in conjunction with a 7^o FOV diversity receiver can produce communication channels with 3 dB bandwidths of more than 2 GHz. This increase in channel bandwidth is accompanied by an increase in the path loss (7^o FOV receiver instead of the previous 12^o FOV receiver).

In this chapter, we show that a channel bandwidth of about 2.14 GHz can be achieved if spots are clustered and distributed on different surfaces, and diversity is employed (8^o FOV, 0.63 μW received power). The latter limits the rays captured by utilising narrow FOV photodetectors and selecting the branch with the best received power (select best diversity here). It should be noted that identically distributing the power among the beams can result in wasting the power allocated to the spots outside the receiver FOV, as well as introducing a time delay between the signals from the spots within the receiver FOV, limiting the bandwidth. Therefore, assigning higher power levels to spots nearest to the receiver can effectively increase the direct power component contribution and reduce the contribution of reflections, hence, significantly increasing the channel bandwidth, ultimately from 37.6 MHz (CDS) to 10.2 GHz as shown in Fig 4.5 (b). This significant bandwidth efficiency is one of the factors that can help increase the achievable data rate. The increased bandwidth, coupled with an increase in the SNR through beam power adaptation allows the OW system to operate at high data rates and provides multi-user capabilities.

Fig. 4.5 shows the impulse responses and frequency responses of different OW channels at transmitter and receiver locations of (2m, 4m, 1m) and (2m, 1m, 1m) respectively. As previously mentioned, a practical OW system produces a continuous impulse response, however, our simulator subdivides the reflecting surfaces into discrete elements. The discretisation effect can be reduced by grouping the powers received within a time bin (0.3 ns duration was used, we have also examined the impact of using a smaller bin, the results will be reported in Section 8.4.1) into a single received power resulting in the smoothness seen in the impulse responses.

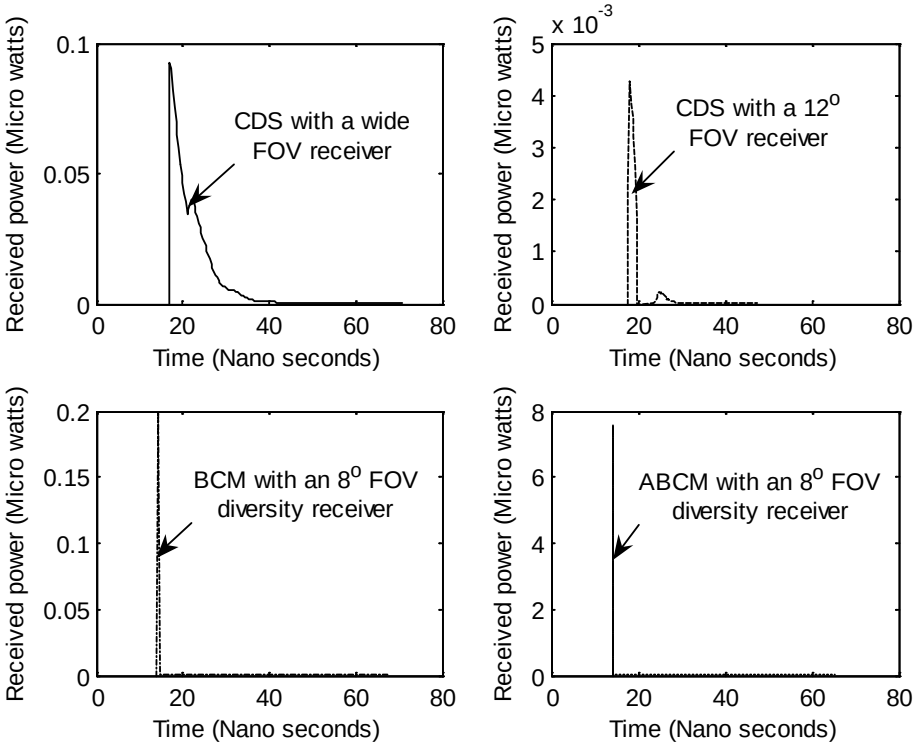

(a)

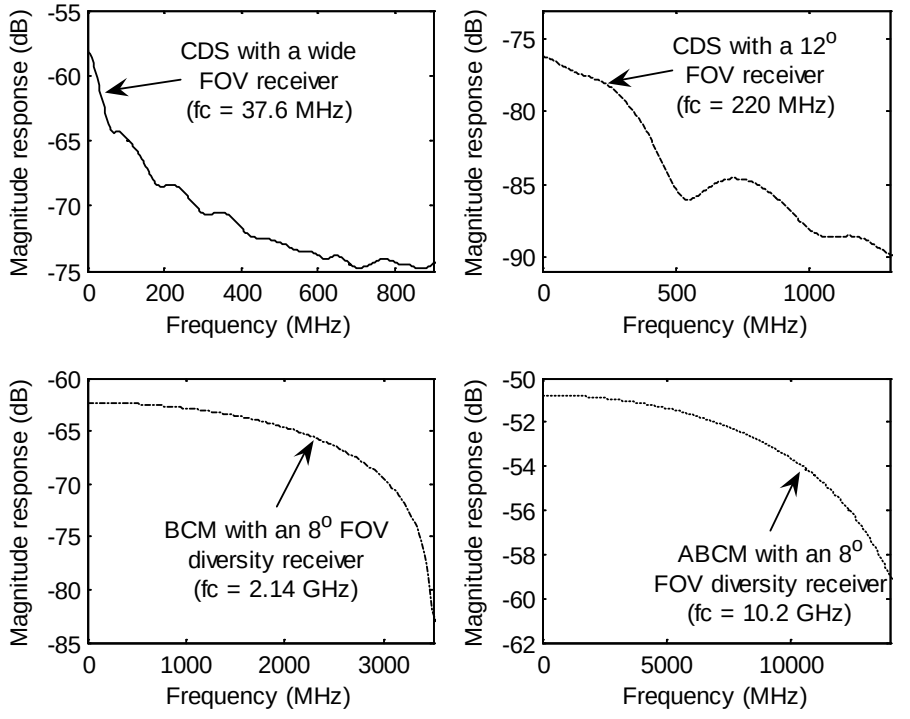

(b)

Figure 4-5: Impulse response and frequency response of different OW configurations at transmitter and receiver locations of (2m, 4m, 1m) and (2m, 1m, 1m); (a) shows impulse responses and (b) shows frequency responses

4.4.4. SNR

In this section, we investigate the performance in terms of SNR for all the configurations considered. The robustness of our ALSMS against shadowing and signals blockage in a real indoor environment is considered in the next Chapter. SNR calculations were performed using equation (3.31) taking into account the eye closure (where $P_{s1} - P_{s0}$ caters for eye closure due to dispersion). To enable comparison to previous work [175], we used a bit rate of 50 Mbit/s. Higher bit rates of 2.5 Gbit/s and 5 Gbit/s are also considered in our proposed ABCM. The pre-amplifier used for the 50 Mbit/s OOK system (20 ns pulse duration) is the 70 MHz PIN-BJT design proposed by Elmirghani et. al [22] with noise spectral density of $2.7\ \mathrm{pA}/\sqrt{\mathrm{Hz}}$. This receiver introduces little or no distortion onto the 50 Mbit/s pulse stream. For our proposed 2.5 Gbit/s and 5 Gbit/s ABCM systems, we used the PIN-FET design proposed by Kimber et al. [180]. This pre-amplifier has a noise current spectral density of $10\ \mathrm{pA}/\sqrt{\mathrm{Hz}}$ and a bandwidth of 10 GHz. The pre-amplifier bandwidth can be limited to 2.5 GHz and 5 GHz through the use of appropriate filters. The impact of this filter on the signal is minimal as the bandwidth considered is higher than 0.7 × bit rate (Personick's analysis [131]), and is not considered here. It has to be noted that the receiver in [22] has been designed for an OW system while that in [180] has not. We had to use the latter receiver since, to our knowledge, there is no receiver to date with such large bandwidth that has been specifically designed for indoor OW (we will design such a receiver in the future). In effect, although the receiver in [22] has $35\ pF$ detector capacitance, following bootstrapping, its equivalent value is $35(1-0.97) = 1.05\ pF$. A custom designed OW receiver at the large bandwidth needed should also use circuit design techniques to reduce the

detector capacitance while allowing a large detector area to be used. In this study we have used an equal detector area (1 cm^2) for both receivers, however this means that the receiver design in [180] has to be improved to allow the use of a large area detector with small equivalent capacitance, as was done in [22]. We believe that a fairer comparison is achieved by using equal detector areas in both receivers and addressing receiver design, than by comparing the two systems based on unequal detector areas which lead to significant performance difference, mainly due to poor receiver design. Also note that an optical concentrator can allow the FOV to be adjusted while allowing a large exit area (detector area) to be employed [181]. Furthermore, in order to show the effect of the detector collection area on the proposed systems performance, we reduced the collection area from 1 cm^2 to 0.1 cm^2 in steps of 0.1 cm^2 and computed the SNR at each step. The trade-off between the collection area and power penalty is depicted in Fig. 4.6. The results show that a power penalty of 20 dB approximately can be induced when the detector collection area is reduced from 1 cm^2 to 0.1 cm^2.

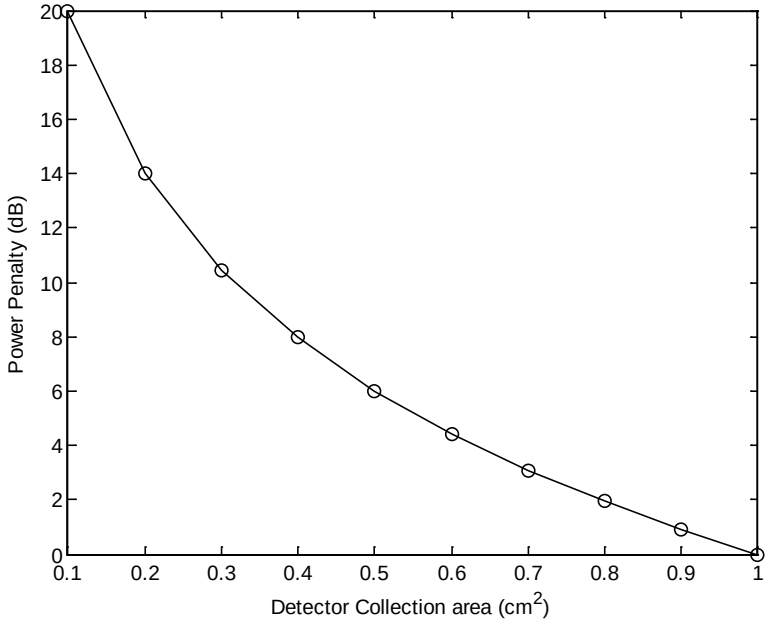

Figure 4-6: Trade-off between the power penalty and detector collection area

Figs. 4.7 (a) shows the SNR levels of four mobile OW systems: CDS with a wide FOV receiver, LSMS, ALSMS and ABCM in conjunction with an angle diversity receiver. The results are quoted when the system operates under the constraints of BN and multipath dispersion, when the transmitter is placed at two different positions (1m, 1m, 1m), (2m, 4m, 1m), and the receiver moves at constant x = 1 m, and along the y-axis over the CF. Our proposed systems (ALSMS and ABCM) are examined at points exactly underneath directive noise sources, (y = 1, 3, 5, and 7 m), as well as points near to the corner of the room, which represent the worst communication path. Simulation results indicate that the SNR is at maximum level in the positions when the transmitter and receiver are nearest each other. The results also show that at transmitter and receiver locations of (2m, 4m, 1m) and (1m, 1m, 1m) an angle diversity LSMS system provides a 23 dB SNR gain over the CDS, in agreement with previous work [100]. This SNR improvement is the result of adopting a spot-diffusing geometry combined with a diversity receiver. The fluctuations observed in the CDS SNR (attributed to the noise distribution) are mitigated by employing angle diversity with LSMS. Degradation in the LSMS SNR is, however, observed due to the transmitter and receiver mobility. For example in an LSMS system, when the transmitter is in the corner of the room (1m, 1m, 1m) the SNR degrades from 30 dB to 18 dB as the receiver moves at constant x = 2 m from y = 1 m to y = 7 m respectively. The opposite trend is observed when the transmitter is placed at (2m, 7m, 1m) and the receiver moves at constant x = 1 m and along the y-axis. A significant performance improvement in the mobile LSMS system is achieved when our transmit beam power adaptation method is implemented. This is due to assigning higher power levels to spots nearest to the receiver resulting in a very strong received power, hence enhancing the receiver SNR.

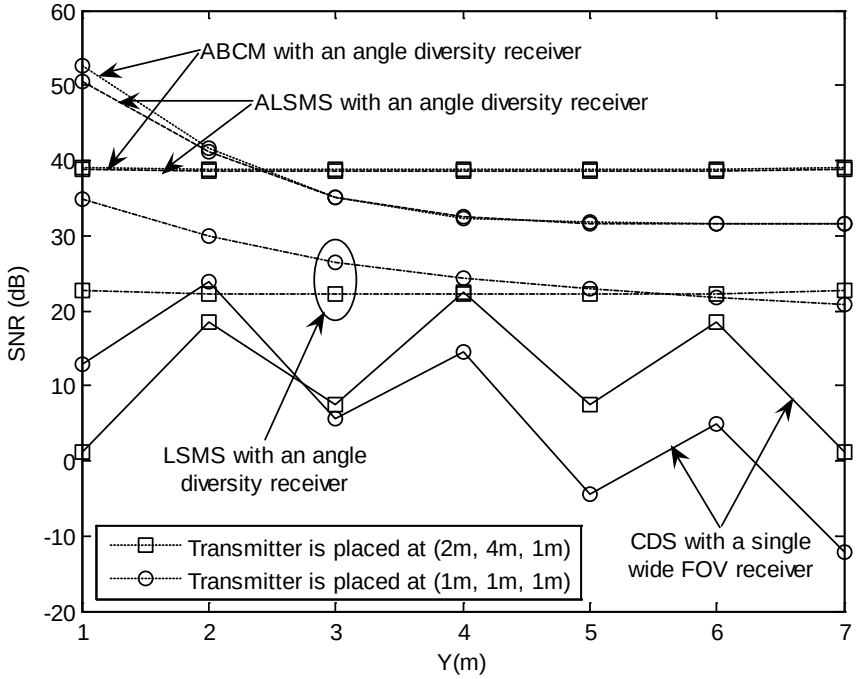

(a)

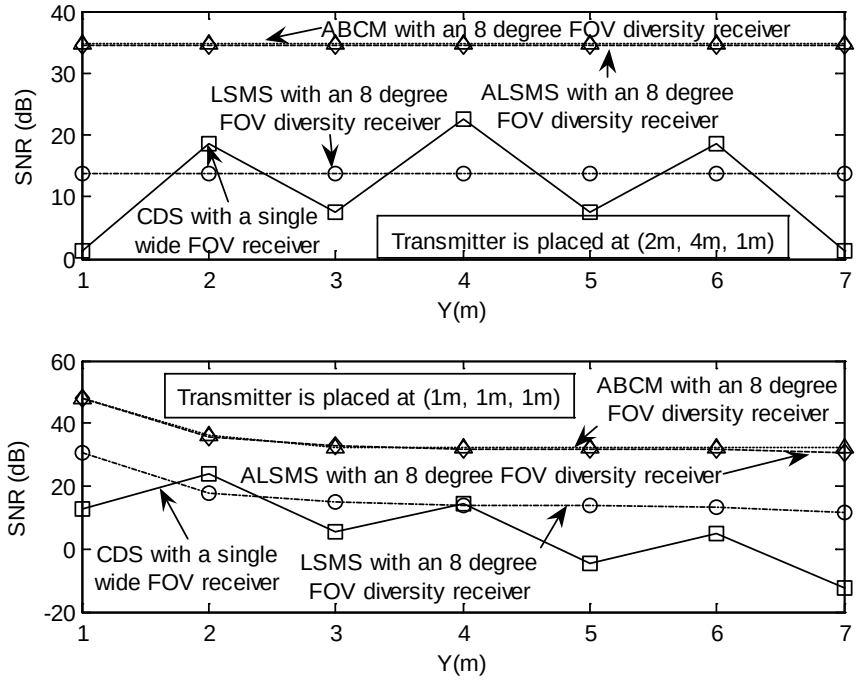

(b)

Figure 4-7: SNR of four mobile OW systems: CDS, LSMS, ALSMS and ABCM when the transmitter is placed at two different positions: (2m, 4m, 1m) and (1m, 1m, 1m) and the receiver is at constant x = 1 m, and along the y-axis; (a) FOV=12^o angle diversity receiver and (b) FOV=8^o angle diversity receiver

At a 6 m transmitter-receiver horizontal separation, almost 12 dB SNR improvement is achieved when an adaptive LSMS replaces the non-adaptive LSMS. Furthermore, our mobile ABCM system offers a 3 dB SNR improvement over the mobile ALSMS system, illustrating the gain achieved through beam clustering. The comparable ALSMS and ABCM SNR performance can be explained on a similar basis to those highlighted in relation to delay spread when transmit power adaptation is implemented. It should be noted that the performance of the proposed adaptive multibeam systems (ALSMS and ABCM) can be further improved if MRC is used at the diversity receiver. Figs. 4.7 (a) and (b) show that a power penalty of 9 dB can be induced in the LSMS SNR when an 8^o FOV diversity receiver replaces the 12^o diversity receiver at a transmitter-receiver distance of 6 m. This performance penalty can be reduced to 2 dB when beam power adaptation is implemented.

Table 4.2 gives a comparison between the BCM and ABCM systems which can be similarly explained. Table 4.2 also illustrates the impact of limiting the diversity receiver's FOVs to 8^o in both systems (BCM and ABCM). The significant SNR achieved through the combination of transmit power adaptation, beam clustering and diversity reception (SNR of 30 dB at the worst communication path considered when an 8^o FOV diversity receiver is employed) can be used to reduce the transmit power.

TABLE 4-2: SNR OF THE PROPOSED SYSTEMS (BCM & ABCM)

Configuration		**SNR (dB)**						
		Y (m)						
		1	**2**	**3**	**4**	**5**	**6**	**7**
12^o diversity receiver	**BCM**	35.02	31.95	28.54	26.27	24.6	23.27	20.23
	ABCM	42.78	37.7	33.68	32.82	32.7	32.62	32.48
8^o diversity receiver	**BCM**	14.04	13.73	13.37	13	12.94	12.91	11.95
	ABCM	32.13	31.73	31.14	30.84	30.8	30.75	30.27

In order to achieve a BER of 10^{-9}, the SNR has to be 15.6 dB for conventional OOK systems. Therefore, at the worst communication path considered in the 50 Mbit/s OOK systems, the combination of these methods can reduce the transmit power by almost 7 dB while achieving 10^{-9} BER. In a non adaptive system and with a total of 1 W transmit power, each of the 80 spots receives 12.5 mW power and the SNR performance is met as shown in Fig. 4.7 (b) for LSMS (SNR of 8 dB at the worst communication path when an 8^{o} FOV diversity receiver is employed). If an optical concentrator, coupled with an optical bandpass filter (to reduce background noise), is used in front of the detectors in the LSMS system and with a typical concentrator gain of 20 dB [30, 181], the power per spot is reduced to 0.3 mW (i.e. a total transmit power of 24 mW is used) which is lower than the typically quoted 1 mW eye safe limit at the near infrared wavelengths. To investigate eye safety, in our adaptive algorithm we used a total of 24 mW transmit power and introduced a limitation so that no spot power exceeds 1 mW and used the same optical concentrator and filter. The SNR obtained through the use of our adaptive algorithm in this case was 25 dB at the worst communication path, which is less than the 30 dB obtained without the restriction and without using any concentrator or filter, but is still significant. The degradation is due to the reduction in the transmit power, from 1 W to 24 mW, and due to the inability of the algorithm to allocate high power freely to spots at good locations due to eye safety. Also note that the transmitter shape and size have to be taken into account to determine if an eye can see more than one beam at a time. The source size also has to be taken into account to complete the assessment.

The high SNR achieved (SNR of 66.8 dB at the worst communication path considered, as shown in Fig. 4.8, when our ABCM system is employed with an 8^{o} FOV diversity receiver that has a collection area of 1 cm^2 and uses an optical

concentrator, coupled with an optical filter with a typical concentrator gain of 20 dB), together with the increase in channel bandwidth shown in Fig. 4.4 (b), can be used to achieve higher data rates or to enable multi-user communication. We consider higher data rates (2.5 Gbit/s and 5 Gbit/s) here and multi-user communication in Chapter 5. Higher bit rate indoor optical wireless systems operating at 2.5 Gbit/s and 5 Gbit/s are shown to be feasible through the combination of three approaches: transmit beam power adaptation, beam clustering, and an 8^o FOV receiver diversity using an optical concentrator coupled with an optical filter (with a typical concentrator gain of 20 dB). The SNR levels of the 50 Mbit/s and 2.5 Gbit/s ABCM systems, in conjunction with an angle diversity receiver, are depicted in Fig. 4.8, when the transmitter is placed in the corner of the room and the receiver moves along the x = 2 m line. SNR results of the 5 Gbit/s ABCM system with two detection areas: 1 cm^2 and 0.1 cm^2 are also included. The results show that the angle diversity ABCM can achieve an SNR of 36.8 dB at the worst communication link while operating at a bit rate of 5 Gbit/s. This is due to three factors. Firstly, the availability of direct path components (between the diffusing spots and receiver at all transmitter/receiver locations considered) due to beam clustering. These direct path components can be improved through beam power adaptation, and in turn can be significantly enhanced by using an optical concentrator. Secondly, a narrow FOV (FOV = 8^o) diversity receiver employing an optical filter can dramatically reduce the background noise. The pre-amplifier noise dominates in both higher data rates (2.5 Gbit/s and 5 Gbit/s) ABCM systems. In addition, the large channel bandwidth achieved (a bandwidth of 8 GHz approximately at the worst communication path) can guarantee that ISI does not occur at the data rates considered (2.5 Gbit/s and 5 Gbit/s). Furthermore, the design of a 1 cm^2 detector, 10 GHz receiver (we only need

5 GHz bandwidth maximum) is a challenging task, but it is not an impossible one. Therefore, we believe that our system is technically feasible. However (without producing a 5 GHz 1 cm^2 receiver design), here we show that a 10^{-9} BER can be met even with a detector area of 0.1 cm^2 where our system achieves an SNR of 17 dB (see Fig. 4.8) which is greater than the 15.6 dB needed. The link budget can be further improved through the use of error correction codes, and these warrant further study.

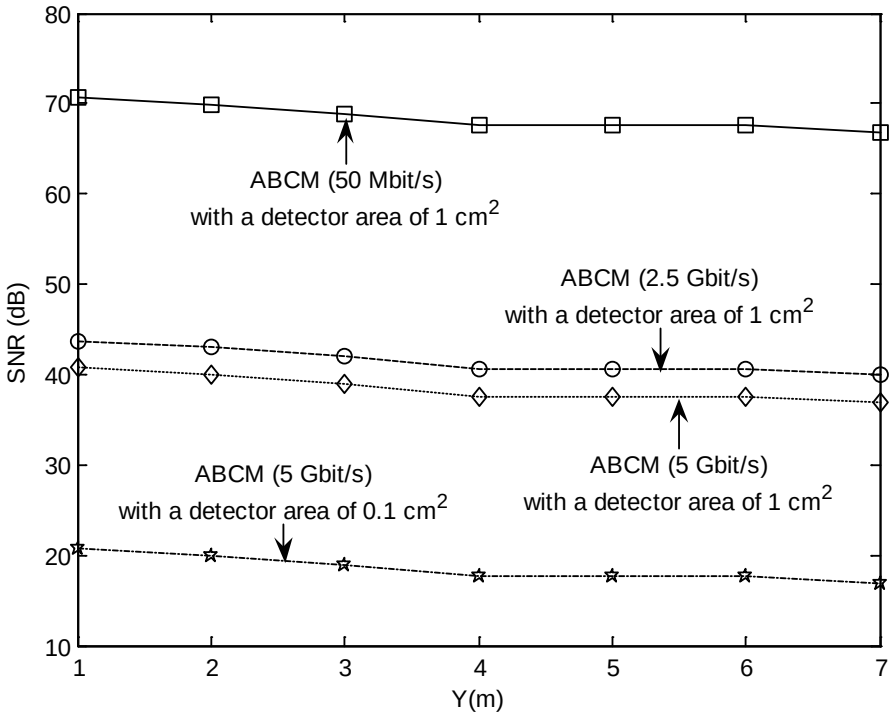

Figure 4-8: SNR of the proposed ABCM system operating at 50 Mbit/s and 2.5 Gbit/s, when the transmitter is placed in the corner of the room (1m, 1m, 1m) and the diversity receiver moves along the x = 2 m line, and the 5 Gbit/s angle diversity ABCM system with two detection areas: 1 cm^2 and 0.1 cm^2

4.5. Summary

In this chapter, we designed and investigated a novel mobile adaptive OW system (ABCM system with an angle diversity receiver) which can provide robustness against BN, multipath dispersion, and transmitter/receiver mobility. Performance degradation is observed in the mobile LSMS system at large transmitter receiver separation. This is attributed to collecting low direct path components, resulting in a low received power compared to the ambient noise level. Our goal was to increase the received optical power, reduce the effect of ISI, and improve the SNR when the system operates under the constraints of BN and multipath dispersion. Simulation results show that a significant performance improvement is achieved (including a reduction in the BN effect, reduction in delay spread, and improvement in SNR) in the two mobile OW system proposed (ALSMS and ABCM) over LSMS and BCM systems when all the systems use an angle diversity receiver. This is due to assigning high power levels to the spots nearest to the receiver, resulting in a strong received optical power as well as an increase in the SNR. The new ABCM system improves the SNR by 22 dB over the LSMS system at one of the worst communication paths considered, when both systems employ an 8^o FOV diversity receiver and operate at 50 Mbit/s. Note that LSMS outperforms the conventional diffuse systems. The significant SNR achieved can be used to reduce the transmit power which helps meet eye safety requirements. An increase in the channel bandwidth from 37.6 MHz (CDS system) to 10.2 GHz is achieved when the 8^o angle diversity ABCM is implemented. This additional bandwidth, coupled with the high SNR (43 dB improvement over the CDS), can be used to achieve higher data rates and 2.5 Gbit/s and 5 Gbit/s were shown to be feasible.

It should be noted that narrower FOVs can be used to restrict the range of incident rays accepted and, hence, reduce the signal spread as well as increase the channel bandwidth at the cost of poor power efficiency. The power efficiency can be enhanced by clustering and distributing the spots on different surfaces which gives the receiver an option to collect the signals through the nearest diffusing spots and the shortest paths. Furthermore, the link design can be significantly improved if beam power adaptation is implemented to effectively increase the direct path components and reduce the effect of reflections (by allocating more power to spots at key locations). The combination of these methods (beam power adaptation, beam clustering and diversity receivers) adds a number of degrees of freedom to link design.

It should also be noted that our approaches are less sensitive to the room layout than other methods (e.g. LSMS or CDS), as the power is adaptively distributed among the spots so as to maximise the receiver SNR, and the spots are clustered on different surfaces. The adaptation can be done in milliseconds based on typical liquid crystal device characteristics. This is fast enough given that the adaptation has to track the channel variation which happens at the rate at which humans or indoor objects move.

5. MC-CDMA ADAPTIVE MOBILE ANGLE DIVERSITY MULTIBEAM OPTICAL WIRELESS SYSTEMS IN A REAL INDOOR ENVIRONMENT

5.1. Introduction

Multicarrier code division multiple access (MC-CDMA) is a transmission scheme that combines the robustness of orthogonal modulation with the flexibility of CDMA schemes. It can lower the symbol rate and is therefore suited to the bandwidth limited optical wireless indoor channel. In this chapter, new work is presented for an optical wireless system that utilises MC-CDMA to improve the BER performance. The first analysis on an OW MC-CDMA system is reported. The results indicate that at a BER of 10^{-4} 7 dB and 10 dB SNR, improvements are obtained through the use of MC-CDMA in a 4-user system, compared to a single user OW OOK system and a 4-user OW CDMA system respectively. This improvement is obtained while enabling multi-user communication. The performance degrades gradually with increase in the number of users. This chapter demonstrates that the significant improvement in the channel bandwidth and SNR, achieved through the combination of transmit power adaptation, spot-diffusing and diversity receiver, can enable the system to provide multi-user communication, in our case, through the use of an MC-CDMA scheme. At transmitter and receiver locations of (2m, 4m, 1m) and (1m, 1m, 1m), the MC-CDMA ALSMS system achieves a BER of 5×10^{-10} in a 4-user scenario compared to a BER of 5×10^{-1} when MC-CDMA CDS is considered. Furthermore, a zero forcing (ZF) equalisation technique was employed to reduce multiple access interference and improve the BER performance. The results confirm that while the CDS and the LSMS systems benefit, the equalisation scheme, which increases receiver complexity, is not necessary when the adaptive LSMS (ALSMS) replaces

CDS or LSMS at the data rate considered. In addition, a real communication environment, which takes into account partition design, cubical design, window availability, and cabinets, is considered.

5.2. Mobile OW Model and Room Configurations

In this section we aim to demonstrate the robustness of our adaptive multibeam systems against shadowing and signal blockage. Due to the comparable performance realised in both ALSMS and ABCM systems (as shown in Chapter 4), it is expected that their performance under shadowing is comparable (due to beam power adaptation). Therefore, we examine our proposed ALSMS system coupled with a diversity receiver in a real office environment that consists of windows, a door, mini-cubicles, bookshelves, and other objects. For comparison purposes a mobile LSMS system with an angle diversity receiver of seven branches is considered in two room scenarios: an empty room, and a real office environment. Moreover, consideration is also given to the other elements of the real indoor environment namely ambient light noise and multipath dispersion, and the performance is evaluated.

The channel characteristics of mobile infrared links, based on adaptive spot-diffusing geometry combined with diversity reception, have been modelled in a highly impaired environment in the presence of windows, office cubicles, bookshelves, and shadowing. The simulation model was developed using as an example room, dimensions similar to those used in the previous chapters, an 8 m × 4 m room having a ceiling of 3 m for two different room configurations denoted as A and B. Fig. 5.1 shows Room B that has three large glass windows, a door, a number of rectangular-shaped cubicles with surfaces parallel to the room walls, and other furniture such as bookshelves and filing cabinets. In Room A, the reflectivity of the walls and ceiling

is 0.8, while it is 0.3 for the floor. In Room B, The glass windows are expected not to reflect any signal hence their diffuse reflectivities are set to zero. In Room B, the reflectivity of ceiling and walls surrounding the windows is 0.8, while the floor has a 0.3 reflectivity. Two perpendicular walls in Room B are covered with bookshelves and filing cabinets with a 0.4 reflectivity. We assumed that, cubical office partitions either absorb or block signals. Furthermore, several tables and chairs are placed in the room with a 0.3 reflectivity. The complicated environment in Room B results in shadowing created by physical partitions and low reflectivity objects. To model the reflections in the two rooms considered, the room reflecting surfaces were divided into a number of equal reflection elements. These reflective elements were modelled as Lambertian reflectors. Up to second-order reflections were considered.

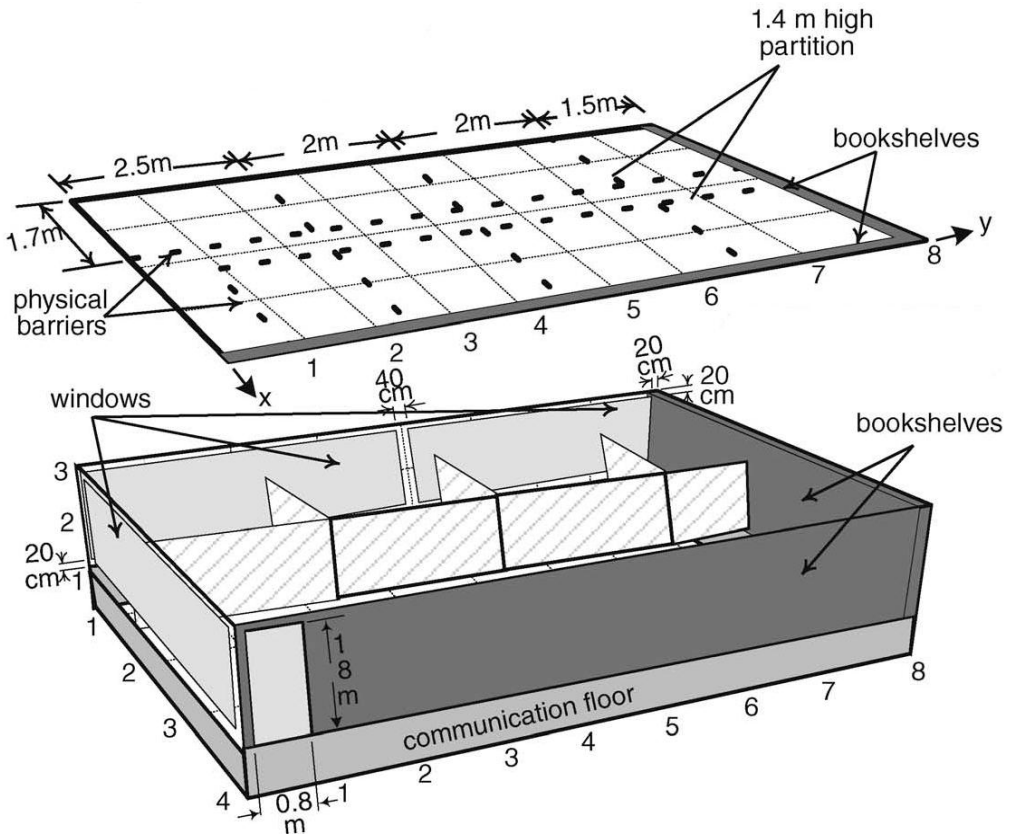

Figure 5-1: A real environment office that has three large glass windows, a door, a number of rectangular-shaped cubicles with surfaces parallel to the room walls, and other furniture such as bookshelves and filing cabinets

An OW simulation package, similar to the one used in the previous chapter, where transmit power adaptation is implemented, was developed. Results were obtained at several receiving positions within the complicated room considered, where the transmitters are placed at three different locations on the CF: (2m, 4m, 1m), (1m, 1m, 1m), and (2m, 7m, 1m) and a total transmit power of 1 W is used. Eight directive lamps (described in the previous chapters) represented the ambient light noise, and allowed BN impairments to be taken into account. A diversity receiver with seven photodetector branches, designed and used in Chapter 3, is employed here in order to reduce the effect of background noise and multipath dispersion. A photodetector with a photosensitive area of 1 cm^2 and a responsivity of 0.5 A/W is used. The performance under a mobile adaptive multibeam transmitter was evaluated and compared at different receiver locations on the CF.

5.3. Performance Evaluation of the Adaptive Spot-Diffusing Systems

In this section, we investigate multipath propagation effects on two room configurations taking into account several types of obstacles that might be seen in real environments. Comparisons are also given for two OW systems (LSMS and ALSMS with diversity receivers) in terms of delay spread and SNR. The 'select best' (SB) diversity approach is considered for processing the received optical signals where the detector that has the highest SNR is chosen.

5.3.1. Delay Spread

Figs. 5.2 (a) and (b) compare the delay spread distribution of two mobile OW systems (LSMS and ALSMS) with an angle diversity receiver in the two room

scenarios (Rooms A and B), when the transmitter is placed at three different positions (2m, 4m, 1m), (1m, 1m, 1m), and (2m, 7m, 1m), and the receiver moves at constant x = 1 m and x = 2 m respectively, and along the y-axis over the CF. It can be seen that the LSMS in Room B has a lower delay spread compared to the LSMS in Room A when the transmitter is placed at (1m, 1m, 1m) due to the limited range of rays captured by the receiver. This is due to the fact that some rays are blocked by opaque objects, and some spots, which fall on the glass windows (according to the transmitter location), are lost. Note that the reduction in delay spread here is accompanied by a reduction in collected power and therefore the SNR is a better measure of performance. Moreover, the delay spread of the mobile LSMS increases, as the receiver moves away from the transmitter in Rooms A and B, and reaches almost 6 ns and 2.4 ns respectively at one of the least successful locations when the transmitter is placed at (1m, 1m, 1m) and the receiver is at (2m, 7m, 1m). The effect of the windows (reflection coefficients are set to zeros) and bookshelves (reflection coefficients = 0.4) is manifest as a loss in delay spread symmetry in the room. This symmetry is seen in Room A, when the transmitter is located at (1m, 1m, 1m) and (2m, 7m, 1m) and the receiver moves at constant x = 1 m, x = 2 m, and along the y-axis over the CF. Our results indicate that a significant reduction in the delay spread is achieved by utilising an adaptive mobile multibeam transmitter in both rooms (Rooms A and B). This is due to assigning the majority of the transmitted power to the spots nearest to the receiver resulting in high direct path contribution and low contribution of reflections. The ALSMS delay spread in Room B, which represents a shadowed environment, is lower than that associated with Room A. This is due to a number of rays being blocked by opaque objects such as, office cubicles, and bookshelves in the environment considered (Room B). It should be noted that the

reduction in the ALSMS delay spread, due to signal obstruction, comes with a reduction in the received power, hence, degradation in the SNR, see Figs. 5.3 (a) and (b). Furthermore, the degradation in the delay spread of the mobile OW system, due to user mobility, is reduced by employing the adaptive multibeam transmitter configuration in conjunction with diversity detection at all transmitter and receiver locations in the worst reception environment where shadowing is created. This improvement in the delay spread is reflected as an increase in the channel bandwidth, which is one of the factors that can help increase the per-user achievable data rate (as shown in Chapter 4), or enable multi-user capabilities, see Section 5.4.

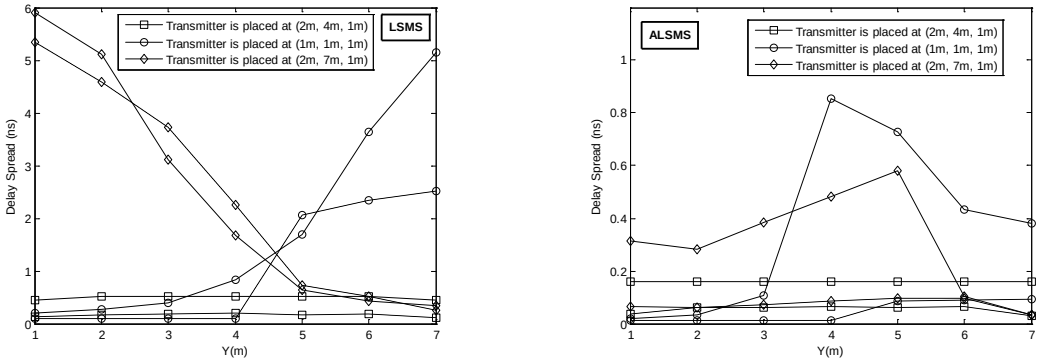

(a)

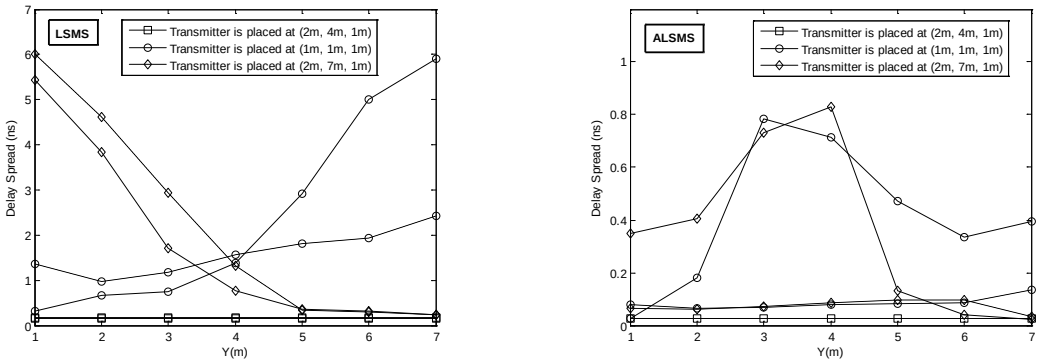

(b)

Figure 5-2: Delay spread distribution of two mobile OW systems (LSMS and ALSMS) in the two room scenarios (Rooms A and B); solid lines represent the delay spread in Room A, dotted lines represent the delay spread in Room B, when the transmitter is placed at three different positions and the receiver moves at constant: (a) x = 1 m, (b) x = 2 m, and along the y-axis

5.3.2. SNR

SNR results are reported based on pulse propagation simulations. The pulse response was found through convolution of the impulse response with a rectangular pulse of 20 ns duration, which corresponds to a 50 Mbit/s bit rate. The received pulse shapes corresponding to the configurations studied were considered in calculating P_{s0} and P_{s1}, the powers associated with logic 0 and 1 respectively. The conventional OOK BER, BER_{OOK} of the indoor mobile OW communication system was calculated using (3.26). Three types of noise are considered in this chapter including receiver noise, that is normally generated in the pre-amplifier components, σ_{pr}, background light induced shot noise σ_{bn}, and shot noises σ_{s0} and σ_{s1} associated with P_{s0} and P_{s1} respectively. This signal-dependent noise σ_{si} is very small, and can be neglected. Two pre-amplifiers were used in this study. For the MC-CDMA system the pre-amplifier used is the PIN-FET design proposed by Kimber et al. [180]. This pre-amplifier has a noise current spectral density of $10\,\mathrm{pA}/\sqrt{\mathrm{Hz}}$ and a bandwidth of 10 GHz. A bit rate of 50 Mbit/s was assumed. The MC-CDMA system requires a bandwidth of 3.25 GHz (64 subcarriers sent at the data rate, see Section 5.4) and the pre-amplifier bandwidth can be limited to this value (or just higher), through the use of an appropriate filter. The impact of this filter on the signal is minimal (bandwidth > 3.25 GHz) and is not considered here. The pre-amplifier used for the 50 Mbit/s OOK system (20 ns pulse duration) is the 70 MHz PIN-BJT design proposed by Elmirghani et al. [22] with noise spectral density of $2.7\,\mathrm{pA}/\sqrt{\mathrm{Hz}}$. This receiver will introduce little or no distortion onto the 50 Mbit/s pulse stream. The use of two different pre-amplifiers is fairer than comparing both systems (OOK and MC-CDMA) based on the larger bandwidth pre-amplifier, (which introduces

unnecessarily large noise to OOK systems, even if its bandwidth is limited through post filtering - note the higher noise power spectral density (PSD) of the 10 GHz receiver, even in the flat low frequency part). In this study we have used an equal detector area (1 cm^2) for the 70 MHz receiver (OOK) and the 10 GHz receiver (MC-CDMA). We believe that a fairer comparison is achieved by using equal detector area in both receivers, than comparing the two systems based on unequal detector areas. This issue was previously explained in Chapter 4, Section 4.4.4. Furthermore, the 10 GHz receiver collection area is varied between 0.1 cm^2 and 1 cm^2 to show the impact on the two systems, (the performance penalty versus collection area trend is shown in Fig. 4.6). With a detection area of 1 cm^2 (for both OOK and MC-CDMA systems), and a BER of 10^{-9}, the MC-CDMA system requires an SNR of 9 dB less than the OOK system, see Fig. 5.5. Reducing the receiver collection area from 1 cm^2 to 0.4 cm^2 incurs an 8 dB power penalty due to a reduction in the received optical power, while an SNR degradation of 10 dB is induced when the detector area is set to 0.3 cm^2, see Fig. 4.6. This means that at a detector area of 0.4 cm^2, the MC-CDMA still requires an SNR of 1 dB less than the OOK system using 1 cm^2 detection area. However, with a detector area of 0.35 cm^2, the two systems require the same SNR, which defines the crossover point. The pre-amplifiers shot noise is given by

$$\sigma_{pr_{OOK}} = 2.7 \times 10^{-12} \times \sqrt{BW_{OOK}}\,, \tag{5.1}$$

$$\sigma_{pr_{MC-CDMA}} = 10 \times 10^{-12} \times \sqrt{BW_{MC-CDMA}}\,, \tag{5.2}$$

where BW_{OOK} and $BW_{MC-CDMA}$ are the receiver bandwidths associated with OOK and MC-CDMA systems respectively. The background noise σ_{bn} can be calculated as

$$\sigma_{bn_{OOK}} = \sqrt{2 \times q \times P_{bn} \times R \times BW_{OOK}}\,, \tag{5.3}$$

$$\sigma_{bn_{MC-CDMA}} = \sqrt{2 \times q \times P_{bn} \times R \times BW_{MC-CDMA}}\,, \tag{5.4}$$

where q and P_{bn} are the electron charge and the received background optical power respectively.

Figs. 5.3 (a) and (b) illustrate the detected SNR of the mobile ALSMS OW system in conjunction with an angle diversity receiver in the two room scenarios (Rooms A and B) when the transmitter is placed at three different positions (1m, 1m, 1m), (2m, 4m, 1m), and (2m, 7m, 1m), and the receiver moves along the x = 1 m and x = 2 m lines respectively. A comparison of the LSMS SNR performance is also included.

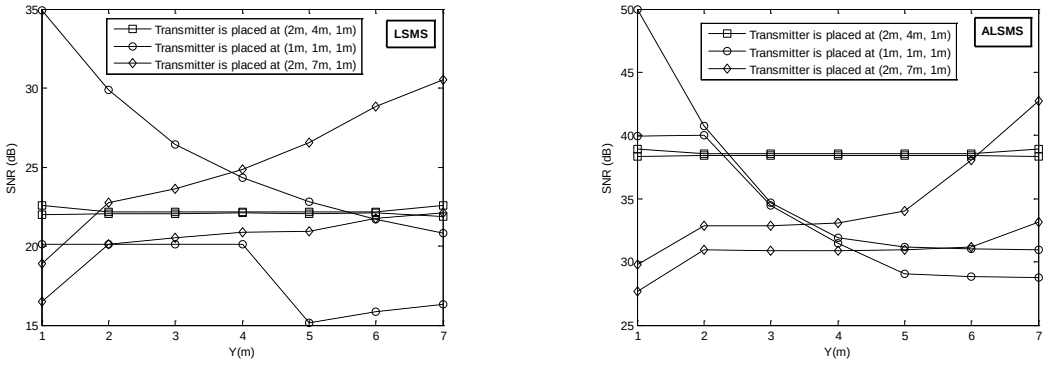

(a)

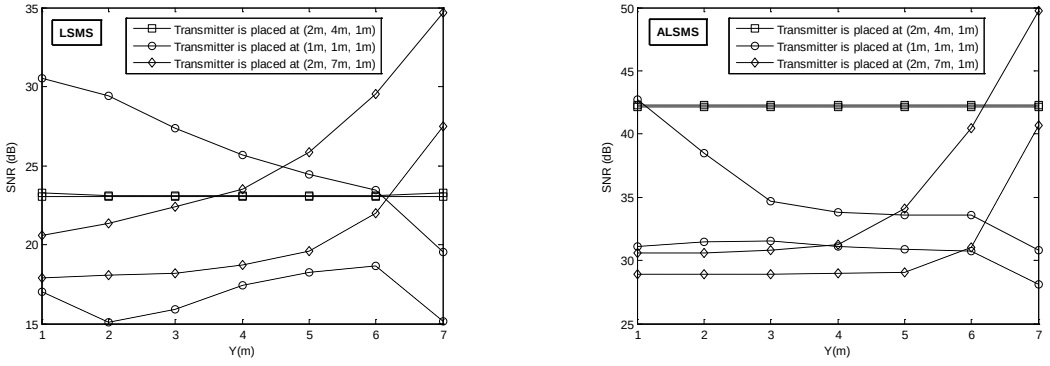

(b)

Figure 5-3: SNR of two mobile OW systems (LSMS and ALSMS) in two room scenarios (Rooms A and B); solid lines represent the SNR in Room A, dotted lines represent the SNR in Room B, when the transmitter is placed at three different positions and the receiver moves at constant: (a) x = 1 m, (b) x = 2 m, and along the y-axis

The results show that the SNR assumes its maximum value at positions where the transmitter and receiver are nearest each other, and degrades as the receiver moves away from the transmitter. Our results show a significant degradation in the performance of the mobile LSMS OW system, due to the reduction in the total received power as a result of shadowing in Room B, which represents a poor communication environment at all transmitter and receiver locations. The SNR performance in Room A (an empty room) shows reciprocal symmetry when the transmitter is placed at (1m, 1m, 1m) and (2m, 7m, 1m) and the receiver assumes one of 7 positions in each case. This symmetry is lost in Room B, with performance degradation as a result of having windows in two perpendicular walls and having bookshelves on the other two walls, yielding a reduction in reflections. The effect of windows can be evidently seen as a significant SNR degradation of 15 dB approximately in the LSMS SNR when the transmitter and receiver are co-located at the corner of the room (1m, 1m, 1m). This SNR degradation can be reduced to about 10 dB when beam power adaptation is implemented. The 10 dB SNR degradation in the shadowed ALSMS SNR (compared to that produced in Room A) is attributed to the inability of the adaptive multibeam transmitter to assign higher power levels to the spots, that are located on the wall adjacent to the receiver, due to the existence of windows, and instead, the majority of the power is allocated to the ceiling spots near the receiver. Furthermore, in the presence of shadowing, a significant SNR improvement of 14 dB is achieved when the ALSMS replaces LSMS at the least successful position when the transmitter is placed at (1m, 1m, 1m) and the receiver is at (2m, 7m, 1m). Note that the LSMS outperforms the CDS and the conventional hybrid system (CHS) [101]. The adaptive technique provides a significant reduction in the performance degradation due to user mobility and optical signal blockage (that

are caused by the presence of windows, office cubicles, and bookshelves in the environment considered).

5.4. OW MC-CDMA System Model

The OW MC-CDMA transmitter and receiver are shown in Fig. 5.4. We assume that there are K simultaneous active users, each utilising N subcarriers and binary phase shift keying (BPSK) modulation. The MC-CDMA transmitter spreads the original data stream of each user using a given spreading code. Each user (k^{th} user) is assigned a different spreading code $\mathbf{c}^k = \left(c_0^k, c_1^k, ..., c_{N-1}^k\right)^T$ with length N_{code} and chip duration T_c, which is the same as the bit duration T_b. Each chip of a data bit is then modulated on a subcarrier separated from its neighbouring subcarrier by $1/T_b$. These signals can be efficiently modulated and demodulated using Fast Fourier Transform (FFT) devices without substantially increasing the receiver's complexity [170]. In a practical FFT implementation, the modulation and demodulation processes can be operated using a single oscillator, where BPSK modulation is used. It should be noted that the use of a cyclic prefix ensures the orthogonality between carriers. Furthermore, the receiver can perform a complex multiplication per frequency to equalise the channel. The light source can be directly driven by the MC-CDMA symbol after adding an appropriate DC offset to avoid negative values. This DC offset would incur performance degradation, almost 3 dB, which can be mitigated by using the power adaptation method introduced, see Fig. 5.3. The peak to average power ratio (PAPR) analysis of the OW MC-CDMA warrants further study.

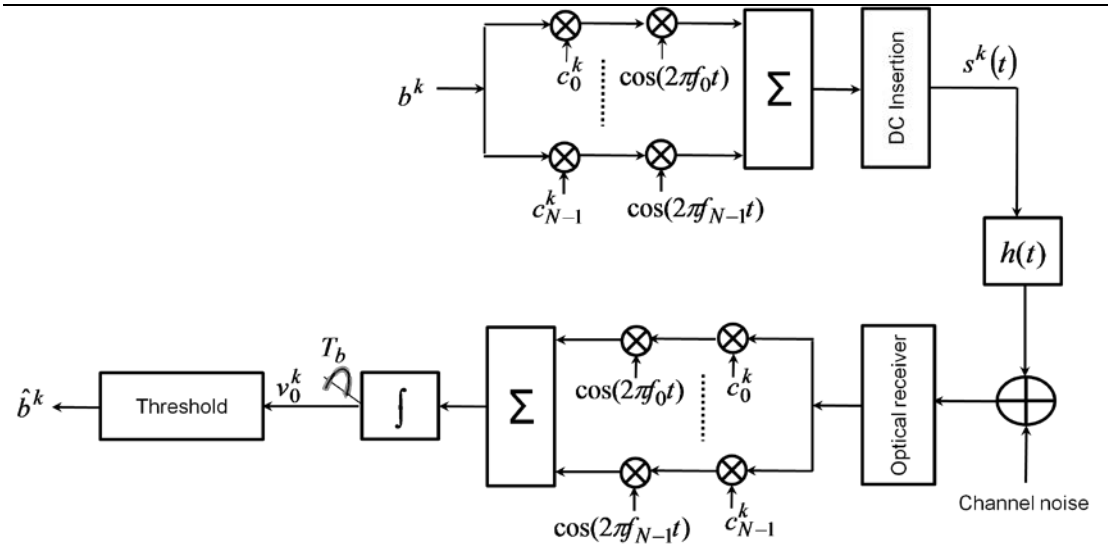

Figure 5-4: Transmitter and receiver models of the OW MC-CDMA system for user k

The transmitted signal corresponding to the m^{th} data bit of the k^{th} user is written as

$$s^k(t) = \sum_{n=0}^{N-1} \sqrt{\frac{P}{N}}\, b_m^k c_n^k \left(1+\cos(2\pi f_n t)\right) \cdot p(t - mT_b) \ , \tag{5.5}$$

where P represents the electrical transmitted power of the data bit, N is the number of subcarriers as well as the spreading gain, b_m^k is the m^{th} data bit of user k, and is assumed to be a random variable taking values of -1 or 1 with equal probability, c_n^k is the n^{th} chip of the spreading code $\mathbf{c}^k = \left(c_0^k, c_1^k, ..., c_{N-1}^k\right)^T$ assigned to user k, which is also assumed to be a random variable taking values of -1 or 1 with equal probability, the term "1" represents the DC shift introduced to avoid negative values, $f_n = n/T_b$ with $n = 0,1,\ldots,N-1$ are the subcarrier frequencies, and $p(\cdot)$ is a rectangular pulse defined over $[0, T_b]$. The signal $s^k(t)$ is proportional to the electrical current which, in turn, is proportional to the transmitted optical power. If the laser transfer characteristics are assumed to be ideal then $s^k(t)$ can be used to represent the transmitted optical power. An exact analysis will have to consider the

laser transfer characteristics, which are not included here. Observe in Fig. 5.4 that this scheme does not include serial-to-parallel conversion and there exists no spreading modulation on each subcarrier. Therefore, the data rate on each of the N sub-carriers is the same as the input data rate. In this MC-CDMA system the subcarrier frequencies are chosen to be 50 % overlapped and orthogonal to each other. The transmission bandwidth required in our case is $(N+1)/T_b$. In [182], Sourour and Nakagawa have shown that significant transmission bandwidth efficiency can be achieved by (serial-to-parallel) converting the bit stream with bit duration T_b into *M* parallel streams with a new bit duration MT_b. When the number of subcarriers increases, the MC-CDMA symbol duration $T_s = NT_c$ becomes large compared to the duration of the impulse response $\tau_{\max}$ of the channel, and the amount of ISI reduces. This transmitted signal $s^k(t)$ is distorted by the channel response and corrupted by noise (channel noise and pre-amplifier noise). The overall noise process is modelled as zero-mean additive white Gaussian noise (AWGN) with two-sided power spectral density $N_0/2$. In the receiver, the received signal is copied and fed to N branches. Each branch is demodulated and multiplied by one chip of the spreading code, and then the branches are summed up and integrated. Finally, the original data may be recovered. The received signal $y(t)$ can be given as

$$y(t) = \sum_{k=0}^{K-1} R\, s^k(t) \otimes h^k(t) + n(t)\ , \tag{5.6}$$

where $n(t)$ is AWGN with two-sided power spectral density $N_0/2$, and $h^k(t)$ is the optical impulse response of the k^{th} user channel which can be represented as [165]

$$h^k(t) = \sum_{\gamma=0}^{\Gamma_{rays}-1} \beta_\gamma^k\, \delta\left(t - \tau_\gamma^k\right), \tag{5.7}$$

where β_γ^k is the gain associated with the γ^{th} ray of the k^{th} user and is received after a delay, τ_γ^k. Γ_{rays} represents the number of received rays. The discretisation is the result of dividing the reflecting surfaces in the room into small elements. Since the positions of the transmitter, receiver, and the reflecting elements are fixed, the received optical power and the delay spread can be considered deterministic for given transmitter and receiver locations. Upon substituting (5.5) and (5.7) into (5.6), the received signal $y(t)$ is given as

$$y(t) = \sum_{k=0}^{K-1}\sum_{n=0}^{N-1}\sum_{\gamma=0}^{\Gamma_{rays}-1}\sqrt{\frac{P}{N}}Rb_m^k c_n^k \beta_\gamma^k \left(1+\cos\left(2\pi f_n\left(t-\tau_\gamma^k\right)\right)\right)\cdot p\left(t-mT_b-\tau_\gamma^k\right)+n(t). \qquad (5.8)$$

5.5. Performance Analysis of OW MC-CDMA System

The aim here is to evaluate the OW MC-CDMA signal-to-noise-and-interference-ratio (SNIR). As such, we derive expressions for the signal, noise and interference powers. In our analysis, we assume that the signal from the first user ($k=0$) is the desired signal and the signals from all other users are interfering signals. We used SB diversity as it results in simple implementation in a practical system. Previous work [96] has compared MRC and SB for the OW OOK system. SB performs slightly worse than MRC, but is simpler. In considering the first user as the reference user, with coherent demodulation, the decision variable v_0 of the m^{th} data bit of the first user is given by

$$v_0 = \frac{1}{T_b}\int_{mT_b}^{(m+1)T_b} y(t)\sum_{n=0}^{N-1} c_n^0 \cos(2\pi f_n t)\,dt, \qquad (5.9)$$

where T_b is the bit duration, and it has been assumed that one data bit is transmitted on all subcarriers, and the receiver is synchronised with the desired user $(k=0)$.

Upon substituting (5.8) for (5.9), and if time synchronisation for user $(k=0)$ is perfect ($\tau^0 = 0, \tau^k \neq 0$), then the decision variable v_0 for $m=0$ can be simplified to

$$v_0 = S + I_1 + I_2 + \eta, \tag{5.10}$$

where S is the desired signal component from the desired user ($k=0$), I_1 is the subcarrier interference between subcarrier f_i in the desired user and the signal components represented by f_i in the other users, I_2 is the equivalent interference among the users subcarriers f_i, $f_j, i \neq j$, and η is the noise component. Each term will be discussed in detail.

A. Signal Component from the desired user, S, and Noise component, η

The first term S is written as

$$S = \sqrt{\frac{P}{N}} \frac{RN}{2} b_0^0 \sum_{n=0}^{N-1} \sum_{\gamma=0}^{\Gamma_{rays}-1} \beta_\gamma^0 . \tag{5.11}$$

The last term η is a zero-mean Gaussian random variable. The variance σ_η^2 can be written as

$$\sigma_\eta^2 = \frac{N_o N}{4T_b}. \tag{5.12}$$

The interference can be written as

$$I = \sqrt{\frac{P}{N}} \frac{R}{T_b} \sum_{k=1}^{K-1} \sum_{n=0}^{N-1} \sum_{l=0}^{N-1} \sum_{\gamma=0}^{\Gamma_{rays}-1} \beta_\gamma^k c_l^0 c_n^k \left[b_{-1}^k L^{(n,l)} + b_0^k R^{(n,l)} \right]. \tag{5.13}$$

The two distinct cases $n=l$ and $n \neq l$ give rise to I_1 and I_2 respectively.

B. Same subcarrier interference component from the other users ($k \neq 0$), I_1

The second term of (5.10) I_1 is the same subcarrier interference from the other users, and can be expressed as

$$I_1 = \sqrt{\frac{P}{N}} \frac{R}{T_b} \sum_{k=1}^{K-1} \sum_{n=0}^{N-1} \sum_{\gamma=0}^{\Gamma_{rays}-1} \beta_\gamma^k c_n^0 c_n^k \left[b_{-1}^k L^{n=l} + b_0^k R^{n=l} \right], \tag{5.14}$$

where

$$\begin{aligned} L^{n=l} &= \int_0^{\tau_\gamma^k} \left(1 + \cos\left(2\pi f_n \left(t - \tau_\gamma^k\right)\right)\right) \cos\left(2\pi f_n t\right) dt \\ &= \frac{1}{2\pi f_n} \sin\left(2\pi f_n \tau_\gamma^k\right) + \frac{\tau_\gamma^k}{2} \cos\left(2\pi f_n \tau_\gamma^k\right) \end{aligned} . \tag{5.15}$$

$$\begin{aligned} R^{n=l} &= \int_{\tau_\gamma^k}^{T_b} \left(1 + \cos\left(2\pi f_n \left(t - \tau_\gamma^k\right)\right)\right) \cos\left(2\pi f_n t\right) dt \\ &= -\frac{1}{2\pi f_n} \sin\left(2\pi f_n \tau_\gamma^k\right) + \frac{\left(T_b - \tau_\gamma^k\right)}{2} \cos\left(2\pi f_n \tau_\gamma^k\right) \end{aligned} . \tag{5.16}$$

We treat the information bit b_m^k and the delay time τ_γ^k of each user as mutually independent random variables. Then, I_1 can be considered as a Gaussian random variable with zero-mean and variance, $\sigma_{I_1}^2$ written as

$$\sigma_{I_1}^2 = \frac{PR^2}{NT_b^2} N(K-1) \sum_{n=0}^{N-1} \sum_{\gamma=0}^{\Gamma_{rays}-1} \left|\beta_\gamma\right|^2 \sum_{n=0}^{N-1} \left(E\left[\left(L^{n=l}\right)^2\right] + E\left[\left(R^{n=l}\right)^2\right] \right), \tag{5.17}$$

where

$$\begin{aligned} E\left[\left(L^{n=l}\right)^2\right] &= \frac{1}{T_b} \int_0^{T_b} \left(\frac{1}{2\pi f_n} \sin\left(2\pi f_n \tau_n^k\right) + \frac{\tau_n^k}{2} \cos\left(2\pi f_n \tau_n^k\right) \right)^2 d\tau_n^k \\ &= \frac{1}{2} \left(\frac{T_b}{2\pi n} \right)^2 + \frac{T_b^2}{24} \end{aligned} . \tag{5.18}$$

$$\begin{aligned} E\left[\left(R^{n=l}\right)^2\right] &= \frac{1}{T_b} \int_0^{T_b} \left(-\frac{1}{2\pi f_n} \sin\left(2\pi f_n \tau_n^k\right) + \frac{\left(T_b - \tau_n^k\right)}{2} \cos\left(2\pi f_n \tau_n^k\right) \right)^2 d\tau_n^k \\ &= \frac{1}{2} \left(\frac{T_b}{2\pi n} \right)^2 + \frac{4T_b^2}{48} \end{aligned} . \tag{5.19}$$

Moreover, as the total power conveyed by the channel's impulse response is normalised so that $E\left\{\sum_{\gamma=0}^{\Gamma-1} \left|\beta_\gamma\right|^2\right\} = 1$, the frequency domain channel response satisfies

$E\left\{\sum_{n=0}^{N-1}\left|H_n\right|^2\right\}=N$ according to the discrete form of Parseval's theorem which can be written as

$$\sum_{n=0}^{N-1}\left|x[n]\right|^2=\frac{1}{N}\sum_{k=0}^{N-1}\left|X[k]\right|^2, \tag{5.20}$$

where $X[k]$ is the discrete Fourier transform (DFT) of $x[n]$, both of length N. After some manipulation, (5.17) can be rewritten as

$$\sigma_{I_1}^2=PR^2N(K-1)\left[\frac{1}{8}+\frac{1}{4\pi^2}\sum_{n=0}^{N-1}\frac{1}{n^2}\right]. \tag{5.21}$$

C. Other subcarrier interference component from the other users ($k\neq 0$), I_2

The third term of (5.10) I_2 is the other subcarrier interference from the other users, and can be expressed as

$$I_2=\sqrt{\frac{P}{N}}\frac{R}{T_b}\sum_{k=1}^{K-1}\sum_{\substack{l=0\\ l\neq n}}^{N-1}\sum_{n=0}^{N-1}\sum_{\gamma=0}^{\Gamma_{rays}-1}\beta_\gamma^k c_l^0 c_n^k\left[b_{-1}^k L^{n\neq l}+b_0^k R^{n\neq l}\right], \tag{5.22}$$

where

$$\begin{aligned}L^{n\neq l}&=\int_0^{\tau_\gamma^k}\left(1+\cos\left(2\pi f_n\left(t-\tau_\gamma^k\right)\right)\right)\cos\left(2\pi f_l t\right)dt\\&=\frac{T_b}{2\pi l}\sin\left(2\pi f_l\tau_\gamma^k\right)+\frac{T_b}{4\pi(n-l)}\left[\sin\left(2\pi f_n\tau_\gamma^k\right)-\sin\left(2\pi f_l\tau_\gamma^k\right)\right]\end{aligned}. \tag{5.23}$$

$$\begin{aligned}R^{n\neq l}&=\int_{\tau_\gamma^k}^{T_b}\left(1+\cos\left(2\pi f_n\left(t-\tau_\gamma^k\right)\right)\right)\cos\left(2\pi f_l t\right)dt\\&=-\frac{T_b}{2\pi l}\sin\left(2\pi f_l\tau_\gamma^k\right)+\frac{T_b}{4\pi(n-l)}\left[\sin\left(2\pi f_l\tau_\gamma^k\right)-\sin\left(2\pi f_n\tau_\gamma^k\right)\right]\end{aligned}. \tag{5.24}$$

I_2 can be considered as a Gaussian random variable with zero-mean and variance $\sigma_{I_2}^2$ given as

$$\sigma_{I_2}^2 = \frac{PR^2}{NT_b^2}(K-1)\sum_{n=0}^{N-1}\sum_{\gamma=0}^{\Gamma_{rays}-1}\left|\beta_\gamma\right|^2\sum_{\substack{l=0\\ l\neq n}}^{N-1}\left(E\left[\left(L^{n\neq l}\right)^2\right]+E\left[\left(R^{n\neq l}\right)^2\right]\right), \tag{5.25}$$

where

$$E\left[\left(L^{n\neq l}\right)^2\right]=\frac{1}{T_b}\int_0^{T_b}\left(\frac{T_b}{2\pi l}\sin\left(2\pi f_l\tau_n^k\right)+\frac{T_b}{4\pi(n-l)}\left[\sin\left(2\pi f_n\tau_n^k\right)-\sin\left(2\pi f_l\tau_n^k\right)\right]\right)^2 d\tau_n^k$$
$$=\frac{1}{2}\left(\frac{T_b}{2\pi l}\right)^2+\left(\frac{T_b}{4\pi(n-l)}\right)^2-\left(\frac{T_b}{4\pi l}\right)\left(\frac{T_b}{4\pi(n-l)}\right) \tag{5.26}$$

$$E\left[\left(R^{n\neq l}\right)^2\right]=\frac{1}{T_b}\int_0^{T_b}\left(-\frac{T_b}{2\pi l}\sin\left(2\pi f_l\tau_n^k\right)+\frac{T_b}{4\pi(n-l)}\left[\sin\left(2\pi f_l\tau_n^k\right)-\sin\left(2\pi f_n\tau_n^k\right)\right]\right)^2 d\tau_n^k$$
$$=\frac{1}{2}\left(\frac{T_b}{2\pi l}\right)^2+\left(\frac{T_b}{4\pi(n-l)}\right)^2+\left(\frac{T_b}{4\pi l}\right)\left(\frac{T_b}{4\pi(n-l)}\right) \tag{5.27}$$

After some manipulation, (5.25) can be rewritten as

$$\sigma_{I_2}^2 = PR^2(K-1)\left[\frac{1}{4\pi^2}\sum_{l=0}^{N-1}\frac{1}{l^2}+\frac{1}{8\pi^2}\sum_{n=0}^{N-1}\sum_{\substack{l=0\\ l\neq n}}^{N-1}\frac{1}{(n-l)^2}\right]. \tag{5.28}$$

Then, the SINR can be obtained as

$$SNIR=\frac{S^2}{\sigma_{I_1}^2+\sigma_{I_2}^2+\sigma_\eta^2}. \tag{5.29}$$

Thus, the BER of the OW MC-CDMA system is obtained as

$$BER=\frac{1}{2}erfc\left(\sqrt{SNIR/2}\right). \tag{5.30}$$

5.6. Theoretical and Simulation Results

In this section, both computer simulation and theoretical results are presented and used to assess the BER performance of the OW MC-CDMA system with multiple active users in an indoor OW channel. The system operated at a data rate of 50 Mbit/s. Orthogonal gold codes are utilised as the signature sequence in our simulated

system. Different codes are assigned to different users. The length of the signature sequence is the same as the number of subcarriers considered which is 64 in both the computer simulation and the theoretical analysis.

5.6.1. Description of the Analytic and Simulation Environments

Analytic performance results were obtained for the OW MC-CDMA system using the analysis in Section 5.5 [110]. The SNIR was evaluated using (5.29) where the signal, interference, and noise are given by (5.11), (5.21), (5.28), and (5.12) respectively. In (5.11), the responsivity is 0.5 A/W and the number of subcarriers is 64. In (5.21), the number of users that is considered is 1, 4, 8, 10, 20 and the subcarrier index *n* takes values of 1, 2, …, 64. In (5.28), the subcarrier indices *n* and l take values of 1, 2, …, 64. In (5.12), the bit duration is 20 ns and $N_0/2$ is the two-sided power spectral density of AWGN.

Computer simulation of a mobile MC-CDMA OW system is carried out in two OW configurations, LSMS and ALSMS with an angle diversity receiver. Two transmitter and receiver locations in each OW configuration are considered; the transmitter is placed at (2m, 4m, 1m) and (1m, 1m, 1m), and the receiver is located at (1m, 1m, 1m) and (2m, 7m, 1m). Comparisons of MC-CDMA LSMS and MC-CDMA CDS systems with a wide FOV receiver are also given. The effect of all the parameters such as the symbol rate, delay spread, transmitter and receiver structures and positions of transmitter and receiver are considered. As shown in Fig. 5.4, at the transmitter, a random serial data of -1 and +1 was generated and spread using an orthogonal gold code sequence which consists of -1, +1 bits. The serially spread data was converted into a parallel data stream to enable parallel transmission with 64

subchannels where each channel was modulated using BPSK modulation. The parallel data was fed to an IFFT processor and the serial output is used for transmission. A DC shift was introduced to avoid negative values, and the transmitted signal was passed through the optical channel (the channel response of the particular OW configuration $h_{conf}(t)$). At the receiver, the received signal is impaired by AWGN (due to the channel and pre-amplifier) at different SNR levels. The corrupted received signal was fed into the FFT circuit where, after processing, the serial data was converted into parallel data. Each column of the parallel data is multiplied by the spreading code, summed up and integrated. Finally, the original data was recovered, and BER performance was evaluated.

Furthermore, a zero forcing (ZF) equalisation technique, which applies channel inversion, was employed to reduce the impact of the channel induced dispersion. Simulation results, with and without using ZF equalisation, were obtained and compared for the OW MC-CDMA systems considered. The results confirm that equalisation, which increases receiver complexity, is not necessary when our new adaptation method is implemented at the bit rate considered. Our non-equalised ALSMS configuration demonstrates significant performance improvement over equalised LSMS and CDS configurations (without transmit power adaptation). Equalisation will, however, become essential if the data rate is further increased in the channel considered.

The performance of the MC-CDMA and the CDMA systems is depicted in Fig. 5.5 in an indoor OW channel based on the LSMS configuration with an angle diversity receiver with multiple active users when both the transmitter and the receiver are co-located at the centre of the room. Fig. 5.5 also compares the performance of these systems to that of the conventional OOK OW system. The results indicate that in a

multi-user scenario, the OW MC-CDMA BER simulation results agree very well with the theoretical BER predictions. The MC-CDMA system provides multiple access facilities compared to OOK and OFDM systems. These facilities are provided at channel rates much lower than those associated with CDMA. Compared to OOK and CDMA systems, the MC-CDMA system offers a significant performance improvement which can be quoted as a reduction in the SNR required at a given BER. For example at a BER of 10^{-4} 7 dB and 10 dB SNR improvements are obtained in a 4-user MC-CDMA OW system compared to a single user OW OOK system and a 4-user OW CDMA system respectively.

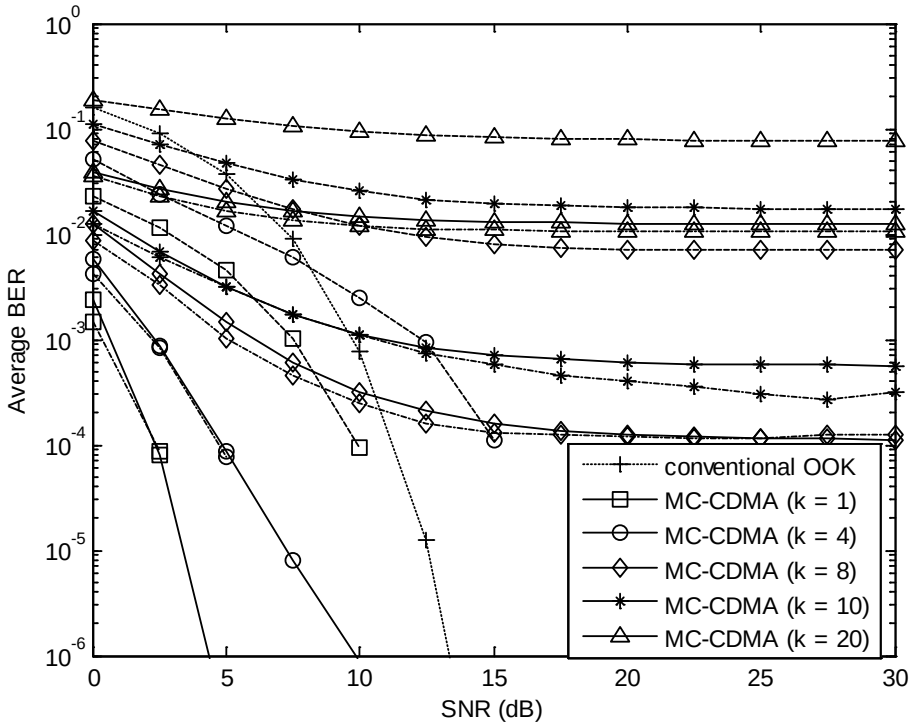

Figure 5-5: BER of the MC-CDMA system and the CDMA system with multiple active users over an indoor OW channel at different SNR levels; compared to the BER performance of the conventional OOK system. Solid lines represent the theoretical results of the OW MC-CDMA system, dashed lines represent the simulation results of the OW CDMA system, and dot-dashed lines represent the simulation results of the OW MC-CDMA system

It should be observed that the performance degrades gradually as the number of users increases due to the increase in multiple access interference (MAI). Simulation results of both OW MC-CDMA and OW CDMA systems using an orthogonal gold code sequence are demonstrated over LSMS configuration with an angle diversity receiver, which is placed in the centre of the room, throughout Room A.

5.6.2. Effect of Delay Spread, Transmitter and Receiver Structures, and Positions of Transmitter and Receiver on the OW MC-CDMA BER

In this section, we compare the BER of several OW systems (CDS, LSMS with a single wide FOV receiver, LSMS and ALSMS with diversity receivers) characterised by different channel delay spreads. The results indicate that the BER performance depends on the symbol rate, delay spread, transmitter and receiver structures, and positions of transmitter and receiver.

Figs. 5.6 (a) and (b) illustrate the BER (simulation results) of three OW MC-CDMA systems: MC-CDMA CDS and MC-CDMA LSMS with a single wide FOV receiver and MC-CDMA in conjunction with an angle diversity receiver in Room A with 8 and 10 users respectively. The BER results quoted are obtained at two receiver locations of (2m, 4m, 1m) and (1m, 1m, 1m) when the transmitter is placed at the room centre (2m, 4m, 1m). The MC-CDMA LSMS system with an angle diversity receiver at the room centre (2m, 4m, 1m) demonstrates the best BER performance over MC-CDMA LSMS system and MC-CDMA CDS system with a single wide FOV receiver at all receiver positions. This is due to the fact that the MC-CDMA LSMS system, based on an angle diversity receiver at the best successful receiver position (the centre of the room), has a minimum delay spread which is small, compared to the OW MC-CDMA symbol duration, the amount of ISI is low.

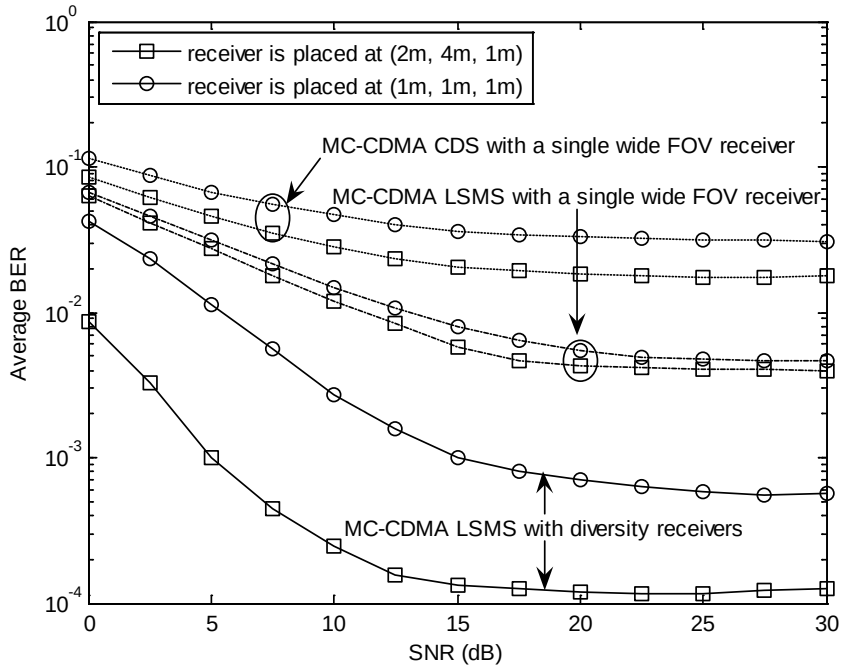

(a)

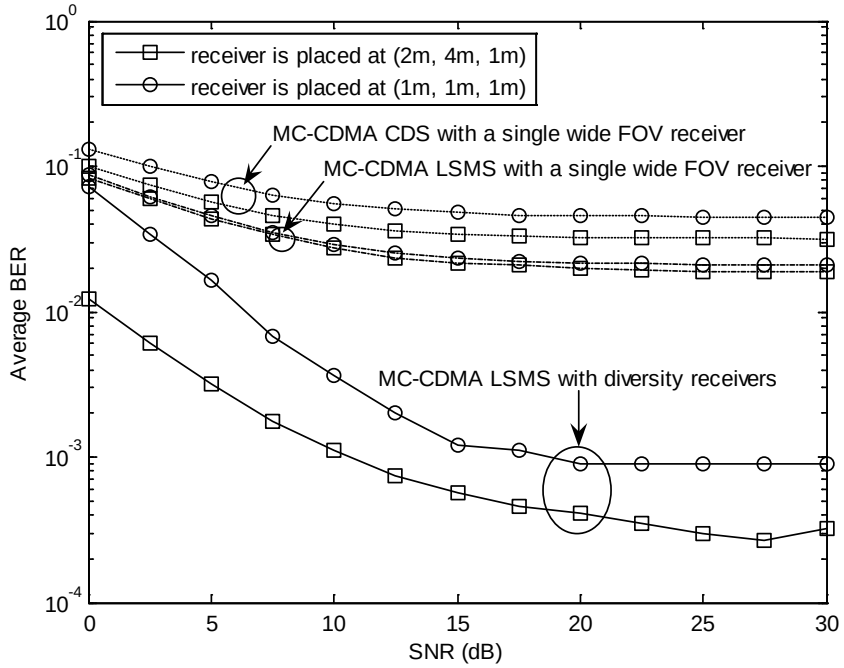

(b)

Figure 5-6: BER of three OW MC-CDMA systems: MC-CDMA CDS and MC-CDMS LSMS with a single wide FOV receiver and MC-CDMA with an angle diversity receiver at two receiver positions; (2m, 4m, 1m) and (1m, 1m, 1m) when the transmitter is placed at the room centre (2m, 4m, 1m) in Room A with multiple users: (a) 8 users and (b) 10 users

Replacing the single wide FOV receiver by an angle diversity receiver in the MC-CDMA LSMS system improves BER by almost an order of magnitude. At a BER of 10^{-2}, an 8-user MC-CDMA angle diversity LSMS system calls for an SNR that is 7.5 dB lower than that required for an 8-user MC-CDMA system based on LSMS with a wide FOV receiver. This is attributed to the significant reduction in the delay spread, from 1.1 ns to 0.45 ns, as a result of limiting the range of rays captured through the diversity scheme.

Fig. 5.7 (a) shows the BER (simulation results) of two mobile OW MC-CDMA systems: MC-CDMA LSMS and MC-CDMA ALSMS with an angle diversity receiver in Room A, at two transmitter locations of (2m, 4m, 1m) and (1m, 1m, 1m) and two receiver locations of (1m, 1m, 1m) and (2m, 7m, 1m) with 10 users. The results show that the BER performance of the mobile OW MC-CDMA system degrades with increase in the delay spread associated with transmitter and receiver locations. In a 10-user mobile MC-CDMA LSMS system, a BER improvement of almost an order of magnitude is obtained as a result of reduction in the delay spread by a factor of 20, approximately, based on moving the receiver from (2m, 7m, 1m) toward the transmitter location of (1m, 1m, 1m). Also, at a BER of 10^{-3} a 7 dB SNR improvement is obtained as the delay spread reduces from 0.45 ns to 0.2 ns when the transmitter moves from (2m, 4m, 1m) toward the receiver position of (1m, 1m, 1m). Furthermore, the mobile MC-CDMA ALSMS system demonstrates an enhanced BER performance, compared to the mobile MC-CDMA LSMS system, at all transmitter and receiver locations within the two rooms considered with multiple active users. At an SNR of 15 dB, for example, the mobile MC-CDMA ALSMS system offers a BER improvement from 1.2×10^{-2} to 3.8×10^{-5} over the mobile MC-CDMA LSMS system at transmitter-receiver separation of 6 m with 10 active users.

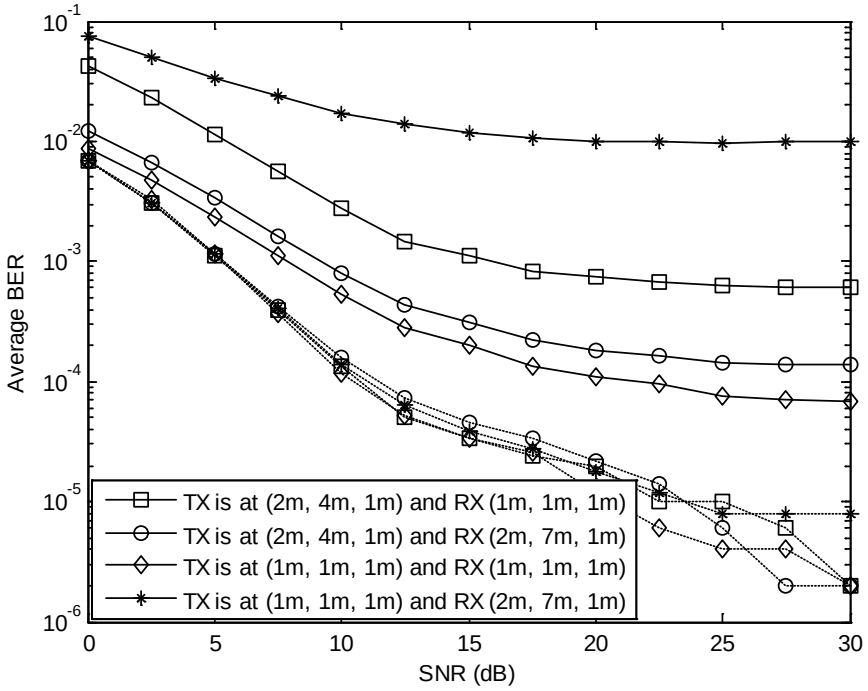

(a)

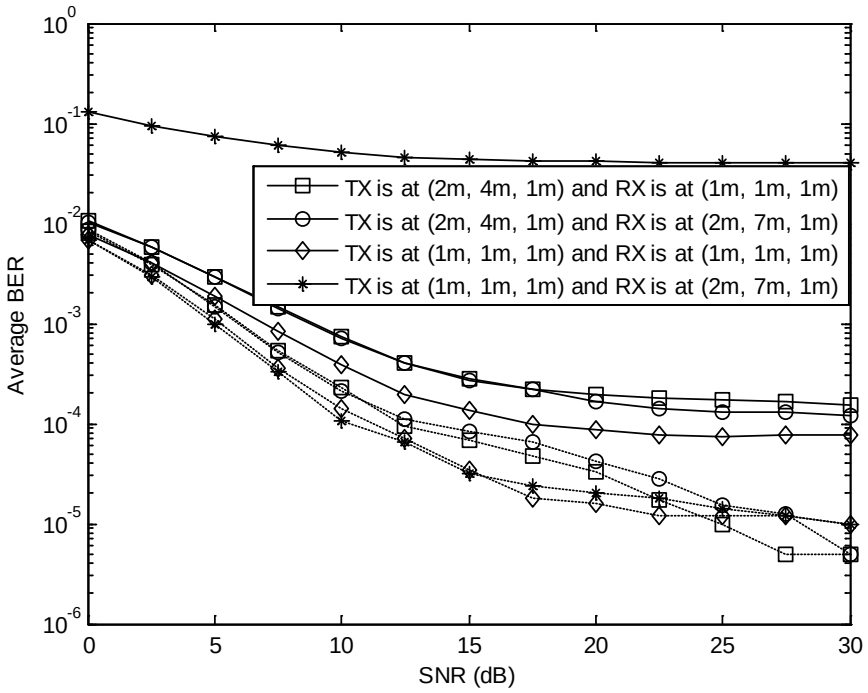

(b)

Figure 5-7: BER of two mobile OW MC-CDMA systems (MC-CDMA LSMS and MC-CDMS ALSMS), at different transmitter and receiver positions with 10 active users in the two room scenarios: (a) Room A and (b) Room B. Sold lines represent the MC-CDMA LSMS system and dotted lines represent the MC-CDMA ALSMS system

This is due to assigning high power levels to spots nearest to the receiver, which significantly improves the BER as a result of the delay spread reduction. A comparison of the BER performance (simulation results) of both systems (MC-CDMA ALSMS and MC-CDMA LSMS systems), under a highly impaired environment (Room B) with 10 active users, is shown in Fig. 5.7 (b). At transmitter and receiver locations of (1m, 1m, 1m) and (2m, 7m, 1m) and at an SNR of 10 dB, the BER improves from 5.12×10^{-2} to 1×10^{-4} when our new ALSMS replaces the multi-spot LSMS technique, in a 10-user MC-CDMA system in Room B where shadowing exists.

Fig. 5.8 shows the BER performance (simulation results) of three mobile OW MC-CDMA systems: mobile MC-CDMA CDS system, mobile MC-CDMA LSMS system and mobile MC-CDMA ALSMS system in Room A, when the transmitter and receiver are co-located at (1m, 1m, 1m) with 20 active users. Results are quoted with and without using the ZF equalisation technique. A significant improvement in BER performance is observed in all the mobile OW MC-CDMA systems considered when ZF equalisation is applied. For example, at an SNR of 20 dB the BER improves from 6.62×10^{-2} to 2.7×10^{-3} and from 1.9×10^{-3} to 1×10^{-4} in a 20 user mobile MC-CDMA CDS and LSMS systems respectively, when ZF equalisation is implemented. In contrast, a slight BER improvement is achieved in a 20 user mobile MC-CDMA ALSMS system by employing ZF equalisation. This is due to the large bandwidth of the ALSMS channel, almost 7 GHz, which can accommodate the MC-CDMA stream which requires a bandwidth of 3.25 GHz. This result confirms that equalisation, which increases the receiver complexity, is not necessary when our new adaptation method is implemented at the data rate and system parameters considered. Furthermore, at an SNR of 10 dB our non-equalised MC-CDMA ALSMS system

achieves a BER of 7×10^{-4} in a 20 user scenario compared to a BER of 1×10^{-1} when MC-CDMA CDS is considered. In addition, performance degradation is observed at lower SNR values in a ZF OW MC-CDMA system attributed to the noise enhancement.

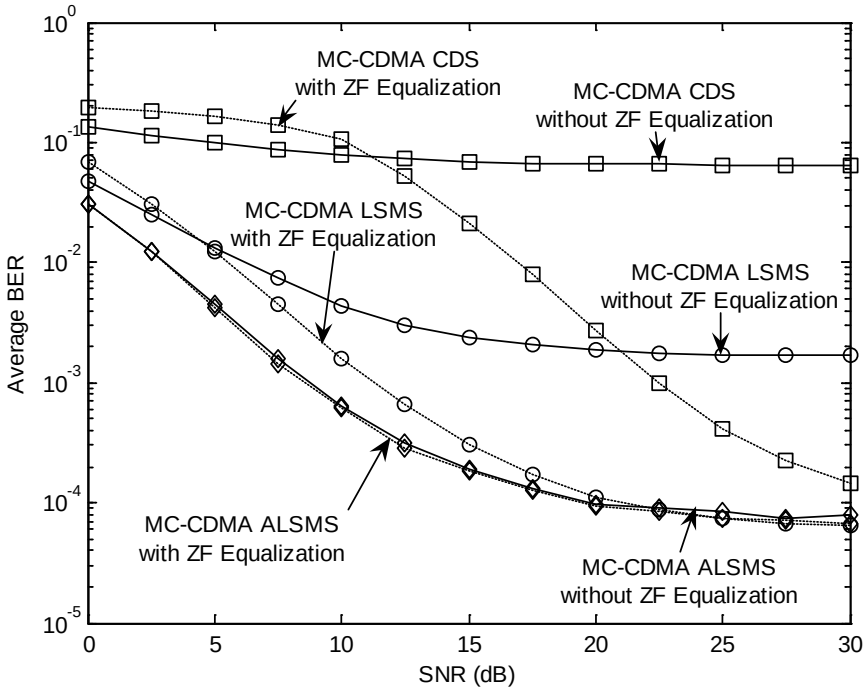

Figure 5-8: BER of three mobile OW MC-CDMA systems with and without zero forcing (ZF) equalisation, when the transmitter and receiver are co-located at the room corner (1m, 1m, 1m) with 20 users

5.6.3. Effect of SNR on the OW MC-CDMA BER

In this section, we consider the effect of SNR on the BER of the OW MC-CDMA, and show simulation results of BER versus receiver locations. The results clearly show that the OW MC-CDMA system performance is a function of the channel characteristics (delay spread and SNR which are position dependent), and on transmitter and receiver structures which affect both.

Fig. 5.9 (a) compares the BER of the mobile MC-CDMA LSMS system with an angle diversity receiver in two room scenarios (Rooms A and B). Meanwhile, Fig. 5.9 (b) shows the BER of the mobile OW MC-CDMA system for the case of LSMS and ALSMS over the worst communication environment (Room B), when the transmitter is placed at (1m, 1m, 1m) in the corner of the room, and the receiver moves along the x = 1 m line with multiple users. The results in Fig. 5.9 (a) show a reduction in the BER of the mobile MC-CDMA LSMS system in Room B, which is a poorer communication environment, compared to Room A, for example, with 4 active users and at y = 1 m (i.e. the transmitter and receiver are co-located in the corner of the room) the BER degrades from 9×10^{-6} to 7.6×10^{-2}. This BER degradation is a result of some spots being absorbed by windows and some rays being blocked by opaque objects such as office cubicles, and bookshelves in the environment considered. This drop in the BER can be significantly improved from 7.6×10^{-2} to 4.6×10^{-8} when beam power adaptation is employed, due to the strong received power based on assigning higher powers to spots nearest to the receiver. Fig. 5.9 also shows that the presence of cubicles and the shadowing introduced have a larger impact on the MC-CDMA LSMS system. These effects are significantly reduced through transmit power adaptation in MC-CDMA ALSMS system. The results show that the BER improvement in the mobile MC-CDMA ALSMS system over the mobile MC-CDMA LSMS system with 20 users is lower than the improvement with 4 users. This is due to the fact that the amount of MAI is markedly high compared to the BN influence when many users access the system.

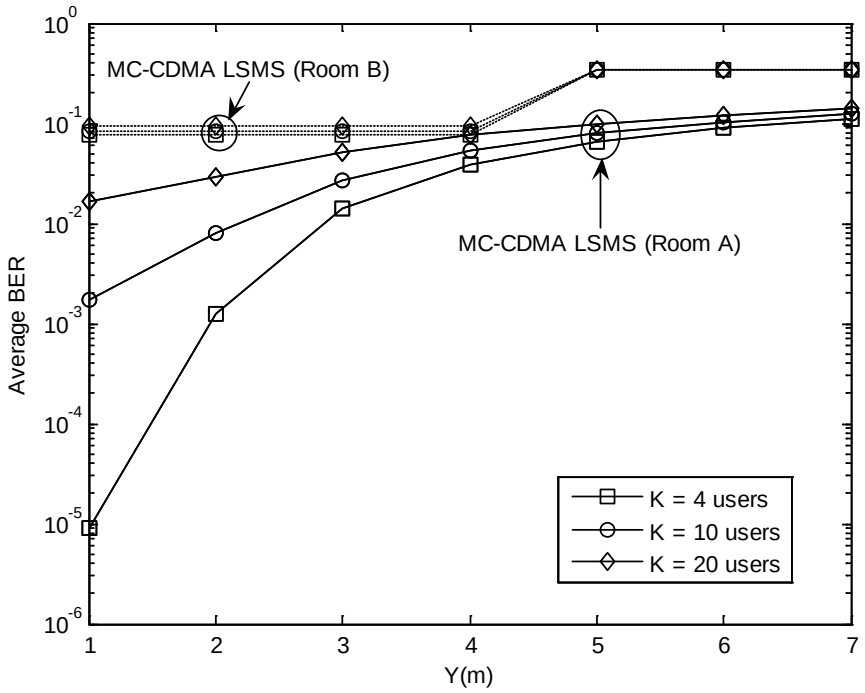

(a)

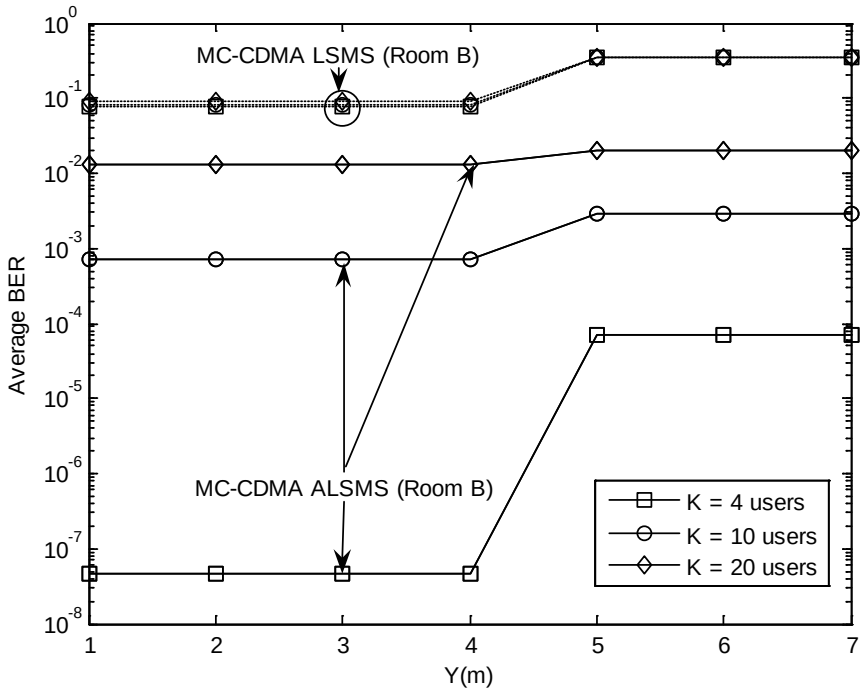

(b)

Figure 5-9: BER of the mobile OW MC-CDMA system with an angle diversity receiver for the case of LSMS and ALSMS, when the transmitter is placed in the corner of the room (1m, 1m, 1m), and the receiver moves at constant x = 1 m , and along the y-axis with multiple users; (a) compares the mobile LSMS MC-CDMA system for Room A and B, (b) compares the mobile MC-CDMA ALSMS system and MC-mobile CDMA LSMS over a real indoor environment (Room B)

Figs. 5.10 (a) and (b) illustrate the BER (simulation results) of the MC-CDMA CDS and ALSMS systems when the transmitter is placed at two positions of (1m, 1m, 1m) and (2m, 4m, 1m) respectively, and the receiver moves along the x = 1 m line in Room A in a multi-user scenario. The results show that a BER improvement from 5×10^{-1} to 5×10^{-10} is achieved in a 4-user mobile OW MC-CDMA system when our new ALSMS replaces the CDS at transmitter and receiver locations of (2m, 4m, 1m) and (1m, 1m, 1m). This is due to the fact that the mobile MC-CDMA ALSMS system, with an angle diversity receiver, takes advantage of beam power adaptation among the spots to maximise the receiver SNR and increase the bandwidth.

5.7. Summary

The use of OW MC-CDMA is proposed for the first time as a method that can provide multiple access facilities suited to the limited bandwidth in OW systems. Performance improvement was achieved by using an MC-CDMA system, compared to the conventional OOK system and OW CDMA system. For example, at an error rate of 10^{-4}, a 4-user MC-CDMA optical wireless system calls for an SNR that is 7 dB and 10 dB lower than that needed for a single user OW OOK system and a 4-user OW CDMA system respectively. The improvement obtained in other conditions has been evaluated and reported. BER analysis of the MC-CDMA system with multiple active users in an indoor OW channel was performed and reported. There is a reduction in performance when the number of active users increases due to the increase in MAI. This is mainly due to the behaviour of our MC-CDMA system as shown in (5.29). At low received powers, the receiver noise dominates and SNIR improves by increasing the signal power leading to a reduction in BER as shown in Fig. 5.5. At large signal powers, interference dominates and the BER curves saturate.

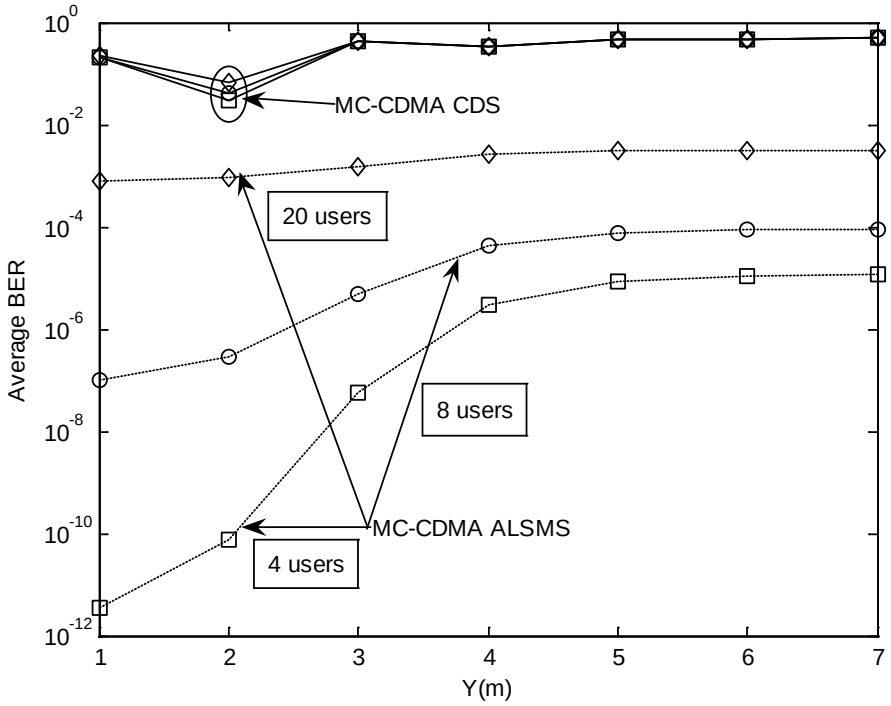

(a)

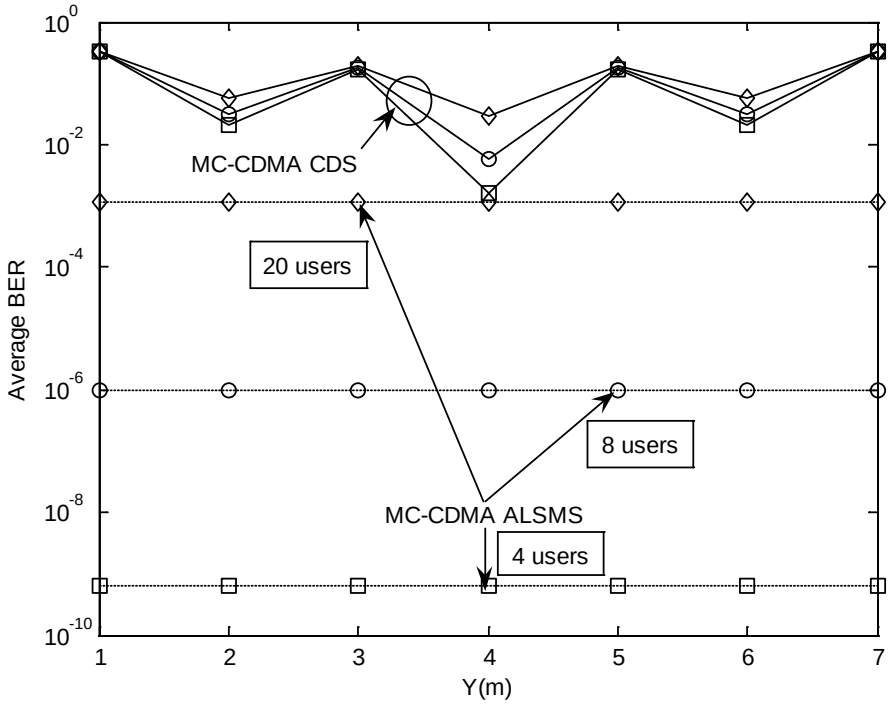

(b)

Figure 5-10: BER of two mobile OW MC-CDMA systems: MC-CDMA CDS and MC-CDMA ALSMS, when the transmitter is placed at two positions: (1m, 1m, 1m) and (2m, 4m, 1m), and the receiver moves along the x = 1 m line in Room A with multiple users

An adaptive LSMS system has been proposed, studied and shown to be a desirable means for improving the performance of mobile OW MC-CDMA systems in a highly impaired environment where shadowing exists. Degradation in the BER from 9×10^{-6} to 7.6×10^{-2} is observed in a 4-user mobile MC-CDMA LSMS system, due to the low received power as a result of the presence of windows, office cubicles, and bookshelves in the environment considered. This BER degradation is significantly reduced from 7.6×10^{-2} to 4.6×10^{-8} through transmit power adaptation. In addition, ZF equalisation was employed to mitigate multiple access interference as well as improve the BER performance of the OW MC-CDMA system. The results confirm that an equalisation scheme, which increases receiver complexity, is not necessary when our new adaptation method replaces standard CDS or LSMS at the data rate and channel conditions considered.

6. PERFORMANCE EVALUATION OF 2.5 GBIT/S AND 5 GBIT/S OPTICAL WIRELESS SYSTEMS EMPLOYING A TWO DIMENSIONAL ADAPTIVE BEAM CLUSTERING METHOD AND IMAGING DIVERSITY DETECTION

6.1. Introduction

Mobile OW systems are significantly affected by the presence or absence of a LOS component which hugely influences the amount of received power. The latter also varies with the distance between the diffusing spot and the receiver. Due to this fact, an adaptive technique (which was introduced in Chapter 4) is employed here to enhance the received optical power at a given receiver location, and also to reduce the performance degradation due to mobility. The purpose of our adaptation method (as indicated in Chapter 4) is to optimise the power levels among the spots to maximise the receiver SNR in the presence of a single transmitter and a single receiver at different locations (i.e., under transmitter and/or receiver mobility).

A useful observation is that the diffuse signal reaches the receiver from a multitude of directions, whereas the noise in an indoor environment tends to be directional. Therefore, diversity receivers can be beneficially employed. The performance improvements achieved by non-imaging angle diversity receivers have been studied [33, 38, 44-47]. Although an improvement in performance was achieved, the proposed implementation which requires a separate optical concentrator for each receiving element is excessively bulky and costly. An appropriate technique that can provide robustness against ambient light noise and multipath dispersion as well as improve the system performance is an imaging receiver [93-94, 98]. It was reported that multibeam transmitters and imaging receivers can reduce the required transmit power by more than 20 dB [94]. The imaging receiver offers two advantages over a non-imaging angle diversity receiver. Firstly, all photodetectors share a common

imaging concentrator, reducing the size and cost. Secondly, all the photodetectors can be laid out in a single planar array which facilitates the use of a large number of photodetector pixels, leading to enhanced performance.

Previous indoor mobile optical wireless systems operated typically at 30 Mbit/s to 100 Mbit/s and here we report on systems that operate at 2.5 Gbit/s and 5 Gbit/s. We are able to achieve these improvements through the introduction of three new approaches: transmit beam power adaptation, a two-dimensional beam clustering method (2DBCM), and diversity imaging. Through channel and noise modelling we evaluated the performance of our systems. The performance of a novel OW configuration that employs a 2DABCM in conjunction with imaging diversity receivers is evaluated under multipath dispersion and background noise impairments. The new proposed system (2DABCM transmitter with imaging diversity receiver) can help reduce the effect of ISI and improve the SNR even at high bit rate. At a bit rate of 30 Mbit/s, previous work has shown that imaging conventional diffuse systems with MRC offer 22 dB better SNR than the non-imaging CDS. Our results indicate that the 2DABCM system with an imaging diversity receiver provides an SNR improvement of 45 dB over the imaging CDS with MRC when both operate at 30 Mbit/s. In the CDS system, an increase in bandwidth from 38 MHz (non-imaging CDS) to 200 MHz approximately, is achieved when an imaging receiver is implemented. Furthermore, the three new methods introduced increase the bandwidth from 38 MHz to 5.56 GHz. Our 2.5 Gbit/s and 5 Gbit/s imaging 2DABCM systems with MRC offer significant SNR improvements, almost 26 dB and 19 dB respectively over a lower bit rate (30 Mbit/s) non-imaging CDS.

6.2. Receiver Structure

Angle diversity detection can be deployed in two main ways: using an imaging receiver that employs a detector segmented into multiple pixels [94] or using a number of photodetectors oriented in different directions [26]. Two different receiver structures, an angle diversity receiver and an imaging diversity receiver are considered.

6.2.1. Angle Diversity Receiver

Unlike the single wide FOV receiver, in this section, the receiver is a collection of narrow-FOV detectors pointed in different directions, forming an angle diversity configuration. The optical signal power received in the various receivers can be amplified separately, and can be processed using several techniques, such as combining or selection methods. The main drawbacks of this approach are the potentially large size and high cost of the multiple receiving elements. As illustrated in Fig. 6.1, the diversity receiver system considered consists of three photodetector branches. Each face bears a certain direction that can be defined by two angles (*Az* and *El* angles). While the *El* of two photodetectors remains at 20^o, the third one faces up with *El* of 90^o, and the *Az* for the three branches of the receiver are fixed at 90^o, 0^o, and 270^o. The selection of these angles and their optimisation was previously considered [44, 50]. Each photodetector is assumed to employ a compound-parabolic concentrator (CPC), which has an acceptance semi-angle ψ_C so that when the reception angle δ exceeds ψ_C, the concentrator transmission factor, $T_{C,NIMG}(\delta)$ rapidly approaches zero.

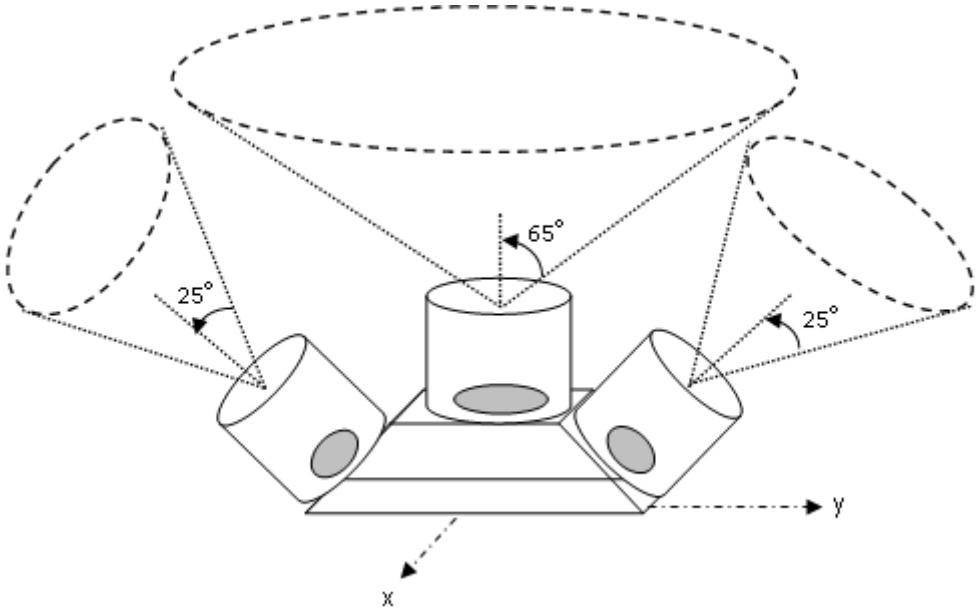

Figure 6-1: Physical structure of an angle diversity non-imaging receiver

The CPC is a common non-imaging concentrator and has $\psi_C < 90^0$, a refractive index of $N_C = 1.7$ is considered, and the entrance area is $A = 9\pi/4\ cm^2$. The transmission factor of the CPC is given by

$$T_{C,NIMG}(\delta) = T\left[1 + (\delta/\psi_C)^{2R}\right]^{-1}, \tag{6.1}$$

where $T = 0.9$ and $R = 13$ [183]. The CPC has an exit area of $A' = A\sin^2(\psi_C)/N_C^2$. In our analysis, the photodetector that faces up is assumed to employ a CPC with an acceptance semi-angle of $\psi_C = 65^0$, while the corresponding concentrator's acceptance semi-angle of each side photodetector was restricted to 25°. These acceptance semi-angles have been selected in order to enable each photodetector to view the whole surface it faces. Furthermore, each photodetector is assumed to be fitted exactly into its associated concentrator's exit area. Therefore, the photosensitive area of the photodetector facing up is 2 cm^2, while it is 0.44 cm^2 for each side photodetector. Each photodetector has a responsivity of 0.54 A/W. A

photodetector that faces up is used in the case of a single non-imaging receiver. The source used is coherent. The concentrator's size is acceptable in mobile terminals and it can be ruggedly fixed to the photodetector.

6.2.2. Imaging Diversity Receiver

As an alternative, imaging receivers have been proposed as a method that can be implemented to combat the limitations (multipath dispersion and ambient light) of the non-directed LOS OW communications [94]. The imaging receiver, depicted in Fig. 6.2, utilises an imaging concentrator that forms an image onto photodetector pixels where each pixel is equipped with a separate pre-amplifier. In order to combine the advantages of imaging receivers and diversity schemes, and hence, provide robustness to ambient light noise and multipath dispersion, we introduce imaging diversity receivers. These can be realised by using the diversity receivers discussed earlier in this section with imaging concentrators and arrays of photodetectors. Each of the three faces has an array of photodetectors (a two-dimensional array of pixels) instead of one photodetector. The imaging diversity receiver employs a detector array segmented into J equal-sized rectangular-shaped pixels, as shown in Fig. 6.2. We assume that there are no gaps between the pixels. Therefore, the area of an individual pixel is the photodetector's area, which is exactly equal to the exit area of the concentrator employed, divided by the number of pixels. In this case and under most circumstances, the signal (image of each spot) falls on no more than four pixels. The photodetector array that faces up is segmented into 200 pixels, while each side photodetector array is segmented into 100 pixels.

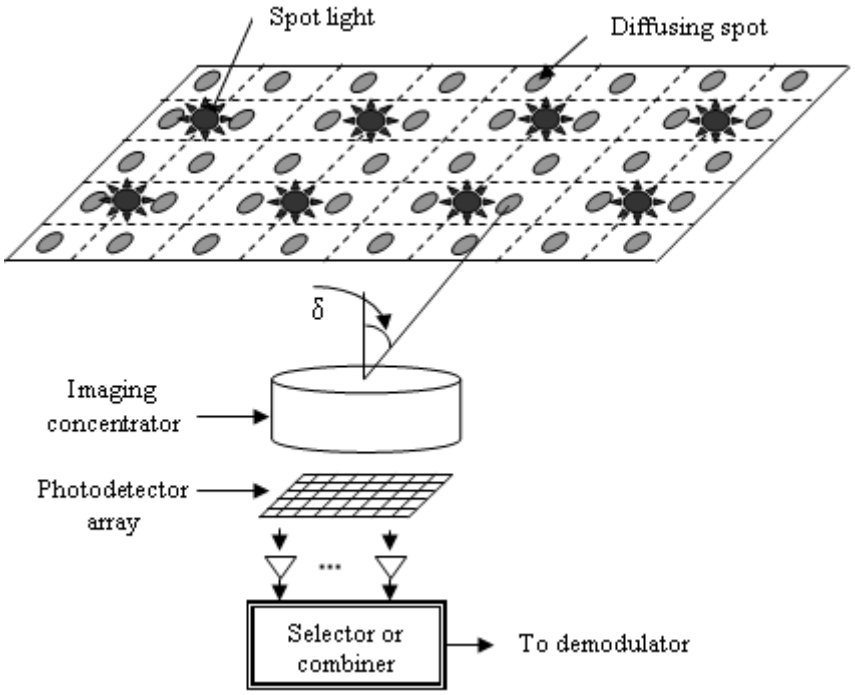

Figure 6-2: Physical structure of an imaging receiver, which utilises a single imaging lens and a photodetector segmented into multiple pixels

In our imaging receiver's analysis, we employ the imaging concentrator that was used in [94]. The transmission factor of this imaging concentrator is given by

$$T_{C,IMG}(\delta) = -0.1982\delta^2 + 0.0425\delta + 0.8778, \quad (6.2)$$

where δ is measured in radians. We emphasise that in all calculations, both the angle diversity receiver and the imaging diversity receiver considered employ equal entrance area of $A = 9\pi/4\ cm^2$ and equal acceptance semi-angles ($\psi_C = 65^0$ for the branch facing up, while it is 25^o for each side photodetector). The results show that MRC offers further improvement when implemented to combine the signals at the outputs of the imaging pixels. A photodetector array that faces up is implemented in the case of a single imaging receiver.

In our imaging diversity receiver's analysis, the reception area observed by each pixel varies as the imaging diversity receiver moves. When placed at the centre of the

room, the imaging diversity array which faces up is designed to see the entire ceiling. In effect the ceiling is subdivided, in this case into 200 segments (10 × 20), and each segment or reception area is cast onto a single pixel. This geometry is used to compute the reception angles associated with each pixel (reception angles α_x and α_y with respect to the receiver's normal along the *x* and *y* lines as shown in Fig. 6.3 (a)), and can be calculated as;

$$\alpha_x = \tan^{-1}\left(\frac{d_x}{h}\right) \quad \text{and} \quad \alpha_y = \tan^{-1}\left(\frac{d_y}{h}\right), \tag{6.3}$$

where d_x and d_y are the *x*-axis and *y*-axis horizontal separations between the receiver's normal and the reception area centre respectively, and h is the reception area height. These reception angles become a design property (reference points) of the imaging receiver at all locations. As the imaging receiver starts moving, the reception areas change accordingly. At certain locations on the CF, some of the reception areas on the ceiling start to appear on one of the walls. For instance, at locations close to the corner (the imaging receiver is at the corner of the room (1m, 1m, 1m)), some of the ceiling reception areas appear on the walls as shown in Fig. 6.3 (b). The height of the centre of a reception area above the communication floor z_y or z_x on the *x*-*z* wall or the *y*-*z* wall respectively can be calculated, by observing Fig. 6.3 (b), as;

$$z_y = \frac{y_r}{\tan\alpha_y} \quad \text{and} \quad z_x = \frac{x_r}{\tan\alpha_x}, \tag{6.4}$$

where y_r and x_r are the horizontal separation distances between the imaging receiver and the *x*-*z* and *y*-*z* walls.

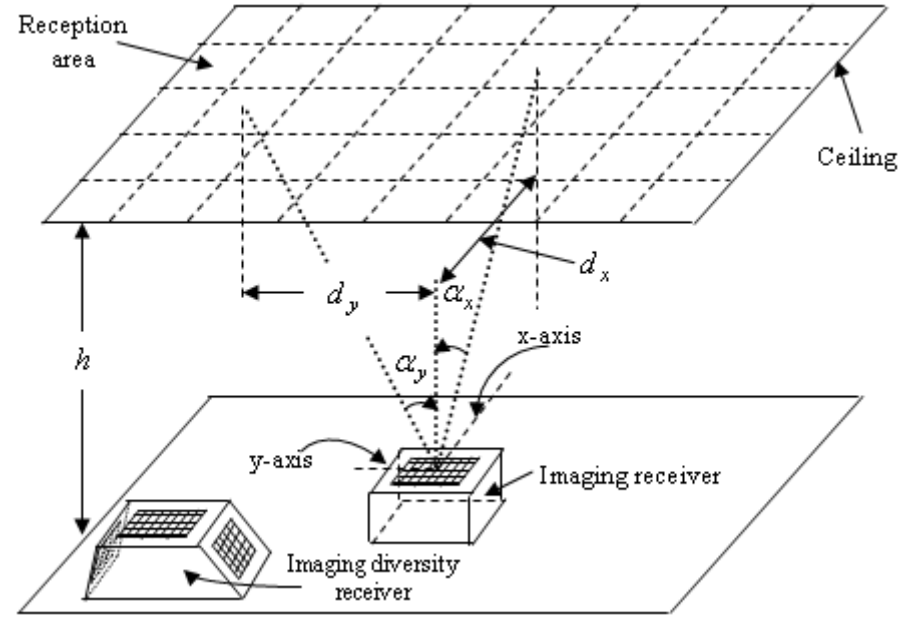

(a)

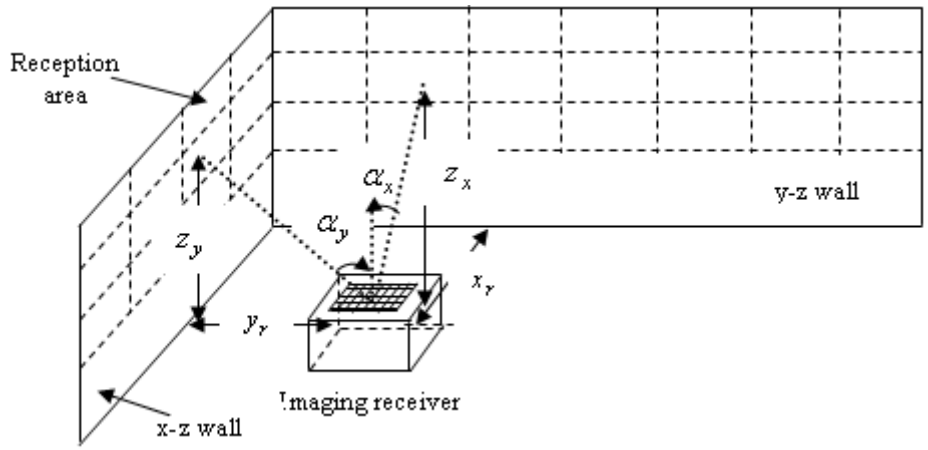

(b)

Figure 6-3: Reception areas associated with the photodetector array showing the *x-z* wall and *y-z* wall at two receiver locations: (a) (2m, 4m, 1m) and (b) (1m, 1m, 1m)

Throughout this chapter, computations were carried out following the procedure given above where the new reception areas are determined, based on the reference points and the imaging receiver location. Taking into account the number of rows and columns of the photodetector array, the centre of each new reception area is determined based on the receive angles associated with the pixel and the new

receiver location. The reception area associated with the side arrays in the diversity receiver can be computed in a similar fashion.

6.3. Propagation Model

The characteristics of the mobile channel, formed by an adaptive two dimensional beam clustering transmitter coupled with an imaging diversity receiver are investigated. The transmitted signal propagates to the receiver through multiple reflections from room surfaces. Simulation was conducted in an empty room (real environment studies were reported in Chapter 5 and is considered in Chapter 7), which has a width of 4 m, a length of 8 m, and a height of 3 m. Up to second order reflections were taken into account and full wall reflectivity was assumed. High reflectivity was chosen as it results in the highest multipath dispersion (worst case), thus significant pulse spread. In order to assess the system performance, in a realistic situation, the room illumination was provided by the same previous eight spotlight lamps of 65 W powers positioned equidistantly in the ceiling as shown in Fig. 3.2. For our purpose these represent ambient background interference. Interference from daylight through windows and doors was not considered in this work. No optical filters were used in this Chapter. Furthermore, in order to minimise the BN effect and reduce multipath dispersion, an imaging diversity receiver is implemented. Significant performance improvements can be achieved by receiving the signal from multiple pixels having narrow FOVs and using appropriate combining techniques. Imaging diversity receivers were discussed in Section 6.2.2. Additional simulation parameters are given in Table 6.1.

TABLE 6-1: SIMULATION PARAMETERS

Parameter	**Configuration Uplink Transmission**		
Room			
Length	8 m		
Width	4 m		
Height	3 m		
ρ _x_z Wall	0.8		
ρ _y_z Wall	0.8		
ρ _x_z op. Wall	0.8		
ρ _y_z op. Wall	0.8		
ρ _Floor	0.3		
Transmitter			
Number of transmitter	1		
Location (x, y, z)	(2,4,1)		
Elevation	90^o		
Azimuth	0^o		
Diversity Receiver			
Number of branches	3		
Photodetector's area	2 cm^2	0.44 cm^2	0.44 cm^2
Acceptance semi-angle	65^o	25^o	25^o
Location (x, y, z)	(1,1,1), (1,2,1), (1,3,1), (1,4,1), (1,5,1), (1,6,1), (1,7,1) (2,1,1), (2,2,1), (2,3,1), (2,4,1), (2,5,1), (2,6,1), (2,7,1)		
Elevation	90^o	20^o	20^o
Azimuth	0^o	90^o	270^o
Pixels			
Number of pixels	200	100	100
Pixel's area	1 mm^2	0.44 mm^2	0.44 mm^2
Time bin duration	0.3 ns	0.3 ns	0.3 ns
Bounces	1		2
Number of elements	32000		2000
dA	5 cm × 5 cm		20 cm × 20 cm
Spot lamps			
Number of spot lamps	8		
Locations (x, y, z)	(1,1,3), (1,3,3), (1,5,3), (1,7,3) (3,1,3), (3,3,3), (3,5,3), (3,7,3)		
Wavelength	850 nm		
Preamplifier design	PIN-FET	PIN-FET	PIN-FET
Receiver Bandwidth	30 MHz	2.5 GHz	5 GHz
Bit rate	30 Mbit/s	2.5 Gbit/s	5 Gbit/s

To quantify the proposed system performance, two configurations were considered: 2DBCM, and 2DABCM, in conjunction with different detection techniques. Firstly, the 2DBCM system performance was evaluated based on the non-imaging angle diversity receiver. Secondly, both the 2DBCM and the 2DABCM systems performances were assessed with the imaging diversity receiver, and compared with the imaging and non-imaging CDS system. The transmitter was placed at the centre of the room at (2m, 4m, 1m) on the CF, pointed upwards, and emitted 1 W total optical power in an ideal Lambertian radiation pattern. Computer generated holographic beam-splitters are assumed to be mounted on the emitter, resulting in multiple narrow beams which illuminate multiple small areas, forming a lattice of diffusing spots (clusters) on the ceiling and one on each of the end walls resulting a BCM configuration [102]. In the 2DBCM configuration, each cluster is made up of a two-dimensional set of spots (instead of a line of spots), as described below (see Section 6.4.2). Previous work in [39, 51] has shown that static beam intensities can be produced by using computer generated holograms. In addition, as previously mentioned a liquid crystal device can be used to adapt the power among the beams at relatively low complexity.

Under receiver mobility, a simulation tool, similar to the one developed for adaptive multibeam system with diversity receiver in Chapter 4, was developed here where each face of the diversity receiver has a photodetector array (2D array of pixels) instead of one photodetector, see Fig. 6.3 (a). This developed simulation algorithm was used to calculate the received power at each pixel based on its FOV and the area (on the ceiling or wall) it observes, and produce the impulse response. Our simulation results have been compared with experimental and theoretical results reported by other researchers in the case of simple CDS [10] and imaging CDS [94]

and a good match was observed giving confidence in our simulator when examining other systems. As previously mentioned in the case of the multibeam geometry, we assume that the journey of the beam from the transmitter (on the CF) to the spot (on the ceiling or walls) is an ideal journey where no power is lost and the pulse width does not increase. Several parameters including SNR, 3 dB channel bandwidth, and delay spread are of interest and can be derived from the simulated impulse response.

6.4. Transmitter Structure

In this section, two novel multibeam clustering configurations (2DBCM and 2DABCM) are presented and analysed. Simulations were carried out in order to evaluate the improvement achieved through the combination of our new approaches (transmit power adaptation, 2D beam clustering, and diversity imaging). The proposed systems were simulated and compared with the CDS.

6.4.1. Conventional Diffuse System (CDS)

This is the basic configuration of the diffuse transmission and reception and has been investigated in [3, 10, 17, 26-27, 53, 121]. The conventional diffuse system uses a single beam transmitter typically with a Lambertian radiation pattern and a wide single element receiver (FOV = 90^{o}). For comparison purposes, a diffuse transmitter has been simulated with different detection techniques (a single non-imaging receiver with (FOV = 65^{o}) and an imaging diversity receiver) to generate channel impulse responses. The BCM is one of the attractive OW transmitter configurations [102-103]. Therefore, it is developed (where 2D beam clustering is employed instead of the previously introduced 1D beam clustering approach) and evaluated here for

the first time with imaging receivers. Furthermore, we also introduce and evaluate our new adaptive 2DBCM.

6.4.2. Two Dimensional Beam Clustering Method (2DBCM)

The spot distribution pattern based on a beam clustering method, proposed and examined in [102] (and presented in Chapter 3), is extended in this system and the results show a significant SNR improvement using MRC at the receiver. Our proposed system employs 400 diffusing spots with total power of 1 W and therefore each spot is allocated 2.5 mW. A two-dimensional beam clustering transmitter is assumed to produce (rows ×columns) beams that form three two-dimensional groups of spots aimed at three different surfaces: ceiling and two end walls. These spots become secondary distributed emitters, which emit Lambertian radiation. The 2DBCM employs three two-dimensional clusters of spots distributed as follows: 200 diffusing spots (10 row × 20 columns) on the ceiling and 100 spots (10 row × 10 columns) on each of the two end walls when the transmitter is at the centre of the room. The difference in distance between the adjacent spots in each row and column in the ceiling is 40 cm, while it is 40 cm and 20 cm on the walls respectively. To help visualise the 2DBCM configuration, Fig. 6.4 displays a limited number of diffusing spots (rows and columns) when the transmitter and receiver are co-located at the centre of the room at (2m, 4m, 1m). The structure has the ability to view and cover its surroundings through the three two dimensional clusters of diffusing spots, which give the receiver the option to collect a number of direct path components (i.e., paths between diffusing spots and a receiver), through the nearest diffusing spots and the shortest paths over the entire CF. In order to maximise the benefits of this structure,

imaging diversity receivers were employed. Each diversity photodetector is segmented into a number of equal-sized rectangular-shaped pixels. A lens system in front of the receiver array ensures that the image of the spots (e.g., on the ceiling) is cast directly on the receiver array. If the system is designed properly, then when the transmitter and receiver are placed at the centre of the room as shown in Fig. 6.4, each signal (image of each spot) is received in one pixel and there are as many pixels rows and columns as there are spot rows and columns on the ceiling. Higher order diversity receivers, such as a 7-face diversity receiver [100], if used with our imaging receiver, can reduce the impact of receiver rotation and can result in improved SNR due to the increase in the number of diversity branches and orientations. However, the implementation complexity increases.

In order to simulate the proposed geometry, the imaging diversity receiver was placed at various locations on the CF. The received multipath profiles, due to each spot, were computed at each pixel based on the pixel's FOV, and the area (on the ceiling and/or walls) the pixel observes at each receiver location. The resultant power profile at each pixel is the sum of the powers due to the 400 diffusing spots.

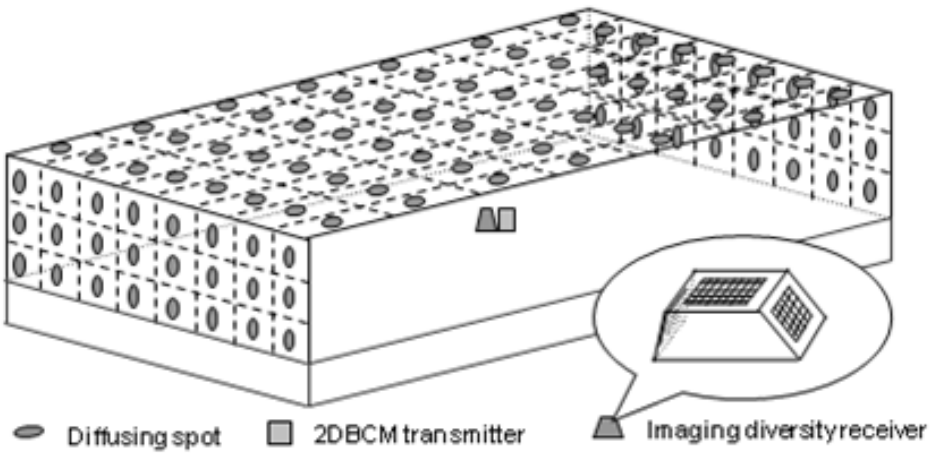

Figure 6-4: 2DBCM configuration when the transmitter and receiver are co-located at the room centre (2m, 4m, 1m)

6.4.3. Two Dimensional Adaptive Beam Clustering Method (2DABCM)

In contrast to the previous method (2DBCM), where the multibeam clustering transmitter distributes the total power, 1 W, on the diffusing spots in equal intensities, in this new system the total power is distributed unequally so as to optimise the receiver SNR. In effect, the spot, having the strongest path to the receiver, is allocated the highest power level, whilst the farthest spot is assigned the lowest power level, hence maximising the receiver SNR. A block diagram that illustrates the operation of our adaptive algorithm and our simulator is given in Fig. 6.5. The adaptation algorithm adapts the transmit powers among the beams according to the following steps:

1. Individually turn on each spot, compute the power received at the imaging diversity receiver, and calculate the SNR.
2. Inform the transmitter of the SNR associated with the spot by sending a feedback signal at low rate.
3. Repeat steps 1 and 2 for all the spots.
4. Re-distribute the transmit power among the spots in proportion to the SNR they produce, where a spot that produces maximum SNR is allocated the highest power level.

We extend our proposed system (2DBCM system) by introducing transmit power adaptation implemented on the beam (spot) powers. The results demonstrate that significant performance (SNR) improvement can be obtained. The transmit powers associated with the beams are adjusted according to the adaptation algorithm described above. As mentioned previously, it has to be noted that the adaptive algorithm described applies to a single transmitter and a single receiver position.

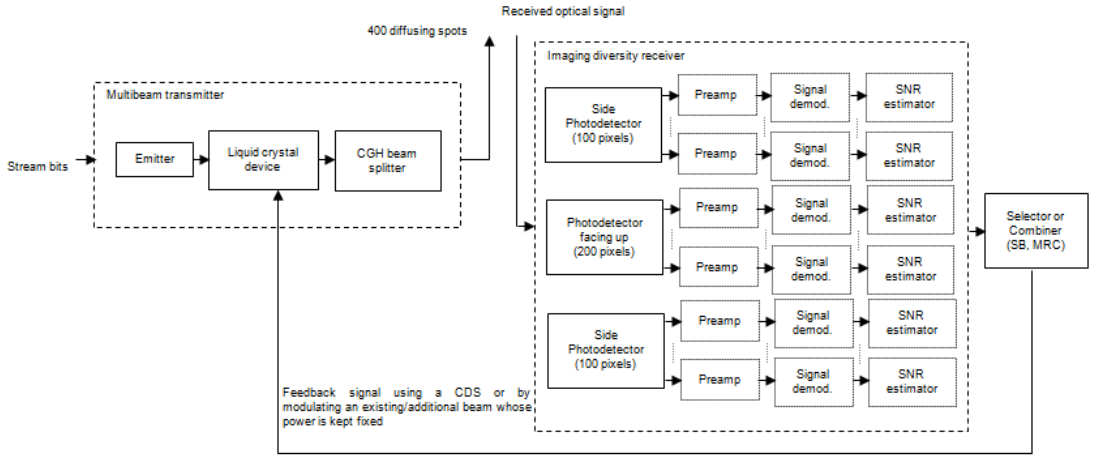

Figure 6-5: Block diagram of the simulator

6.5. Performance Analysis and Simulation Results

In this section the optical signal collected under the constraints of BN and multipath dispersion has been assessed in different link configurations. Simulation results are presented in terms of impulse response, delay spread, channel bandwidth, and SNR. The performance, under the two dimensional adaptive beam clustering transmitter coupled with an imaging diversity receiver, was evaluated and compared with the other geometries at different receiver locations on the CF, when the transmitter is stationary at the centre of the room (2m, 4m, 1m). Transmitter mobility is not taken into account in this chapter. Further research into the effect of transmitter and receiver mobility on our proposed imaging system performance will be considered in the next chapter (Chapter 7). In the previous chapters we have considered the impact of mobility on other OW systems.

6.5.1. Impulse Responses

The SB impulse response of the three configurations (2DBCM with non-imaging angle diversity receiver, 2DBCM, and 2DABCM in conjunction with imaging diversity receivers) at transmitter and receiver locations of (2m, 4m, 1m) and (1m, 1m, 1m) respectively, is depicted in Fig. 6.6. Fig. 6.6 shows the received power levels (μW) versus the time (ns), i.e. impulse responses. The results indicate that the adaptive multibeam clustering transmitter, coupled with an imaging diversity receiver, increases the received power level and reduces the signal spread. This is due to (i) assigning higher power levels to spots nearest to the receiver resulting in high direct path components, and (ii) the limited rays captured by a pixel associated with its narrow FOV.

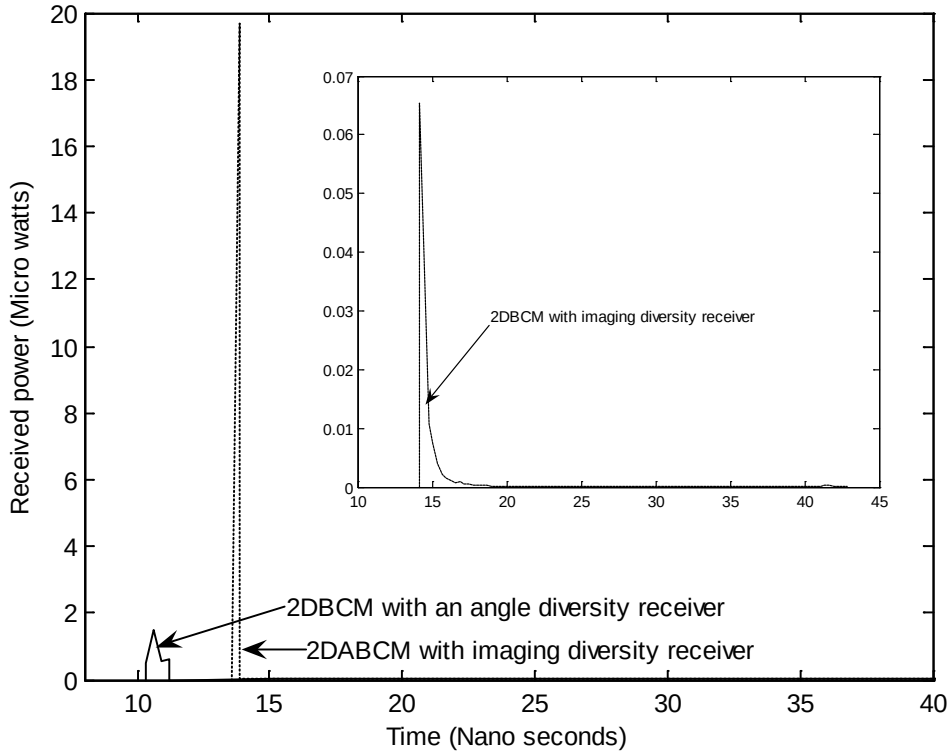

Figure 6-6: Impulse response of three configurations; 2DBCM with angle diversity receivers, 2DBCM, and 2DABCM in conjunction with imaging diversity receivers, when the transmitter is placed at the centre of the room (2m, 4m, 1m) and the receiver is in the corner of the room (1m, 1m, 1m)

In a 2DBCM channel, a drop in the received power level by a factor of 22 can be observed when the imaging diversity receiver replaces the non-imaging angle diversity receiver. This reduction is attributed to the limited range of rays that can be received within the pixel's narrow FOV. It has to be observed however, that the imaging diversity receiver (with MRC) yields a better overall SNR performance due to the significant reduction in background noise it collects. Furthermore, the imaging diversity receiver results in lower delay spread and therefore the reduction in received power can be compensated for through beam power adaptation, which is able (for this transmitter and receiver set of locations) to increase the received power from $0.09\,\mu W$ to $20\,\mu W$ approximately. In addition, the impulse responses for all cases studied are analysed to compare the effect of a large distance between the transmitter and receiver on the received optical power. A practical OW system has a continuous impulse response; however the simulation algorithm segments the reflecting surfaces into discrete elements. The effect of discretisation is reduced through grouping the powers received with a time bin (0.3 ns duration) into a single received power. This results in the smoothness shown in the impulse responses. The impulse response seen by a single detector that faces up are composed of clusters (depending on spot geometry and receiver position), however the impulse response results in Fig. 6.6 correspond to systems that use angle diversity. As a result the direction (or cluster) that produces the best received power is selected.

6.5.2. Delay Spread Assessment and Bandwidth Efficiency

Fig. 6.7 (a) compares the delay spread of the configurations considered when the transmitter is stationary at the centre of the room and the receiver moves along the *x*

= 1 m line, while the bandwidth is depicted in Fig. 6.7 (b). The results show that our imaging 2DABCM system provides the lowest delay spread and the largest bandwidth compared to the other systems at all receiver positions considered.

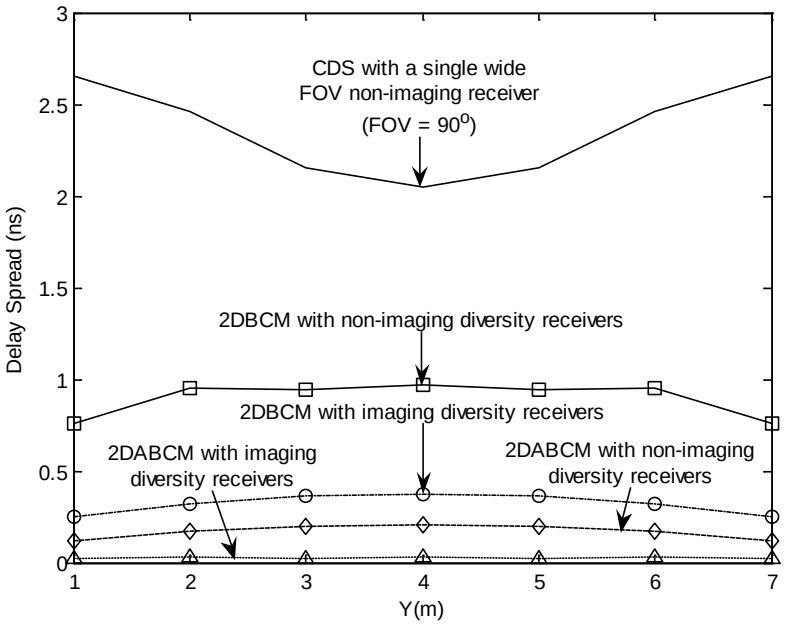

(a)

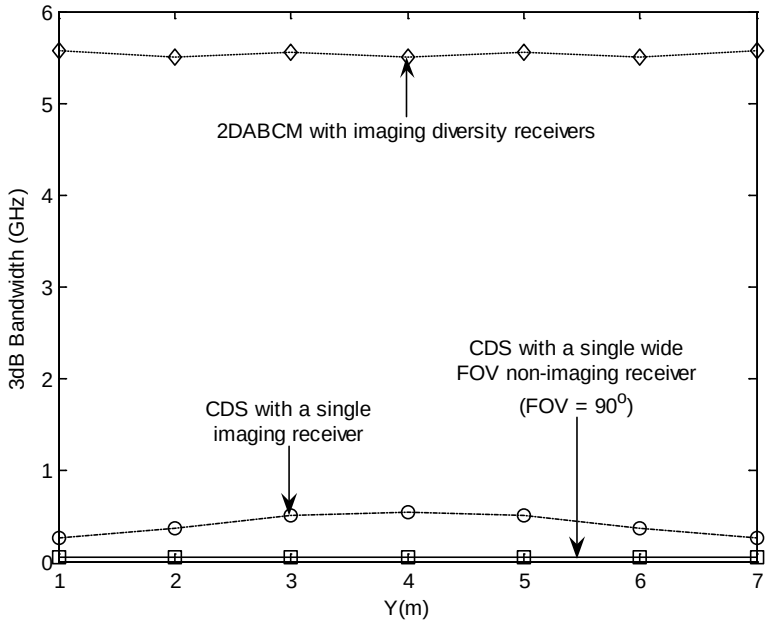

(b)

Figure 6-7: (a) Delay spread distribution and (b) 3 dB channel bandwidth of the proposed systems when the transmitter is placed at the centre of the room and the receiver moves at constant x = 1 m and along the y-axis

This is due to allocating higher power levels to the spots nearest to the receiver and also due to the very high direct power component contribution and the reduction in the contribution of reflections. In the 2DBCM system, the results indicate that employing an imaging diversity receiver instead of an angle diversity receiver can reduce the delay spread by a factor of 3 at one of the least successful receiver locations considered (1m, 1m, 1m), as a result of receiving a limited range of rays in a small pixel with narrow FOV. Furthermore, our imaging 2DABCM offers a reduction in the delay spread, by a factor more than 11 and an increase in the bandwidth, from almost 400 MHz to 5.56 GHz over the imaging 2DBCM. Also, at the worst communication path considered, a significant bandwidth improvement, from 38 MHz to 5.56 GHz approximately, is achieved when our imaging 2DABCM system replaces the non-imaging CDS. In addition, the non-imaging 2DABCM system improves the delay spread by a factor of 7 over the non-imaging 2DBCM system. It can be clearly seen that the two-dimensional adaptive beam clustering transmitter, in conjunction with imaging diversity receivers, is an appropriate choice to combat multipath dispersion, as well as, to reduce the ISI.

6.5.3. SNR Performance Analysis

In this section, we investigate the performance of our proposed imaging configurations in terms of SNR when the system operates at different bit rates: 30 Mbit/s, 2.5 Gbit/s and 5 Gbit/s under the constraints of background noise and multipath dispersion. Also, non-imaging OW systems (CDS with a 65^{o} FOV single receiver, 2DBCM and 2DABCM with an angle diversity receiver) operating at 30 Mbit/s are investigated and their performances are evaluated and compared at

different receiver locations on the CF. We follow the SNR analysis given in (3.31) which accounts for the impact of the pulse spread caused by ISI where $P_{s1} - P_{s0}$ represents the eye opening at the sampling instant. Three noise sources are considered including the pre-amplifier noise variance component σ_{pr}^2, the background light-induced shot noise variance σ_{bn}^2 and the shot noise variance components σ_{s0}^2 and σ_{s1}^2 associated with P_{s0} and P_{s1}, respectively. This signal-dependent noise σ_{si}^2 is very small, particularly in imaging diversity receivers and can be neglected. The pre-amplifier used in this chapter for the 30 Mbit/s OOK system is the PIN FET transimpedance pre-amplifier that was used in [94]. For simplicity, the FET gate leakage and $1/f$ noise have been neglected. Therefore, the pre-amplifier noise variance is given by [94]

$$\sigma_{pr}^2 = \frac{4kT}{R_F} I_2 B + \frac{16\pi^2 kT\Gamma}{g_m} \left(C_d + C_g\right)^2 I_3 B^3 . \tag{6.5}$$

Observing (6.5), the pre-amplifier noise variance consists of two noise terms. The first term represents thermal noise from the feedback resistor: k is the Boltzmann's constant, T is absolute temperature, R_F is the feedback resistance, $I_2 = 0.562$, and B is the bit rate. The second term represents thermal noise from the FET channel resistance: Γ is the FET channel noise factor, g_m is the FET transconductance, $I_3 = 0.0868$, C_d and C_g are the detector and FET gate capacitances respectively. For simplicity, we assume that $C_g << C_d$. We also assume that the receiver bandwidth is equal to the bit rate B, which requires the condition $R_F = G/2\pi BC_d$, where G is the open-loop voltage gain. To facilitate comparison with previous work [94], we consider a bit rate of 30 Mbit/s. Higher bit rates of 5 Gbit/s and 2.5 Gbit/s

are also considered. The photodetector capacitance C_d is proportional to the photodetector area A_d, i.e., $C_d = \eta_c A_d$, where η_c is a fixed capacitance per unit area. Therefore, (6.5) can be rewritten as

$$\sigma_{pr}^2 = \frac{8\pi kT}{G}\eta_c A_d I_2 B^2 + \frac{16\pi^2 kT\Gamma}{g_m}\eta_c^2 A_d^2 I_3 B^3. \tag{6.6}$$

In an imaging diversity receiver, each pixel has an area equal to the photodetector area divided by the number of pixels. Therefore, it should be noted that the pre-amplifier noise is reduced because a small pixel size reduces the pre-amplifier input capacitance, which is proportional to the pixel area, hence allowing a large resistance to be used.

The ambient-induced shot noise σ_{bn}^2 can be calculated from its respective associated power level P_{bn} using (3.29). In an imaging diversity receiver, this noise term is reduced because the small FOV associated with a small pixel size reduces the received ambient light power. In our calculations, we chose the following parameter values that were used in [94]: $T = 295\,K$, $R = 0.54$ A/W, $G = 10$, $g_m = 30$ mS, $\Gamma = 1.5$, and $\eta_c = 112$ pF/cm^2. For the 2.5 Gbit/s and 5 Gbit/s systems, we have used the PIN FET receiver in [184] and the bandwidth was limited to 2.5 GHz and 5 GHz respectively by using appropriate filters. As previously mentioned, the impact of this filter on the signal is minimal as the bandwidth considered is higher than 0.7 × bit rate (Personick's analysis [131]), and is not considered here. We consider two approaches: SB and MRC in our imaging diversity receiver to process the resulting electrical signals. SB represents a simple form of diversity where the receiver simply chooses the pixel with the largest SNR. The SNR obtained using SB receiver is given by

$$SNR_{IMG,SB} = \underset{j}{MAX}\left(\frac{R\times\left(P_{s1j}-P_{s0j}\right)}{\sigma_{0j}+\sigma_{1j}}\right)^2 \quad 1\le j\le J\,, \tag{6.7}$$

where J is the number of pixels considered $(J=400)$.

In contrast to the SB approach, where the multiple signals resulting from the individual pixels are not fully used, in MRC the output signals of all the pixels are combined through an adder circuit, where each input to the circuit is summed with a weight directly proportional to its SNR. To maximise the MRC SNR, all pixels are combined using weights equal to $w_j = \frac{R\times\left(P_{s1j}-P_{s0j}\right)}{\left(\sigma_{0j}+\sigma_{1j}\right)^2}$, $1\le j\le J$, i.e., proportion to the pixel SNR [94]. The SNR obtained using MRC is given by

$$SNR_{IMG,MRC} = \frac{\left(\sum_{j=1}^{J} R\left(P_{s1j}-P_{s0j}\right)w_j\right)^2}{\sum_{j=1}^{J}\left(\sigma_{0j}+\sigma_{1j}\right)^2 w_j^2}\,. \tag{6.8}$$

$$\begin{aligned} SNR_{IMG,MRC} &= \frac{\left(\sum_{j=1}^{J} R\left(P_{s1j}-P_{s0j}\right)\frac{R\left(P_{s1j}-P_{s0j}\right)}{\left(\sigma_{0j}+\sigma_{1j}\right)^2}\right)^2}{\sum_{j=1}^{J}\left(\frac{R\left(P_{s1j}-P_{s0j}\right)}{\left(\sigma_{0j}+\sigma_{1j}\right)^2}\right)^2\left(\sigma_{0j}+\sigma_{1j}\right)^2}\,. \\ &= \sum_{j=1}^{J}\left(\frac{R\left(P_{s1j}-P_{s0j}\right)}{\left(\sigma_{0j}+\sigma_{1j}\right)}\right)^2 = \sum_{j=1}^{J} SNR_j \end{aligned} \tag{6.9}$$

Equation (6.9) indicates that the overall SNR of the imaging diversity receiver is, in fact, the sum of the SNR values of all pixels. MRC can achieve better performance than SB, at the cost of increased circuit complexity. This is associated with the increased signal processing in order to determine the correct weighting gain factor compared to the SB. It is demonstrated that as the number of pixels in the imaging receiver is increased, the MRC SNR increases further at the expense of receiver complexity [94].

6.5.3.1. 30 Mbit/s Non-Imaging OW Systems

The performance of the three non-imaging OW systems operating at 30 Mbit/s: CDS, 2DBCM, and 2DABCM, is depicted in Fig. 6.8 under the constraints of BN and multipath dispersion when the transmitter is placed at the centre of the room and the receiver moves at constant x = 1 m, and along the y-axis over the CF. Our non-imaging systems (2DBCM and 2DABCM) are examined at noise impaired receiver locations within the room considered, based on SB and MRC techniques. The results indicate that a consistent SNR performance is observed in the non-imaging 2DBCM system in contrast to the fluctuation displayed in the non-imaging CDS SNR.

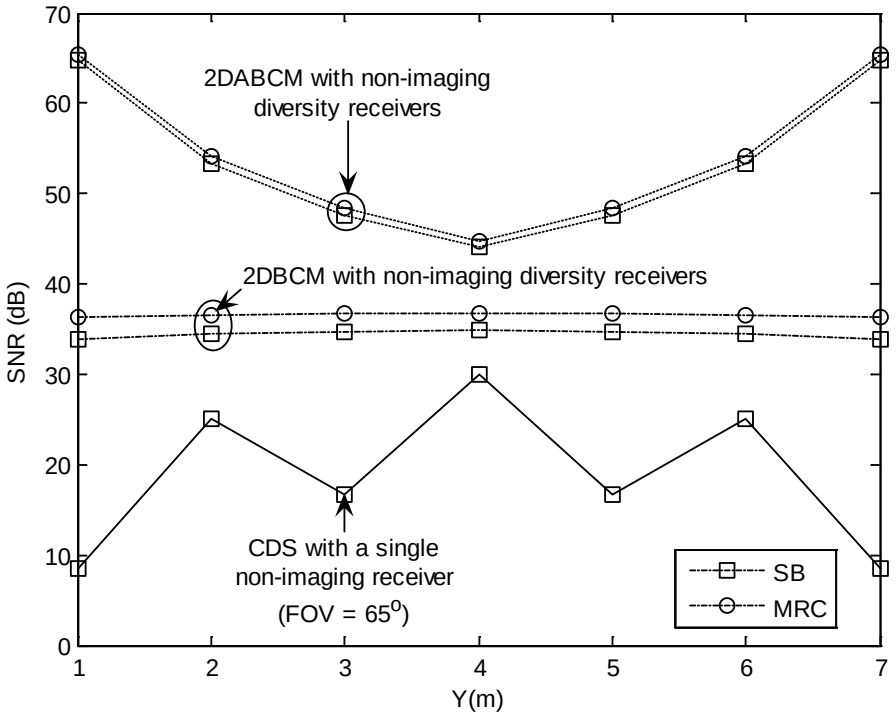

Figure 6-8: SNR of three OW systems operating at 30 Mbit/s; CDS with a single non-imaging receiver, 2DBCM, and 2DABCM in conjunction with non-imaging diversity receivers

This is due to the fact that the 2DBCM configuration has the ability to cover its surroundings through the diffusing spots (on the ceiling and two end walls), which gives the non-imaging angle diversity receiver the option to collect the signals through the nearest diffusing spots and the shortest paths (within the transmitter location considered, direct path components can be collected at every non-imaging angle diversity receiver location). The SB non-imaging 2DBCM system offers an improvement in the SNR level, 25 dB approximately, over the non-imaging CDS system at the worst communication path considered when the receiver is placed at the room corner (1m, 1m, 1m). Furthermore, the non-imaging 2DABCM demonstrates a significant performance improvement of 31 dB compared with the non-imaging 2DBCM system when both systems employ SB. This is attributed to allocating high power levels to spots nearest to the receiver, resulting in a strong received optical power. However, employing a 2DABCM transmitter accompanied by a three face non-imaging angle diversity receiver results in a reduction in SNR towards the centre of the room. This can be explained by observing that at all the receiver locations considered, the narrow FOV (FOV = 25^{o}) associated with the side photodetector leads to reducing the impact of the BN compared to that experienced by the photodetector that faces up with FOV = 65^{o}, hence the 2DABCM transmitter assigns high power levels to spots located within the FOV of the side photodetector. Therefore, when the receiver moves towards the edge of the room, the distance between the spots allocated high power levels and the receiver becomes shorter, which is a critical factor in spot-diffusing indoor optical wireless systems. This results in a very high received power. This decline in SNR is reduced by replacing the non-imaging angle diversity receiver with our new imaging diversity receiver (see Figs. 6.9 (a) and (b)).

6.5.3.2. 30 Mbit/s, 2.5 Gbit/s and 5 Gbit/s Imaging OW Systems

Figs. 6.9 (a) and (b) show the SNR of the proposed systems operating at 30 Mbit/s and 2.5 Gbit/s respectively, when the systems operate under the constraints of BN (eight directed spotlights n_{Lamp} = 33.1) and multipath dispersion, when the transmitter is placed at the centre of the room and the receiver moves at constant x = 1 m, and along the y-axis over the CF. Also, the 5 Gbit/s imaging 2DABCM SNR is given in Fig. 6.9 (b). These locations were selected in order to examine some of the key cases, i.e., points exactly underneath directive noise sources, as in y = 1, 3, 5, and 7 m, as well as points near to the corner of the room, which represent the worst communication paths. Under these conditions, all the proposed configurations are compared. The results indicate that at a bit rate of 30 Mbit/s, the 2DABCM system, in conjunction with imaging diversity receivers, offers a significant SNR improvement of 32 dB over the non-imaging 2DBCM system, using SB approach. This improvement is attributed to two effects. Firstly, assigning high power levels to the spots nearest to the receiver results in a high received power. Secondly, the small size of the pixel associated with narrow FOV yields a reduction in the amount of BN detected by the pixel, and reduces the pre-amplifier thermal noise. Furthermore, in the 2DBCM system, with an angle diversity receiver that is placed at the corner of the room, a slight performance improvement of less than 3 dB can be achieved by using MRC instead of SB scheme. In contrast, an SNR improvement of 19 dB is obtained in the imaging 2DBCM when MRC replaces SB. This is due to the fact that imaging diversity receivers with MRC fully benefit from combining the SNRs associated with multiple small sized pixels that observe spatially low noise levels. In effect, the imaging MRC receiver (with 2DABCM) is able to select the area(s) (in the ceiling and/or walls) to observe (images) so that the receiver SNR is maximised.

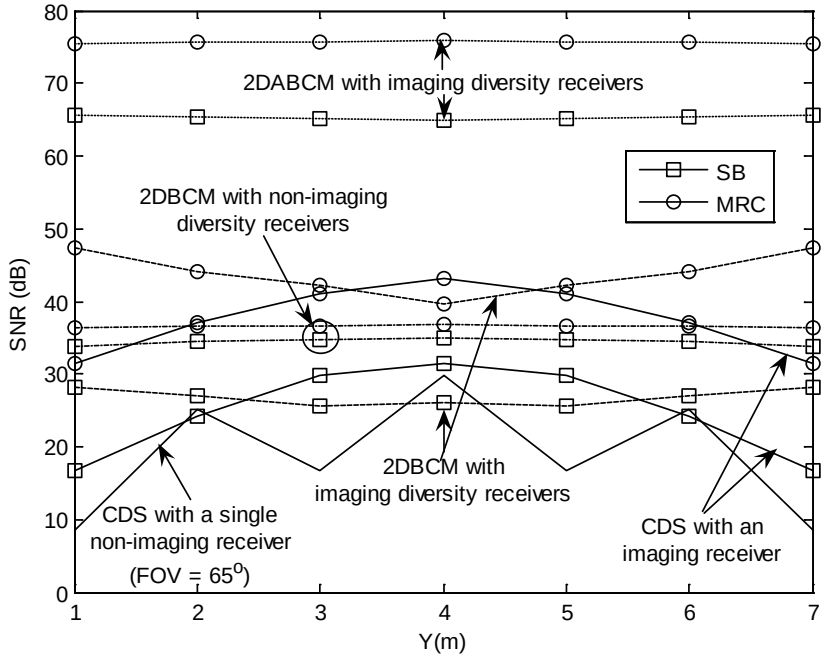

(a)

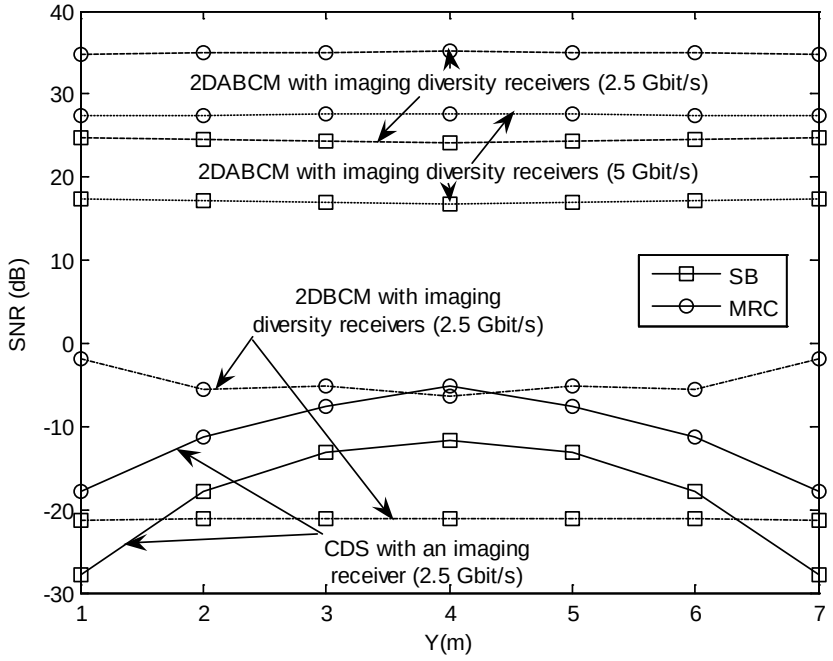

(b)

Figure 6-9: SNR of the proposed systems operating at (a) 30 Mbit/s and (b) 2.5 Gbit/s when the transmitter is placed at the centre of the room and the receiver moves at constant x = 1 m and along the y-axis. Also, (b) shows SNR level of our proposed 5 Gbit/s 2DABCM system with an imaging diversity receiver

This observation also explains the performance penalty of approximately 5 dB observed when MRC is replaced by SB. Note that an imaging CDS operating at 30 Mbit/s with MRC offers 22 dB SNR improvement over the non-imaging 30 Mbit/s CDS. This SNR improvement is in agreement with that presented in [94]. Furthermore, our new imaging 2DABCM, which operates at 30 Mbit/s, demonstrates a further SNR improvement of 45 dB over the imaging 30 Mbit/s CDS system. Observing Fig. 6.9 (b), at one of the least successful receiver locations (1m, 1m, 1m), our new 2.5 Gbit/s 2DABCM system, in conjunction with our new imaging diversity receivers based on the SB method, demonstrates significant performance improvements of 16 dB and 8 dB compared with the non-imaging and imaging SB CDS systems operating at 30 Mbit/s. However, a reduction in the imaging MRC 2DABCM SNR performance of 7 dB is observed when the bit rate increases from 2.5 Gbit/s to 5 Gbit/s. Our new 5 Gbit/s imaging SB 2DABCM system offers an SNR improvement of 9 dB over the non-imaging CDS system operating at 30 Mbit/s. In addition, an SNR improvement of 10 dB in the high bit rates (2.5 Gbit/s and 5 Gbit/s) imaging 2DABCM systems, is achieved when MRC replaces SB. Finally, our results confirm that the new methods introduced (transmit power adaptation, 2D beam clustering, and diversity imaging) assist an optical wireless communication system in reducing the effect of BN and multipath dispersion even at high bit rates (2.5 Gbit/s and 5 Gbit/s). Table 6.2 provides a comparison between the different systems examined in this chapter when the receiver moves along the x = 2 m line.

TABLE 6-2: SNR OF THE PROPOSED IMAGING SYSTEMS AND COMPARISON WITH IMAGING CDS

Configuration		SNR (dB)						
		Y (m)						
		1	2	3	4	5	6	7
CDS (30 Mbit/s)	SB	18.62	26.54	32.2	34.1	32.2	26.54	18.62
	MRC	32.74	38.84	43.34	45.13	43.34	38.84	32.74
2DBCM (30 Mbit/s)	SB	31.32	27.21	26.3	26.22	26.3	27.21	31.32
	MRC	45.79	42.75	41.74	41.78	41.74	42.75	45.79
2DABCM (30 Mbit/s)	SB	65.53	65.3	65.17	64.94	65.17	65.3	65.53
	MRC	75.55	75.63	75.78	75.81	75.78	75.63	75.55
2DABCM (2.5 Gbit/s)	SB	24.8	24.65	24.43	24.21	24.43	24.65	24.8
	MRC	34.83	34.91	35.04	35.14	35.04	34.91	34.83
2DABCM (5 Gbit/s)	SB	17.33	17.15	16.9	16.7	16.9	17.15	17.33
	MRC	27.24	27.43	27.52	27.63	27.52	27.43	27.24

6.6. Summary

In this chapter, we have designed and investigated a novel adaptive OW system (2DABCM system) and have shown that it can provide robustness against BN and multipath dispersion. The new proposed system (imaging 2DABCM transmitter with imaging diversity receiver) can help reduce the effect of intersymbol interference and improve the SNR even at high bit rates. At a bit rate of 30 Mbit/s, previous work has shown that imaging CDS with MRC offers 22 dB better SNR than the non-imaging CDS. Our results indicate that the 2DABCM system, with an imaging diversity receiver based on MRC, achieves an SNR improvement of 45 dB over the imaging MRC CDS, when both systems operate at 30 Mbit/s. This is due to three factors. Firstly, a strong received power due to allocating high power levels to the spots

nearest to the receiver. Secondly, a significant reduction in the ambient shot noise and pre-amplifier thermal noise is achieved due to the small pixel size and its associated narrow FOV. Furthermore, the use of MRC with imaging receivers and 2DABCM means that the receiver is able to select the area (on the ceiling or walls) that provides the best SNR (combination of presence of spots and absence of ambient light noise in the observed part of the image). In addition, the new methods introduced (transmit power adaptation, 2D beam clustering, and diversity imaging) increase the bandwidth from 38 MHz (non-imaging CDS) to 5.56 GHz. The increase in channel bandwidth and SNR can assist the OW system to achieve higher data rates and 2.5 Gbit/s and 5 Gbit/s OW systems are shown to be feasible. At the worst communication paths considered, our 2.5 Gbit/s and 5 Gbit/s imaging 2DABCM systems based on MRC demonstrate SNR gains of 26 dB and 19 dB respectively over the non-imaging CDS that operates at 30 Mbit/s.

It should be noted that the OW link design can benefit significantly if spots are clustered and distributed on different surfaces as shown in this study. Furthermore, the link design can be improved if spot power adaptation is allowed and more so if imaging reception is employed. The latter allows the receiver to observe locations in space where the SNR is at maximum level. The combination of these methods adds a number of degrees of freedom to link design. The power consumed by the proposed systems is relatively low and the transmit power can be significantly reduced below the current 1 W level by making use of the SNR improvements achieved. The system makes use of commercially available components and can therefore be implemented at relatively low cost.

7. IMPACT OF MOBILITY AND SHADOWING ON MULTIGIGABIT INDOOR SPOT DIFFUSING OPTICAL WIRELESS SYSTEMS EMPLOYING MULTIBEAM POWER ADAPTATION, IMAGING DIVERSITY AND MC-CDMA SCHEME

7.1. Introduction

The link design presented in the previous chapter (Chapter 6) (where shadowing, signal blockage and transmitter mobility were not taken into account) has shown that a 5 Gbit/s optical wireless communication system can be realised through the combination of transmit beam power adaptation, a two-dimensional beam clustering method and diversity MRC imaging. This significant performance improvement comes with an increase in complexity in terms of the computational time required where 400 diffusing spots are employed. The complexity results from computing the SNR produced by each spot at the imaging diversity receiver and adapting the power levels among the spots at the transmitter. Here we show that this bit rate (5 Gbit/s) is achievable with full mobility in the presence of shadowing and signal obstruction by employing a less complex multibeam transmitter structure (i.e. replacing the 2DBCM by an LSMS) that is combined with beam power adaptation and diversity MRC imaging. However, this computational saving is combined with a power penalty in the order of 10 dB compared to SNR reported in the previous chapter.

This chapter introduces three methods (line strip spot-diffusing, beam power adaptation and diversity imaging) to the design of multigigabit optical wireless systems to improve link performance. The aim is to reduce the effect of intersymbol interference and to enhance the SNR, thus enabling the system to achieve mobility while operating at high bit rates in the presence of very directive noise, multipath propagation, mobility and shadowing typical in a real indoor environment. The

simulation results show that the combination of transmit power adaptation, spot-diffusing and diversity imaging methods can help suppress the limitations of the OW communication links even in the presence of shadowing. Significant performance improvements can be achieved and used to enable higher data rates and/or multi-user optical wireless communication systems with full mobility. Multi-user capabilities can be provided, in our case, by employing an MC-CDMA scheme.

7.2. Modelling Room: Transmitter, Receiver, and Noise Sources

In order to present the benefits of our new methods (spot-diffusing, transmit power adaptation, imaging diversity reception and MC-CDMA) in indoor mobile OW multigigabit systems, a simulation was developed in two room scenarios denoted as A and B, similar to those described in Chapter 5, where room dimensions of 8 m × 4 m × 3 m were used. Room A is an empty room (without furniture) with a reflectivity of 0.8 for the walls and ceiling and 0.3 for the floor. Room B represents a real office environment that consists of windows, a door, mini-cubicles, bookshelves, and other objects. Two walls (except the door) in Room B are covered with bookshelves and filing cabinets having a 0.4 diffuse reflectivity. It is assumed that glass windows do not reflect any signal. However, ceiling and walls surrounding windows diffusely reflect signals with a reflectivity of 0.8. It is also assumed that those signals that reach the cubical office partitions are either absorbed or blocked. The complicated environment in Room B introduces shadowing attributed to physical partitions and low reflectivity objects. The reflections in the two room scenarios (Rooms A and B) are modelled through the segmentation of the reflecting surfaces into a number of equal size reflection elements that act as Lambertian reflectors. In order to assess the system's performance, the eight halogen spotlight lamps used in the previous

chapters were chosen to illuminate the two environments considered. These lamps produced a well-illuminated environment. Furthermore, an imaging diversity receiver, discussed in Chapter 6, is implemented to provide a robust link against BN, multipath dispersion and signal blockage. A photodetector array that faces up is used as a single imaging receiver. Optical filters were not used in this chapter.

In this chapter, we model an adaptive LSMS in conjunction with an imaging diversity receiver, and compare the results with two other OW systems: CDS and LSMS systems that employ imaging diversity receivers. Also, for comparison purposes, two imaging receivers (i) a single imaging receiver and (ii) an imaging diversity receiver are employed in all the systems considered. In order to judge the proposed systems under mobility, the transmitter was placed at three different locations on the CF (2m, 4m, 1m), (1m, 1m, 1m) and (2m, 7m, 1m), pointed upwards, and emitted 1 W total optical power with an ideal Lambertian radiation pattern. LSMS uses a diffusing spot distribution pattern where a line of spots with equal intensities (in our case 80 spots) is formed in the middle of the ceiling, i.e. at x = 2 m and along the y-axis when the transmitter is placed at the centre of the room. It is developed and evaluated here for the first time with imaging receivers. The spot distribution structure in ALSMS is similar to that in LSMS, but the total power is adaptively distributed among the spots in ALSMS so as to optimise the receiver SNR. Throughout this chapter, computations were carried out following the procedure given in Chapter 6, Section 6.2.2 to determine the new reception area of each pixel based on the receive angles associated with the pixel and the new receiver location. Additionally, as the transmitter moves, the distribution of the spots can be determined in the room following the procedure given in Fig. 3.7.

In a real OW environment in the presence of transmitter and receiver mobility, a simulation algorithm, similar to that developed in the previous chapter (Chapter 6), was used to obtain the channel impulse response and the full channel characteristics (delay spread, 3dB channel bandwidth and SNR) due to each pixel based on its FOV and the area it observes. In our imaging receiver, two approaches (SB and MRC) are considered to process the resulting electrical signals.

7.3. Delay Spread Evaluation and Bandwidth

In this section, we evaluate the multipath propagation effects on the proposed OW configurations in the two room scenarios, and simulation results are presented in terms of delay spread and 3 dB channel bandwidth. Comparisons are also made among the proposed OW systems in terms of SNR, and the results are discussed in Section 7.4.

Figs. 7.1 (a) and (b) compare the delay spread distribution of the proposed mobile OW systems (CDS with a 65^{o} FOV non-imaging receiver, CDS, LSMS, and ALSMS based on an imaging receiver with SB) in the two room scenarios (Room A and B) respectively, when the transmitter is placed in the corner of the room (1m, 1m, 1m) and the receiver moves at constant x = 2 m, and along the y-axis over the CF. It can be seen that the delay spread of all systems considered in Room B is lower than that in Room A due to the limited range of rays captured by the receiver. This is a result of the fact that some rays are blocked by the objects in Room B, and some spots which fall on the glass windows (according to the transmitter location) are lost. Note that the reduction in delay spread here is accompanied by a reduction in collected power and therefore the SNR is a better measure of performance.

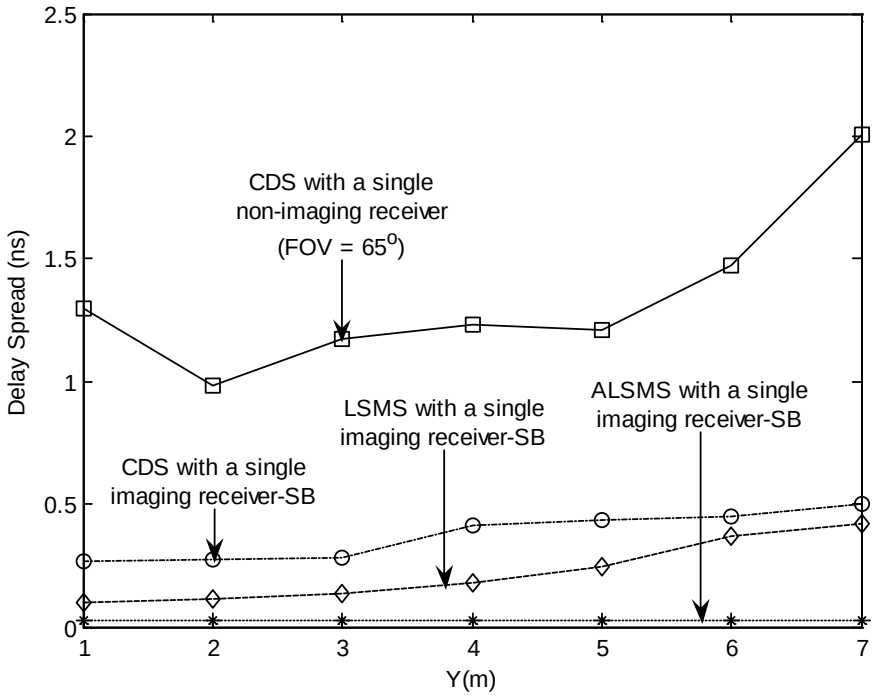

(a)

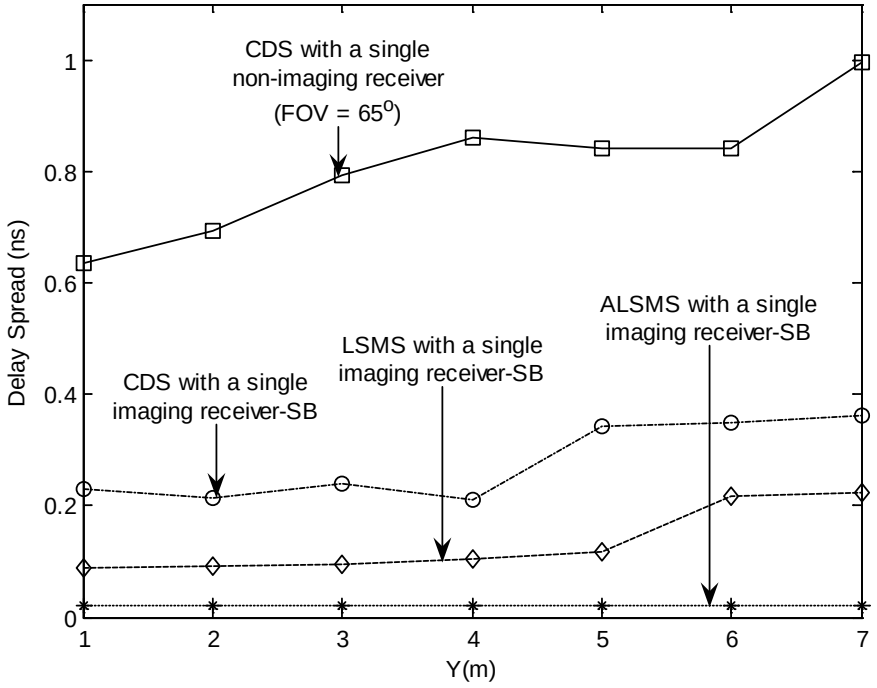

(b)

Figure 7-1: Delay spread distribution of four mobile OW systems; CDS with a single non-imaging receiver, CDS, LSMS, and ALSMS in conjunction with a single imaging receiver based on SB in two room scenarios (Rooms A and B) when the transmitter is placed in the corner of the room (1m, 1m, 1m) and the receiver is at constant x = 2 m and along the y-axis. (a) Room A (b) Room B

In the CDS system, a reduction in the delay spread from almost 2 ns to 0.5 ns is obtained when an imaging receiver replaces the non-imaging receiver at one of the least successful locations and where the transmitter is placed at (1m, 1m, 1m) and the receiver is at (2m, 7m, 1m). This is attributed to the small pixels and their narrow FOV which results in a limited range of received rays. Fig. 7.1 (b) also indicates that the imaging ALSMS system reduces the delay spread by a factor of 22 over the imaging CDS. This reduction is due to assigning higher power levels to spots nearest to the receiver which increases the power captured through the direct path and reduces the influence of the reflecting elements, resulting in a lower multipath dispersion. The results confirm the benefits of our methods (spot power adaptation and imaging reception). The results can also be expressed in terms of bandwidth improvement, see Table 7.1. The 3 dB channel bandwidth of our proposed imaging OW systems is quoted in Table 7.1.

TABLE 7-1: A 3 dB BANDWIDTH OF THE PROPOSED IMAGING SYSTEMS AND COMPARISON WITH NON-IMAGING CDS

Configuration	**3 dB Channel Bandwidth (GHz)**						
	Y (m)						
	1	**2**	**3**	**4**	**5**	**6**	**7**
CDS with a single non-imaging receiver (FOV = 65^o)	0.064	0.084	0.071	0.067	0.068	0.056	0.041
CDS with a single imaging receiver-SB	0.31	0.3	0.29	0.2	0.19	0.18	0.16
LSMS with a single imaging receiver-SB	0.83	0.75	0.62	0.46	0.34	0.22	0.19
ALSMS with a single imaging receiver-SB	7.61	7.58	7.57	7.56	7.54	7.51	7.5

The imaging ALSMS system increases the bandwidth from 41 MHz (CDS with a 65^{o} FOV non-imaging receiver) to 7.5 GHz at a transmitter-receiver horizontal separation of 6 m. This significant bandwidth improvement can help increase the individual user data rate or can help in a multi-user system.

7.4. SNR

The SNR under the adaptive line strip spot-diffusing transmitter combined with imaging diversity receiver was evaluated and compared with two other proposed systems: CDS and LSMS with imaging diversity receiver at different transmitter and receiver locations on the CF. The imaging ALSMS system produces a significant performance improvement compared to the other geometries.

7.4.1. Comparison of Imaging and Non-Imaging 30 Mbit/s CDS Systems

Figs. 7.2 (a) and (b) show the detected SNR for both imaging and non-imaging CDS systems under the impairments of ambient light noise and multipath dispersion in Room A, when the transmitter is placed at (2m, 4m, 1m) and (2m, 7m, 1m) respectively, and the receiver moves along the x = 1 m line. The results are quoted when the systems operate at a bit rate of 30 Mbit/s. This low bit rate (30 Mbit/s) was considered to enable comparison to previous work [94]. The pre-amplifier used for the 30 Mbit/s systems is the PIN FET transimpedance receiver used in [94]. The peaks and troughs of the BN are manifest in the SNR in the non-imaging CDS system. This is due to the noise distribution having a very low value at y = 2, 4, and 6 m, as the receiver is not underneath a spotlight, while high noise levels are detected at y = 1, 3, 5, and 7 m.

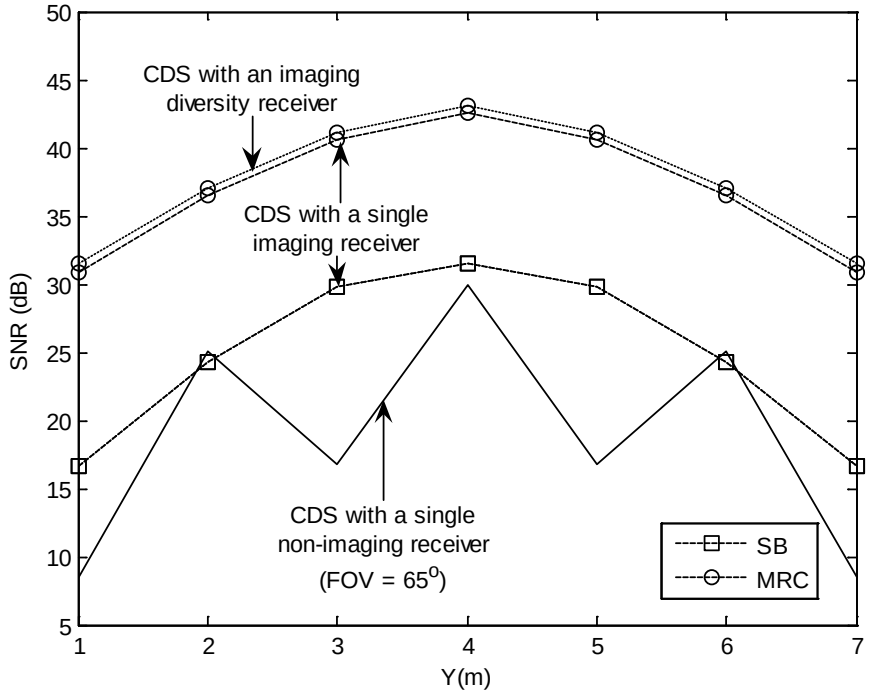

(a)

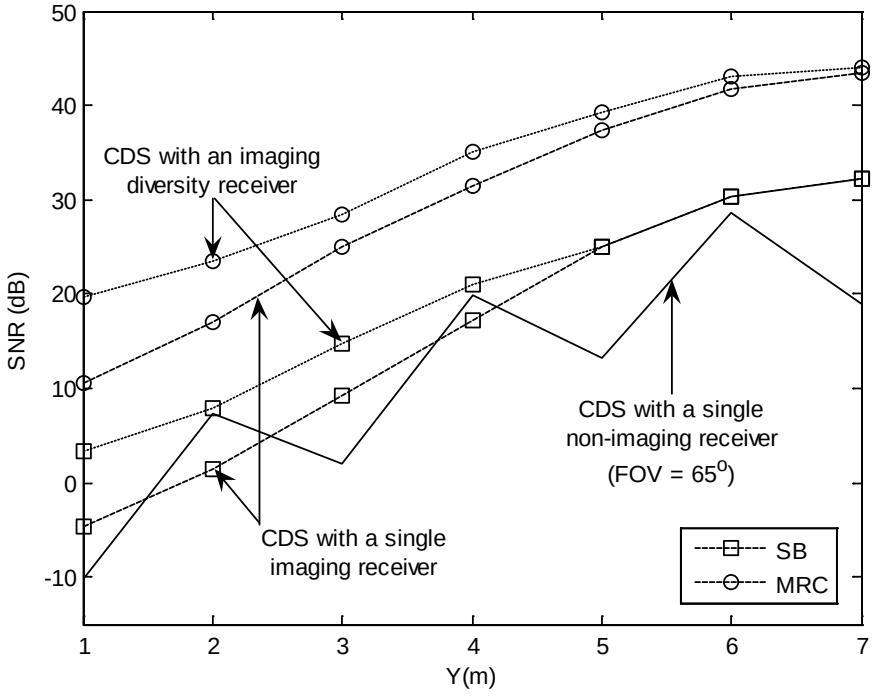

(b)

Figure 7-2: SNR of CDS system in conjunction with a single non-imaging receiver, a single imaging receiver, and an imaging diversity receiver when the receiver moves along the x = 1 m line and the transmitter is placed at: (a) (2m, 4m, 1m) and (b) (2m, 7m, 1m)

The fluctuation in the CDS SNR is mitigated when the imaging receiver replaces the non-imaging receiver. For example, at the least successful transmitter and receiver locations when the transmitter is located at (2m, 7m, 1m) and the receiver is in the corner of the room (1m, 1m, 1m), the imaging MRC CDS system offers a significant SNR improvement of 20 dB approximately over the conventional non-imaging diffuse system. This result agrees very well with that presented in [94]. This enhancement in the SNR level is attributed to the ability of the imaging receiver to spatially select (or MRC combine) those pixels that observe minimum background noise. Moreover, there is a reduction in the noise level that is collected by the small pixels and their associated narrow FOV. Furthermore, degradation in the imaging CDS performance is observed when the imaging receiver moves away from the transmitter towards the edges. This is due to the weak optical power collected at a large transmitter-receiver separation. The results also indicate that an SNR improvement is achieved when the imaging diversity MRC receiver is used instead of a single imaging MRC receiver in the CDS system. For example at transmitter and receiver locations of (2m, 7m, 1m) and (1m, 1m, 1m) respectively, replacing the single imaging MRC receiver by an imaging diversity MRC receiver can increase the SNR by almost 8 dB. This SNR improvement is attributed to the wider ceiling area that can be covered by the imaging diversity receiver compared to the ceiling area covered by a single imaging receiver.

7.4.2. 30 Mbit/s Imaging Non-Adaptive LSMS Systems

At a bit rate of 30 Mbit/s, the performance of a non-adaptive LSMS in conjunction with a single imaging receiver and an imaging diversity receiver is depicted in Fig.

7.3 (a), when the transmitter is placed at the centre of the room and the receiver moves along the x = 1 m line within Room A. Fig. 7.3 (b) provides performance results when the transmitter is located in the corner of the room (1m, 1m, 1m) and the receiver moves along the x = 2 m line. The results in Fig. 7.3 (a) indicate that a constant SNR in both imaging SB and MRC LSMS systems is observed, in contrast to those displayed in both imaging SB and MRC CDS systems. This is due to the fact that the LSMS configuration has the ability to more uniformly cover its surroundings through the diffusing spots, which gives the imaging receiver an option to collect the signals through the nearest diffusing spots and the shortest paths. In Figs. 7.2 (b) and 7.3 (b), at the worst communication path considered when the transmitter is placed at the room corner (1m, 1m, 1m) and the imaging receiver is at (2m, 7m, 1m), the imaging SB LSMS system offers an improvement in the SNR level, 28 dB approximately, over the imaging SB CDS system, while 17 dB SNR improvement is obtained when both systems employ MRC. Note that due to room symmetry a transmitter at (2m, 7m, 1m) and a receiver that moves along the x = 1 m line (i.e. Fig. 7.2 (b)) is the same case as a transmitter that is placed at (1m, 1m, 1m) and a receiver that moves along the x = 2 m line (i.e. Fig. 7.3 (b)) and therefore Figs. 7.2 (b) and 7.3 (b) can be compared. Furthermore, the mobile LSMS system performance with MRC improves by 1 dB when the imaging diversity receiver is implemented instead of a single imaging receiver. This observation confirms the presence of direct path components that the LSMS configuration can provide at every transmitter and/or receiver location in the configurations considered.

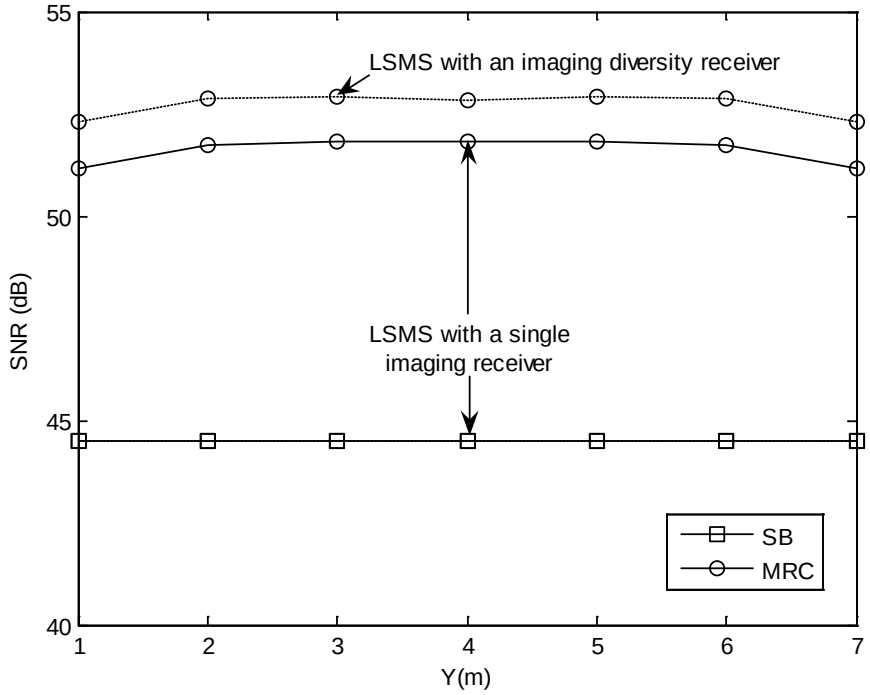

(a)

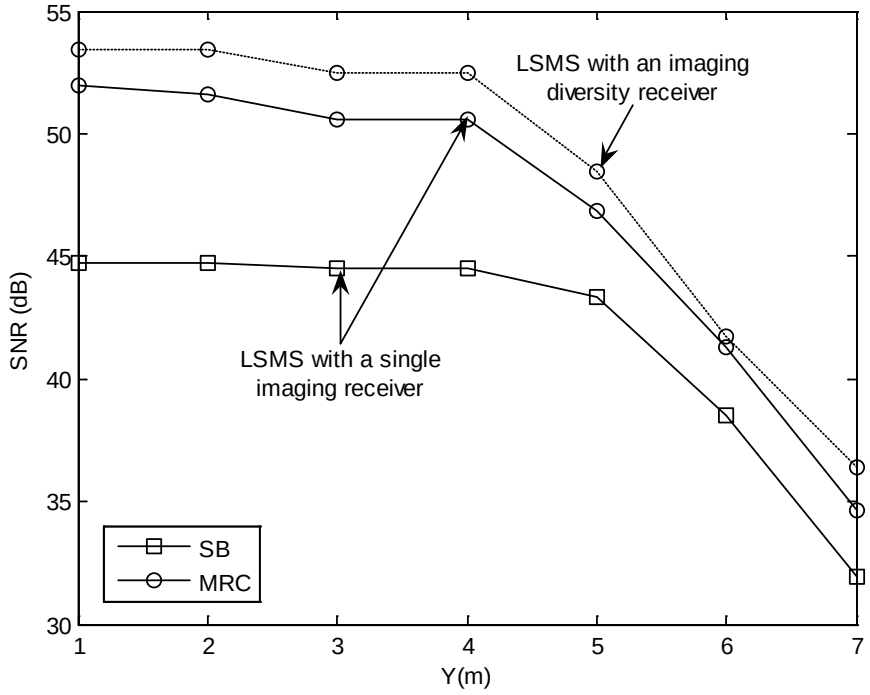

(b)

Figure 7-3: SNR of LSMS system in conjunction with a single imaging receiver and imaging diversity receivers (a) when the transmitter is placed at (2m, 4m, 1m) and the receiver moves along the x = 1 m line (b) when the transmitter is placed at (1m, 1m, 1m) and the receiver moves along the x = 2 m line

7.4.3. 30 Mbit/s, 2.5 Gbit/s and 5 Gbit/s Imaging Adaptive LSMS Systems

The performance of our proposed system (adaptive LSMS with an imaging diversity receiver) is assessed under the impairments of ambient light noise, multipath propagation, mobility and signal blockage, i.e. in the presence of windows, office cubicles, and bookshelves in the environment considered (Room B). Our system SNR (imaging ALSMS SNR) is compared to that of other OW systems (imaging LSMS, non-imaging and imaging CDS systems) when all systems operate at a bit rate of 30 Mbit/s. The results are depicted in Figs 7.4 (a) and (b) when the receiver moves along the x = 1 m line within room A at two transmitter positions: the room centre (2m, 4m, 1m) and one of the room edges (2m, 7m, 1m) respectively. Figs. 7.5 (a) and (b) show the shadowed SNR of the proposed systems. In the unshadowed CDS system at one of the worst communication paths considered, replacing the non-imaging receiver by an imaging receiver with MRC increases the SNR by 20 dB. This SNR improvement is attributed to the reduction in the collected noise level by spatially selecting (or MRC combining) those pixels that observe minimum BN, and due to the minimisation of the thermal noise level based on the small pixel and its narrow FOV. Further SNR enhancement of 24 dB is achieved when the LSMS replaces the CDS when both systems employ an imaging MRC receiver, again at the worst location. This is due to the ability of the spot-diffusing structure to maintain direct path components at every imaging receiver location. Furthermore, previous work [96] has shown that a slight performance improvement, less than 1 dB can be achieved by using MRC instead of the SB scheme in the LSMS system with a 3-face non-imaging diversity receiver. In contrast, an improvement, almost 7 dB in the SNR is observed in the LSMS with an imaging receiver when using an MRC instead of the SB approach.

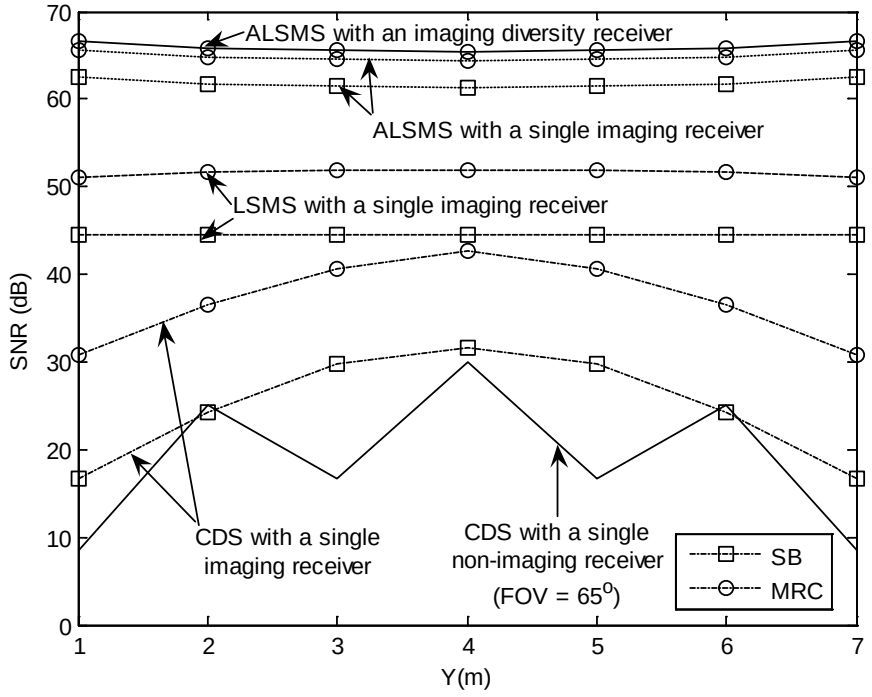

(a)

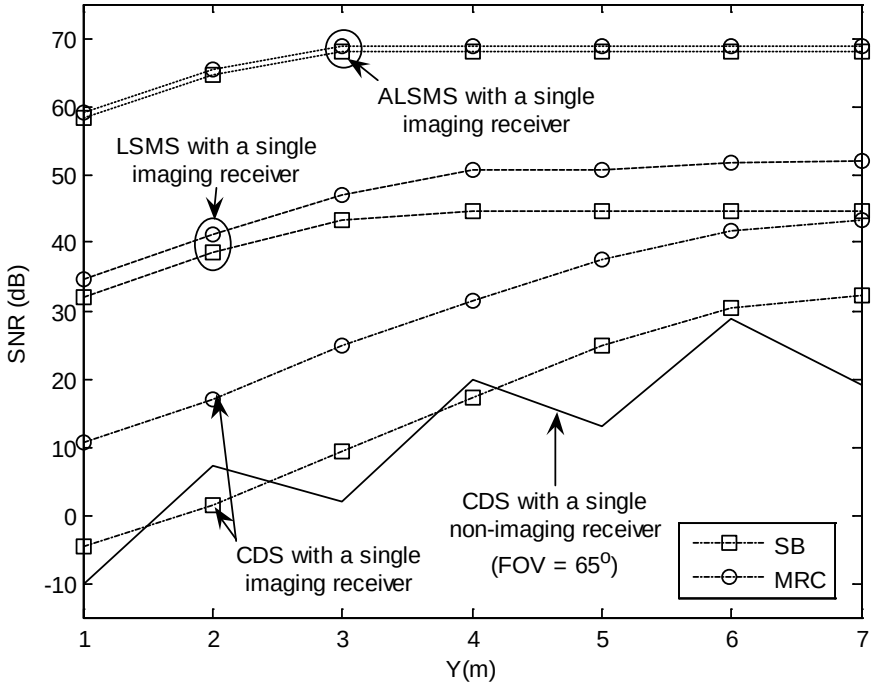

(b)

Figure 7-4: SNR of the proposed imaging OW systems (CDS, LSMS and ALSMS) operating at a bit rate of 30 Mbit/s, and comparison with the 30 Mbit/s non-imaging CDS when the receiver moves along the x = 1 m line within room A at transmitter locations of (a) (2m, 4m, 1m) and (b) (2m, 7m, 1m)

Our imaging MRC ALSMS system offers 23 dB SNR improvement over the imaging MRC LSMS system at a 6 m transmitter-receiver horizontal separation. It is also observed that employing an imaging diversity MRC receivers instead of a single imaging receiver based on MRC can improve the ALSMS SNR by less than 1 dB.

In the presence of shadowing (Room B) i.e. comparing Rooms A and B, the non-imaging CDS performance degrades by 12.8, 15.5, 11.2, 14.3, 7.7, 8.8, and 11 dB when the non-imaging receiver is placed at y = 1, 2, 3, 4, 5, 6, and 7 m respectively and the transmitter is positioned at (2m, 7m, 1m). This performance degradation is reduced to 8.1, 6.1, 2.1, 1.4, 0.66, 0.66, and 0 dB at the receiver locations mentioned when an imaging SB receiver is implemented instead of the non-imaging receiver. When the transmitter is stationary at the centre of the room, the shadowing-based degradation in the imaging CDS SNR is smaller than that observed when the transmitter is placed at (2m, 7m, 1m). This can be explained by observing the fact that most of the reflections in CDS are due to the ceiling, which is a key factor when using imaging receivers, and hence, the effect of shadowing is limited in this case (when the transmitter is at the centre of the room). In addition, employing an LSMS configuration coupled with an imaging receiver helps mitigate the impact of shadowing by providing a direct path component to the receiver. These direct path components can be significantly enhanced by utilising an adaptive spot-diffusing transmitter, which assigns high power levels to spots nearest to the receiver. The larger bandwidth (7.5 GHz) made available through the use of an ALSMS transmitter and an imaging receiver coupled with the high SNR in Fig. 7.5 (a) and (b) can be used to increase the system data rate or to enable multi-user communication. We consider higher data rates here and multi-user communication in Section 7.5.

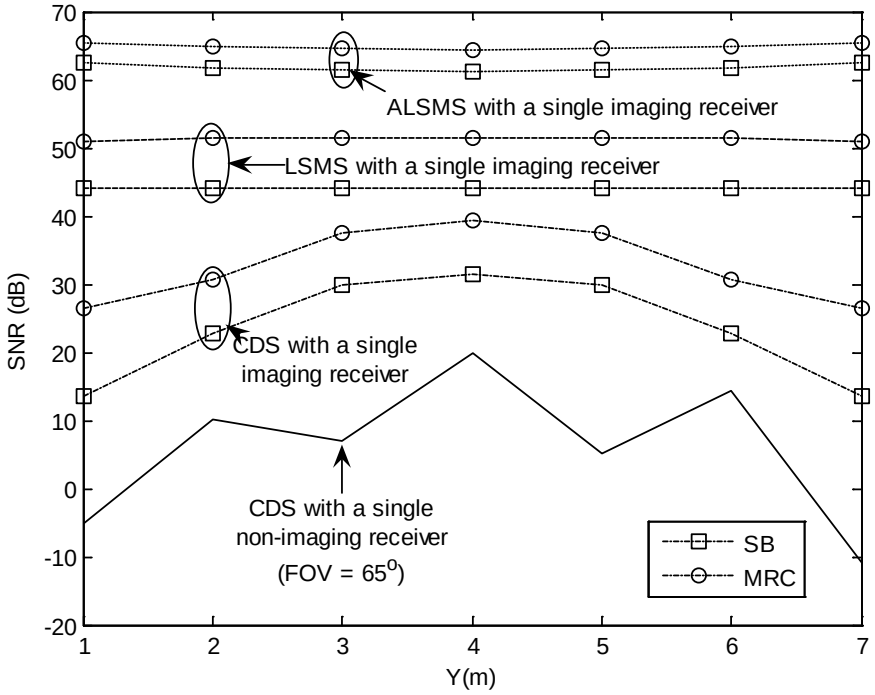

(a)

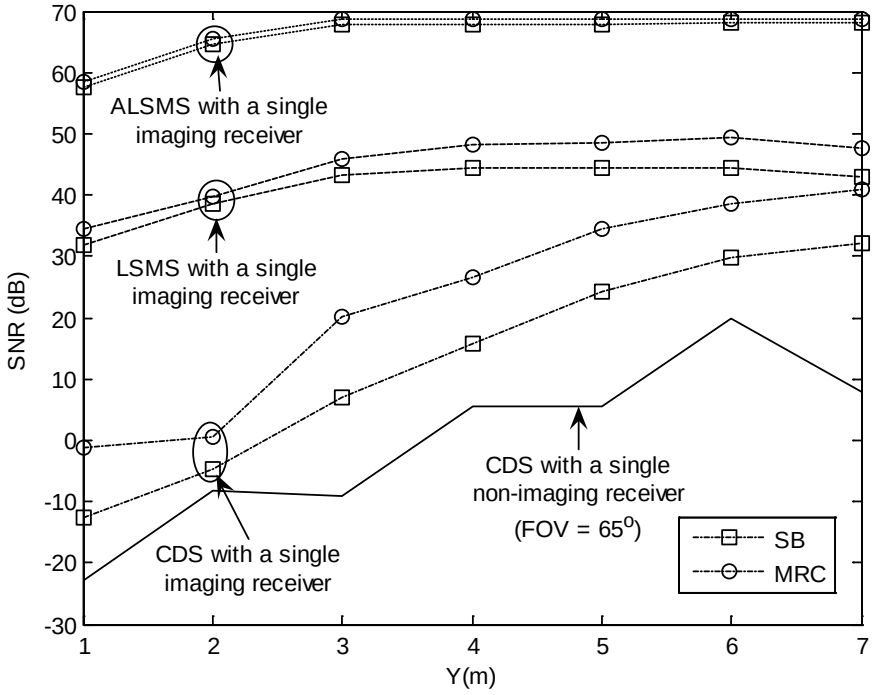

(b)

Figure 7-5: SNR of the proposed imaging OW systems (CDS, LSMS and ALSMS) operating at a bit rate of 30 Mbit/s, and a comparison of the 30 Mbit/s non-imaging CDS when the receiver moves along the x = 1 m line within room B at transmitter locations of (a) (2m, 4m, 1m) and (b) (2m, 7m, 1m)

Figs. 7.6 (a) and (b) (Room B) show the MRC SNR performance at high bit rates of 2.5 Gbit/s and 5 Gbit/s (when using the PIN FET receiver in [184] and when the bandwidth was limited to 2.5 GHz and 5 GHz respectively) when the receiver moves along the x = 1 m line and the transmitter is placed at (2m, 4m, 1m) and (2m, 7m, 1m) respectively. Our new 5 Gbit/s imaging MRC ALSMS system offers an SNR improvement of 20 dB over the non-imaging CDS system that operates at 30 Mbit/s at the worst communication path considered in the shadowed environment (Room B). In order to achieve acceptable performance, the SNR has to be 15.6 dB or better for conventional OOK systems. Therefore, among the systems considered, only ALSMS with an imaging MRC receiver is able to achieve the required performance. This is achieved with full mobility at 5 Gbit/s which is a useful result for wireless communications.

7.5. Multi-User OW Communication Systems

In this section, we aim to demonstrate how the significant bandwidth and SNR improvements achieved can be used to provide multi-user OW communication systems by using an MC-CDMA scheme. The OW MC-CDMA system employs N subcarriers and each user transmits M bits during a signalling interval, leading to the spreading factor (the processing gain) $N_{code} = N/M$. The modelling of OW MC-CDMA was given in Chapter 5, Section 5.4, and its performance was first analysed in Section 5.5. Here we present both computer simulation and theoretical results and used to assess the BER of the proposed MC-CDMA OW imaging systems based on an SB approach in a multi-user scenario (note that the Chapter 5 systems were non-imaging). The system operated at a data rate of 30 Mbit/s.

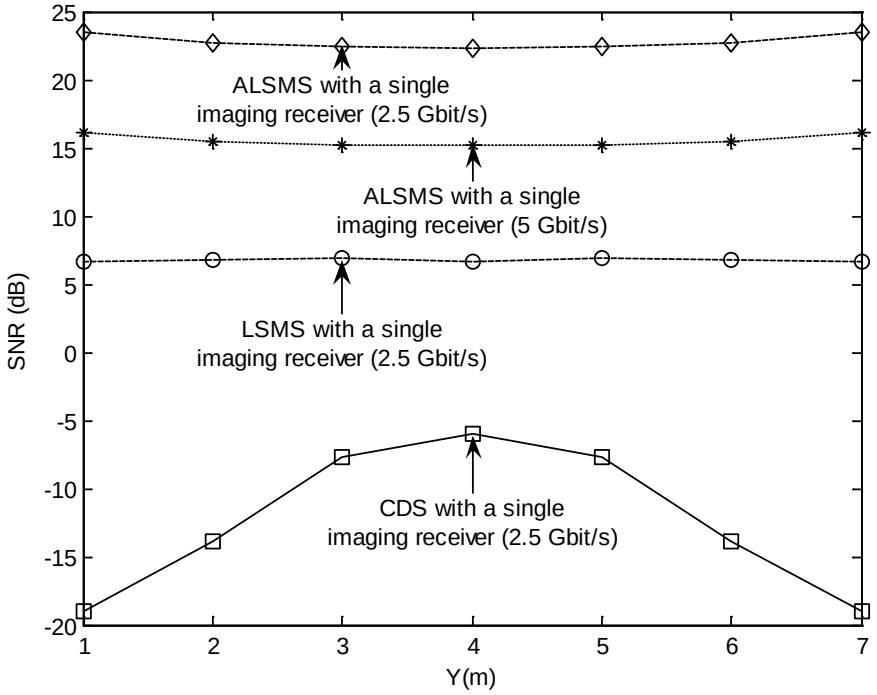

(a)

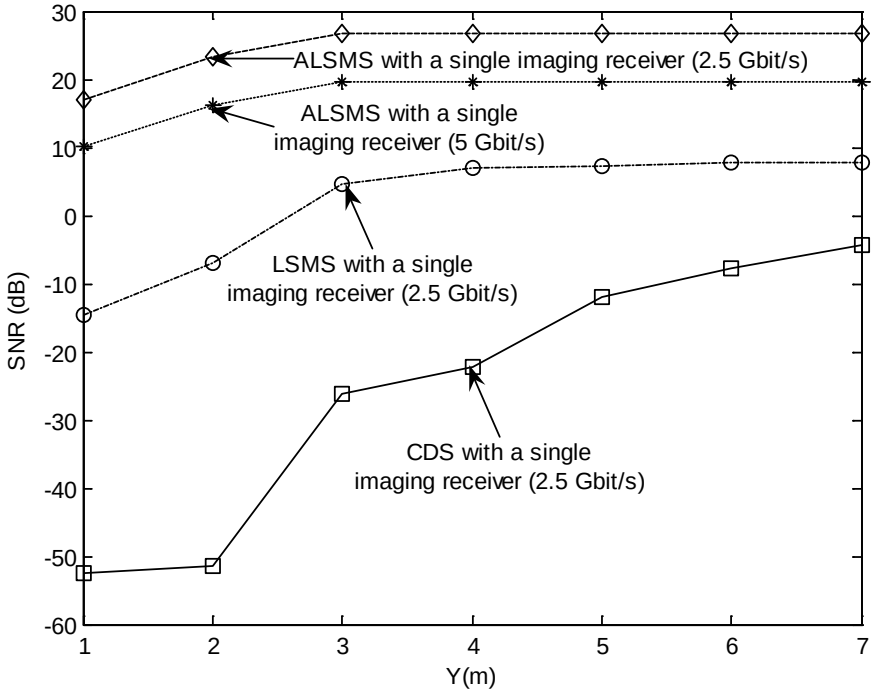

(b)

Figure 7-6: SNR of the proposed imaging MRC OW systems (CDS, LSMS and ALSMS) operating at a bit rate of 2.5 Gbit/s, and a comparison with the 5 Gbit/s imaging ALSMS when the receiver moves along the x = 1 m line in room B at transmitter locations of (a) (2m, 4m, 1m) and (b) (2m, 7m, 1m)

For the MC-CDMA OW system, we have used the PIN FET receiver in [184] and the bandwidth was limited to 2 GHz to accommodate the MC-CDMA symbol that requires a bandwidth of 1.95 GHz (64 subcarriers send at the data rate). The effect of all the parameters such as the delay spread, receiver structure, SNR and positions of transmitter and receiver are studied. Orthogonal gold codes are used as the signature sequence. Each user is assigned a different sequence code. The length of the signature sequence is equal to the number of subcarriers used which is 64 in both the computer simulation and the theoretical analysis. The analytic and simulation environments were previously described in Chapter 5, Section 5.6.1. The SNIR was evaluated using (5.29). Theoretical BER predictions are quoted versus SNR, see Fig. 7.7.

Fig. 7.7 compares the BER (BER simulation results) of two OW MC-CDMA systems (an MC-CDMA LSMS system with an angle diversity non-imaging receiver and an MC-CDMA imaging ALSMS system) when both transmitter and receiver are co-located at the centre of the room within Room A, in a multi-user scenario. Fig. 7.7 also illustrates the theoretical BER predictions of the OW MC-CDMA system. The MC-CDMA non-imaging LSMS BER simulation results with multiple users are in agreement with the theoretical BER predictions [171]. The performance degrades gradually as the number of users increases due to the increase in MAI. The results indicate that the MC-CDMA imaging ALSMS system offers a BER improvement over the MC-CDMA non-imaging LSMS system. This BER improvement is attributed to the reduction in the MAI influence as a result of reduction in the delay spread. For example, in an 8-user OW MC-CDMA system at a 15 dB SNR, the BER improves from 1.3×10^{-4} to 1.8×10^{-5} when our new imaging ALSMS replaces the non-imaging LSMS.

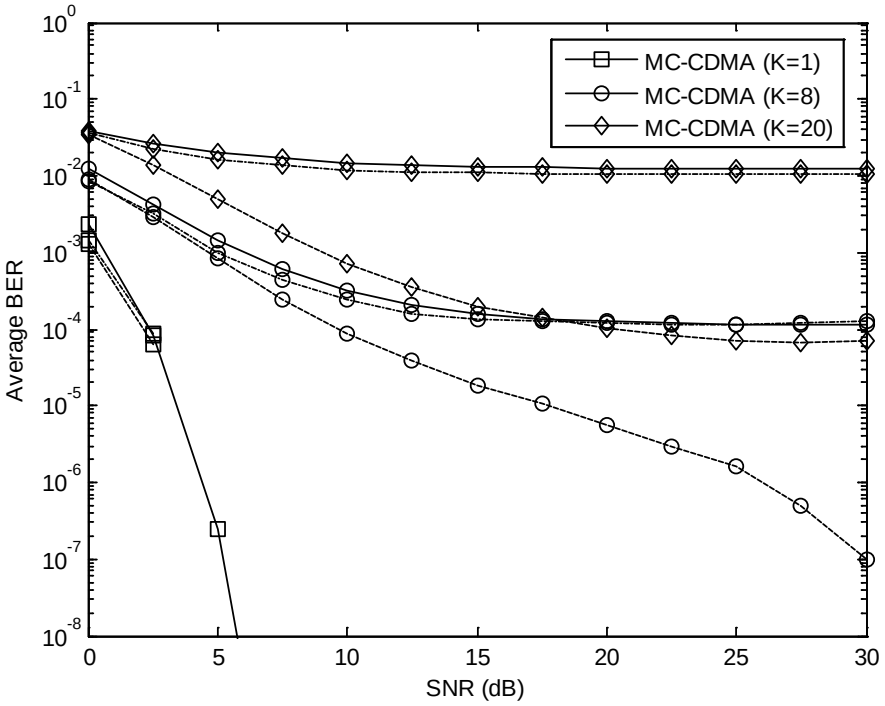

Figure 7-7: BER of the MC-CDMA system with multiple active users over indoor OW channels at different SNR levels, sold lines represent the theoretical results, dot-dashed lines represent the simulation results of the MC-CDMA LSMS system with a non-imaging diversity receiver, and dashed lines represent the simulation results of the MC-CDMA imaging ALSMS system

Fig. 7.8 shows the degradation in the BER of the mobile MC-CDMA non-imaging CDS system due to an increase in the delay spread from 0.63 ns to almost 1 ns (as shown in Fig. 7.1 (b)) associated with moving the non-imaging receiver 6 m away from the transmitter. The results indicate that in a 20 user mobile MC-CDMA CDS system at a 10 dB SNR, the BER improves from 6.4×10^{-2} to 4.8×10^{-3} when the imaging SB receiver replaces the non-imaging receiver at a 6 m transmitter-receiver horizontal separation. Also, at a BER of 10^{-2} a 4 dB SNR improvement is obtained by replacing the conventional diffuse transmitter by an adaptive spot-diffusing transmitter when both are combined with an imaging SB receiver with 20 active users.

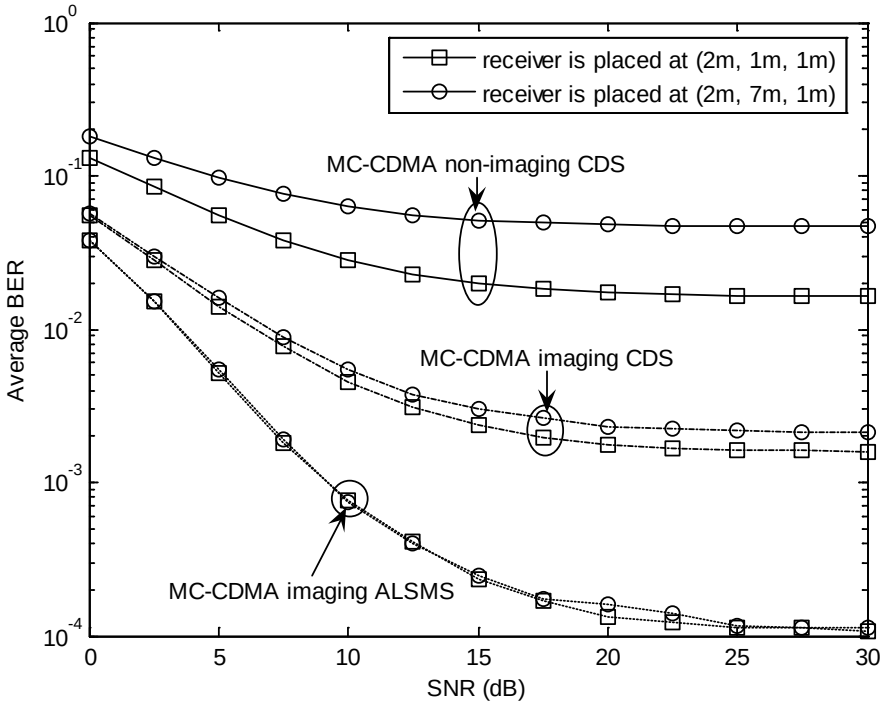

Figure 7-8: BER of three mobile OW MC-CDMA systems, MC-CDMA CDS system with a single non-imaging receiver, MC-CDMA CDS and MC-CDMA ALSMS with a single imaging receiver based on SB in Room B when the transmitter is placed in the corner of the room (1m, 1m, 1m) and the receiver is at (2m, 1m, 1m) and (2m, 7m, 1m) with 20 active users

Figs. 7.9 (a) and (b) compare the BER of two mobile MC-CDMA OW systems (LSMS, and ALSMS in conjunction with an imaging receiver based on SB) over a poor communication environment (Room B), with multi-user scenario when the imaging receiver moves along the x = 1 m line at transmitter positions of (2m, 4m, 1m) and (2m, 7m, 1m) respectively. These receiver locations have been chosen since they represent the worst communication links over the entire CF (movement inside the office cubicles). Our new MC-CDMA imaging ALSMS system offers a BER improvement over the MC-CDMA imaging LSMS system at all the transmitter and receiver locations considered.

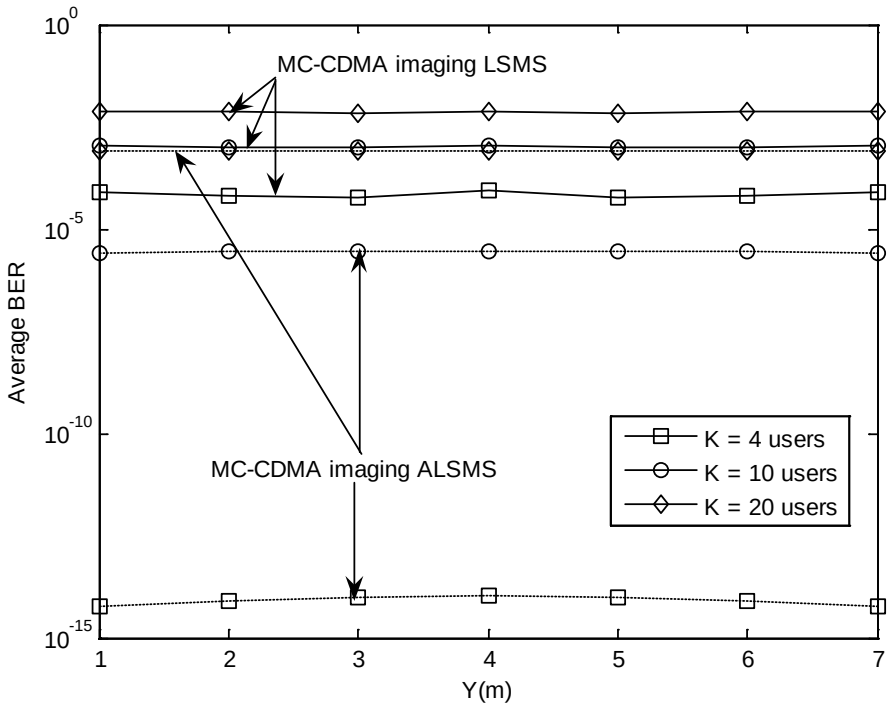

(a)

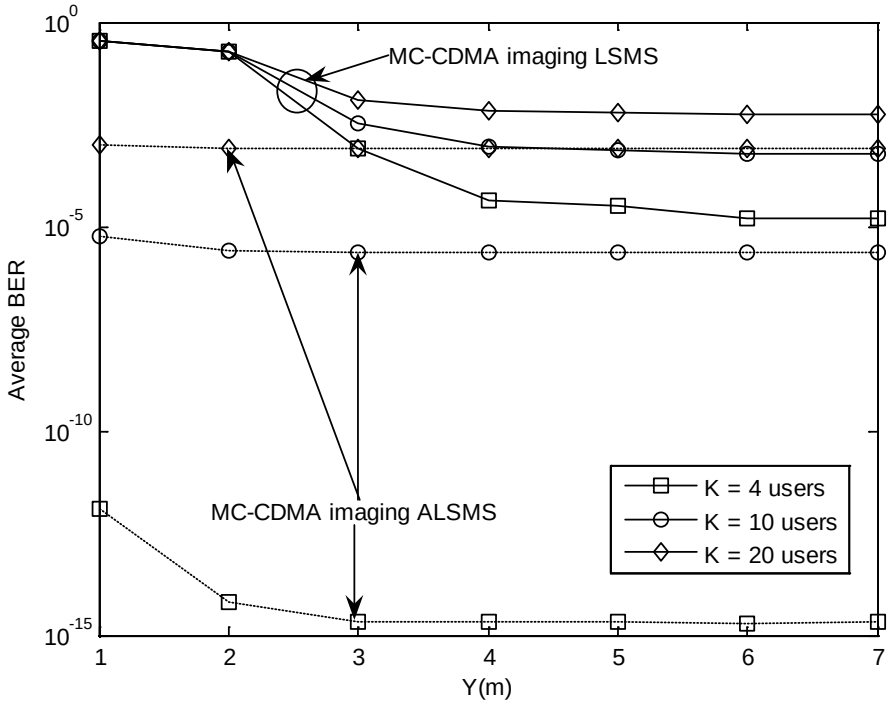

(b)

Figure 7-9: BER of two mobile OW MC-CDMA systems: MC-CDMA LSMS and MC-CDMA ALSMS with a single imaging receiver based on SB in Room B with multiple users when the receiver moves along the x = 1 m line at transmitter locations of (a) (2m, 4m, 1m) and (b) (2m, 7m, 1m)

For example an improvement in the 10-user MC-CDMA OW system BER from 1×10^{-3} to 2.6×10^{-6} is achieved when the ALSMS is employed instead of the LSMS, at the worst communication environment (Room B) when the transmitter is placed at (2m, 4m, 1m) and the imaging receiver is at (1m, 1m, 1m). This significant BER improvement is due to the large bandwidth of the imaging ALSMS channel almost 8 GHz and the enhanced SNR. The results in Fig. 7.9 (a) shows a constant BER in the MC-CDMA imaging LSMS system when the transmitter is placed at the centre of the room. This is due to the ability of the LSMS configuration at this transmitter location (i.e. the room centre (2m, 4m, 1m)), to maintain a direct path component between the transmitter and the receiver through its multiple diffusing spots, even in the presence of office partitions. The diffusing spots provide a large number of potential LOS paths in this case. However, shadowing significantly decreases the BER in the MC-CDMA imaging LSMS system when the transmitter moves towards the edges of the room, for example, in a 4-user MC-CDMA imaging LSMS, the BER performance degrades from 7.5×10^{-5} to 3.5×10^{-1} when the imaging receiver is located in the corner of the room (1m, 1m, 1m) and the transmitter moves from (2m, 4m, 1m) to (2m, 7m, 1m). This BER degradation is dramatically improved from 3.5×10^{-1} to 0.12×10^{-11} through transmit power adaptation.

7.6. Summary

This chapter introduced three methods (spot-diffusing, beam power adaptation and imaging reception) to improve the OW system performance even in the presence of shadowing. Imaging receivers can help mitigate the BN effect by selecting (or MRC combining) those pixels that observe a lower BN, and by minimising the pre-amplifier thermal noise through the use of small sized pixels (that correspond to

photodetectors with a low capacitance allowing a large resistance to be used). In the absence of shadowing at a 6 m transmitter-receiver separation, an SNR improvement of 20 dB is achieved in the 30 Mbit/s CDS system when an imaging receiver with MRC replaces a single non-imaging receiver in agreement with previous results in the field. The CDS SNR performance further improves by 8 dB when an imaging diversity receiver with MRC replaces the single imaging MRC receiver. Further SNR enhancement of 17 dB is obtained when the spot-diffusing transmitter is implemented instead of a conventional diffuse transmitter when both transmitters use an imaging diversity receiver based on MRC. This improvement is due to the presence of direct path components made possible through the use of the spot-diffusing transmitter configuration. Furthermore, our new ALSMS can help enhance those direct path components and reduce the influence of reflections by assigning higher power levels to spots nearest to the receiver. The imaging MRC ALSMS system offers an SNR improvement of 23 dB over the imaging MRC LSMS when both systems operate at 30 Mbit/s. The lower bit rate (30 Mbit/s) facilitates comparison with previous work.

This significant SNR improvement achieved through the combination of transmit power adaptation, spot-diffusing and imaging reception can help reduce the transmit power. In order to achieve a BER of 10^{-9}, the SNR has to be 15.6 dB for conventional OOK systems. Therefore, at the worst communication path considered in the 30 Mbit/s OOK system, the combination of the spot-diffusing geometry and imaging reception with MRC can reduce the transmit power by almost 10 dB while achieving 10^{-9} BER. A further reduction in the transmit power requirement of 12 dB can be achieved when the beam power adaptation method is implemented. As such,

in our proposed systems, the power required in each beam is relatively low and can be transmitted in compliance with eye safety regulations.

The combination of the adaptive spot-diffusing transmitter and imaging receiver increases the bandwidth from 46.5 MHz to 7.5 GHz compared to the non-imaging CDS system, thus helping to increase the channel capacity. The increase in channel bandwidth and SNR can be used to achieve higher data rates and 2.5 Gbit/s and 5 Gbit/s OW systems were shown to be feasible. Alternatively, these improvements can be used to enable multi-user communication. We introduced an MC-CDMA ALSMS imaging OW system to provide multiple access facilities and improve the BER. The MC-CDMA imaging ALSMS system achieves a BER of 0.12×10^{-11} in a 4-user scenario compared to a BER of 3.5×10^{-1} when MC-CDMA imaging LSMS is considered. This significant improvement is achieved in a highly impaired environment where shadowing is present.

8. BEAM POWER AND ANGLE ADAPTATION IN MULTIBEAM SPOT DIFFUSING OPTICAL WIRELESS SYSTEMS

8.1. Introduction

Mobility and shadowing can induce significant SNR performance degradation in OW systems based on diffuse as well as spot-diffusing configurations. Therefore, efficient schemes are in demand to reduce the link performance degradations as well as provide robustness against shadowing. Our previous work [104-105, 110-111] has shown that adaptively distributing the power among the beams can significantly improve the link performance under the constraints of ambient light noise, multipath dispersion, mobility and shadowing, compared to the other non-adaptive systems. Although a significant performance improvement has been achieved, SNR degradation can be observed due to transmitter mobility, shadowing and signal blockage. The positions of the spots are dictated by the transmitter position when the beam angles are fixed. With fixed beam angles and when the transmitter and receiver are at opposite room corners (or far from each other) the spots are clustered near the transmitter in the ceiling and the corner adjacent to the transmitter. Beam power adaptation does not help much in this case, however if the beams can be moved near to the receiver the performance can improve. In addition, the possibility of signal obstruction by moving objects may be more detrimental when the beam angles are fixed, i.e. when they rely on the transmitter position. In order to solve this problem as well as mitigate the SNR degradation due to transmitter mobility and shadowing, beam angle adaptation is considered which introduces a degree of freedom allowing the spatial distribution of the spots to be adjusted (to positions near the receiver) regardless of the transmitter position.

In this chapter, we introduce a novel method (beam angle adaptation) to the design of multi-spot-diffusing optical wireless systems to effectively reduce the effect of mobility as well as improve the link performance in the presence of shadowing. The main goal is to spatially optimise the spots distribution in an area (ceiling and/or walls) based on a multibeam transmitter whose beam angles can be adapted and controlled by a digital signal processor (DSP). The ultimate goal is to maximise SNR at a given receiver location. The multibeam transmitter initially produces a single spot and scan this spot along a number of possible locations (in the ceiling and walls) to identify the location with the best receiver SNR. Simulation results prove that a significant performance improvement can be achieved in a multi-spot-diffusing optical wireless system when our beam angle adaptation method is implemented. However, there is a moderate increase in receiver complexity. This is associated with the computation time required to identify the optimum spot location. The SNRs due to the beam at each scan are computed at the receiver and the optimum spot location is selected at the transmitter. Furthermore, once the optimum beam direction is identified using a single spot, all the beam spots are switched ON (i.e. a line strip of spots is generated centred at the optimum spot location), the beam angles are adapted and a transmit beam power adaptation method is then employed to obtain further SNR improvements. The beam power adaptation is carried out at each step in beam angle adaptation (see Section 8.3.2). This method can enable our proposed transmitter to adaptively distribute the power among the spots to produce a higher receiver SNR. The results show that the proposed system (multibeam angle and power adaptive transmitter with an angle diversity receiver) offers an SNR improvement of 29 dB over the traditional angle diversity spot-diffusing system at the worst communication paths considered when both systems operate at 50 Mbit/s,

enabling a reduction in the transmit power requirements. This SNR improvement coupled with an increase in the channel bandwidth from 647 MHz (LSMS) to 5.57 GHz allows the OW system to operate at high bit rates (2.5 Gbit/s, 5 Gbit/s and beyond). The trade-off between complexity and performance enhancement is of interest and is investigated. A significant computational saving in our proposed system (computation time reduction from 12.5 ms to 80 μs) can be achieved at the cost of a performance penalty of 11.7 dB again at the worst communication path considered. Intermediate complexity and hence lower power penalties are also possible. The system robustness against shadowing and signal blockage is also considered.

8.2. System Description

In order to evaluate the advantages of our methods (beam angle and beam power adaptation) in an indoor OW system, a simulation was performed using an empty room with dimensions of 8 m × 4 m × 3 m (length × width × height). It was shown that plaster walls reflect light rays in a form close to a Lambertian function [3]. Therefore the walls (including ceiling) and floor were modelled as Lambertian reflectors with reflectivity of 80 % and 30 % respectively. Reflections from doors and windows are considered to be identical to reflections from walls. The transmitted signal propagates to the receiver through multiple reflections from the room reflecting surfaces which were divided into a number of equal-size, square-shaped reflection elements. The reflection elements have been treated as small transmitters that diffuse the received signals from their centres in the form of a Lambertian pattern. It is noted that third-order reflections and higher do not produce a significant

change in the received optical power [3, 10, 17, 27], and therefore reflections up to the second order are considered. The surface element size used in this work was set to 5 cm × 5 cm for the first-order reflections and 20 cm × 20 cm for the second-order reflections.

To verify the system performance improvements achieved through the combination of our new methods under mobility, three transmitter configurations were considered: line stripe multibeam system (LSMS), multibeam angle adaptive system (MBAAS), and multibeam power and angle adaptive system (MBPAAS), in conjunction with an angle diversity receiver of seven branches. The transmitter was placed at three different locations on the communication floor (2m, 4m, 1m), (1m, 1m, 1m), and (2m, 7m, 1m), pointed upwards, and emitted 1 W total optical power with an ideal Lambertian radiation pattern. Computer-generated holographic beam-splitters are assumed to be mounted on the emitter, resulting in multiple narrow beams, which illuminate multiple small areas forming a line of diffusing spots on the ceiling (LSMS configuration). The illumination direction can be chosen by varying the angles of the beams that produce the spots. Static beam intensities can be produced by employing computer-generated holograms. The beam angles can be varied if a liquid crystal device is used to generate the 2D hologram. Such a device can be used to dynamically generate variable optical spot intensities and optical spot locations on the ceiling and/or walls. As previously mentioned, these devices have μs to ms response times [178] which are adequate given that the beam power and angle adaptation has to be carried out at the rate at which the environment changes (for example, human motion) and not at the data rate. The feasibility of generating multiple beams (2D spots on ceiling) using holograms has been experimentally verified by many [39, 42, 51-52, 179, 185-186]. The implementation of our

technique should be viewed as selecting some of these many possible beams at any one given point in time, rather than "beam steering". The feasibility is then obvious. It is also believed that the holograms used can handle a 1 W optical power. Furthermore, the high SNR performance obtained, 36 dB at the worst communication path, can be used to reduce the transmit power to 93 mW reducing the power density on the hologram and helping with eye safety.

The proposed systems are assessed in the presence of directive noise sources, eight halogen spotlights, which cause high optical spectral corruption levels to the received data stream. PAR38 was chosen and this emits a power of 65 W in Lambertain beams with n_{Lamp} = 33.1. The eight spotlights, which represent ambient background interference were regularly spaced across the ceiling (as shown in Fig. 3.2) at coordinates of (1, 1, 3), (1, 3, 3), (1, 5, 3), (1, 7, 3), (3, 1, 3), (3, 3, 3), (3, 5, 3), and (3, 7, 3). Interference from daylight through windows and doors was not considered in this study. In order to reduce the effect of ambient light noise and multipath dispersion, an angle diversity receiver is employed. The receiver diversity system considered consists of seven photodetector branches. Each face is oriented to a different direction that can be characterised by two angles (*Az* and *El* angles). The *El* of the seven photodetectors are set at 90^o, 65^o, $65^{o,}$ 20^o, 65^o, 65^o, and 20^o. The *Az* for the seven branches of the receiver are fixed at 0^o, 0^o, 90^o, 90^o, 180^o, 270^o, and 270^o. The corresponding FOVs were restricted to 12^o for all the detectors. The *Az*, *El*, and FOVs were chosen through an optimisation similar to that in [44, 46] to achieve the best SNR considering the transmitter locations as well as the system motion. Moreover, the angle diversity receiver is designed so that all the diffusing spots are always positioned within the receiver FOV when our new multibeam angle adaptive transmitter produces a line of 80 diffusing spots with an angle of 0.28^o (at this angle

the spots just touch) between adjacent beams. This choice of the receiver FOV produces a link that is robust against diffusing spot blockage. Furthermore, as will be seen in the results section, the optimum spot geometry in many cases is a geometry where all the spots just touch each other in the line strip (i.e. the angle between adjacent beams is 0.28^{o}). The photosensitive area of each photodetector was set to 1 cm^2 with a detector responsivity of 0.5 A/W. The angle diversity receiver was always placed on the CF (a plane 1 m above the ground). A simulation similar to the one developed and used in Chapter 4 with additional modification (to cater for adapting the beams angles in addition to the beam power adaptation) is used to generate the channel impulse response and obtain its characteristics (delay spread, channel bandwidth and SNR) for a mobile multibeam OW system.

8.3. Transmitter Configurations

In this section, two new multibeam transmitter configurations are presented, analysed, and compared in order to identify the most suitable geometry for use in indoor OW systems. Simulations were carried out to evaluate the improvement achieved through the use of our new methods (beam angle and beam power adaptation) and the influence of optimising the distribution, direction and the intensities of the diffusing spots. The line strip multibeam system is an attractive configuration [95-97, 99-101, 175]. Therefore, it is used for comparison purposes in order to evaluate the proposed novel configurations. Our new adaptive multibeam system configurations (MBAAS and MBPAAS) are introduced and evaluated next.

8.3.1. Multibeam Angle Adaptive System (MBAAS)

The distance between the diffusing spot and the receiver is a key factor in mobile indoor multibeam OW systems. Due to this fact, beam angle adaptation is an effective technique that can help identify the optimum distribution of the diffusing spots to provide the strongest paths between the diffusing spots and the receiver at every transmitter and receiver location. In effect, given the optimum spot positions, the receiver is able to collect high direct path components, which significantly enhances the receiver SNR. A multibeam angle adaptive transmitter is composed of an optical transmitter followed by an adaptive hologram that generates spots whose locations and intensities can be varied where the transmission angles (θ_x and θ_y) in the *x-y* axes are varied between -90^o and 90^o with respect to the transmitter's normal in both the *x* and the *y* directions respectively. A depiction of the MBAAS configuration at transmitter and receiver locations of (1m, 1m, 1m) and (2m, 4m, 1m) is shown in Fig. 8.1. An angle adaptive algorithm is used to automatically aim the transmitter so that it concentrates its diffusing spots at an area (on the ceiling and/or walls) so that the best SNR is produced at the receiver. Essentially the adaptive hologram is made to initially produce a single spot. The spot is scanned along a range of rows and columns in the ceiling and walls to identify the location that yields the best SNR at the receiver. This is then used as the centre of the line strip. This beam angle adaptation step can be followed by beam power adaptation. For a single transmitter and a single receiver at a given set of coordinates (x_T, y_T, z_T) and (x_r, y_r, z_r), the new angle adaptation algorithm determines the two transmission angles θ_x and θ_y, which identify the centre coordinates (x_c, y_c, z_c) of the line strip, according to the following steps:

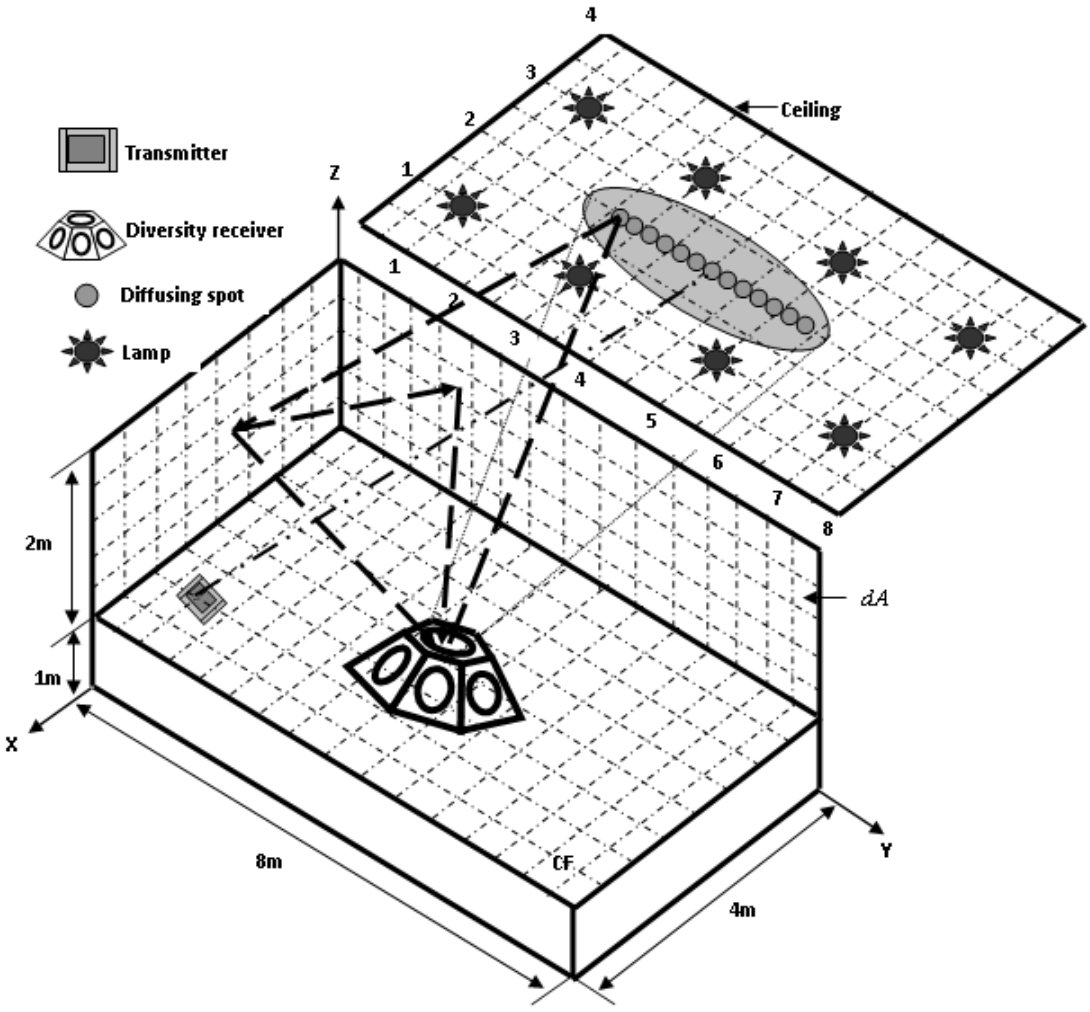

Figure 8-1: OW MBAAS architecture at transmitter and receiver locations of (1m, 1m, 1m) and (2m, 4m, 1m) respectively

1. Move the single spot by changing the beam angles between -90^o and 90^o in steps of 2.29^o along the *x-y* axes (i.e. at each step the spot moves 8 cm resulting in a total of 50 × 100 possible locations in the ceiling of the room). If each SNR computation is carried out in 1 μs, then the optimum spot location can be identified in 5 ms. If the walls have to be scanned as well, then the total time will be less than 3 times this figure owing to the small size of the walls compared to the ceiling. This rate is fast enough given that the beam angles have to be adapted at the rate at which the environment changes, (for example, pedestrian motion).

2. Compute the receiver SNR at each step. In a practical implementation, circuits can be designed with an appropriate MAC protocol to facilitate the computation of the SNR as discussed earlier.
3. Send a feedback signal at low rate to inform the transmitter of the SNR associated with the step. The feedback channel can be implemented using a CDS or by modulating an existing/additional beam whose power is kept fixed (as the data rate is low).
4. At the step where the receiver SNR is maximum, record the associated transmission angles θ_x and θ_y.
5. Determine the x_c, y_c, and z_c position of the spot that maximised the receiver SNR. This (x_c, y_c, z_c) coordinate can be defined based on the transmission angles θ_x and θ_y.
6. Deploy a line strip of spots (80 spots in our case) whose centre is this coordinate, i.e. (x_c, y_c, z_c).
7. Start with an angle of 0.28^o between the beams (all the spots just touch each other in the line strip where each spot has a diameter of 1 cm and the angle is measured between the centres of adjacent beams), vary the angle ϕ_b between the beams in steps of 0.57^o, which makes a lattice space of 2 cm, and compute the SNR at each step. It should be noted that in the line strip multibeam configuration all the angles between the beams are equal. A maximum of 10 cm spacing between the adjacent spots is considered.
8. Send a feedback signal at low rate to inform the transmitter of the SNR associated with the step. Select the angle $\phi_{optimum}$ that gives maximum SNR.

9. Operate the proposed multibeam transmitter using the (x_c, y_c, z_c) coordinate and the angle $\phi_{optimum}$, and distribute the power among the beams in equal intensities.

The complexity can be reduced by increasing the beam angle adaptation step size, see Section 8.5.

8.3.2. Multibeam Power and Angle Adaptive System (MBPAAS)

In contrast to the previous configuration (MBAAS), where the multibeam angle adaptive transmitter distributes the total power, 1 W, equally among the diffusing spots, in this system the total power is distributed unequally so as to further optimise the receiver SNR. In effect, the spots nearest to the receiver are allocated the highest power level, whilst the farthest spot is assigned the lowest power level, so as to maximise the receiver SNR. Once the optimum centre of the line strip (of diffusing spots) is determined and the line strip multibeam transmitter chooses a certain angle ϕ_b, the new power adaptation algorithm adjusts the transmit powers of the individual beams as follows:

1. Switch on each spot individually, compute the power received at the receiver, and calculate the SNR.
2. Inform the transmitter of the SNR associated with the spot by sending a feedback signal at low rate.
3. Repeat steps 1 and 2 for all the spots.
4. Re-distribute the total power among the spots in proportion to the receiver SNR they produce, where a spot that produces maximum SNR gets the highest power level.
5. Increase the angle ϕ_b by 0.57^o and repeat steps 1 to 4.

6. Stop when the maximum allowed spot spacing of 10 cm is reached.
7. Configure the transmitter to operate at the optimum beam angles and beam powers.

The MAC protocol should include a repetitive training period that allows steps 1-5 to be performed. Training should be carried out at the rate at which the environment changes. This is usually a slow rate commensurate with human motion. It has to be noted that the two adaptation algorithms described (angle adaptation algorithm and power adaptation algorithm) apply to a single transmitter and a single receiver position. In a multi-user scenario a number of different methods can be considered. For example opportunistic scheduling [177] can be used to select optimum beam angles and beam powers to maximise the SNR in a given region (set of users) for a given time period. The beam angles and powers can be adjusted using a liquid crystal device that implements different (adaptable) holographic 2D functions. The adaptation takes place at a rate comparable to the rate at which the environment changes and/or the rate of transmitter and receiver motion. This is typically a low pedestrian rate in indoor OW systems which relaxes the demands placed on the feedback channel, the computation circuits and the liquid crystal device and ensures that the associated MAC overheads are minimal. Assigning optical beam powers to spots according to the SNR they produce at the receiver mimics maximum ratio combining techniques, although this is a transmitter approach. The absolute optimality of the angle and power adaptation algorithm is worth further investigation, however we show here the amount of improvement it offers. The examination of the optimality of the algorithm in the presence of shadowing and beam obstruction is worth further investigation. An algorithmic description of the angle and power adaptation algorithm is given in Table 8.1.

TABLE 8-1: ANGLE AND POWER ADAPTATION ALGORITHM

Algorithm 1: Angel and power adaptation

$N_s = 80$; (number of spots), J = 7; (number of photodetectors)

$p(.)$ is a rectangular pulse defined over $[0, T_b]$, $T_b = 1/B$ (B is a bit rate)

For i = 0 : 2.29 : 180

  For l = 0 : 2.29 : 180

    $\theta_x = i$; $\theta_y = l$;

    Produce a single spot in a direction associated with θ_x and θ_y

    For j = 1 : J

      Calculate and sum the received power levels within a time bin (0.3 ns duration)

      Produce the impulse response $h_j(t)$

      Calculate the pulse response = $h_j(t) \otimes p(t - T_b)$ and then calculate $(P_{s1} - P_{s0})_j$

      Compute $SNR_j = \left(\frac{R \times (P_{s1} - P_{s0})_j}{(\sigma_t)_j} \right)^2$

    end

    $SNR(i,l) = \max(SNR_j)$;

  end

end

$SNR_{\max} = \max(SNR(i,l))$;

$[\theta_{x,optimum}, \theta_{y,optimum}] = find(SNR(i,l) == SNR_{\max})$;

For k = 0:5

  $\phi(k) = 0.28 + 0.57 \times k$; (the angle between adjacent beams)

  $W_{total} = 0$;

  For S = 1 : N_s

    $P_{spot} = 1/N_s$; (the power per spot)

    For j = 1 : J

      Compute $SNR_j = \left(\frac{R \times (P_{s1} - P_{s0})_j}{(\sigma_t)_j} \right)^2$;

    end

    $W_s = \max(SNR_j)$;

    $W_{total} = W_{total} + W_s$;

  end

  For j = 1 : J

    For S = 1 : N_s

      $P_{spot} = W_s / W_{total}$;

      Calculate and sum the received power levels within a time bin (0.3 ns duration)

    end

    Compute $SNR_j = \left(\frac{R \times (P_{s1} - P_{s0})_j}{(\sigma_t)_j} \right)^2$;

  end

  $SNR_k = \max(SNR_j)$;

end

$SNR_{optimum} = \max(SNR_k)$;

$\phi_{optimum} = find(SNR_k = SNR_{optimum})$;

8.4. Simulation Results

In this section, we investigate the performance of the proposed multibeam geometries in the presence of BN, multipath propagation, and mobility. Simulation results are presented in terms of impulse response, delay spread, 3 dB channel bandwidth and SNR. The two novel adaptive multibeam systems (MBAAS and MBPAAS) are discussed and compared with LSMS, when all systems employ an angle diversity receiver with seven branches. For simplicity, SB was considered in order to process the resulting electrical signals. SB represents a simple form of diversity, where the receiver simply selects the branch with the best SNR. The performance of the proposed mobile adaptive multibeam systems was evaluated and compared at different receiver locations on the CF.

8.4.1. OW Channel Characteristics

Figs. 8.2 (a) and (b) show the impulse responses and frequency responses, respectively, of different OW channels at transmitter and receiver locations of (2m, 4m, 1m) and (2m, 1m, 1m). The impulse response in a practical OW system is continuous; however the simulator subdivides the reflecting surfaces into discrete elements. We have tried to reduce the effect of discretisation by grouping the powers received within a time bin (0.3 ns duration) into a single received power. This accounts for the smoothness seen in the impulse responses. A smaller time bin (0.01 ns duration) was also used resulting in a slightly higher delay spread result compared to that obtained using a 0.3 ns time bin, see Fig. 8.3 (b). Note that at very small delay spread levels a time bin with a smaller duration has to be used.

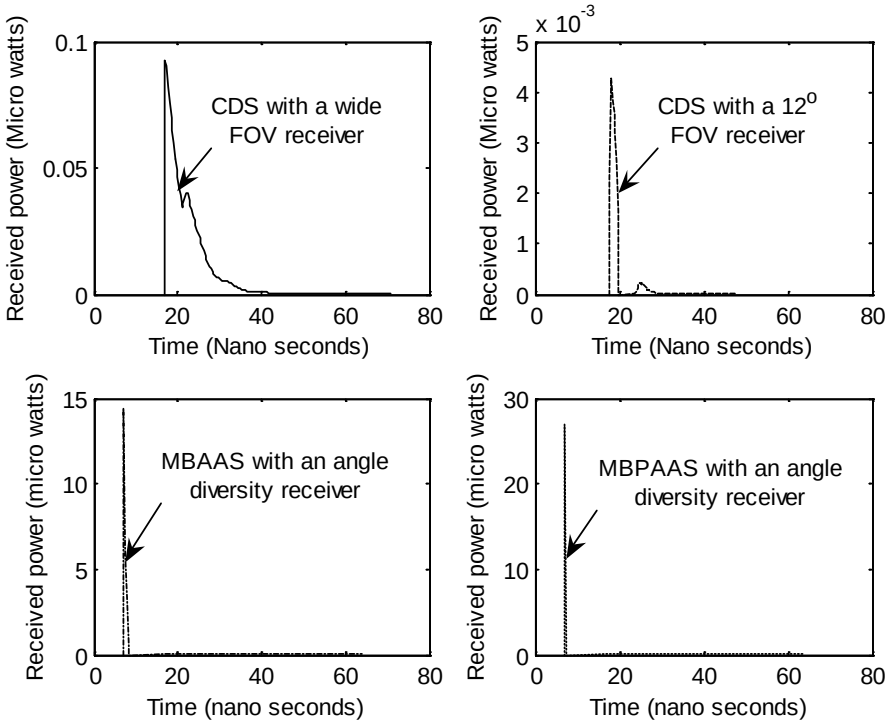

(a)

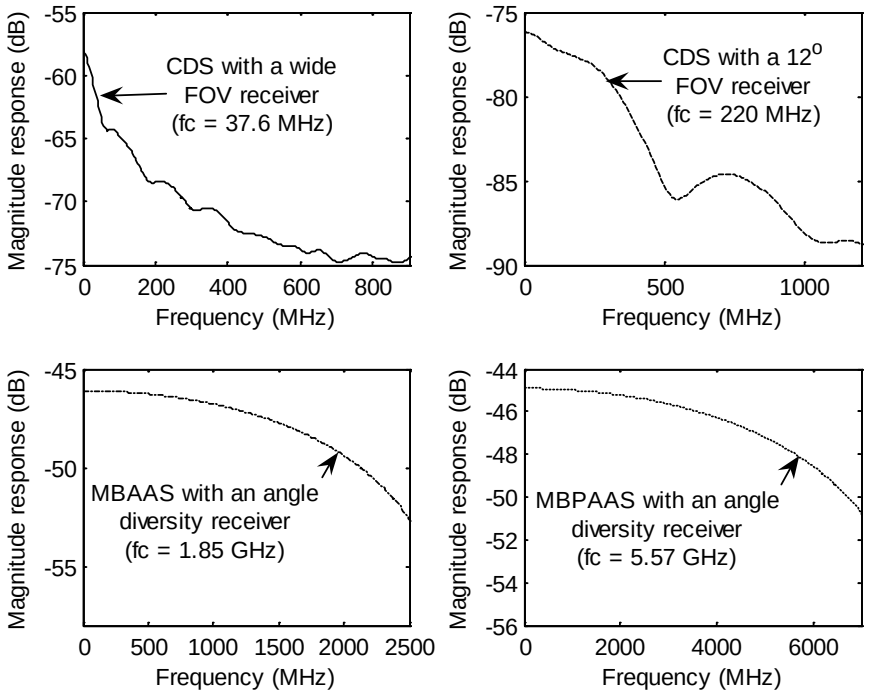

(b)

Figure 8-2: Impulse response and frequency response of different OW configurations at transmitter and receiver locations of (2m, 4m, 1m) and (2m, 1m, 1m): (a) Impulse responses (b) Frequency responses

This reduces the smoothing effect introduced through the use of time bins (that group rays with comparable delays together). At the same time a smaller time bin duration enables better discrimination between the rays (delay wise) which is essential at small delay spread levels. The results show that a 38 MHz channel bandwidth is achieved by employing a diffuse transmitter with a wide FOV receiver (FOV = 90^o). This result agrees very well with that reported in [10]. Limiting the receiver's FOV to 12^o can improve the bandwidth from 38 MHz to 220 MHz at the cost of a power penalty, where the collected power drops from 1.56 μW to 24.18 nW. Replacing the diffuse transmitter by a spot-diffusing transmitter enhances the received power, which increases from 24.18 nW to 1.29 μW and increases the channel bandwidth from 220 MHz to 647 MHz. It was shown that systems employing a spot-diffusing transmitter with a 7^o diversity receiver can achieve a channel bandwidth more than 2 GHz [42]. This improvement in channel bandwidth comes with an increase in the path loss, where a 7^o FOV receiver is employed instead of the previous 12^o FOV receiver. In this chapter, we show that a channel bandwidth of about 1.85 GHz can be achieved if the spots distribution is spatially adjusted to positions near the receiver, and diversity is employed (12^o FOV, 24.3 μW received power). A diversity receiver limits the range of rays collected by using narrow FOV photodetectors and selecting the branch with the largest SNR. It should be noted that an equal distribution of the transmit power among the beams can result in wasting the power assigned to the spots outside the receiver FOV as well as introducing a time delay between the signals from the spots within the receiver FOV, limiting the bandwidth. Therefore, allocating higher power levels to spots nearest to the receiver can significantly increase the direct path contribution and reduce the contribution of reflections, hence markedly increasing the channel bandwidth ultimately from 37.6

MHz (CDS) to 5.57 GHz as shown in Fig 8.2 (b). This significant bandwidth efficiency is one of the factors that can increase the achievable data rate. The increase in bandwidth coupled with an increase in the SNR (SNR of 29 dB compared with LSMS, see Section 8.4.2) through beam angle and power adaptation allows the OW system to operate at higher data rates.

For delay spread assessment, the transmitter is placed at one of the room corners (1m, 1m, 1m) and the receiver moves along the x = 2 m line, in order to examine the proposed systems at poor communication paths. At a given receiver location, the spots are automatically distributed based on the new method (beam angle adaptation). The angles between the adjacent spots are also optimised. Fig. 8.3 (a) compares the delay spread performance of the three multibeam configurations (LSMS, MBAAS, and MBPAAS) using a 0.3 ns bin duration. The delay spread distribution of the MBPAAS configuration using two different bin times (0.3 ns and 0.01 ns) is shown in Fig. 8.3 (b). In the LSMS configuration, the results indicate that the delay spread increases as the transmitter-receiver distance increases. The delay spread is almost independent of the transmitter-receiver separation in our new MBAAS configuration as the beam angles are adapted to yield the best SNR. Fig. 8.3 (a) also shows that a significant delay spread improvement is achieved when the multibeam angle adaptive system replaces the LSMS. At transmitter and receiver locations of (1m, 1m, 1m) and (2m, 7m, 1m), the MBAAS reduces the delay spread from almost 6 ns (LSMS) to 0.09 ns. A further delay spread improvement, from 0.09 ns (MBAAS) to 0.03 ns, is obtained when the transmit power adaptation method is implemented. It has to be noted that with a narrow field of view receiver, the delay spread is dictated by the number of spots seen within the FOV and their relative positions and therefore small delay spread values can be obtained.

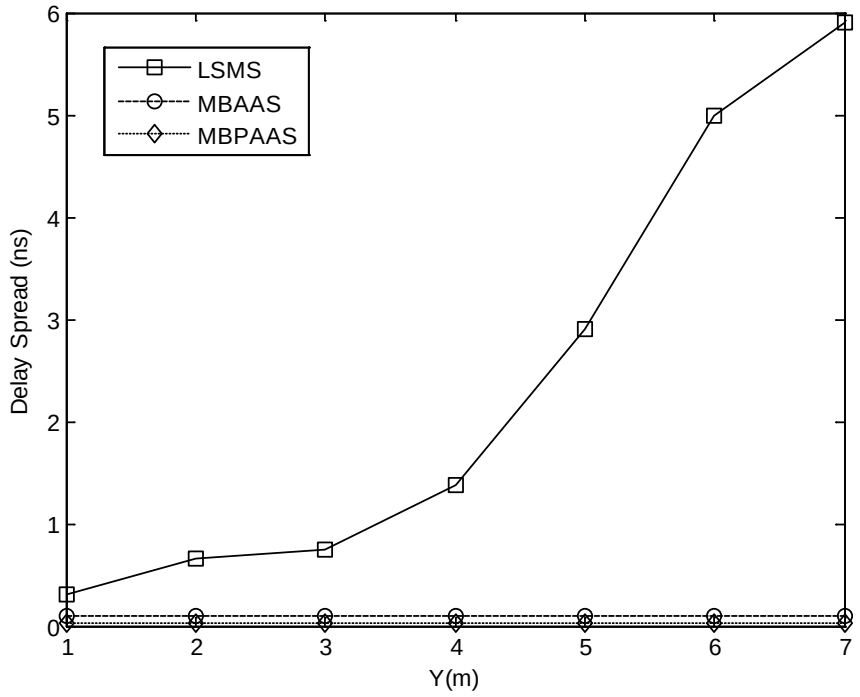

(a)

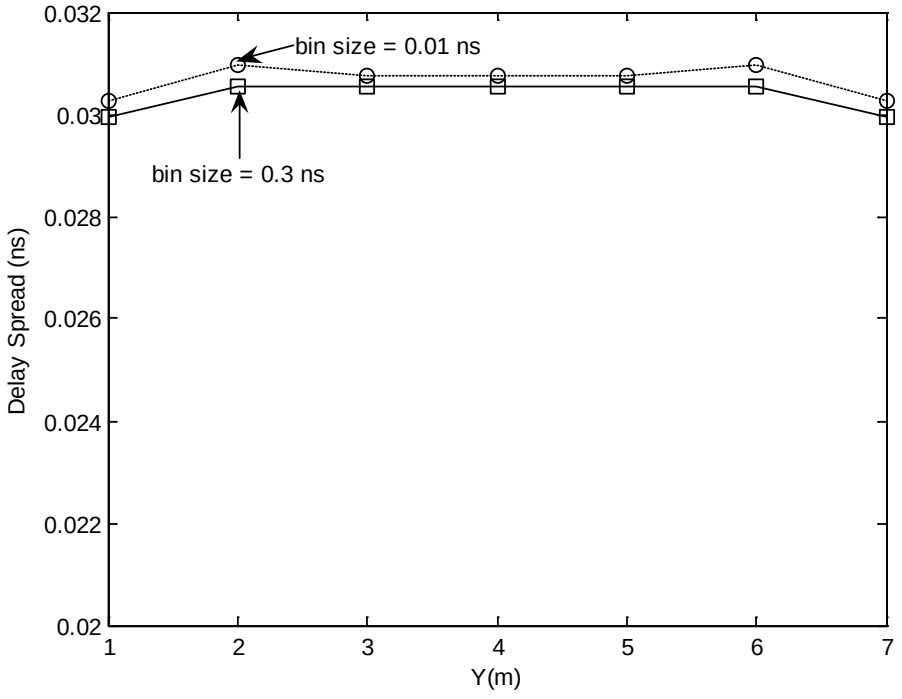

(b)

Figure 8-3: (a) Delay spread distribution of three multibeam transmitter configurations (LSMS, MBAAS, and MBPAAS), in conjunction with an angle diversity receiver when the transmitter is placed at (1m, 1m, 1m) and the receiver moves along the x = 2 m line (b) Delay spread distribution of the MBPAAS configuration using two different bin times: 0.3 ns and 0.01 ns

Unequally distributing the power among the spots can further reduce the delay spread. This significant reduction in delay spread reflects directly on the system bandwidth when our methods (beam angle and beam power adaptation) are implemented. The 3 dB channel bandwidth of three configurations: LSMS, MBAAS and MBPAAS systems with an angle diversity receiver is depicted in Fig. 8.4 when the transmitter is placed at the room centre and the receiver moves along the x = 2 m line.

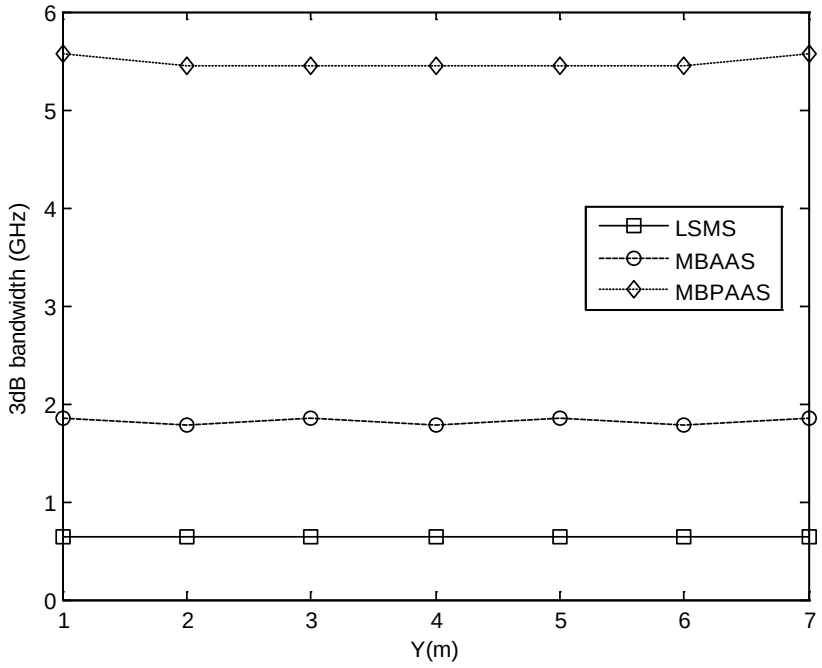

Figure 8-4: 3dB channel bandwidth of the proposed multibeam configurations (LSMS, MBAAS, and MBPAAS) with an angle diversity receiver when the transmitter is placed at the centre of the room and the receiver moves along the x = 2 m line.

8.4.2. SNR of the Mobile Multibeam OW Systems

Indoor OW communication links are strongly impaired by the shot noise induced by ambient light. The received pulse shapes corresponding to the proposed multibeam configurations were considered in calculating P_{s0} and P_{s1} (the powers associated

with logic 0 and 1 respectively). The SNR of the multibeam OW systems was calculated using (3.31). To facilitate comparison with previous work [175], we used a bit rate of 50 Mbit/s. Higher bit rates of 2.5 Gbit/s and 5 Gbit/s are also considered in our proposed MBPAAS. For the 50 Mbit/s OOK system (giving a pulse duration of 20 ns), we used the PIN-BJT preamplifier design proposed by Elmirghani et. al. [22]. This preamplifier has a noise spectral density of $2.7\,\mathrm{pA}/\sqrt{\mathrm{Hz}}$ and a bandwidth of 70 MHz which is large enough to ensure that the receiver introduces little or no distortion onto the 50 Mbit/s pulse stream. For our proposed 2.5 Gbit/s and 5 Gbit/s MBPAAS systems, we used the PIN-FET design proposed by Kimber et al. [180]. This preamplifier has a noise current spectral density of $10\,\mathrm{pA}/\sqrt{\mathrm{Hz}}$ and a 10 GHz bandwidth. The preamplifier bandwidth can be limited to 2.5 GHz and 5 GHz through the use of appropriate filters. The impact of this filter on the signal is minimal (as the bandwidth considered is higher than 0.7 × bit rate) and is not considered here.

The performance of our proposed multibeam systems (MBAAS and MBPAAS) combined with an angle diversity receiver is assessed under the impairments of BN, multipath propagation and mobility. Our systems' SNR is compared with that of the LSMS with diversity detection, when the transmitter is placed at (1m, 1m, 1m) and (2m, 7m, 1m) and the receiver moves along the x = 2 m line, and the results are depicted in Fig 8.5. Previous work [175] has shown that the LSMS SNR performance is almost independent of the receiver location when the transmitter is stationary at the room centre (2m, 4m, 1m). It was also found that degradation in the SNR is observed when the transmitter is mobile. This SNR degradation attributed to the transmitter mobility can be mitigated by replacing the LSMS with the MBAAS. Regardless of the transmitter position, the new method introduced (beam angle adaptation) can

guide the multibeam transmitter to target its diffusing spots at an area on the ceiling and/or walls based on the receiver location so as to maximise the receiver SNR. The results confirm that the MBAAS SNR is completely independent of the transmitter location. The results also indicate that a significant SNR improvement is achieved at all the transmitter and receiver locations considered, when the MBAAS replaces LSMS. At transmitter and receiver locations of (1m, 1m, 1m) and (2m, 7m, 1m), our new MBAAS improves the SNR by 28 dB over the LSMS. Further SNR improvement of about 1 dB is achieved when the transmit power adaptation method is implemented with beam angle adaptation. Note that beam angle adaptation in this case is able to achieve the majority of the improvement by concentrating the power near the receiver. If shadowing exists (i.e. some beams are obstructed), then beam power adaptation can help further by re-allocating the power to unobstructed beams.

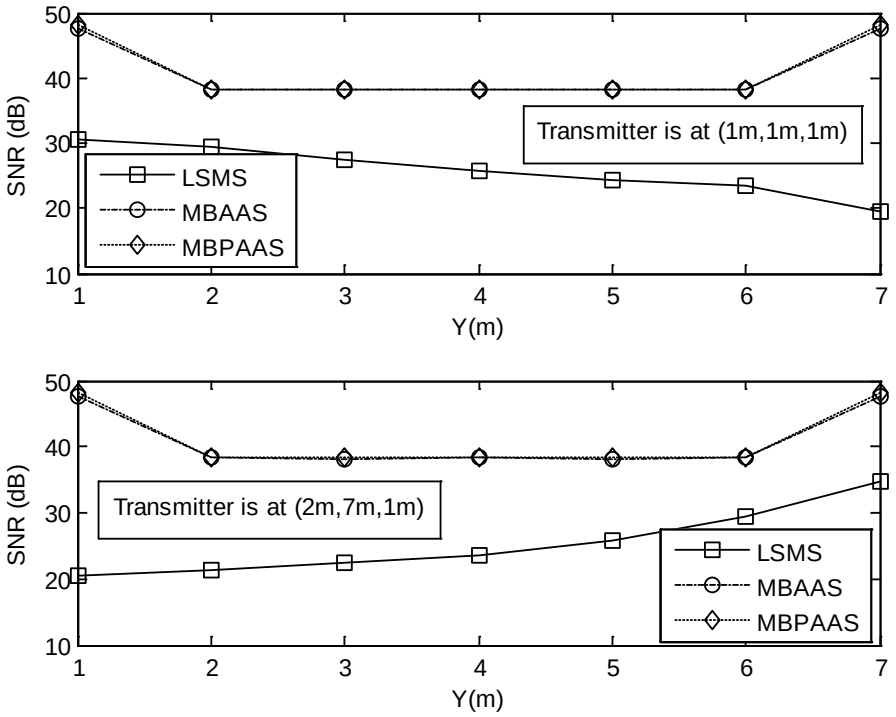

Figure 8-5: SNR of the proposed multibeam systems (LSMS, MBAAS, and MBPAAS), in conjunction with an angle diversity receiver when the transmitter is placed at (1m, 1m, 1m) and (2m, 7m, 1m) and the receiver moves along the x = 2 m line

Furthermore, the best MBAAS SNR is achieved when the receiver is near the room edges (i.e., at y = 1, 7 m), where the distance between the diffusing spots and the receiver is shorter than that associated with other receiver locations. In addition, joint optimisation of the angle between the adjacent beams and the transmit power among the beams was carried out, and the SNR results at one of the worst communication paths considered, where the transmitter is placed at the room corner (1m, 1m, 1m) and the receiver is at (2m, 7m, 1m), are given in Fig. 8.6. Fig. 8.6 shows the SNR levels of the proposed systems (MBAAS and MBPAAS with diversity detection) as a function of the spacing between the adjacent beams (cm). The LSMS angle diversity receiver SNR is given for comparison. In both MBAAS and MBPAAS systems the distance between adjacent beams increases from 0 (where the spots just touch each other) to 10 cm (the maximum distance considered) in steps of 2 cm which represents an angle step of 0.57^{o}. The SNR is computed at each step and the result is shown in both MBAAS and MBPAAS systems. In contrast, in the LSMS configuration the angle between the beams is fixed and is 10 cm. Therefore, one value of SNR is illustrated at 10 cm spacing between the adjacent beams in the LSMS. It is evident that the MBAAS produces the best SNR when its diffusing spots are contiguous. This is due to illuminating a line of touching spots (80 spots are considered) centred at the optimum position, which is determined based on our angle adaptation algorithm (discussed in Section 8.3.1). In order to mitigate the SNR degradation attributed to the increase in the angle between the adjacent spots, the transmit power is distributed among the beams based on the transmit beam power algorithm (discussed in Section 8.3.2). The multibeam OW spot diffusing system coupled with beam power and beam angle adaptation methods provides a significant SNR improvement in all the scenarios considered. The SNR improvement can be

used to reduce the transmit power of the system to help comply with eye safety requirements.

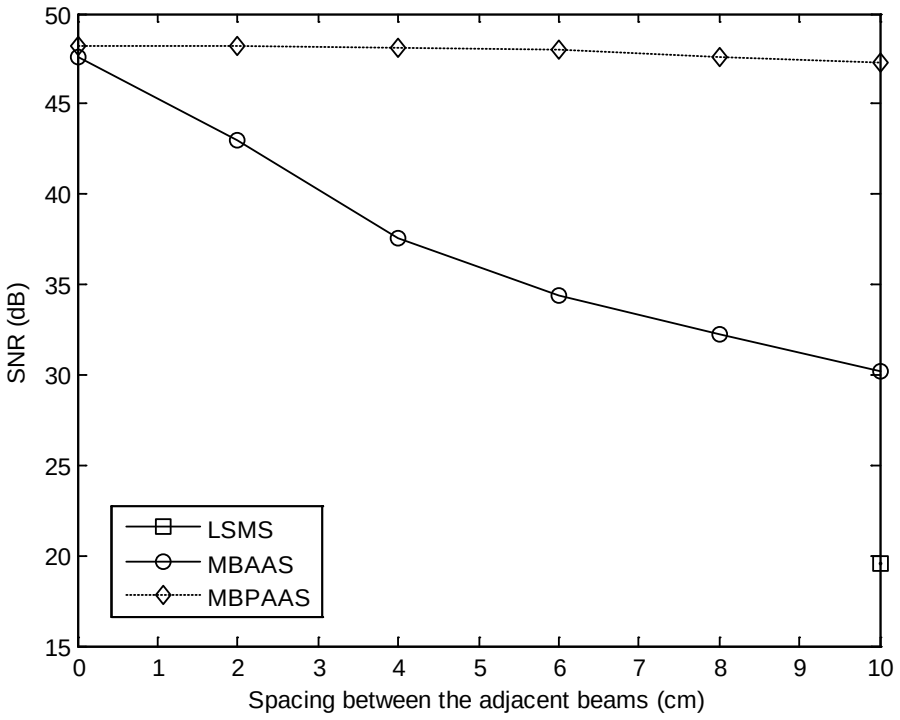

Figure 8-6: SNR of the proposed multibeam systems (LSMS, MBAAS, and MBPAAS) with an angle diversity receiver at transmitter and receiver locations of (1m, 1m, 1m) and (2m, 7m, 1m)

8.5. Performance Penalty versus Computational Saving

A significant SNR improvement can be achieved through the use of our new methods (beam angle and beam power adaptation) in OW multibeam systems coupled with diversity detection however a cost in terms of complexity has to be paid. This complexity is associated with the computational time and resources required to identify the optimum spot position when the receiver SNR at each possible beam location is computed and the optimum spot direction is selected at the transmitter. Furthermore, the increase in implementation complexity associated with the beam power adaptation method is modest compared to the complexity induced by

employing the beam angle adaptation approach. It should be noted that the majority of the complexity introduced is proportional to the number of possible locations (in the ceiling and walls), which have to be scanned to identify the optimum direction, and can therefore be reduced by increasing the beam angle adaptation step size as mentioned earlier in Section 8.3.1. In order to investigate the trade-off between the performance penalty and computational saving, the beam angle and power adaptation algorithm (discussed in Section 8.3.1 and 8.3.2) is employed, however with an increase in the beam angle adaptation step size, where steps of 2.29^o are now used. At each step the receiver SNR is calculated and stored. A maximum of 26.57^o angle step size (i.e. the spot moves 100 cm resulting in a total of 80 possible locations on the ceiling and walls of the room) is considered. The performance penalty versus computation time is depicted in Fig. 8.7 at receiver locations of (1m, 1m, 1m) and (1m, 3m, 1m). When the receiver is located at the room edges, increasing the beam angle step size from 2.29^o to 15.64^o reduces the number of locations, which have to be scanned to identify the optimum location, from 12500 locations to 245 locations resulting in a reduction in the computation time from 12.5 ms to 0.245 ms (as mentioned earlier, it is assumed that the SNR computation associated with each location is carried out in 1 μs). This reduction in complexity comes with a slight performance degradation of 1.7 dB. However, a power penalty of 10.3 dB can be incurred if the beam angle step size is set at 17.74^o to achieve a computational saving from 12.5 ms to 0.195 ms. This is due to the fact that at beam angle step sizes up to 15.64^o the angle adaptive algorithm can scan some possible locations in the wall adjacent to the receiver within the FOV associated with the side photodetector hence identifying the optimum location. When the beam angle step size exceeds 15.64^o the locations scanned in that wall are outside the side photodetector's FOV (in this case)

resulting in identifying an optimum position on the ceiling where the distance between the diffusing spots and the receiver is larger. Furthermore, increasing the beam angle step size from 17.74^o to 26.57^o to achieve a reduction in computation time from 0.195 ms to 80 μs can result in an increase in the SNR penalty from 10.6 dB to 11.6 dB. In contrast, when the receiver is located elsewhere (receiver positions are not at the room edges) the angle and power adaptation algorithm can reduce the computational time from 12.5 ms to 80 μs by increasing the beam angle step size from 2.29^o to 26.56^o at the cost of a 1.3 dB power penalty. These observations give confidence in modifying our main angle and power adaptive algorithm where the angle scan step size is increased possibly up to 26.57^o where 80 possible positions need to be scanned to identify the spot direction that maximises the receiver SNR.

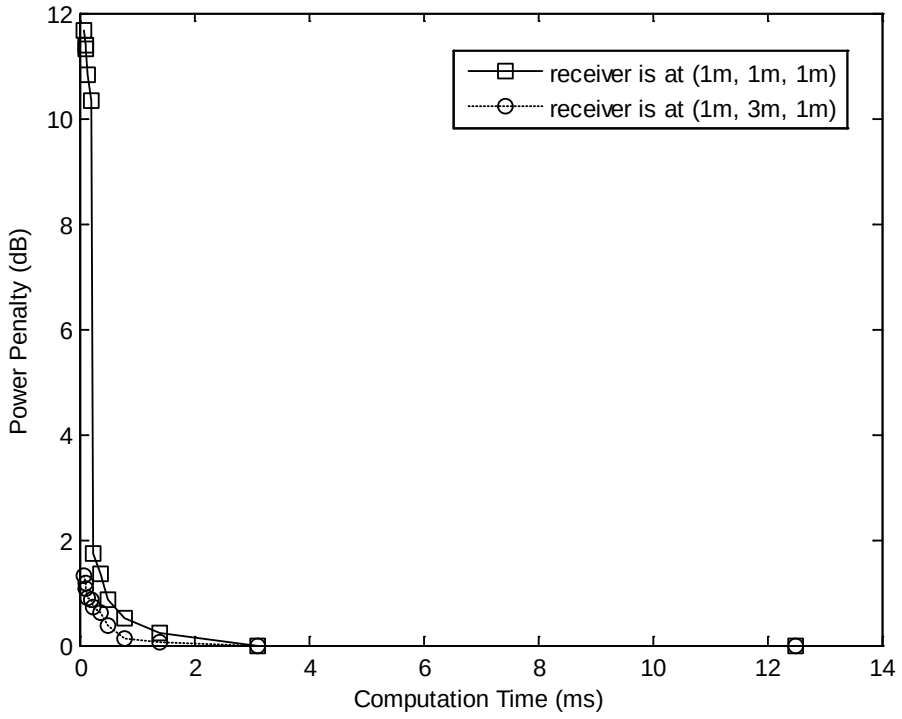

Figure 8-7: Trade-off between the performance penalty and computational saving of the MBPAAS system when a receiver is placed at (1m, 1m, 1m) and (1m, 3m, 1m)

A comparison of the SNR of the main MBPAAS and modified MBPAAS systems operating at 50 Mbit/s is shown in Fig. 8.8. Replacing the main MBPAAS by our modified MBPAAS can reduce the computation time from 12.5 ms to 80 μs when the environment changes, however a degradation in the receiver SNR can be induced. A worst case performance penalty of 11.6 dB has to be paid when the receiver is placed at the room corner. This penalty can be put in context by observing that an SNR improvement of 18 dB can be achieved when the modified MBPAAS replaces the traditional LSMS at the worst communication path considered when both systems operate at 50 Mbit/s. Note that the LSMS offers a 30 dB SNR gain over the conventional diffuse system [175].

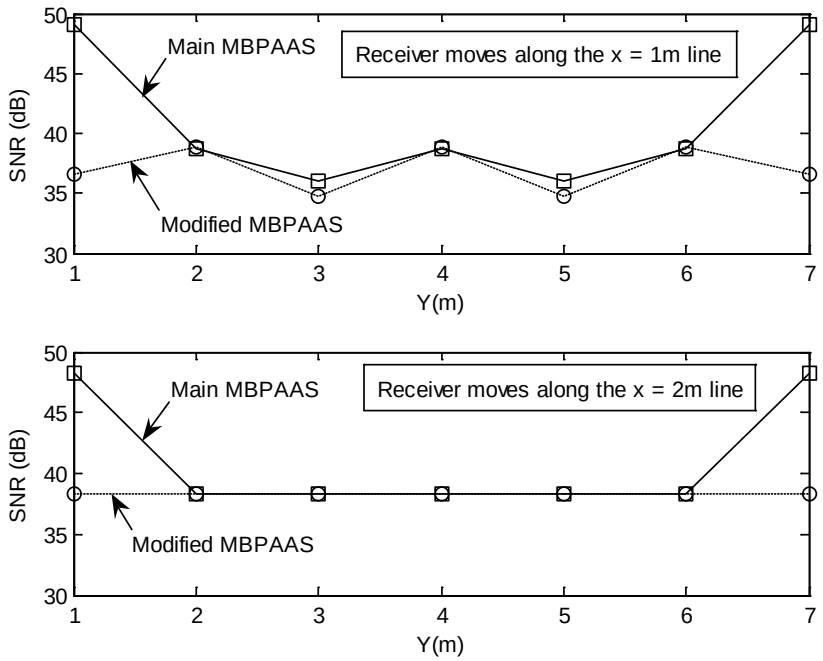

Figure 8-8: SNR of the proposed multibeam systems (main MBPAAS, and modified MBPAAS) operating at 50 Mbit/s, when both systems employ an angle diversity receiver that moves along the x = 1 m and x = 2 m lines

The high SNR obtained through the combination of beam angle and beam power adaptation, spot-diffusing and diversity reception (SNR of 36 dB at the worst communication path considered) can enable a transmit power reduction (below the current 1 W level). Conventional OOK systems require an SNR of 15.6 to achieve a BER of 10^{-9}. Therefore, in the 50 Mbit/s OOK systems at the worst communication path considered, the transmit power can be reduced by almost 10.7 dB while achieving 10^{-9} BER through the combination of these methods. A non adaptive LSMS system emitting a total of 1 W transmit power, where each of the 80 spots receives 12.5 mW powers, can achieve the SNR performance shown in Fig. 8.5. The power per spot can be reduced to 0.22 mW (which is lower than the typically quoted 1 mW eye safe limit at the near infrared wavelengths) when an optical concentrator coupled with an optical bandpass filter are used in front of the detectors in the LSMS system with a typical concentrator gain of 17 dB corresponding to a 12^{o} FOV [30, 181]. To consider eye safety, a restriction is imposed to our angle and power adaptation algorithm where the power per beam is restricted to less than 1 mW and a total transmit power of 18 mW is used. The same optical concentrator and filter are also used. Our beam angle and power adaptation algorithm, in this case and at the worst communication path, can achieve an SNR of 30 dB which is less than the 36 dB obtained without the restriction and without using any concentrator or filter, but is still significant. The degradation is due to the reduction in the transmit power, from 1 W to 18 mW, and due to the inability of the algorithm to assign high power freely to spots at good locations due to eye safety. As previously mentioned, it should be noted that the shape and size of the transmitter have to be considered to determine if an eye can see more than one beam at a time. The source size also has to

be considered to complete the assessment, where the source size determines the size of the image cast on the retina.

8.6. Effectiveness of the Proposed Link Design against Shadowing

The effectiveness of our modified multibeam power and angle adaptive system is evaluated in a harsh environment with mobility. Such an environment is typically encountered in real office configurations where optical signal blockage (due to cubicles), windows, doors, furniture, ambient light noise, and multipath propagation all exist. To simulate shadowing and signal blockage of the communication link, we consider a room similar to that shown in Fig. 5.1, which has three large glass windows, a door, a number of rectangular-shaped cubicles with surfaces parallel to the room walls, and other furniture such as bookshelves and filing cabinets. The dimensions of this room are similar to those of the previous room considered. The glass windows are assumed not to reflect any signal. The reflectivity of the ceiling, walls surrounding the windows, and floor are similar to those previously stated. Two perpendicular walls are covered with bookshelves and filing cabinets with a 0.4 reflectivity. Cubical office partitions are assumed to either absorb or block signals. Furthermore, several tables and chairs are placed on the floor with a 0.3 reflectivity. The complicated environment in this room results in shadowing created by physical partitions and low reflectivity objects.

Comparisons were carried out between the traditional line strip multibeam system and a multibeam system that adopts our modified beam angle adaptation method followed by beam power adaptation when both systems employ an angle diversity receiver in a complicated room design with full mobility. The SNR results (simulation) of both systems operating at 50 Mbit/s in the two room scenarios

(shadowed and unshadowed rooms) are depicted in Fig. 8.9, when the receiver moves along the x = 2 m line at transmitter locations of (1m, 1m, 1m) and (2m, 7m, 1m). The SNR of the modified MBPAAS system is evaluated when an optical concentrator coupled with an optical bandpass filter with a typical concentrator gain of 17 dB are used. Fig. 8.9 shows the weakness of the LSMS and the robustness of the modified MBPAAS against shadowing, signal blockage, and mobility. The effect of mobility on the LSMS performance can be observed as an SNR degradation of 15 dB when the receiver is at (2m, 7m, 1m) and the transmitter moves from (2m, 7m, 1m) to (1m, 1m, 1m). In contrast, the SNR of our modified MBPAAS is independent of the transmitter position.

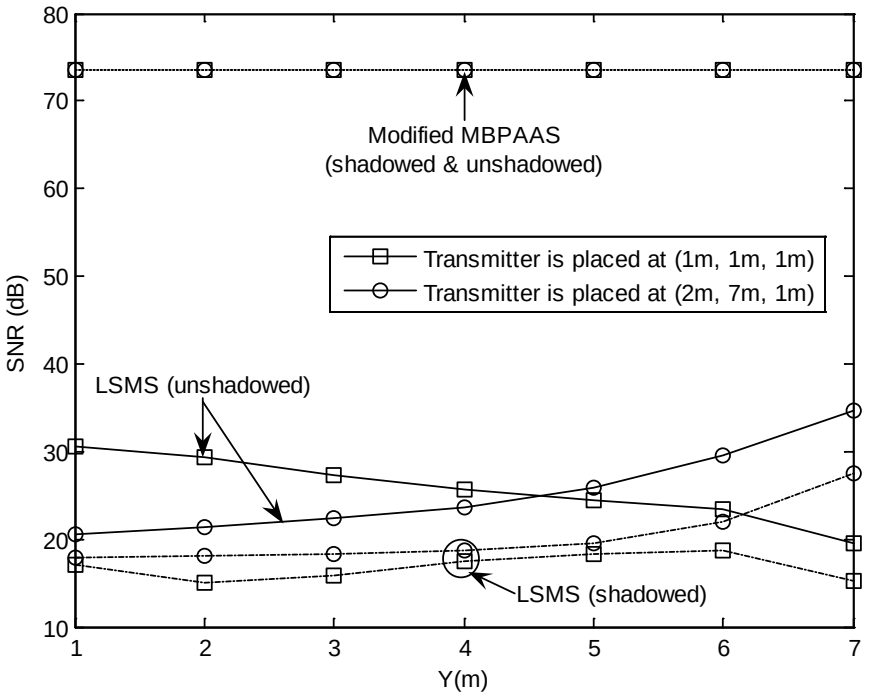

Figure 8-9: SNR of the LSMS and the modified MBPAAS systems operating at 50 Mbit/s, with an angle diversity receiver in the two room scenarios (unshadowed and shadowed) when the transmitter is placed at (1m, 1m, 1m) and (2m, 7m, 1m) and the receiver moves along the x = 2 m line

Furthermore, the worst impact of shadowing and signal blockage in the LSMS performance is observed in the form of a decline in the SNR by 15 dB when the transmitter and receiver are co-located at the room corner (1m, 1m, 1m). This degradation is due to the presence of windows that causes a large signal loss and hence larger path losses near the room corner. The modified MBPAAS with an angle diversity receiver is more robust against shadowing and signal blockage, owing to its ability to allocate the power to regions in the ceiling with the shortest path to the receiver, and also due to re-allocating the power to unblocked spots. These benefits are manifest as an SNR improvement in the modified angle diversity MBPAAS system in both shadowed and unshadowed environments. In shadowed communication links, the results show that a significant SNR improvement of 55 dB can be achieved when the modified MBPAAS with a 12^o FOV diversity receiver using a 17 dB optical concentrator replaces the traditional angle diversity LSMS at a transmitter-receiver separation of 6 m. This high SNR coupled with the excess bandwidth shown in Fig. 8.4 can prove extremely useful in increasing the data rate of the system. Higher bit rates (2.5 Gbit/s and 5 Gbit/s) indoor optical wireless systems are shown to be feasible through the combination of three approaches: beam angle and power adaptation, spot-diffusing and receiver diversity using optical concentrators and filters. The SNRs associated with the 2.5 Gbit/s modified MBPAAS and the LSMS systems, in conjunction with an angle diversity receiver, are depicted in Fig. 8.10 when the transmitter is placed at the room corner (1m, 1m, 1m) and the receiver moves along the x = 2 m line in the shadowed and the unshadowed rooms. SNR results associated with the 5 Gbit/s modified MBPAAS system with two photodetection areas: 1 cm^2 and 0.1 cm^2 are also included.

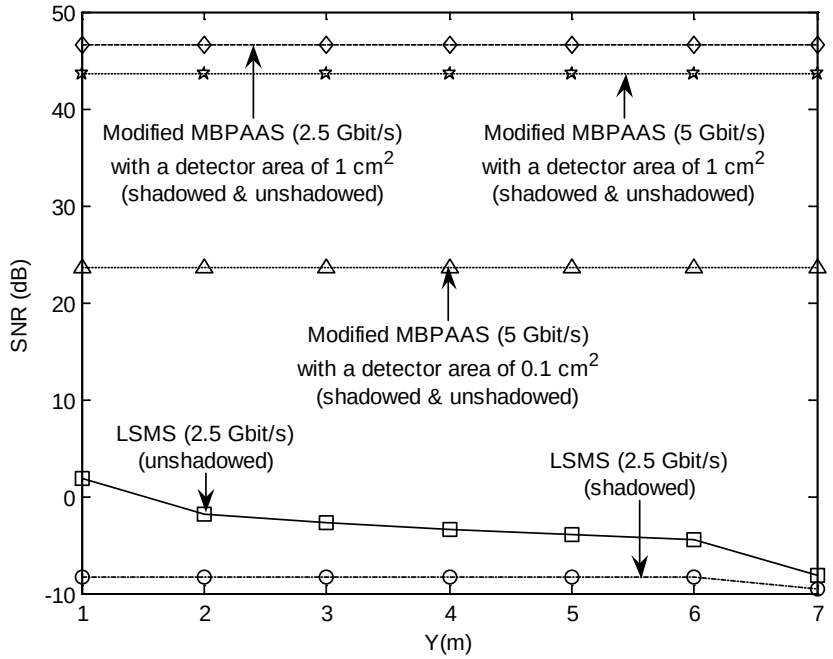

Figure 8-10: SNR of the proposed multibeam systems (LSMS and modified MBPAAS) operating at 2.5 Gbit/s, when the transmitter is placed at the room corner (1m, 1m, 1m) and the diversity receiver moves along the x = 2 m line, and the 5 Gbit/s modified angle diversity MBPAAS system with two photodetection areas: 1 cm^2 and 0.1 cm^2

The results indicate that among the systems considered, only the angle diversity modified MBPAAS system is able to achieve the required performance (BER of 10^{-9}) while operating at high bit rates (2.5 Gbit/s and 5 Gbit/s). This is achieved with full mobility at 2.5 Gbit/s and 5 Gbit/s which is a useful result. Our previous work in Chapter 4 (where shadowing and signal blockage were not taken into account) has shown that a 5 Gbit/s optical wireless communication system can be realised through the combination of transmit beam power adaptation, beam clustering method and diversity reception. Here we show that this bit rate (5 Gbit/s) is achievable with an SNR improvement of 7 dB over that quoted in Fig. 4.8 (where a better optical concentrator, with a typical concentrator gain of 20 dB, was used) due to the introduction of beam angle adaptation in addition to beam power adaptation.

Furthermore, in the current work beam angle adaptation allows this improvement to be achieved with full mobility in the presence of shadowing and beam obstruction. In addition, this SNR improvement can be used to reduce the photodetector area to 0.1 cm^2 where the optical wireless system is still able to operate at 5 Gbit/s (using existing detectors) and meet a 10^{-9} BER by achieving an SNR of 23.6 dB which is greater than the 15.6 dB needed.

8.7. Summary

The line strip multibeam transmitter is one of the attractive configurations considered in the literature. It provides a better SNR than the CDS, but its SNR can be degraded due to shadowing, signal blockage and mobility. In this chapter, we introduced two methods (beam angle and beam power adaptation) to the spot-diffusing design to mitigate the SNR degradation attributed to mobility in the presence of shadowing, and to improve the system performance. The beam angle adaptation method can help the multibeam transmitter to automatically target the diffusing spots at an area on the ceiling and/or walls where the receiver can collect a strong signal through LOS components and through the shortest paths, resulting in SNR enhancement. The transmit power adaptation approach can enable the transmitter to assign higher power levels to spots nearest to the receiver to produce further SNR improvement. Our new MBPAAS improves the SNR by 29 dB, and reduces the delay spread from almost 6 ns to 0.03 ns compared to the traditional LSMS. An increase in the channel bandwidth from 647 MHz to 5.57 GHz can be achieved when the new MBPAAS replaces the LSMS allowing the OW system to operate at high bit rates.

The significant improvements achieved through the use of our new methods (beam angle and beam power adaptation) are coupled with an increase in complexity. The

latter can be reduced from a typical beam angle and beam power adaptation time of 12.5 ms to 80 µs by modifying the beam angle adaptation method to concentrate the power on the ceiling and also reduce the number of locations that have to be scanned to identify the optimum direction. However, a performance penalty of 11.6 dB at receiver locations near the room edges (i.e. y = 1, 7 m) and 1.3 dB elsewhere, can be induced when the modified MBPAAS replaces the main MBPAAS. Intermediate complexity-penalty trade-offs are also possible. Furthermore, our new modified MBPAAS with diversity receivers, where each receiver uses an optical concentrator coupled with an optical filter, provides robustness against transmitter mobility and shadowing while offering an SNR gain of 55 dB over the shadowed LSMS with diversity receivers at a 6 m transmitter-receiver horizontal distance. The SNR improvement achieved can be used to reduce the transmit power which helps meet eye safety requirements. This SNR improvement and the excess bandwidth obtained can be used to achieve higher data rates and 2.5 Gbit/s and 5 Gbit/s OW systems are shown to be feasible.

It should be noted that from bandwidth and SNR points of view a single beam system may be desirable, but such a system will be prone to beam blockage, shadowing and may violate eye safety if all the available power is allocated to a single beam. Our angle and power adaptive multibeam system offers advantages in this regard. A constraint was introduced in the adaptation algorithm to limit the power per beam to less than 1 mW to help comply with eye safety, and the results show that good performance is obtained. Our design is less sensitive to the room geometry (than CDS and LSMS) as the diffusing spots can be targeted at the optimum location that yields the best SNR at the receiver. The power can also be re-distributed among the spots to further improve the receiver SNR. Our algorithm adapts the beam angles and

beam powers. This enables the system to adapt to the room geometry and to transmitter and receiver mobility hence maximising the SNR, reducing the delay spread and increasing the channel bandwidth. The angle adaptation and power allocation are optimised with respect to the SNR, but our SNR expression, as shown in (4.31), contains the effect of pulse spread and ISI ($P_{s1}- P_{s0}$), and hence accounts for the impact of channel bandwidth as well as signal power and noise and therefore is a good cost metric to be used in the optimisation as it reflects the BER of the system which is the quantity of interest to the optical wireless system user. Our proposed system makes use of commercially available components and can therefore be implemented at relatively low cost.

9. HIGH-SPEED SPOT DIFFUSING MOBILE OPTICAL WIRELESS SYSTEMS EMPLOYING BEAM ANGLE AND POWER ADAPTATION AND IMAGING RECEIVERS

9.1. Introduction

Chapter 8 demonstrated that the combination of beam angle and power adaptation, spot-diffusing and diversity reception can help reduce the limitations of OW communication links. Significant performance improvements were achieved and used to significantly increase the data rate to 5 Gbit/s with full mobility. Although, an improvement in performance is achieved by using non-imaging diversity detection; cost and complexity have to be considered where each receiving element requires the use of a separate optical concentrator. Chapters 6 and 7 have shown that an imaging receiver is an effective technique that can help combat background noise, significantly reduce ISI, and improve system performance. Compared to the non-imaging angle diversity receiver, an imaging receiver provides two advantages. Firstly, all photodetectors share a common imaging concentrator, which helps reduce size and cost. Additionally, all the photodetectors can be laid out in a single planar array which facilitates the use of a large number of photodetector pixels, hence improving the link performance (under MRC the resultant SNR is the sum of the SNRs of the individual detectors). In this chapter, we develop and evaluate our proposed link design (MBPAAS) with imaging receivers. The results show a promising system performance.

9.2. Simulation Model

The characteristics of a mobile channel formed by a multibeam power and angle adaptive transmitter coupled with an imaging receiver are investigated. Propagation simulations were conducted for such systems in an environment similar to that described in the previous chapters, where an empty room is considered. The OW communication system architecture associated with a multibeam power and angle adaptive transmitter combined with an imaging receiver is shown in Fig. 9.1. Three mobile multibeam transmitter configurations (LSMS, MBAAS and MBPAAS) with an imaging receiver were considered. Comparisons between imaging and non-imaging CDS systems were also considered. A single source and a liquid crystal holographic element can generate the beams. Changing the holographic 2D function (through a liquid crystal device) can generate variable optical spot intensities and optical spot locations on the ceiling and/or walls. The optimum spots distribution and their associated power levels that yield the best SNR at the imaging receiver can be chosen through the angle and power adaptation algorithm given in Table 8.1. A beam angle adaptation step size of 2.29^{o} is considered resulting in a total of 12500 possible locations (on the ceiling and walls) that have to be scanned to identify the optimum direction of a line of spots. In order to assess the system's performance as well as evaluate the benefits of our methods (beam angle adaptation, transmit power adaptation, spot-diffusing, and imaging reception), the room illumination was provided by the same previous eight-halogen spotlights. Throughout this work interference from daylight through windows and doors was not considered. Furthermore, an imaging receiver is employed to reduce the effect of ambient light noise and multipath dispersion. No optical filters were used in this chapter. The

simulations were carried out at several receiving locations within the room when the transmitter is positioned at (1m, 1m, 1m), (2m, 4m, 1m) and (2m, 7m, 1m).

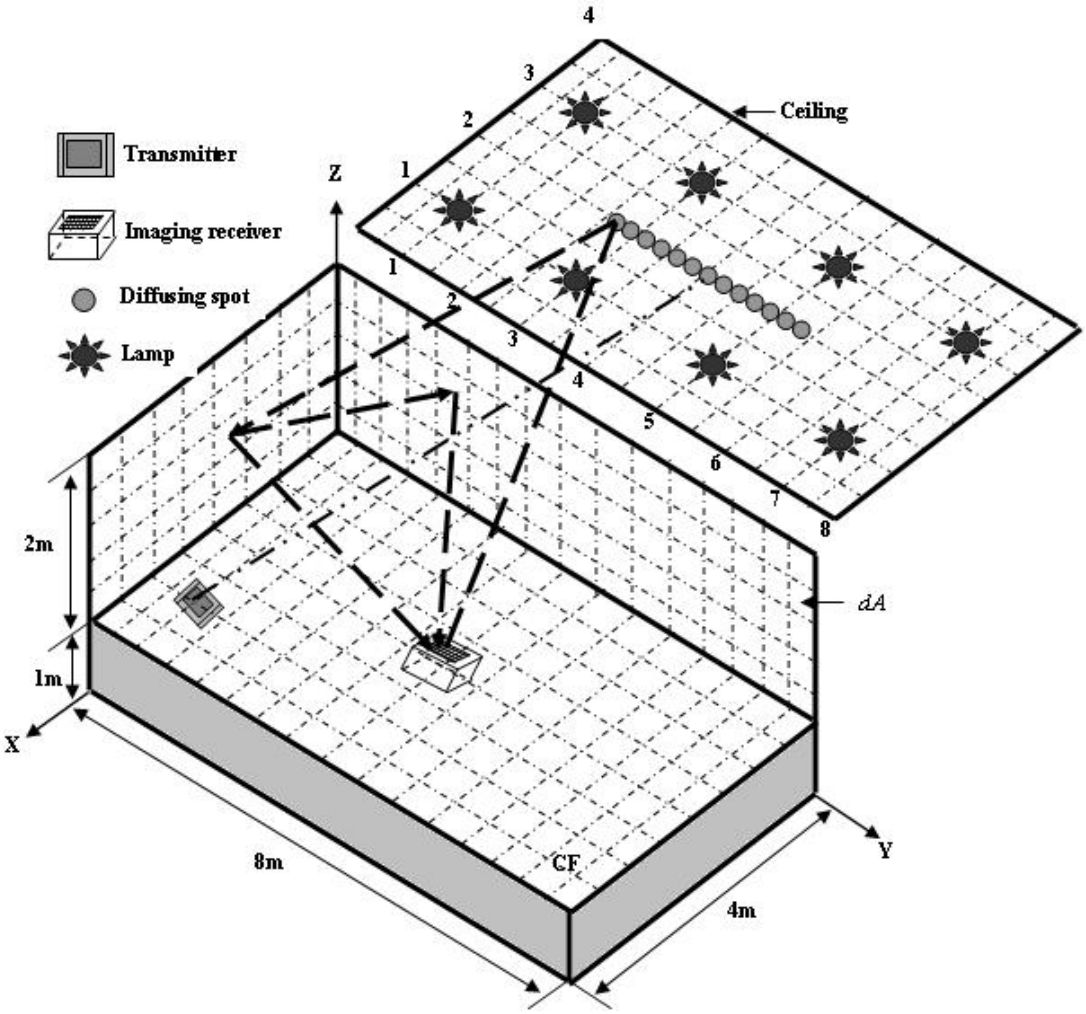

Figure 9-1: OW MBPAAS configuration

9.3. Receiver Structure

Two different receiver structures: a non-imaging receiver and an imaging receiver are considered.

9.3.1. Non-Imaging Receiver

A single-element receiver was considered here. It employs a compound-parabolic concentrator (CPC) whose output is coupled to a single photodetector equipped with a preamplifier. The CPC is a common non-imaging concentrator and has an acceptance semi-angle ψ_C such that when the reception angle δ exceeds ψ_C, the concentrator transmission factor, $T_{C,NIMG}(\delta)$ rapidly approaches zero. The single non-imaging receiver is assumed to employ a CPC with an acceptance semi-angle of $\psi_C = 65^0$ in order for the photodetector to view the whole ceiling when the receiver is at the room centre. A refractive index $N_C = 1.7$ is considered, and the entrance area is $A = 9\pi/4\ \text{cm}^2$. The transmission factor of the CPC is given by (6.1). The CPC has an exit area $A' = A\sin^2(\psi_C)/N_C^2$. The photodetector is assumed to be fitted exactly into its associated concentrator's exit area. Therefore, the photosensitive area of the photodetector is 2 cm^2. The concentrator's size is acceptable in mobile terminals and it can be ruggedly fixed to the photodetector. The photodetector has a responsivity of 0.54 A/W.

9.3.2. Imaging Receiver

An imaging receiver made up of a single imaging lens and a detector that is segmented into multiple pixels is depicted in Fig. 9.2. An MBAAS configuration was considered with transmitter and receiver locations of (1m, 1m, 1m) and (2m, 4m, 1m). The optical signal power received in the pixels can be amplified separately and can be processed using appropriate combining techniques. The results show that MRC offers further improvement when used to combine the signals at the outputs of

the imaging pixels. The imaging receiver employs a photodetector array segmented into 200 pixels. It is assumed that there are no gaps between the pixels, and therefore, the area of an individual pixel equals to the photodetector's area (which is exactly equal to the exit area of the concentrator employed) divided by the number of pixels. The imaging concentrator that was used in [94] is employed. Its acceptance semi-angle was restricted to 65^{o} and its transmission factor was given in (6.2). The imaging receiver considered employs an entrance area of $A = 9\pi/4\,\text{cm}^2$. The reception area observed by each pixel changes according to the imaging receiver movement.

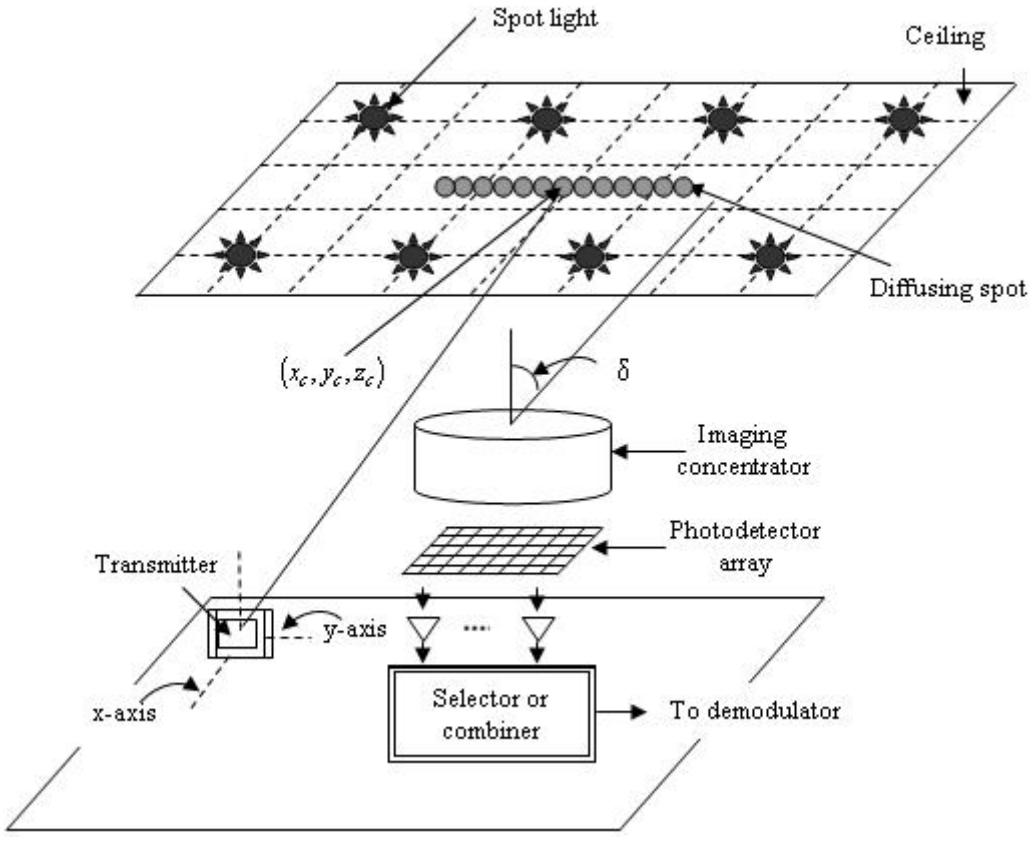

Figure 9-2: The physical structure of an imaging receiver made up of a single imaging lens and a photodetector that is segmented into multiple pixels. An MBAAS configuration is considered at the transmitter together with receiver locations of (1m, 1m, 1m) and (2m, 4m, 1m)

Computations were carried out following the procedure given in Chapter 6, Section 6.3.2 to determine the reception areas of the pixels at a given receiver location. In turn the received power at each pixel can be calculated based on the reception area it observes.

9.4. Imaging OW Systems: Comparison and Performance Analysis

In this section, the two new adaptive spot-diffusing systems (MBAAS and MBPAAS) coupled with an imaging receiver are studied and compared with LSMS and CDS systems employing an imaging receiver. Comparison with a non-imaging CDS is also considered. The systems are assessed and evaluated in the presence of ambient light noise, multipath propagation and mobility.

9.4.1. Delay Spread Assessment

In order to estimate the distortion caused by signal spread, which is a result of multipath propagation, root mean square delay spread can be used. The delay spread gives an indication of the ISI experienced in the received optical signal, and is quantified in (3.25). A comparison of the delay spread distribution of the proposed configurations (CDS, LSMS, MBAAS, and MBPAAS) with an imaging receiver is depicted in Fig. 9.3. The delay spread of the non-imaging CDS channel is also presented. In a CDS configuration, the delay spread decreases from almost 2 ns to 0.5 ns when an imaging receiver replaces the non-imaging receiver at a transmitter-receiver horizontal separation of 6 m. This is attributed to the small pixels and their narrow FOV which results in a limited range of received rays. Furthermore, at that transmitter-receiver distance, the imaging LSMS offers a reduction in the delay

spread, from 0.5 ns to 0.42 ns over the imaging CDS system. It can be seen that the delay spread of both imaging CDS and imaging LSMS systems increases as the transmitter-receiver distance increases. In contrast, our new imaging MBAAS configuration produces an almost constant delay spread (i.e. independent of the transmitter-receiver distance) as the beam angles are adjusted to maximise the receiver's SNR. A significant delay spread reduction, from 0.42 ns to 0.08 ns is achieved when the multibeam angle adaptive system replaces the LSMS at 6 m transmitter-receiver horizontal separation when both systems employ an imaging receiver. The delay spread is further reduced, from 0.08 ns (MBAAS) to 0.02 ns by increasing the power to spots that have a stronger path to the receiver (i.e. transmit power adaptation).

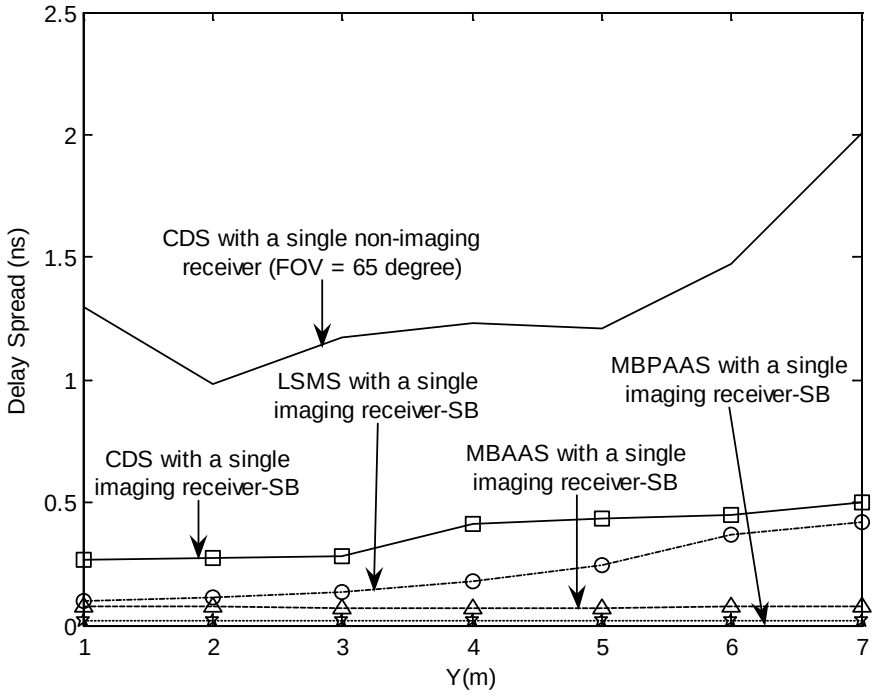

Figure 9-3: Delay spread of the proposed configurations when the transmitter is placed at (1m, 1m, 1m) and the receiver moves along the x = 2 m line

9.4.2. Bandwidth

The 3 dB channel bandwidth of the proposed imaging systems and comparison with the non-imaging CDS is outlined in Table. 9.1. The results show that a diffuse link employing a single wide FOV receiver at 6 m transmitter-receiver separation can achieve an almost 25 MHz channel bandwidth in good agreement with that reported in [10]. The diffuse channel bandwidth can be increased from 25 MHz to 250 MHz when an imaging receiver replaces the wide FOV receiver, see Fig. 9.4. However, a reduction in the received power from 0.26 μW to 21.8 nW is observed. This power penalty can be reduced with the received power increasing from 21.8 nW to 0.36 μW when a spot-diffusing transmitter replaces the diffuse transmitter (both transmitters employ an imaging receiver), see Fig. 9.4 (a). This is attributed to the ability of the spot-diffusing technique to establish a LOS with such diffusing spots. This power improvement is combined with an increase in the channel bandwidth from 250 MHz (imaging CDS) to 400 MHz at that transmitter-receiver distance (a 6 m horizontal separation). However, the imaging LSMS channel can achieve a 1.66 GHz bandwidth when the transmitter and receiver are co-located at the room corner (1m, 1m, 1m) as shown in Table 9.1.

Furthermore, beam angle adaptation coupled with the spot-diffusing geometry can spatially distribute the spots to positions near to the imaging receiver regardless of the transmitter position resulting in improvements in the received power and channel bandwidth. At a 6 m transmitter receiver separation, a spot-diffusing system adopting beam angle adaptation with an imaging receiver can achieve a channel bandwidth of about 1.99 GHz and 10.3 μW received power, see Figs. 9.4 (a) and (b). The imaging receiver limits the rays captured by utilising narrow FOVs pixels (a pixel's FOV of 11.3^{o} is used) and selects the pixel with the best received power (select the best

image pixel here). Allocating higher powers to the spots observed by the selected pixel through transmit beam power adaptation significantly enhances the received power to 25.2 μW and increases the channel bandwidth to 8.19 GHz (see Figs. 9.4 (a) and (b)).

TABLE 9-1: 3 dB BANDWIDTH OF THE PROPOSED IMAGING SYSTEMS AND COMPARSION WITH THE NON-IMAGING CDS

Configuration	**3** dB **Channel Bandwidth (**GHz**)**						
	Y (m)						
	1	2	3	4	5	6	7
CDS with a single non-imaging receiver (FOV = 65^o)	0.055	0.068	0.073	0.075	0.076	0.063	0.043
CDS with a single imaging receiver-SB	0.46	0.45	0.44	0.31	0.29	0.27	0.25
LSMS with a single imaging receiver-SB	1.66	1.51	1.25	0.93	0.68	0.48	0.40
MBAAS with a single imaging receiver-SB	1.99	2.02	1.98	2.03	1.98	2.02	1.99
MBPAAS with a single imaging receiver-SB	8.19	8.16	8.16	8.16	8.16	8.16	8.19

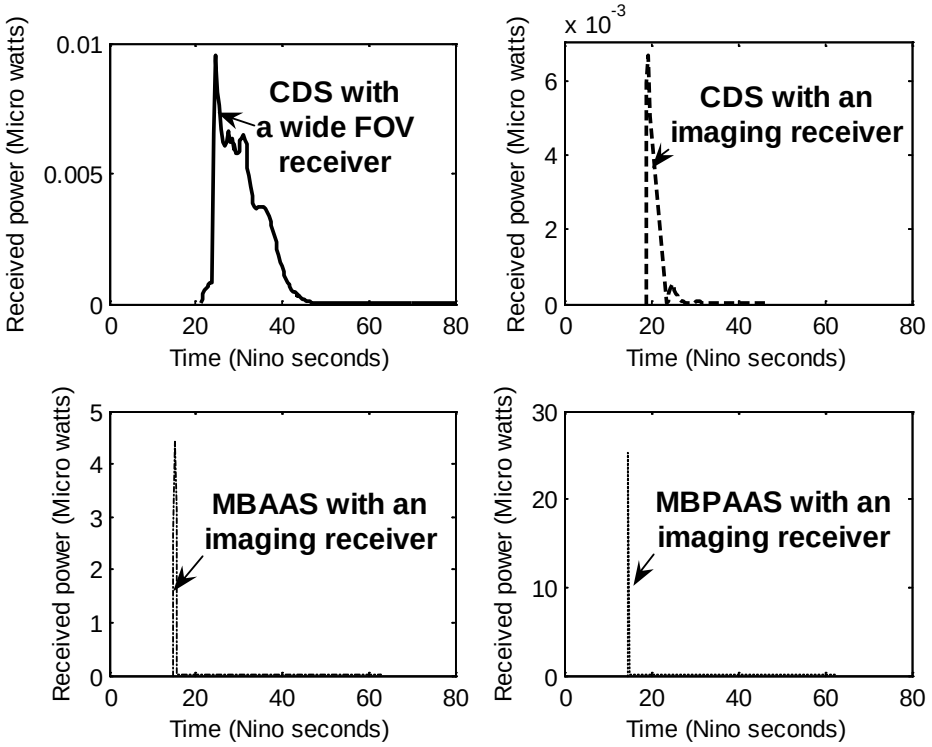

(a)

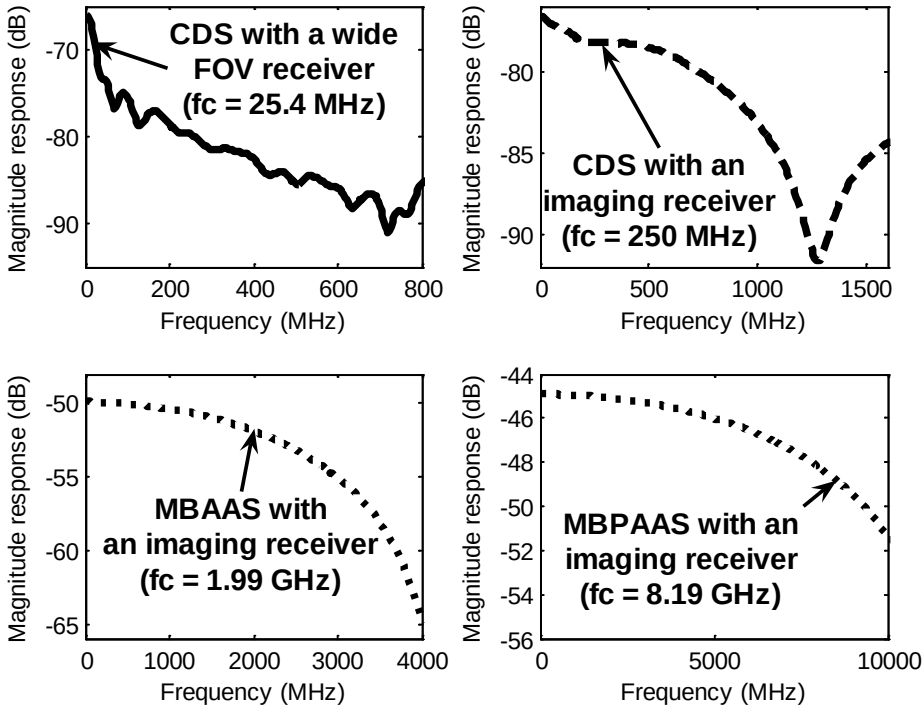

(b)

Figure 9-4: Impulse response and frequency response of different OW configurations at a transmitter-receiver separation of 6 m; (a) Impulse responses (b) Frequency responses

9.4.3. SNR

The performance of our proposed imaging systems operating at 30 Mbit/s is evaluated under the impairments of ambient light induced shot noise, multipath dispersion, and mobility. Our imaging systems' SNR is compared with that of the 30 Mbit/s non-imaging CDS, when the transmitter is placed at (2m, 4m, 1m) and (2m, 7m, 1m) and the receiver moves along the x = 1 m line, and the results are depicted in Figs. 9.5 (a) and (b) respectively. The low bit rate (30 Mbit/s) was considered to enable comparison to previous work. The preamplifier used in the 30 Mbit/s OW systems is the PIN FET transimpedance preamplifier in [94]. The results show that the fluctuation observed in the CDS SNR due to the noise distribution is reduced with more than 20 dB SNR improvement at the worst communication path considered when the MRC imaging receiver replaces the non-imaging receiver. This is due to the ability of the imaging receiver to spatially select (or MRC combine) those pixels that experience low BN. The SNR gain is further improved by 24 dB approximately when the LSMS replaces the CDS. Although, an SNR improvement is achieved through the spot-diffusing geometry with imaging reception, degradation can be induced due to mobility. The effect of transmitter mobility on the imaging MRC LSMS performance can be observed as an SNR degradation of 17 dB when the receiver is at (2m, 7m, 1m) and the transmitter moves from (2m, 4m, 1m) to (1m, 1m, 1m). Spatially distributing the diffusing spots at positions near the imaging receiver through beam angle adaptation can maximise the SNR at all receiver locations regardless of the transmitter position. For example, our imaging MRC MBAAS improves the SNR by 36 dB compared to the imaging LSMS with MRC at transmitter and receiver locations of (2m, 7m, 1m) and (1m, 1m, 1m).

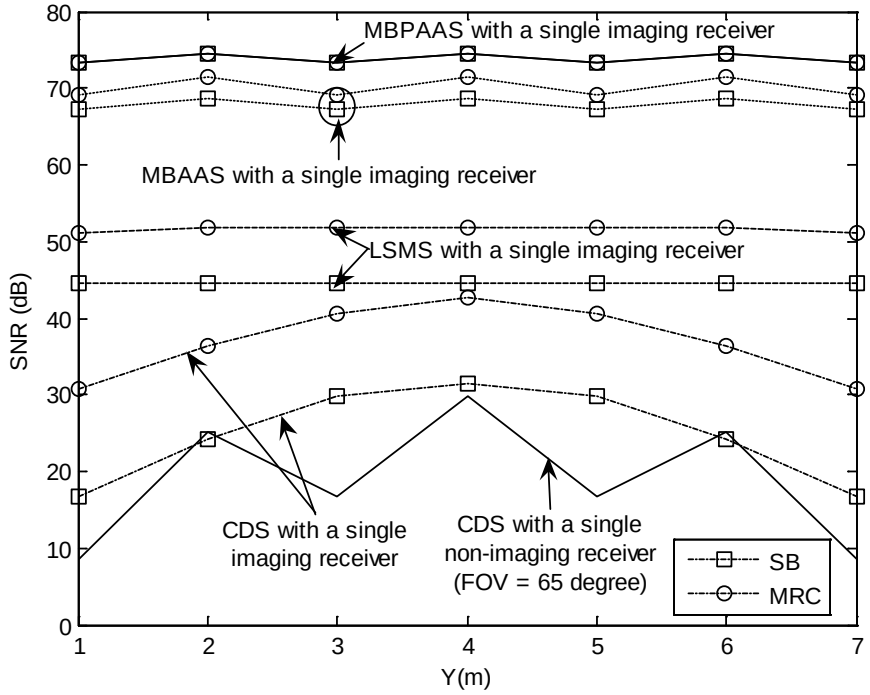

(a)

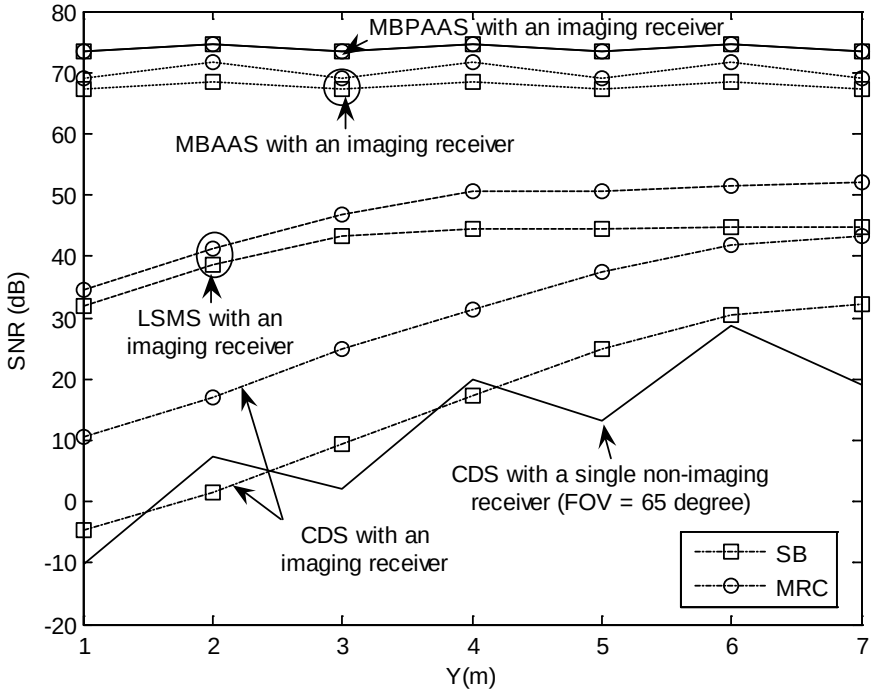

(b)

Figure 9-5: SNR of the proposed systems operating at 30 Mbit/s, when the receiver moves along the x = 1 m line and the transmitter is placed at (a) (2m, 4m, 1m) and (b) (2m, 7m, 1m)

Further SNR improvement of about 4 dB is achieved when the power is adaptively distributed among the spots. It should be noted that the majority of the SNR improvement, in this case, is achieved through beam angle adaptation which concentrates the power near the receiver. Furthermore, joint optimisation of the angle between the beams and the transmitted power amongst the beams, similar to that discussed in Chapter 8, Section 8.4.2, was carried out, and it is evident that the MBAAS produces the best SNR when its diffusing spots just touch.

9.5. Power Penalty versus Computation Time

The combination of the spot-diffusing approach, imaging reception, beam power and beam angle adaptation provides a significant SNR improvement, however the implementation complexity increases. This is a result of computing the imaging receiver SNR based on a single beam scanning over a range of possible locations on the ceiling and walls. A total of 12500 possible locations were scanned when using a beam angle adaptation step size of 2.29^{o} resulting in 12.5 ms computation time. As mentioned previously in Chapter 8, increasing the beam angle adaptation step size can reduce the number of possible locations studied resulting in computational saving at an expected power penalty cost. In order to investigate the trade-off between the power penalty and computational saving, the beam angle and power adaptation algorithm given in Table 8.1 was adopted, however at an increased beam angle adaptation step size, where steps of 2.29^{o} are used now. At each step the MRC imaging receiver SNR is calculated and stored. A maximum step size of 36.64^{o} (i.e. the spot moves 128 cm resulting in a total of 54 possible locations on the ceiling and walls of the room) is considered. It is observed that at all the beam angle step sizes considered the angle adaptation algorithm can identify the optimum location on the

ceiling where the imaging receiver can spatially MRC combine those pixels that observe minimum background noise. The performance penalty versus computation time associated with the imaging MBAAS system is depicted in Fig. 9.6 at receiver locations of (1m, 1m, 1m) and (1m, 2m, 1m). These two locations were selected in order to examine two different cases, i.e. a point exactly underneath spotlights and another point that is not. When the receiver is located underneath a spotlight, increasing the beam angle step size from 2.29^{o} to 27.48^{o} reduces the number of locations, which have to be scanned to identify the optimum location, from 12500 locations to 96 locations resulting in a reduction in the computation time from 12.5 ms to 96 μs (as mentioned earlier, it is assumed that the SNR computation associated with each location is carried out in 1 μs).

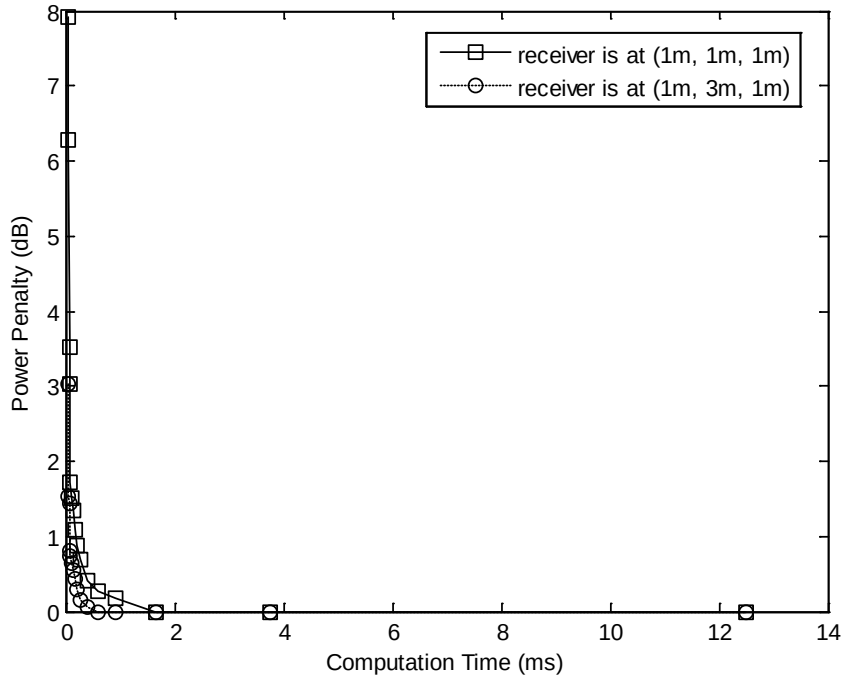

Figure 9-6: Trade-off between the power penalty and computation time saving of the imaging MBAAS system when the receiver is placed at (1m, 1m, 1m) and (1m, 2m, 1m)

This reduction in complexity comes with a slight performance degradation of 1.73 dB. However, a power penalty of 3 dB can be incurred if the beam angle step size is set at 29.77^{o} to achieve a computational saving from 12.5 ms to 77 μs. The penalty is attributed to the fact that at beam angle step sizes up to 27.48^{o} the angle adaptation algorithm can identify the optimum location of the centre of a line of spots observed by pixels that experience minimum background noise. When the beam angle step size exceeds 27.48^{o} some of the spots of the line strip whose centre is the optimum location start to appear on an area associated with a pixel observing a high noise power. Furthermore, increasing the beam angle step size from 29.77^{o} to 36.64^{o} to achieve a reduction in computation time from 77 μs to 54 μs, increases the SNR penalty from 3 dB to 7.92 dB. In contrast, when the receiver is located elsewhere (receiver positions are not underneath spotlights) the angle adaptation algorithm can reduce the computational time from 12.5 ms to 54 μs by increasing the beam angle step size from 2.29^{o} to 36.64^{o} at the cost of a 3 dB power penalty.

Fig. 9.7 compares the SNR of the main MBPAAS and modified MBPAAS systems that operate at 30 Mbit/s and employ an MRC imaging receiver. A reduction in the computation time from 12.5 ms to 54 μs can be achieved when our modified MBPAAS replaces the main MBPAAS. However, SNR degradation can be induced. A worst case performance penalty of 4 dB has to be paid when the receiver is placed at locations underneath spotlights in our communication environment (room). A reduction in the performance penalty, from 7.92 dB to 4 dB is achieved illustrating the gain achieved through transmit power adaptation. An SNR improvement of 35 dB can be obtained when the modified MBPAAS is implemented instead of the LSMS at the worst communication link considered when both systems operate at 30 Mbit/s and employ an MRC imaging receiver.

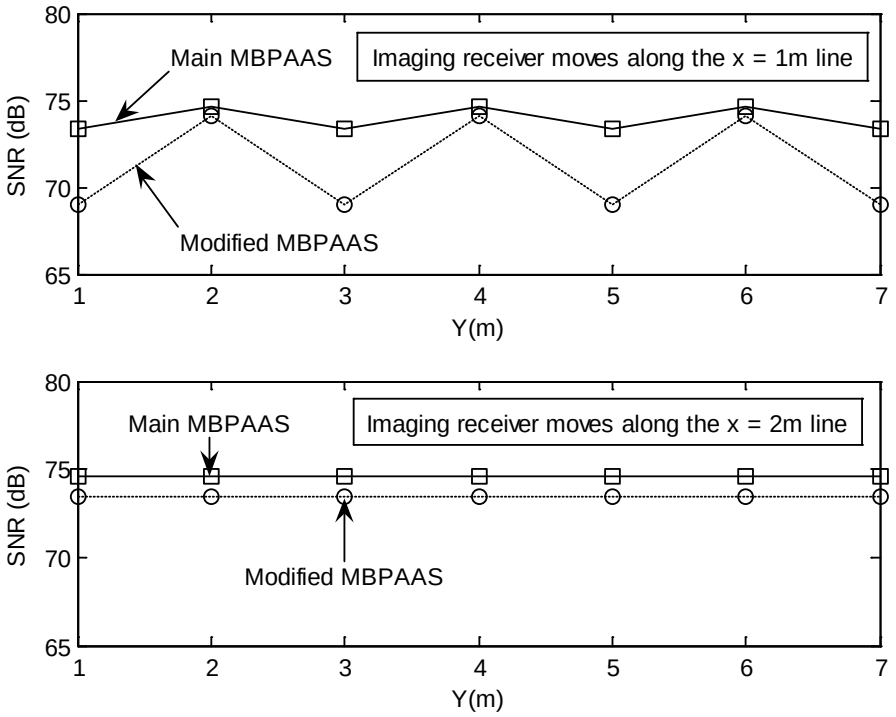

Figure 9-7: SNR of the proposed multibeam systems (main MBPAAS, and modified MBPAAS) operating at 30 Mbit/s, when both systems employ an imaging receiver that moves along the x = 1 m and x = 2 m lines

The excess SNR achieved through the combination of spot-diffusing, imaging reception, beam angle and beam power adaptation (SNR of 69 dB at the worst communication path considered) can prove extremely useful in reducing the transmit power of the system below the current 1 W level to help meet eye safety requirements. At the worst communication path considered in the 30 Mbit/s OOK OW systems, the introduction of these methods can reduce the transmit power by almost 27 dB while achieving 10^{-9} BER. To investigate eye safety, the transmit power is reduced to 10 mW and a restriction is introduced to the beam angle and power adaptation algorithm so that no spot is assigned more than 1 mW (which is the eye safe limit at the near infrared wavelengths). The SNR obtained through the use of

our restricted beam angle and power adaptation algorithm was 33.4 dB at the worst communication path.

9.6. Robustness to Shadowing and Signal Blockage

In this section, the robustness of our multibeam power and angle adaptive system coupled with imaging MRC receivers to shadowing and signal blockage is evaluated and compared to that associated with imaging MRC LSMS. Comparisons of modified imaging MRC MBAAS, imaging with MRC and non-imaging CDS systems are also considered and presented. A realistic office environment similar to that shown in Fig. 5.1 is used to simulate shadowing of the communication links. The SNR of all the systems in the two room scenarios (shadowed and unshadowed rooms) are shown in Fig. 9.8 at a data rate of 30 Mbit/s, when the transmitter is positioned at the room corner (1m, 1m, 1m) and receiver moves along the x = 2 m line. Simulation results show that the worst impact of shadowing and signal blockage in the non-imaging CDS performance translates to an SNR degradation of almost 24 dB at a transmitter-receiver distance of 6 m. This shadowing-induced degradation can be reduced to about 10 dB when an imaging MRC receiver replaces the non-imaging receiver. Furthermore, employing an LSMS geometry coupled with an imaging receiver helps mitigate the impact of shadowing due to its ability to maintain the direct path components at every imaging receiver location. The introduced beam angle adaptation provides a robust link against shadowing and signal blockage due to its ability to position the diffusing spots in regions in the ceiling with the strongest paths to the receiver. The introduction of beam angle and beam power adaptation to the mobile multibeam OW system employing imaging MRC receivers produces a comparable SNR performance in both shadowed and unshadowed environments.

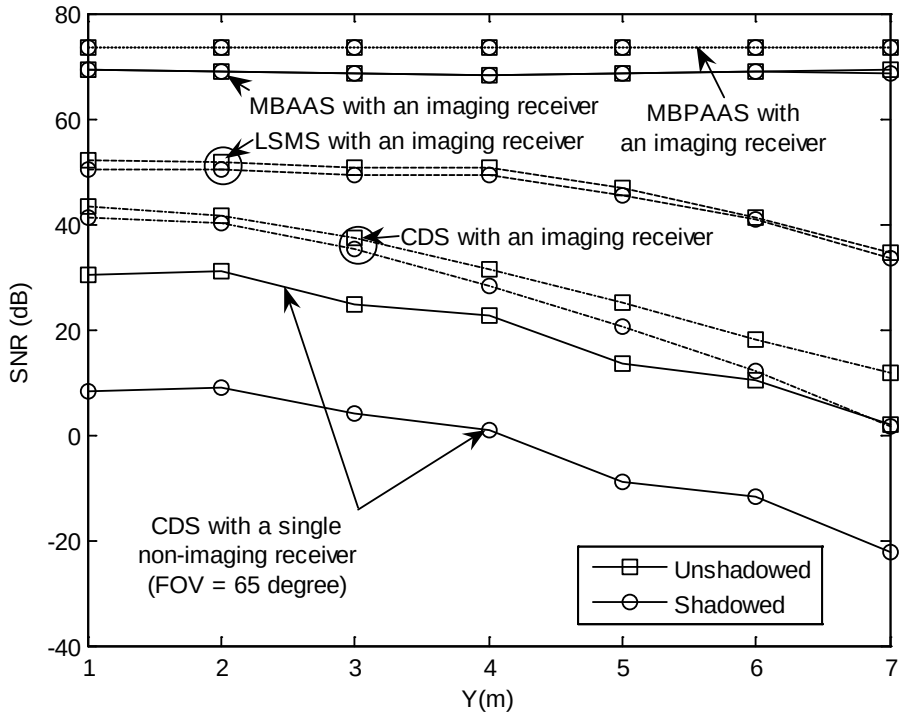

Figure 9-8: SNR of the proposed systems in two room scenarios (unshadowed and shadowed rooms) when the transmitter is placed at (1m, 1m, 1m) and the receiver moves along the x = 2 m line

In the presence of shadowing at the worst communication path considered, a significant SNR improvement of 40 dB can be achieved by replacing the imaging MRC LSMS with the modified imaging MRC MBPAAS. Our previous work in [114] has shown that an adaptive LSMS (ALSMS) system with an imaging MRC receiver offers a 23 dB SNR improvement over the non-adaptive imaging MRC LSMS (when both systems operate at 30 Mbit/s at the worst communication path in the presence of shadowing). This SNR improvement illustrates the gain achieved through power adaptation while the beam angles are kept fixed. Here we show that a further 17 dB SNR improvement can be achieved if adaptation is also applied to beam angles.

The high SNR achieved coupled with the additional bandwidth shown in Table 9.1 can be used to provide high data rate communications (2.5 Gbit/s, 5 Gbit/s and beyond) and multi-user access (see Section 9.7) over optical wireless channels. This system significantly outperforms any optical wireless system published in the literature to the best of our knowledge. Indoor mobile optical wireless systems operating at 2.5 Gbit/s and 5 Gbit/s are shown to be feasible through the combination of four methods: spot-diffusing, imaging reception, beam angle and power adaptation, see Fig. 9.9. The results prove that the mobile modified MBPAAS system in conjunction with imaging MRC receivers can achieve a BER of 10^{-9} while operating at a high bit rate of 5 Gbit/s at all transmitter and receiver locations over the entire CF in the presence of shadowing and signal obstruction.

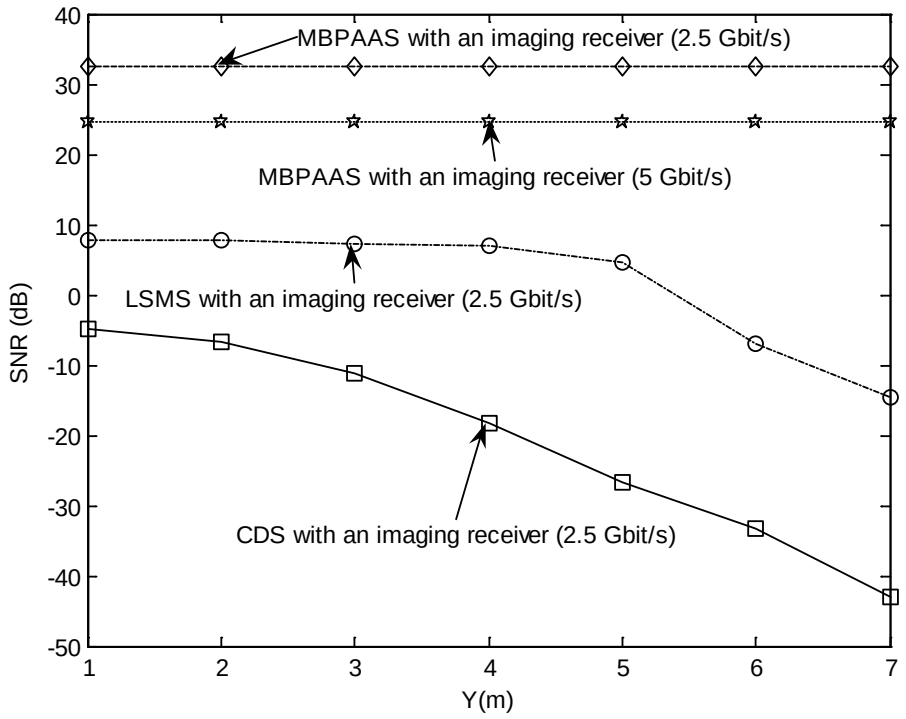

Figure 9-9: SNR of the proposed imaging systems operating at 2.5 Gbit/s, when the transmitter is placed at the room corner (1m, 1m, 1m) and the imaging receiver moves along the x = 2 m line, and the 5 Gbit/s imaging MBPAAS system

At the worst communication path in a shadowed environment, the 5 Gbit/s modified MBPAAS system offers an SNR gain of 23 dB over a lower data rate (30 Mbit/s) CDS system when both systems employ an imaging receiver based on MRC. Our multibeam angle and power adaptation system with an imaging receiver offers a minimum bandwidth of 8.16 GHz, see Table 9.1. This can support a 10 Gbit/s system. We plan to investigate future mobile optical wireless systems that operate at data rates well beyond 10 Gbit/s which is a promising feature in such optical systems.

9.7. Multi-users OW Imaging Systems

In this section, we introduce an MC-CDMA scheme to the modified MBPAAS system to enable multi-user OW communications. Computer simulation of the MC-CDMA system was carried out in a shadowed OW channel. It has to be observed that the PIN FET receiver used in [184] was used in conjunction with the OW MC-CDMA system. The receiver bandwidth was limited to 2 GHz to accommodate the MC-CDMA symbol that requires a bandwidth of 1.95 GHz (64 subcarriers send at a data rate of 30 Mbit/s). This receiver bandwidth is large and was intentionally used so that the effect of the channel dispersion is studied in isolation from any further dispersion that can be induced by the receiver. At the transmitter, as shown in Fig. 5.4, we generated random serial data of -1 and +1 and we spread the data using an orthogonal gold code sequences which consist of -1, +1 bits. The serially spread data was converted into a parallel data stream enabling parallel transmission with 64 sub-channels (where each channel was modulated using a BPSK modulation scheme). The parallel data was fed to an IFFT processor and the serial output was used for transmission. A DC value was added to ensure non-negativity, and the transmitted

signal was passed through the optical channel. At the receiver, the received signal is influenced by AWGN (due to the channel and the preamplifier) at different SNR levels. The corrupted received signal was fed into the FFT circuit where after processing, the serial data was converted into parallel data. Each column of these parallel data is multiplied by the spreading code, is summed up and integrated. Finally, the original data was recovered, and the BER was calculated.

The BER of the MC-CDMA system over an indoor OW channel based on the modified MBPAAS configuration with an imaging SB receiver is evaluated and presented. Comparisons with the MC-CDMA imaging LSMS and CDS systems employing SB approach are also provided. The BER results in a multi-user scenario are quoted in Figs. 9.10 (a) and (b) in the presence of shadowing when the transmitter is located at (2m, 4m, 1m) and (2m, 7m, 1m) respectively, and the imaging receiver moves along the x = 1 m on the CF. It is to be noted that this line (x = 1 m) represents the worst zone that can be scanned due to the presence of office cubicles. A better perspective on how the BER varies with transmitter-receiver distance within the entire CF can be achieved by plotting BER values at different transmitter and receiver locations, as shown in Figs. 9.10 (a) and (b). The results show a decline in BER in both MC-CDMA imaging CDS and LSMS systems when the imaging receiver moves away from the transmitter, while the MC-CDMA imaging modified MBPAAS system produces an almost constant BER independent of the transmitter-receiver separation. This is due to the ability of the beam angle adaptation algorithm to target its diffusing spots to an area near the imaging receiver that maximises the SNR and due to re-allocating the power to unobstructed spots through beam power adaptation. The results also show that background noise and shadowing have a significant effect on the performance of the MC-CDMA imaging

CDS system at all transmitter and receiver positions. This impact is observed as a comparable BER performance in both 4-user and 10-user MC-CDMA imaging CDS systems because the noise dominates and the data signal is weak. This is mainly due to the behaviour of our MC-CDMA system, and can also be seen in the BER trend of the MC-CDMA imaging LSMS, as shown in Fig. 9.10 (b), when the receiver is away from the transmitter, particularly when the receiver is at y = 1, 2 m. Furthermore, in a 4-user MC-CDMA system, a BER reduction from 3.7×10^{-1} to 7.5×10^{-5} is achieved when an LSMS replaces the diffuse system when both systems employ an imaging SB receiver at transmitter and receiver locations of (2m, 4m, 1m) and (1m, 1m, 1m) respectively. This is attributed to the more uniform diffusion of the spots on the entire CF, as a result of positioning the LSMS transmitter at the room centre (2m, 4m, 1m), which yields a strong received signal. As the spot-diffusing transmitter begins to move towards the opposite room edge of the receiver location (1m, 1m, 1m), the BER in the 4-user MC-CDMA imaging LSMS system gradually decreases until it reaches its lowest value of 3.5×10^{-1} when the transmitter is at (2m, 7m, 1m). Our previous work in Chapter 7 has shown that adaptively distributing the power among the spots can improve the BER from 3.5×10^{-1} to 0.12×10^{-11} in a 4-user mobile MC-CDMA imaging LSMS system. Here we show that placing the diffusing spots at regions with the shortest paths to the receiver can offer further BER improvement from 0.12×10^{-11} to 0.9×10^{-15}. This significant BER improvement is due to the large channel bandwidth of almost 8.2 GHz and the increase in SNR achieved through the combination of beam angle and beam power adaptation, spot-diffusing and imaging reception.

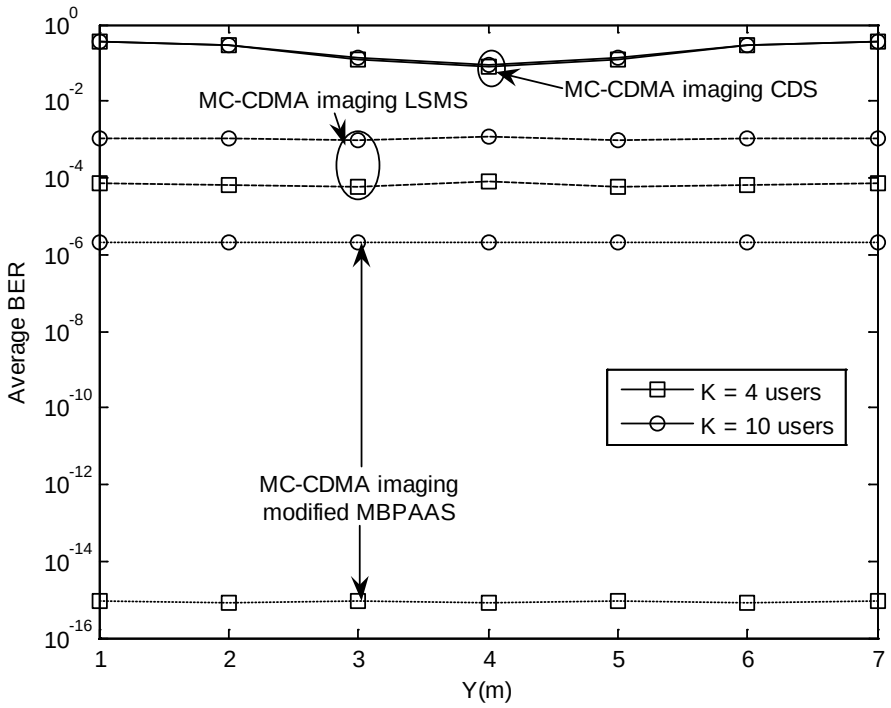

(a)

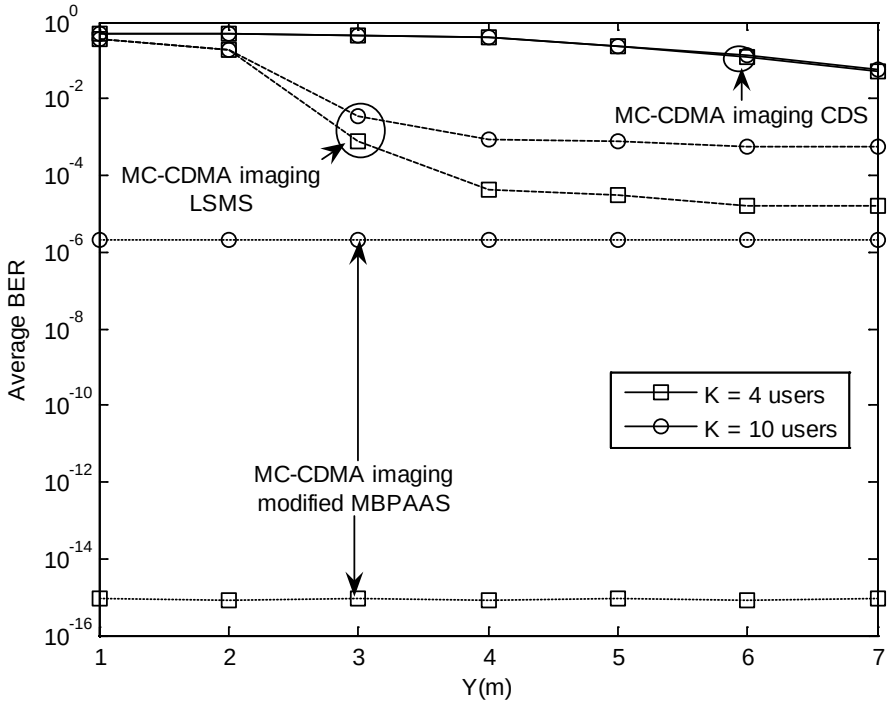

(b)

Figure 9-10: BER of three mobile OW MC-CDMA systems: MC-CDMA CDS, MC-CDMA LSMS and MC-CDMA modified MBPAAS with an imaging receiver based on SB in a shadowed environment with multiple users when the receiver moves along the x = 1 m line at transmitter locations of (a) (2m, 4m, 1m) and (b) (2m, 7m, 1m)

9.8. Summary

This chapter introduced a high-speed spot diffusing mobile optical wireless system employing beam angle and power adaptation and imaging receivers. The aim was to increase the achievable data rate in non LOS infrared communications and enhance the SNR enabling the system to achieve mobility while operating at high bit rates in the presence of shadowing. This was achieved by making use of the significant SNR and channel bandwidth improvements obtained through the introduction of four methods: spot-diffusing, imaging reception, beam angle and beam power adaptation. Our proposed system (MBPAAS with imaging receivers) was evaluated through channel and noise modelling, and results for select best and maximum ratio combining were presented. Imaging receivers can help mitigate the BN effect by selecting (or MRC combining) those pixels that observe lower BN, and by minimising the preamplifier thermal noise through the use of small sized pixels. In a CDS system, replacing a non-imaging receiver by an imaging receiver with MRC can increase the SNR by more than 20 dB. Further SNR improvement of 24 dB was achieved when the spot-diffusing system replaced the CDS when both systems employed an imaging MRC receiver. In the imaging spot-diffusing system, the SNR was independent of the transmitter position and can be maximised at all receiver locations when our new methods (beam angle and beam power adaptation) were implemented. Regardless of the transmitter position, beam angle adaptation can target the spots at the optimum location that yields the best SNR at the receiver. A significant SNR improvement of 36 dB in the imaging spot-diffusing system was achieved when angle adaptation was introduced. A further SNR improvement of 4 dB was obtained when the power was adaptively distributed among the spots. This improvement came at the cost of complexity. The complexity can be reduced by

increasing the beam angle adaptation step size from 2.3^{o} to 36.64^{o} resulting in a typical search time reduction from 12.5 ms to 54 μs when our modified MBPAAS replaced the main MBPAAS. However, a power penalty of 4 dB at receiver locations underneath spotlights and 1 dB elsewhere was induced. Furthermore, the combination of imaging reception, spot-diffusing, beam angle and beam power adaptation increased the bandwidth from 43 MHz to 8.19 GHz compared to the non-imaging CDS system thus helping increase the channel capacity. The results also prove that the influence of shadowing and signal blockage can be sufficiently reduced through the use of these methods. A fully mobile 5 Gbit/s OW communication system was shown to be feasible with an SNR improvement of 15 dB compared to a lower data rate (30 Mbit/s) imaging MRC CDS at the worst communication link in a shadowed environment. In addition, a multi-user OW communication system was evaluated introducing an MC-CDMA scheme to our proposed link design (imaging modified MBPAAS). In a 4-user MC-CDMA OW system, a BER improvement from 3.5×10^{-1} to 0.9×10^{-15} was obtained when the imaging modified MBPAAS replaces the imaging LSMS.

10. CONCLUSIONS

Multipath dispersion is one of the most important concerns in characterising indoor OW systems. Attention was given to multipath propagation, and its influence on the received optical signal was examined. The multipath dispersion impact is negligible in a direct LOS link, as the transmitted optical beam is narrow and is aimed directly into a narrow FOV receiver yielding high power efficiency. A diffuse link is an alternative approach that allows user mobility and provides some immunity to transmission path blockage, but it is more prone to multipath effects than direct LOS links. This is due to the multiple reflections in a diffuse system which cause dispersion and ISI. The severity of ISI can be measured using the channel rms delay spread. Another major impairment that affects optical wireless systems is background noise (BN), which tends to be directional and is typically due to artificial or natural light sources. The effect of multipath dispersion and BN can be reduced by having a choice of reception directions through the use of diversity receivers. This is due to the fact that normally the desired optical signal reaches the receiver from all directions unlike the undesired directional BN. Furthermore, spot-diffusing techniques lead to attractive configurations that combine the advantages of both direct LOS and pure diffuse links. A significant performance improvement can be achieved through the combination of a spot-diffusing transmitter geometry and diversity detection. This improvement is due to the reduction in BN as well as reduction in ISI effects, and also due to the enhanced received power. However, shadowing and user mobility can cause performance degradation in spot-diffusing optical wireless systems.

This thesis has focused on link designs, with emphasis on efficient methods that can combat the impairments discussed enabling the OW system to achieve higher data rates (2.5 Gbit/s, 5 Gbit/s and beyond) and/or provide multi-user communications. The performance of our proposed systems was evaluated through channel and noise modelling in a rectangular room having a width of 4 m, a length of 8 m and a height of 3 m. Simulation results were obtained using a light ray tracing method where the transmitted signal reaches the receiver through various paths based on reflections from reflecting surfaces. Diversity emission and detection have been taken into account. We have compared our results to published simulations and experiments and a good agreement was observed giving confidence in our simulator when examining other systems. LSMS and BCM, which are two attractive configurations in the literature, were modelled and used for comparison purposes in order to evaluate the improvements offered through our proposed novel configurations. Our new systems were also compared with conventional diffuse system which is a reference base line accepted in the community.

A novel beam power adaptation method was proposed, studied and shown to be a desirable means for improving the performance of spot-diffusing optical wireless systems that operate under the constraints of background noise, multipath dispersion, and mobility. We proposed and evaluated new OW configurations based on an adaptive multibeam transmitter and diversity detection. Two mobile adaptive multibeam OW configurations (ABCM and ALSMS) in conjunction with a 7-face diversity receiver were considered. The main goal was to reduce the effect of transmitter/receiver mobility and the associated impacts in terms of a weak received optical power and reduction in bandwidth. Previous work showed that multiple spot diffusing techniques suffer from these two fundamental limitations associated with

mobility. The new adaptive spot-diffusing geometry helped overcome the impairments introduced by mobility. It introduced a gain in the received optical power, and increased the channel bandwidth even at large transmitter receiver separations. Previous work showed that BCM outperforms LSMS as its geometry results in spot clusters (higher powers) nearer to most receiver locations as the transmitter moves. We have shown that with spot power adaptation the performance of ABCM and ALSMS are similar as the adaptation algorithm distributes the power among the spots according to receiver location. It was also demonstrated that employing an adaptive beam clustering transmitter coupled with an 8^o diversity receiver can lead to significant improvements in the SNR and considerable extra bandwidth in the channel compared to non-adaptive systems. This improvement proved extremely useful in increasing the data rate of the system and enabling multi-user facilities. However, a moderate increase in complexity was induced due to SNR computations at the receiver and power adjustment among the spots at the transmitter. A fully mobile 5 Gbit/s OW communication system was shown to be feasible while achieving 37 dB SNR in the worst reception cases through the combination of beam clustering, transmit power adaptation and an 8^o diversity receiver using an optical concentrator coupled with an optical filter with typically 20 dB concentrator gain. This improvement was achieved when using a 1 cm^2 detector, 5 GHz receiver. We showed that 10^{-9} BER can be met even with a detector area of 0.1 cm^2 where our 5 Gbit/s OW system achieves an SNR of 17 dB which is greater than the 15.6 dB needed. Furthermore, our adaptive multibeam OW systems were evaluated in a real environment, and the results confirmed that adaptively distributing the power among the spots can provide more robustness against shadowing.

The use of MC-CDMA was proposed as a method that can provide multi-user capabilities suited to the limited bandwidth in OW systems. BER analysis for the OW MC-CDMA system in a multi-user scenario was first performed and reported. A performance improvement was achieved by using an OW MC-CDMA system, compared to the conventional OOK system and OW CDMA system. It was demonstrated that at a 10^{-4} BER a 4-user OW MC-CDMA system offers SNR improvements of 7 dB and 10 dB over a single user OW OOK system and a 4-user OW CDMA system respectively. MC-CDMA exhibits an interference performance penalty as the number of users increases due to MAI. In a 4-user OW MC-CDMA, a BER improvement from 7.6×10^{-2} to 4.6×10^{-8} was achieved when an ALSMS replaces the traditional LSMS at the worst communication path in a highly impaired environment where shadowing exists. In addition, ZF equalisation was employed to mitigate the multiple access interference and improve the BER performance. It was shown that while the MC-CDMA CDS and LSMS systems benefit, the equalisation scheme, which increases receiver complexity, is not necessary when our new adaptation method is implemented at the data rate and system parameters considered.

Diversity reception can be configured in two main ways: using a number of photodetectors allocated different directions or using an imaging receiver employing a photodetector array segmented into multiple pixels. Imaging receivers offer the advantage of low cost and small size as a single imaging concentrator is used for all photodetectors (pixels), in contrast to using a separate concentrator for each photodetector in angle diversity non-imaging receivers. Additionally, photodetectors in an imaging receiver can be laid out in a single planar array which facilitates the use of a large number of photodetectors pixels, leading to enhanced performance. In order to combine the benefits of imaging receivers and diversity schemes (hence

providing robustness against BN and multipath dispersion), this thesis introduced imaging diversity receivers. Imaging receivers with MRC produced more than 20 dB better SNR than a non-imaging receiver in a conventional diffuse system. This result is in agreement with previous results reported in the literature. Replacing the imaging receivers with imaging diversity receivers achieved a further SNR improvement of 8 dB.

Furthermore, in order to provide full room coverage with uniform distribution of diffusing spots, a two-dimensional beam clustering method was employed (where three two-dimensional clusters of spots are distributed on the ceiling and two end walls with equal intensities). It was found that the 2DBCM SNR was enhanced by 12 dB when imaging diversity receivers replace the non-imaging diversity receivers when both receivers employ MRC. It was also noted that the imaging MRC 2DBCM system offered 17 dB better SNR than an imaging MRC CDS system. A further SNR improvement of 26 dB was obtained when transmit power adaptation is implemented. Moreover, the new methods introduced (transmit power adaptation, 2D beam clustering, and diversity imaging) increased the bandwidth from 38 MHz (non-imaging CDS) to 5.56 GHz. The increase in channel bandwidth and SNR aided the system to maintain higher data rates and a 5 Gbit/s OW system was realised with an SNR of 27 dB resulting in a power saving reward of 5.7 dB while achieving a BER of 10^{-9}. This was achieved at the cost of a substantial increase in complexity and without considering transmitter mobility and signal obstruction. In order to reduce the complexity, this treatment was extended while replacing the 2D beam clustering transmitter by a line strip spot-diffusing transmitter (i.e. employing a line of 80 spots instead of three 2D clusters of 400 diffusing spots in total), and using a single imaging receiver (that faces up) rather than a 3-face imaging diversity receiver. The

results showed that while operating at 5 Gbit/s (when the transmitter is stationary at the room centre and the imaging receiver is located at the room corner), a 10^{-9} BER is achieved with an approximate SNR of 17 dB through the combination of spot power adaptation, spot-diffusing and imaging MRC reception with a photodetector (pixel) area of 0.01 cm^2. However, a reduction in the SNR of 10 dB approximately was observed compared to that produced by the 5 Gbit/s 2DABCM system with imaging diversity receivers (where shadowing and signal blockage were not taken into account). When the transmitter moved to the opposite room corner the SNR of our 5 Gbit/s imaging ALSMS system degraded to almost 10 dB and missed the 10^{-9} BER. This achievement was obtained with full mobility in the presence of shadowing and beam blockage, with a modest complexity. It was also observed that in the adaptive LSMS system, replacement of the imaging receiver by imaging diversity receivers can slightly increase the SNR by 1 dB. In addition, we incorporated the MC-CDMA scheme into the imaging adaptive LSMS to facilitate multi-user communication and achieved a BER of 0.12×10^{-11} in a 4-user scenario compared to a BER of 3.5×10^{-1} when MC-CDMA imaging LSMS is considered.

Finally, a novel beam angle adaptation method was introduced, in addition to beam power adaptation, to the design of spot-diffusing OW systems to mitigate the mobility-induced degradation as well as improve the link performance in the presence of shadowing. A link design adopting the combination of these methods (spot-diffusing, beam angle and beam power adaptation) was investigated and evaluated with two detection techniques (a 7-face diversity non-imaging receiver and an imaging receiver) in a realistic environment with full mobility. The results proved that our introduced methods coupled with either diversity or imaging reception can maximise the receiver SNR over the entire CF regardless of the transmitter position,

and can also reduce shadowing and signal blockage. This is due to the ability of the angle adaptation algorithm to optimise the spots distribution that yields the best SNR at the receiver, and also due to allocating the power to unblocked beams through power adaptation. Significant SNR and bandwidth improvements were achieved combined with complexity expansion in terms of the computation time required to optimise the receiver SNR. This complexity was considerably reduced from a typical beam angle and beam power adaptation time of 12.5 ms to 54 μs when an imaging receiver is employed. However, a worst case power penalty of 4 dB at reception locations underneath spotlights was observed. The high SNR obtained was used to reduce the transmit power to comply with eye safety. A restriction, where the upper limit for spot power is 1 mW, was imposed in our angle and power adaptation algorithm, and a good performance was achieved. Furthermore, the OW system made use of this SNR improvement and the large bandwidth obtained through the combination of our new methods to operate at a high data rate of 5 Gbit/s while meeting 10^{-9} BER, with full mobility in the presence of shadowing and signal blockage. This system significantly outperforms any optical wireless system published in the literature to the best of our knowledge. In addition, multi-user scenarios were evaluated by introducing MC-CDMA, and a BER of 0.9×10^{-15} was achieved in a 4-user scenario.

11. FUTURE WORK

Throughout this thesis a number of original contributions were presented. Analytical expressions and simulation tools were developed and used to characterise a number of known and new OW systems. This work opened the gates to a host of new areas where new techniques can be proposed, examined and used to overcome the limitations associated with OW environments, hence achieving high-speed OW systems.

In this thesis, a novel beam power adaptation method was shown to improve the performance of spot-diffusing OW systems. The power adaptation algorithm given applied to the single user case where the beam powers are adapted so as to maximise the SNR at one given receiver location. In a multi-user scenario a number of different methods can be considered. Future work may employ opportunistic scheduling to handle this situation where the beam powers are chosen to maximise the SNR in a given region for a given time period, or effectively to allocate more power to users who experience lower background noise and/or multipath dispersion at a given time period.

The application of MC-CDMA in OW communication systems was first proposed, studied and investigated in this thesis. Multi-carrier modulation techniques suffer from high peak to average power ratio (PAPR). Although this issue is moderate in MC-CDMA in comparison to OFDM, it may be a severe problem in infrared communications, where infrared power radiation is limited due to eye safety. Here, a DC value was also added to each branch to ensure a positive signal. This incurred a power penalty that was mitigated by making use of the significant SNR improvement

achieved through our methods. The PAPR analysis of the OW MC-CDMA could be studied further.

The results in this thesis assume that the room surfaces reflect the incident optical signal in a Lambertion pattern with a typical reflection coefficient of 0.8. While this is true for most rooms with light coloured plaster walls, it is worth evaluating the sensitivity of the results to different room geometries and reflecting surface properties. Also, the simulation results presented in this thesis included first and second order reflections. Future work may include higher order reflections for producing more accurate channel characteristics.

In this thesis, the proposed systems are designed to interconnect mobile communication devices placed on the communication floor (a surface 1m above the floor). If one (or more) of these devices is fixed and is connected to a backbone network, it can act as an access gateway to the external world and can also act as a base station that shares the resources among the mobile devices and coordinates access to the medium. The design of a suitable medium access control protocol for such a system is not considered here and is worth further investigation.

In addition, the methods introduced in this study may be applicable to other parts of the spectrum where sources and detectors are starting to become available, for example UV. However, a detailed study is needed to characterise the reflective properties of different materials at these parts of the spectrum. The experimental verification of the many results presented in this thesis is essential in any future work.

References

[1] Grubb, J. L.,'The traveler's dream come true,' *Communications Magazine, IEEE,* vol. 29, pp. 48-51, 1991.

[2] Padgett, J. E., Gunther, C. G. and Hattori, T.,'Overview of wireless personal communications,' *Communications Magazine, IEEE,* vol. 33, pp. 28-41, 1995.

[3] Gfeller, F. R. and Bapst, U.,'Wireless in-house data communication via diffuse infrared radiation,' *Proceedings of the IEEE,* vol. 67, pp. 1474-1486, 1979.

[4] Freeman, E. and Forsberg, G.,'A short-range optical transmission system for television signals,' *Optical Engineering,* vol. 13, pp. 396-400, 1975.

[5] Ogawa, K.,'Considerations for Optical Receiver Design,' *Selected Areas in Communications, IEEE Journal on,* vol. 1, pp. 524-532, 1983.

[6] Minami, T., Yano, K., Touge, T., Morikawa, H. and Takahashi, O., "Optical wireless modem for office communication," presented at the Proceedings of the May 16-19, 1983, national computer conference, Anaheim, California, 1983.

[7] Nakata, Y., Kashio, J., Kojima, T. and Noguchi, T., "In-house wireless communication communication system using infrared radiation," in *Proceedings of the International Conference on Computer Communication,* 1984, pp. 333-337.

[8] Takahashi, O. and Touge, T.,'Optical wireless network for office communication,' *JARECT (Japan Electron Rev. Electron. Comput. Telecomm.),* vol. 20, pp. 217-228, 1985/1986.

[9] Pauluzzi, D. R., McConnell, P. R. H. and Poulin, R. L., "Free-space, undirected infrared (IR) voice and data communications with a comparison to RF systems," in *Wireless Communications, 1992. Conference Proceedings., 1992 IEEE International Conference on Selected Topics in,* 1992, pp. 279-285.

[10] Barry, J. R., Kahn, J. M., Krause, W. J., Lee, E. A. and Messerschmitt, D. G.,'Simulation of multipath impulse response for indoor wireless optical channels,' *Selected Areas in Communications, IEEE Journal on,* vol. 11, pp. 367-379, 1993.

[11] Smyth, P. P., McCullagh, M. J., Wisely, D., Wood, D., Ritchie, S., Eardley, P. L., and Cassidy, S.,'Optical wireless local area networks-enabling technologies,' *BT Technol. Journal,* vol. 11, pp. 56-64, April 1993.

[12] Smyth, P. P., Wood, D., Ritchie, S. and Cassidy, S., "Optical wireless: New enabling transmitter technologies," in *Communications, 1993. ICC 93. Geneva. Technical Program, Conference Record, IEEE International Conference on*, 1993, pp. 562-566 vol.1.

[13] Elmirghani, J. M. H. and Cryan, R. A.,'Performance considerations for indoor infrared LANs,' *Proceedings of SPIE - The International Society for Optical Communications,* vol. 2450, pp. 606-612, 1995.

[14] Marsh, G. W. and Kahn, J. M.,'50-Mb/s diffuse infrared free-space link using on-off keying with decision-feedback equalization,' *Photonics Technology Letters, IEEE,* vol. 6, pp. 1268-1270, 1994.

[15] McCullagh, M. J. and Wisely, D. R.,'155 Mbit/s optical wireless link using a bootstrapped silicon APD receiver,' *Electronics Letters,* vol. 30, pp. 430-432, 1994.

[16] McCullagh, M. J., Wisely, D. R., Eardley, P. L. and Smyth, P. P.,'A 50 Mbit/s optical wireless LAN link using novel optical and electronic enabling technologies,' *International Seminar on Digital Communications*, pp. 298-309, 1994.

[17] Audeh, M. D. and Kahn, J. M.,'Performance evaluation of baseband OOK for wireless indoor infrared LAN's operating at 100 Mb/s,' *Communications, IEEE Transactions on*, vol. 43, pp. 2085-2094, 1995.

[18] Greaves, S. D., Nichols, P. J., Wisely, D. R. and Unwin, R. T., "Optical wireless video distribution," in *Proceedings of the International Society for Optical Engineering Conference*, 1995, pp. 280-285.

[19] Goldberg, L.,'Infrared data transmission: the missing link?,' *Electronic Design*, pp. 47-64, 1995.

[20] Boucouvalas, A. C.,'Indoor ambient light noise and its effect on wireless optical links,' *Optoelectronics, IEE Proceedings* -, vol. 143, pp. 334-338, 1996.

[21] Moreira, A. J. C., Valadas, R. T. and de Oliveira Duarte, A. M.,'Performance of infrared transmission systems under ambient light interference,' *Optoelectronics, IEE Proceedings* -, vol. 143, pp. 339-346, 1996.

[22] Elmirghani, J. M. H., Chan, H. H. and Cryan, R. A.,'Sensitivity evaluation of optical wireless PPM systems utilising PIN-BJT receivers,' *Optoelectronics, IEE Proceedings* -, vol. 143, pp. 355-359, 1996.

[23] Phillips, A. J., Cryan, R. A. and Senior, J. M.,'An optically preamplified intersatellite PPM receiver employing maximum likelihood detection,' *Photonics Technology Letters, IEEE*, vol. 8, pp. 691-693, 1996.

[24] Marsh, G. W. and Kahn, J. M.,'Performance evaluation of experimental 50-Mb/s diffuse infrared wireless link using on-off keying with decision-feedback equalization,' *Communications, IEEE Transactions on*, vol. 44, pp. 1496-1504, 1996.

[25] Wisely, D. R., "A 1 Gbit/s optical wireless tracked architecture for ATM delivery," in *Optical Free Space Communication Links, IEE Colloquium on*, 1996, pp. 14/1-14/7.

[26] Carruthers, J. B. and Kahn, J. M., "Angle diversity for nondirected wireless infrared communication," in *Communications, 1998. ICC 98. Conference Record.1998 IEEE International Conference on*, 1998, pp. 1665-1670 vol.3.

[27] Carruthers, J. B. and Kahn, J. M.,'Modeling of nondirected wireless infrared channels,' *Communications, IEEE Transactions on*, vol. 45, pp. 1260-1268, 1997.

[28] Street, A. M., Stavrinou, P. N., O'Brien, D. C. and Edwards, D. J.,'Indoor optical wireless systems - a review,' *Optical and Quantum Electronics*, vol. 29, pp. 349-378, 1997.

[29] Wisely, D. and Neild, I., "A 100 Mbit/s tracked optical wireless telepoint," in *Personal, Indoor and Mobile Radio Communications, 1997. 'Waves of the Year 2000'. PIMRC '97., The 8th IEEE International Symposium on*, 1997, pp. 964-968 vol.3.

[30] Kahn, J. M. and Barry, J. R.,'Wireless infrared communications,' *Proceedings of the IEEE*, vol. 85, pp. 265-298, 1997.

[31] Jungnickel, V., von Helmolt, C. and Kruger, U.,'Broadband wireless infrared LAN architecture compatible with Ethernet protocol,' *Electronics Letters*, vol. 34, pp. 2371-2372, 1998.

[32] Heatley, D. J. T., Wisely, D. R., Neild, I. and Cochrane, P.,'Optical wireless: the story so far,' *Communications Magazine, IEEE,* vol. 36, pp. 72-74, 79-82, 1998.

[33] Sterckx, K. L., Elmirghani, J. M. H. and Cryan, R. A., "Pyramidal fly-eye detection antenna for optical wireless systems," in *Optical Wireless Communications (Ref. No. 1999/128), IEE Colloquium on*, 1999, pp. 5/1-5/6.

[34] Theodorou, P., Elmirghani, J. and Cryan, R., "Performance of ATM optical wireless LANs with fixed channel assignment," in *Global Telecommunications Conference, 1999. GLOBECOM '99*, 1999, pp. 598-602 vol.1b.

[35] Heatley, D. J. T. and Neild, I., "Optical wireless-the promise and the reality," in *Optical Wireless Communications (Ref. No. 1999/128), IEE Colloquium on*, 1999, pp. 1/1-1/6.

[36] Bellon, J., Sibley, M. J. N., Wisely, D. R. and Greaves, S. D.,'Hub architecture for infra-red wireless networks in office environments,' *Optoelectronics, IEE Proceedings* -, vol. 146, pp. 78-82, 1999.

[37] Alvarez, J. R. V., Hernandez, F. J. L., Galdon, A. S., Jimenez, R. P. and Borges, J. A. R., "Infrared wireless DSSS system for indoor data communication links," in *Optical Wireless Communications Ii*. vol. 3850, E. J. Korevaar, Ed., ed Bellingham: Spie-Int Soc Optical Engineering, 1999, pp. 92-99.

[38] Sterckx, K. L., Elmirghani, J. M. H. and Cryan, R. A.,'Sensitivity assessment of a three-segment pyramidal fly-eye detector in a semidisperse optical wireless communication link,' *Optoelectronics, IEE Proceedings* -, vol. 147, pp. 286-294, 2000.

[39] Jivkova, S. and Kavehrad, M., "Indoor wireless infrared local access, multi-spot diffusing with computer generated holographic beam-splitters," in *Communications, 1999. ICC '99. 1999 IEEE International Conference on*, 1999, pp. 604-608 vol.1.

[40] Yun, G. and Kavehrad, M., "Spot-diffusing and fly-eye receivers for indoor infrared wireless communications," in *Wireless Communications, 1992. Conference Proceedings., 1992 IEEE International Conference on Selected Topics in*, 1992, pp. 262-265.

[41] Pohl, V., Jungnickel, V. and von Helmolt, C., "A channel model for wireless infrared communication," in *Personal, Indoor and Mobile Radio Communications, 2000. PIMRC 2000. The 11th IEEE International Symposium on*, 2000, pp. 297-303 vol.1.

[42] Jivkova, S. and Kavehrad, M.,'Receiver designs and channel characterization for multi-spot high-bit-rate wireless infrared communications,' *Communications, IEEE Transactions on,* vol. 49, pp. 2145-2153, 2001.

[43] Jungnickel, V., Haustein, T., Forck, A. and von Helmolt, C.,'155 Mbit/s wireless transmission with imaging infrared receiver,' *Electronics Letters,* vol. 37, pp. 314-315, 2001.

[44] Al-Ghamdi, A. and Elmirghani, J. M. H.,'Optimization of a triangular PFDR antenna in a fully diffuse OW system influenced by background noise and multipath propagation,' *Communications, IEEE Transactions on,* vol. 51, pp. 2103-2114, 2003.

[45] Al-Ghamdi, A. G. and Elmirghani, J. M. H.,'Performance evaluation of a triangular pyramidal fly-eye diversity detector for optical wireless

communications,' *Communications Magazine, IEEE,* vol. 41, pp. 80-86, 2003.

[46] Al-Ghamdi, A. G. and Elmirghani, J. M. H., "Triangular PFDR antenna optimisation under the restriction of background noise and multipath propagation in an optical wireless system," in *Communications, 2003. ICC '03. IEEE International Conference on*, 2003, pp. 2013-2019 vol.3.

[47] Al-Ghamdi, A. G. and Elmirghani, J. M. H.,'Performance evaluation of a pyramidal fly-eye diversity antenna in an indoor optical wireless multipath propagation environment under very directive noise sources,' *Optoelectronics, IEE Proceedings -*, vol. 150, pp. 482-489, 2003.

[48] Kahn, J. M., Barry, J. R., Audeh, M. D., Carruthers, J. B., Krause, W. J., and Marsh, G. W.,'Non-directed infrared links for high-capacity wireless LANs,' *Personal Communications, IEEE,* vol. 1, p. 12, 1994.

[49] Kahn, J. M., Barry, J. R., Krause, W. J., Audeh, M. D., Carruthers, J. B., Marsh, G. W., Lee, E. A., and Messerschmitt, D. G., "High-speed non-directional infrared communication for wireless local-area networks," in *Signals, Systems and Computers, 1992. 1992 Conference Record of The Twenty-Sixth Asilomar Conference on*, 1992, pp. 83-87 vol.1.

[50] Al-Ghamdi, A. G. and Elmirghani, J. M. H.,'Optimization of a pyramidal fly-eye diversity receiver for optical wireless systems under the influence of multipath dispersion and background noise,' *Microwave and Optical Technology Letters,* vol. 36, pp. 401-406, 2003.

[51] Jivkova, S. T. and Kavehard, M.,'Multispot diffusing configuration for wireless infrared access,' *Communications, IEEE Transactions on,* vol. 48, pp. 970-978, 2000.

[52] Jivkova, S., Hristov, B. A. and Kavehrad, M.,'Power-efficient multispot-diffuse multiple-input-multiple-output approach to broad-band optical wireless communications,' *Vehicular Technology, IEEE Transactions on,* vol. 53, pp. 882-889, 2004.

[53] Barry, J. R. and Kahn, J. M.,'Link design for nondirected wireless infrared communications,' *Applied Optics,* vol. 34, pp. 3764-3776, 1995.

[54] Yang, H. and Lu, C.,'Infrared wireless LAN using multiple optical sources,' *Optoelectronics, IEE Proceedings -*, vol. 147, pp. 301-307, 2000.

[55] Maiman, T. H.,'Stimulated Optical Radiation in Ruby,' *Nature,* vol. 187, pp. 493-494, 1960.

[56] Boucouvalas, A. C.,'IEC 825-1 Safety Classification of some consumer electronics products,' *Colloquium on Optical Free Space Communication Links,* (1996), 13/1-13/6.

[57] IrDA standard,'Serial infrared: Physical layer link specification,' 1997, Version 1.2.

[58] IrDA up-to-date standards and http://www.irda.org. *The IrDA can be contacted at P.O. Box 3883, Walnut Creek, CA 94598, USA.*

[59] Jovkova, S. T. and Kavehard, M.,'Multispot diffusing configuration for wireless infrared access,' *Communications, IEEE Transactions on,* vol. 48, pp. 970-978, 2000.

[60] Elmirghani, J. M. H. and Cryan, R. A.,'New PPM-CDMA hybrid for indoor diffuse infrared channels,' *Electronic Letters,* vol. 30, pp. 1646-1647, 1994.

[61] Elmirghani, J. M. H. and Cryan, R. A., "Indoor infrared wireless networks utilising PPM CDMA," in *Singapore ICCS '94. Conference Proceedings.*, 1994, pp. 334-337 vol.1.

[62] Elmirghani, J. M. H. and Cryan, R. A., "Indoor infrared LANs with multiple access facilities based on hybrid PPM CDMA," in *Communications, 1995. ICC '95 Seattle, 'Gateway to Globalization', 1995 IEEE International Conference on*, 1995, pp. 731-734 vol.2.

[63] Elmirghani, J. M. H. and Cryan, R. A.,'Hybrid ppm-cdma systems utilizing optical orthogonal codes for indoor wireless infrared communication,' *Microwave and Optical Technology Letters,* vol. 8, pp. 44-47, 1995.

[64] Chan, H. H. and Elmirghani, J. M. H.,'PPM CDMA networks employing OC and PC signature codes,' *Journal of Optical Communications,* vol. 20, pp. 92-97, 1999.

[65] Chow, F. M. and Kahn, J. M., "Effect of non-reciprocity on infrared wireless local-area networks," in *Global Telecommunications Conference, 1999. GLOBECOM '99*, 1999, pp. 330-338 vol.1a.

[66] Gfeller, F. and Hirt, W.,'A robust wireless infrared system with channel reciprocity,' *Communications Magazine, IEEE,* vol. 36, pp. 100-106, 1998.

[67] Otte, R., De Jong, L. P. and Van Roermund, A. H. M.,'Wireless optical PPM telemetry and the influence of lighting flicker,' *Instrumentation and Measurement, IEEE Transactions on,* vol. 47, pp. 51-55, 1998.

[68] Narasimhan, R., Audeh, M. D. and Kahn, J. M.,'Effect of electronic-ballast fluorescent lighting on wireless infrared links,' *Optoelectronics, IEE Proceedings -,* vol. 143, pp. 347-354, 1996.

[69] Moreira, A., Valadas, R. and de Oliveira Duarte, A. M.,'Optical interference produced by artificial light,' *Wireless Networks,* vol. 3, pp. 131-140, 1997.

[70] Zahedi, S., Salehi, J. A. and Nasiri-Kenari, M., "A photon counting approach to the performance analysis of indoors wireless infrared CDMA networks," in *Personal, Indoor and Mobile Radio Communications, 2000. PIMRC 2000. The 11th IEEE International Symposium on*, 2000, pp. 928-932 vol.2.

[71] Moreira, A. J. C., Valadas, R. T. and de Oliveira Duarte, A. M., "Characterisation and modelling of artificial light interference in optical wireless communication systems," in *Personal, Indoor and Mobile Radio Communications, 1995. PIMRC'95. 'Wireless: Merging onto the Information Superhighway'., Sixth IEEE International Symposium on*, 1995, pp. 326-331 vol.1.

[72] Moreira, A. J. C., Valadas, R. T. and de Oliveira Duarte, A. M., "Reducing the effects of artificial light interference in wireless infrared transmission systems," in *Optical Free Space Communication Links, IEE Colloquium on*, 1996, pp. 5/1-510.

[73] Hsun-Hung, C., Sterckx, K. L., Elmirghani, J. M. H. and Cryan, R. A.,'Performance of optical wireless OOK and PPM systems under the constraints of ambient noise and multipath dispersion,' *Communications Magazine, IEEE,* vol. 36, pp. 83-87, 1998.

[74] Tavares, A., Valadas, R. and Duarte, A. M. d. O., "Performance of wireless infrared transmission systems considering both ambient light interference and intersymbol interference due to multipath dispersion," in *Opt. Wireless Communications, Proc. SPIE*, Boston, MA, 1998, pp. 82-93.

[75] Moreira, A. J. C., Tavares, A. M., Valadas, R. J. M. T. and Duarte, A. M. d. O., "Modulation methods for wireless infrared transmission systems: performance under ambient light noise and interference," in *SPIE Proceedings. on Wireless Data Transmission*, Philadelphia, PA, USA, 1995, pp. 226-237.

[76] Georgopoulos, C. J.,'Suppressing background-light interference in an in-house infrared communication system by optical filtering,' *International Journal of Optoelectronics*, vol. 3, pp. 247-256, 1988.

[77] Kotzin, M. D., "Short-range communications using diffusely scattered infrared radiation," PhD dissertation, Northwestern University, 1981.

[78] Barry, J. R., "Wireless infrared communications," Kluwer Academic Publishers, 1994.

[79] Wong, K. K., O'Farrell, T. and Kiatweerasakul, M.,'Infrared wireless communication using spread spectrum techniques,' *Optoelectronics, IEE Proceedings* -, vol. 147, pp. 308-314, 2000.

[80] O'Farrell, T. and Kiatweerasakul, M., "Performance of a spread spectrum infrared transmission system under ambient light interference," in *Personal, Indoor and Mobile Radio Communications, 1998. The Ninth IEEE International Symposium on*, 1998, pp. 703-707 vol.2.

[81] Carruthers, J. B. and Kannan, P.,'Iterative site-based modeling for wireless infrared channels,' *Antennas and Propagation, IEEE Transactions on*, vol. 50, pp. 759-765, 2002.

[82] Carruthers, J. B., Carroll, S. M. and Kannan, P.,'Propagation modelling for indoor optical wireless communications using fast multi-receiver channel estimation,' *Optoelectronics, IEE Proceedings* -, vol. 150, pp. 473-481, 2003.

[83] Senior, J. M. and Jamro, M. Y., *Optical fiber communications : principles and practice*. Harlow, England; New York: Financial Times/Prentice Hall, 2009.

[84] Commission, I. E., "International standard IEC 60825-1 (1998-01) Ed. 1.1 Consolidated Edition, Safety of laser products - Part 1: Equipment classification, requirements and user's guide," ed. Geneva, Switzerland.

[85] Hirt, W., Hassner, M. and Heise, N.,'IrDA-VFIr (16 Mb/s): modulation code and system design,' *Personal Communications, IEEE*, vol. 8, pp. 58-71, 2001.

[86] Rappaport, T. S.,'Characterization of UHF multipath radio channels in factory buildings,' *Antennas and Propagation, IEEE Transactions on*, vol. 37, pp. 1058-1069, 1989.

[87] Chuang, J.,'The Effects of Time Delay Spread on Portable Radio Communications Channels with Digital Modulation,' *Selected Areas in Communications, IEEE Journal on*, vol. 5, pp. 879-889, 1987.

[88] Einarsson, G. and Leeson, M.,'Principles of Lightwave Communications,' *Physics Today*, vol. 50, pp. 84-86, 1997.

[89] Carruthers, J. B. and Kahn, J. M.,'Multiple-subcarrier modulation for nondirected wireless infrared communication,' *Selected Areas in Communications, IEEE Journal on*, vol. 14, pp. 538-546, 1996.

[90] Feher, K., *Wireless digital communications: modulation & spread spectrum applications*: Prentice-Hall, Inc., 1995.

[91] Ta-Shing, C. and Gans, M.,'High speed infrared local wireless communication,' *Communications Magazine, IEEE*, vol. 25, pp. 4-10, 1987.

[92] Hirt, W., Petrilla, J. and Yuuki, Y., "Proposed changes to IrDA serial infrared physical layer link specification for 16 Mbps addition (VFIR) final proposal," adopted with status final by the IrDA Board of Directors, San Francisco, CA1999.

[93] Tang, A. P., Kahn, J. M. and Keang-Po, H., "Wireless infrared communication links using multi-beam transmitters and imaging receivers," in *Communications, 1996. ICC 96, Conference Record, Converging*

Technologies for Tomorrow's Applications. 1996 IEEE International Conference on, 1996, pp. 180-186 vol.1.

[94] Djahani, P. and Kahn, J. M.,'Analysis of infrared wireless links employing multibeam transmitters and imaging diversity receivers,' *Communications, IEEE Transactions on*, vol. 48, pp. 2077-2088, 2000.

[95] Al-Ghamdi, A. G. and Elmirghani, J. M. H.,'Spot diffusing technique and angle diversity performance for high speed indoor diffuse infra-red wireless transmission,' *Optoelectronics, IEE Proceedings* -, vol. 151, pp. 46-52, 2004.

[96] Al-Ghamdi, A. G. and Elmirghani, J. M. H.,'Analysis of diffuse optical wireless channels employing spot-diffusing techniques, diversity receivers, and combining schemes,' *Communications, IEEE Transactions on*, vol. 52, pp. 1622-1631, 2004.

[97] Al-Ghamdi, A. G. and Elmirghani, J. M. H., "Line strip multibeam transmitter to combat the multipath dispersion and background noise of the indoor optical wireless links," in *Global Telecommunications Conference, 2004. GLOBECOM '04. IEEE*, 2004, pp. 3630-3635 Vol.6.

[98] Kahn, J. M., You, R., Djahani, P., Weisbin, A. G., Beh Kian, T., and Tang, A.,'Imaging diversity receivers for high-speed infrared wireless communication,' *Communications Magazine, IEEE*, vol. 36, pp. 88-94, 1998.

[99] Al-Ghamdi, A. G. and Elmirghani, J. M. H., "Performance analysis of line strip multispot diffusing system, fully diffuse, and hybrid optical wireless techniques in a real environment," in *Global Telecommunications Conference, 2004. GLOBECOM '04. IEEE*, 2004, pp. 1213-1220 Vol.2.

[100] Al-Ghamdi, A. G. and Elmirghani, J. M. H.,'Line strip spot-diffusing transmitter configuration for optical wireless systems influenced by background noise and multipath dispersion,' *Communications, IEEE Transactions on*, vol. 52, pp. 37-45, 2004.

[101] Al-Ghamdi, A. G. and Elmirghani, J. M. H.,'Performance comparison of LSMS and conventional diffuse and hybrid optical wireless techniques in a real indoor environment,' *Optoelectronics, IEE Proceedings* -, vol. 152, pp. 230-238, 2005.

[102] Al-Ghamdi, A. G. and Elmirghani, J. M. H.,'Performance analysis of mobile optical wireless systems employing a novel beam clustering method and diversity detection,' *Optoelectronics, IEE Proceedings* -, vol. 151, pp. 223-231, 2004.

[103] Al-Ghamdi, A. G. and Elmirghani, J. M. H., "Analysis of optical wireless links employing a beam clustering method and diversity receivers," in *Communications, 2004 IEEE International Conference on*, 2004, pp. 3341-3347 Vol.6.

[104] Alsaadi, F., Nikkar, M. and Elmirghani, J. M. H.,'Adaptive mobile optical wireless systems employing a beam clustering method, diversity detection, and relay nodes,' *Communications, IEEE Transactions on*, vol. 58, pp. 869-879, 2010.

[105] Alsaadi, F. E. and Elmirghani, J. M. H., "Adaptive multibeam clustering angle diversity optical wireless system," in *Optical Network Design and Modeling (ONDM), 2010 14th Conference on*, 2010, pp. 1-6.

[106] Jaesang, H., Kyeongyeon, K., Sangheon, K. and Chungyong, L.,'Link-Adaptive MIMO Systems With Ordered SIC Receiver Using Stream-Ordering Algorithms in Multiuser Environments,' *Vehicular Technology, IEEE Transactions on*, vol. 57, pp. 3224-3230, 2008.

[107] Karmokar, A. K. and Bhargava, V. K., "Cross-Layer Design of Optimal Adaptation Technique over Selection-Combining Diversity Nakagami-m Fading Channels," in *Global Telecommunications Conference, 2008. IEEE GLOBECOM 2008. IEEE*, 2008, pp. 1-5.

[108] Karmokar, A. K. and Bhargava, V. K.,'Performance of cross-layer optimal adaptive transmission techniques over diversity Nakagami-m fading channels,' *Communications, IEEE Transactions on,* vol. 57, pp. 3640-3652, 2009.

[109] Vo-Nguyen, B. Q., Duong, T. Q. and Tran, N. N., "Ergodic capacity of cooperative networks using adaptive transmission and selection combining," in *Signal Processing and Communication Systems, 2009. ICSPCS 2009. 3rd International Conference on*, 2009, pp. 1-6.

[110] Alsaadi, F. and Elmirghani, J. M. H.,'Adaptive mobile spot diffusing angle diversity MC-CDMA optical wireless system in a real indoor environment,' *Wireless Communications, IEEE Transactions on,* vol. 8, pp. 2187-2192, 2009.

[111] Alsaadi, F. E. and Elmirghani, J. M. H., "Mobile MC-CDMA Optical wireless System Employing an Adaptive Multibeam Transmitter and Diversity Receivers in a Real Indoor Environment," in *Communications, 2008. ICC '08. IEEE International Conference on*, 2008, pp. 5196-5203.

[112] Alsaadi, F. and Elmirghani, J.,'Performance evaluation of 2.5 Gbit/s and 5 Gbit/s optical wireless systems employing a two dimensional adaptive beam clustering method and imaging diversity detection,' *Selected Areas in Communications, IEEE Journal on,* vol. 27, pp. 1507-1519, 2009.

[113] Alsaadi, F. E. and Elmirghani, J. M. H., "Adaptive 2.5 Gbit/s Optical Wireless Systems Employing a Two Dimensional Beam Clustering Method and Imaging Diversity Receivers," in *Communications, 2009. ICC '09. IEEE International Conference on*, 2009, pp. 1-8.

[114] Alsaadi, F. and Elmirghani, J.,'Adaptive mobile line strip multibeam MC-CDMA optical wireless system employing imaging detection in a real indoor environment,' *Selected Areas in Communications, IEEE Journal on,* vol. 27, pp. 1663-1675, 2009.

[115] Alsaadi, F. and Elmirghani, J.,'Mobile Multigigabit Indoor Optical Wireless Systems Employing Multibeam Power Adaptation and Imaging Diversity Receivers,' *Optical Communications and Networking, IEEE/OSA Journal of,* vol. 3, pp. 27-39, 2011.

[116] Alsaadi, F. E. and Elmirghani, J. M. H.,'Beam power and angle adaptation in multibeam 2.5 Gbit/s spot diffusing mobile optical wireless system,' *Selected Areas in Communications, IEEE Journal on,* vol. 28, pp. 913-927, 2010.

[117] Alsaadi, F. E. and Elmirghani, J. M. H., "Multibeam 2.5 Gbit/s Mobile Optical Wireless Systems Employing Beam Power and Angle Adaptation Method," in *Communications (ICC), 2010 IEEE International Conference on*, 2010, pp. 1-6.

[118] Alsaadi, F. E. and Elmirghani, J. M. H.,'High-Speed Spot Diffusing Mobile Optical Wireless System Employing Beam Angle and Power Adaptation and Imaging Receivers,' *Lightwave Technology, Journal of,* vol. 28, pp. 2191-2206, 2010.

[119] Alsaadi, F. E. and Elmirghani, J. M. H., "Mobile Multi-Gigabit Spot-Diffusing Optical Wireless System Employing Beam Angle and Power

Adaptation and Imaging Reception," in *GLOBECOM 2010, 2010 IEEE Global Telecommunications Conference*, 2010, pp. 1-6.

[120] Street, A. M., Stavrinou, P. N., Edwards, D. J. and Parry, G., "Optical preamplifier designs for IR-LAN applications," in *Optical Free Space Communication Links, IEE Colloquium on*, 1996, pp. 8/1-8/6.

[121] Barry, J. R., Kahn, J. M., Lee, E. A. and Messerschmitt, D. G.,'High-speed nondirective optical communication for wireless networks,' *Network, IEEE,* vol. 5, pp. 44-54, 1991.

[122] Int. Electrotech. Commission and CEI/IEC825-1, "Safety of Laser Products, 1993. J. D. Rancourt, Optical Thin Films," ed. New York: Macmillan 1987.

[123] Eardley, P. L., Wisely, D. R., Wood, D. and McKee, P.,'Holograms for optical wireless LANs,' *Optoelectronics, IEE Proceedings* -, vol. 143, pp. 365-369, 1996.

[124] Pakravan, M. R., Simova, E. and Kavehrad, M., "Holographic diffusers for indoor infrared communication systems," in *Global Telecommunications Conference, 1996. GLOBECOM '96. 'Communications: The Key to Global Prosperity*, 1996, pp. 1608-1612 vol.3.

[125] Simova, E., Tai, M. and Kavehard, M.,'Indoor wireless infrared link with a holographic multi-spot diffuser,' *Applications of Photonic Technology, Plenum Press, New York,* vol. 2, pp. 223-228, 1996.

[126] Pohl, V., Jungnickel, V. and von Helmolt, C.,'Integrating-sphere diffuser for wireless infrared communication,' *Optoelectronics, IEE Proceedings* -, vol. 147, pp. 281-285, 2000.

[127] Ning, X., Winston, R. and O?Gallagher, J.,'Dielectric totally internally reflecting concentrators,' *Applied Optics*, vol. 26, pp. 300-305, 1987.

[128] Savicki, J. P. and Morgan, S. P.,'Hemispherical concentrators and spectral filters for planar sensors in diffuse radiation fields,' *Applied Optics*, vol. 33, pp. 8057-8061, 1994.

[129] Poulin, R. L., Pauluzzi, D. R. and Walker, M. R., "A multi-channel infrared telephony demonstration system for public access applications," in *Wireless Communications, 1992. Conference Proceedings., 1992 IEEE International Conference on Selected Topics in*, 1992, pp. 286-291.

[130] Streetman, B. G. and Banerjee, S., *Solid state electronic devices*, 6th ed.: Prentice Hall, 2009.

[131] Personick, S. D.,'Receiver design for digital fiber optical communication system, Part I and II,' *Bell Systems Technology Journal,* vol. 52, pp. 843-886, 1973.

[132] Nguyen, T. D. and M.S., "report," Univ. Calif., Berkeley1995.

[133] Chan, H. H., Hussain, A., Elmirghani, J. M. H. and Cryan, R. A., "Channel equalisation for optical wireless multi-user systems utilising orthogonal codes," in *Optical Free Space Communication Links, IEE Colloquium on*, 1996, pp. 1/1-1/7.

[134] Qureshi, S. U. H.,'Adaptive equalization,' *Proceedings of the IEEE,* vol. 73, pp. 1349-1387, 1985.

[135] Spectrix Corporation, Evanston and IL. *www.spectrixcorp.com*.

[136] IBM Corporation, Armonk and NY. *www.ibm.com*.

[137] Photonics Corporation San Jose and CA. *www.Photonics.com*.

[138] Lee, D. C. M., Kahn, J. M. and Audeh, M. D.,'Trellis-coded pulse-position modulation for indoor wireless infrared communications,' *Communications, IEEE Transactions on*, vol. 45, pp. 1080-1087, 1997.

[139] Perez-Jimenez, R., Betancor, M. J. and Melian, V. M.,'Improved PPM schemes for IR-wireless LAN,' *Electronics Letters,* vol. 32, pp. 885-887, 1996.

[140] Ungerboeck, G.,'Trellis-coded modulation with redundant signal sets Part I: Introduction,' *Communications Magazine, IEEE,* vol. 25, pp. 5-11, 1987.

[141] Kaluarachi, E. D., Ghassemlooy, Z. and Wilson, B., "Digital pulse interval modulation for optical free space communication links," in *Optical Free Space Communication Links, IEE Colloquium on*, 1996, pp. 3/1-3/5.

[142] You, R. and Kahn, J. M.,'Average power reduction techniques for multiple-subcarrier intensity-modulated optical signals,' *Communications, IEEE Transactions on,* vol. 49, pp. 2164-2171, 2001.

[143] Teramoto, S. and Ohtsuki, T., "Multiple-subcarrier optical communication systems with peak reduction carriers," in *Global Telecommunications Conference, 2003. GLOBECOM '03. IEEE*, 2003, pp. 3274-3278 vol.6.

[144] Hanzo, L., Webb, W. T. and Keller, T., *Single- and Multi-carrier Quadrature Amplitude Modulation: Principles and Applications for Personal Communications, WATM and Broadcasting*: IEEE Press-John Wiley, 2000.

[145] Hanzo, L., Keller, T., Muenster, M. and Choi, B.-J., *OFDM and MC-CDMA for Broadband Multi-User Communications, WLANs and Broadcasting*: John Wiley \& Sons, Inc., 2003.

[146] Bingham, J. A. C.,'Multicarrier modulation for data transmission: an idea whose time has come,' *Communications Magazine, IEEE,* vol. 28, pp. 5-14, 1990.

[147] Pahlavan, K. and Levesque, A., *Wireless information networks*: John Wiley, 2005.

[148] Chung, F. R. K., Salehi, J. A. and Wei, V. K.,'Optical orthogonal codes: design, analysis and applications,' *Information Theory, IEEE Transactions on,* vol. 35, pp. 595-604, 1989.

[149] Salehi, J. A.,'Code division multiple-access techniques in optical fiber networks. I. Fundamental principles,' *Communications, IEEE Transactions on,* vol. 37, pp. 824-833, 1989.

[150] Salehi, J. A. and Brackett, C. A.,'Code division multiple-access techniques in optical fiber networks. II. Systems performance analysis,' *Communications, IEEE Transactions on,* vol. 37, pp. 834-842, 1989.

[151] Shaar, A. A. and Davies, P. A.,'Prime sequences: quasi-optimal sequences for OR channel code division multiplexing,' *Electronics Letters,* vol. 19, pp. 888-890, 1983.

[152] Holmes, A. S. and Syms, R. R. A.,'All-optical CDMA using `quasi-prime' codes,' *Lightwave Technology, Journal of,* vol. 10, pp. 279-286, 1992.

[153] Ravindranathan, K. C. and Selvarajan, A.,'Code generation paradigms on optical orthogonal and other codes in a fiber optic CDMA LAN,' *J. of Scientific & Industrial Research,* vol. 54, pp. 19-23, 1995.

[154] Yang, G. C. and Kwong, W. C.,'Performance analysis of optical CDMA with prime codes,' *Electronics Letters,* vol. 31, pp. 569-570, 1995.

[155] Jian-Guo, Z.,'Flexible optical fiber CDMA networks using strict optical orthogonal codes for multimedia broadcasting and distribution applications,' *Broadcasting, IEEE Transactions on,* vol. 45, pp. 106-115, 1999.

[156] Sung Soo, H., Chanbum, P. and Jae Hong, L.,'Asynchronous multirate optical wireless PPM-CDMA in an indoor non-directed diffuse channel,' *Electronics Letters,* vol. 33, pp. 1565-1567, 1997.

[157] Chan, H. H., Elmirghani, J. M. H. and Cryan, R. A.,'Optical wireless PPM CDMA networks employing OC and PC signature codes,' *Journal of optical communications*, vol. 20, pp. 92-97, 1999.

[158] Ghassemlooy, Z., See, C. K., Holding, J. M. and Lu, C.,'Bit-error-rate analysis for hybrid PIM-CDMA optical wireless communication systems,' *Microwave and Optical Technology Letters*, vol. 31, pp. 40-44, 2001.

[159] Kalofonos, D. N., Stojanovic, M. and Proakis, J. G.,'Performance of adaptive MC-CDMA detectors in rapidly fading Rayleigh channels,' *Wireless Communications, IEEE Transactions on*, vol. 2, pp. 229-239, 2003.

[160] Hara, S. and Prasad, R.,'Overview of multicarrier CDMA,' *Communications Magazine, IEEE*, vol. 35, pp. 126-133, 1997.

[161] Marsh, G. W. and Kahn, J. M.,'Channel reuse strategies for indoor infrared wireless communications,' *Communications, IEEE Transactions on*, vol. 45, pp. 1280-1290, 1997.

[162] Chan, H. H., Elmirghani, J. M. H. and Cryan, R. A., "Performance analysis of indoor infrared wireless networks utilising PPM CDMA," in *Communications, 1996. ICC 96, Conference Record, Converging Technologies for Tomorrow's Applications. 1996 IEEE International Conference on*, 1996, pp. 1467-1471 vol.3.

[163] Yamaguchi, H., Matsuo, R., Ohtsuki, T. and Sasase, I.,'Indoor Infrared Wireless Systems Using OOK-CDMA with Decision-Feedback Equalizer on Diffuse Channels,' *IEICE TRANSACTIONS on Communications*, vol. E84-B, pp. 960-966, 2001.

[164] Griner, U. N. and Arnon, S.,'Multiuser diffuse indoor wireless infrared communication using equalized synchronous CDMA,' *Communications, IEEE Transactions on*, vol. 54, pp. 1654-1662, 2006.

[165] Gonzalez, O., Perez-Jimenez, R., Rodriguez, S., Rabadan, J. and Ayala, A.,'OFDM over indoor wireless optical channel,' *Optoelectronics, IEE Proceedings* -, vol. 152, pp. 199-204, 2005.

[166] Gonzalez, O., Perez-Jimenez, R., Rodriguez, S., Rabadan, J. and Ayala, A.,'Adaptive OFDM system for communications over the indoor wireless optical channel,' *Optoelectronics, IEE Proceedings* -, vol. 153, pp. 139-144, 2006.

[167] Gonzalez, O., RodrÂ¿guez, S., Perez-Jimenez, R., Delgado, F. and Ayala, A.,'Multi-user adaptive orthogonal frequency-division multiplexing system for indoor wireless optical communications,' *Optoelectronics, IET*, vol. 1, pp. 68-76, 2007.

[168] Popovic, B. M.,'Spreading sequences for multicarrier CDMA systems,' *Communications, IEEE Transactions on*, vol. 47, pp. 918-926, 1999.

[169] Aue, V. and Fettweis, G. P., "Multi-carrier spread spectrum modulation with reduced dynamic range," in *Proc. VTC'96*, Atlanta, 1996, pp. 914-917.

[170] Xiang, G. and Tung Sang, N.,'Performance of asynchronous orthogonal multicarrier CDMA system in frequency selective fading channel,' *Communications, IEEE Transactions on*, vol. 47, pp. 1084-1091, 1999.

[171] Alsaadi, F. E. and Elmirghani, J. M. H., "MC-CDMA Indoor Optical Wireless System," in *Global Telecommunications Conference, 2007. GLOBECOM '07. IEEE*, 2007, pp. 2455-2460.

[172] Alsaadi, F. E. and Elmirghani, J. M. H.,'Spot diffusing angle diversity MC-CDMA optical wireless system,' *Optoelectronics, IET*, vol. 3, pp. 131-141, 2009.

[173] Alsaadi, F. E. and Elmirghani, J. M. H.,'Adaptive mobile multicarrier code division multiple access optical wireless systems employing a beam clustering method and diversity detection,' *Optoelectronics, IET,* vol. 4, pp. 95-112, 2010.

[174] Association, I. D., "www.irda.org/ associations/2494/files/Giga-IR_General.pdf," ed, 2009.

[175] Al-Ghamdi, A. G. and Elmirghani, J. M. H., "Characterization of mobile spot diffusing optical wireless systems with diversity receiver," in *Communications, 2004 IEEE International Conference on*, 2004, pp. 133-138 Vol.1.

[176] Desurvire, E., *Erbium-doped fiber amplifiers: principles and applications*. New York: John Wiley and Sons, 1994.

[177] Viswanath, P., Tse, D. N. C. and Laroia, R.,'Opportunistic beamforming using dumb antennas,' *Information Theory, IEEE Transactions on,* vol. 48, pp. 1277-1294, 2002.

[178] Elmirghani, J. M. H. and Mouftah, H. T.,'Technologies and architectures for scalable dynamic dense WDM networks,' *Communications Magazine, IEEE,* vol. 38, pp. 58-66, 2000.

[179] Akhavan, K., Kavehrad, M. and Jivkova, S.,'High-speed power-efficient indoor wireless infrared communication using code combining .I,' *Communications, IEEE Transactions on,* vol. 50, pp. 1098-1109, 2002.

[180] Kimber, E. M., Patel, B. L., Hardcastle, I. and Hadjifotiou, A.,'High performance 10 Gbit/s pin-FET optical receiver,' *Electronics Letters,* vol. 28, pp. 120-122, 1992.

[181] Ho, K. P. and Kahn, J. M.,'Compound parabolic concentrators for narrow-band wireless infrared receivers,' *Opt. Engineering,* vol. 34, pp. 1385-1395, May 1995 1995.

[182] Sourour, E. A. and Nakagawa, M.,'Performance of orthogonal multicarrier CDMA in a multipath fading channel,' *Communications, IEEE Transactions on,* vol. 44, pp. 356-367, 1996.

[183] Welford, W. T. and Winston, R., *High Collection Nonimaging Optics*: San Diego, CA: Academic, 1989.

[184] Leskovar, B.,'Optical receivers for wide band data transmission systems,' *Nuclear Science, IEEE Transactions on,* vol. 36, pp. 787-793, 1989.

[185] Akhavan, K., Kavehrad, M. and Jivkova, S.,'High-speed power-efficient indoor wireless infrared communication using code combining .II,' *Communications, IEEE Transactions on,* vol. 50, pp. 1495-1502, 2002.

[186] Jivkova, S. and Kavehrad, M.,'Transceiver design concept for cellular and multispot diffusing regimes of transmission,' *EURASIP J. Wirel. Commun. Netw.*, vol. 2005, pp. 30-38, 2005.

[187] Agrawal, G. P., *Fiber-optic communication systems*, 3rd ed.: John Wiely and Dons, 2002.

[188] Baher, H., *Analog and digital signal processing*, 2nd ed.: John Wiley and Sons, 2001.

Appendices

Appendix A: Computation of the Parameters used in the Simulation

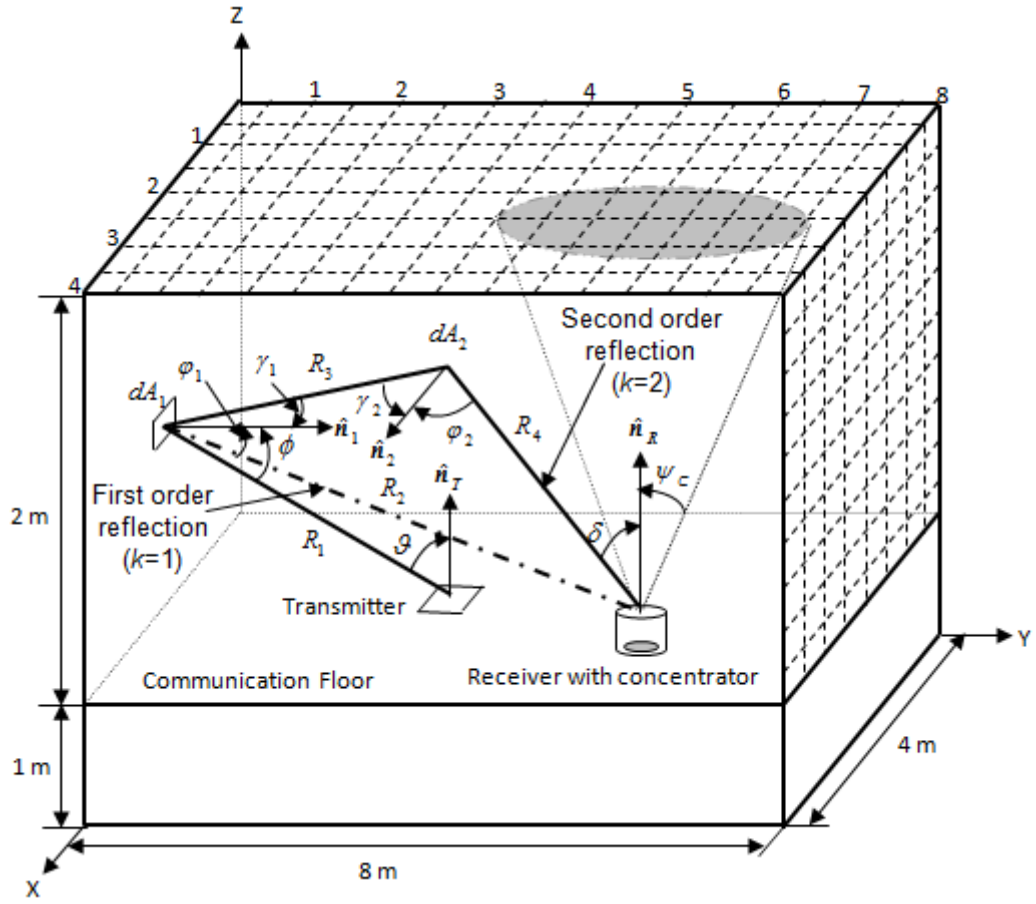

Figure A-1: Ray tracing

$$R_1 = |\mathbf{r}_1 - \mathbf{r}_T| = \sqrt{(x_1 - x_T)^2 + (y_1 - y_T)^2 + (z_1 - z_T)^2} \quad \text{(A.1)}$$

$$R_2 = |\mathbf{r}_R - \mathbf{r}_2| = \sqrt{(x_R - x_2)^2 + (y_R - y_2)^2 + (z_R - z_2)^2} \quad \text{(A.2)}$$

$$R_3 = |\mathbf{r}_2 - \mathbf{r}_1| = \sqrt{(x_2 - x_1)^2 + (y_2 - y_1)^2 + (z_2 - z_1)^2} \quad \text{(A.3)}$$

$$R_4 = |\mathbf{r}_R - \mathbf{r}_2| = \sqrt{(x_R - x_2)^2 + (y_R - y_2)^2 + (z_R - z_2)^2} \quad \text{(A.4)}$$

$$\cos\vartheta = \hat{\mathbf{n}}_T \cdot (\mathbf{r}_1 - \mathbf{r}_T)/R_1 \quad \text{(A.5)}$$

$$\cos\phi = \hat{\mathbf{n}}_1 \cdot (\mathbf{r}_T - \mathbf{r}_1)/R_1 \tag{A.6}$$

$$\cos\varphi_1 = \hat{\mathbf{n}}_1 \cdot (\mathbf{r}_R - \mathbf{r}_1)/R_2 \tag{A.7}$$

$$\cos\gamma_1 = \hat{\mathbf{n}}_1 \cdot (\mathbf{r}_2 - \mathbf{r}_1)/R_3 \tag{A.8}$$

$$\cos\gamma_2 = \hat{\mathbf{n}}_2 \cdot (\mathbf{r}_1 - \mathbf{r}_2)/R_3 \tag{A.9}$$

$$\cos\varphi_2 = \hat{\mathbf{n}}_2 \cdot (\mathbf{r}_R - \mathbf{r}_2)/R_4 \tag{A.10}$$

$$\cos\delta = \hat{\mathbf{n}}_R \cdot (\mathbf{r}_2 - \mathbf{r}_R)/R_4 \ , \tag{A.11}$$

where $\hat{\mathbf{n}}_T$ is the normal to the transmitter at position $\mathbf{r}_T$, $\hat{\mathbf{n}}_R$ is the normal to the receiver at position $\mathbf{r}_R$, $\hat{\mathbf{n}}_1$ and $\hat{\mathbf{n}}_2$ are normal to the surface elements dA_1 and dA_2 at positions $\mathbf{r}_1$ and $\mathbf{r}_2$ respectively, as shown in Fig. A.1.

In computing the total received power at the detector, direct path components between the transmitter and the receiver have to be considered. These can be calculated using equation (3.10) taking into account the incident angle of the direct ray ϑ_d with respect to the transmitter normal and the direct distance R_d between the transmitter and the receiver

$$R_d = |\mathbf{r}_R - \mathbf{r}_T| = \sqrt{(x_R - x_T)^2 + (y_R - y_T)^2 + (z_R - z_T)^2} \tag{A.12}$$

$$\cos\vartheta_d = \hat{\mathbf{n}}_T \cdot (\mathbf{r}_R - \mathbf{r}_T)/R_d \ . \tag{A.13}$$

Appendix B: Derivation of the Q-Factor

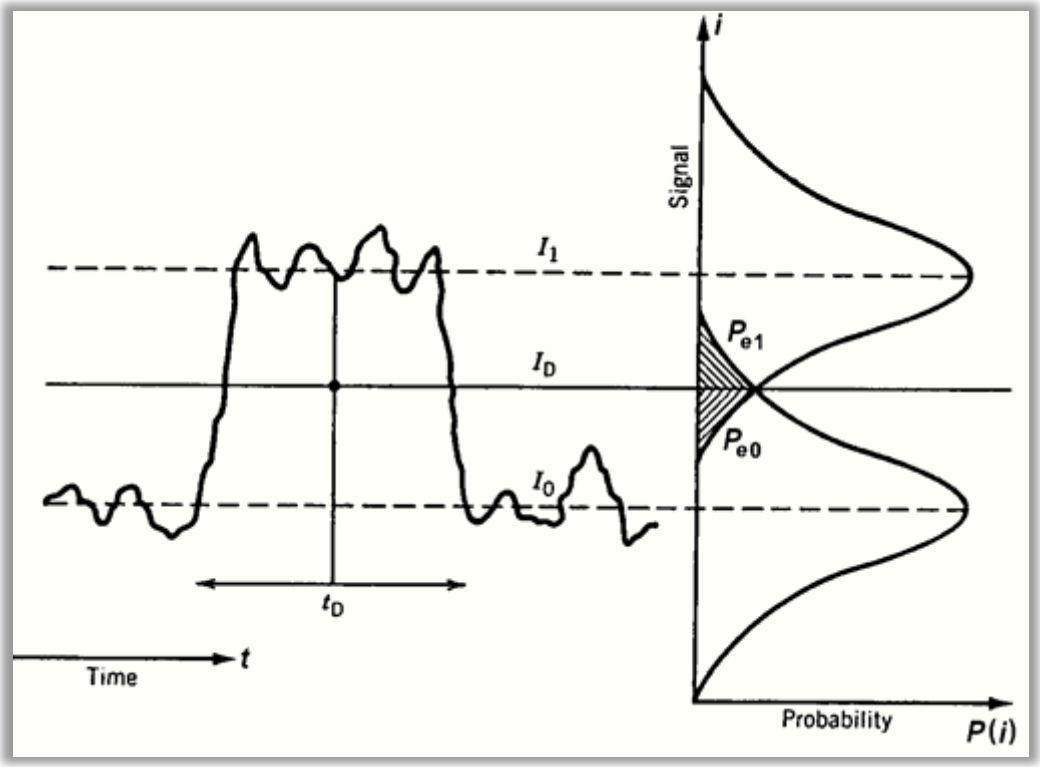

Figure B-1: (a) Signal at input to the decision circuit, (b) Gaussian probability densities for '0' and '1' bits [187-188]

Fig. B.1 shows examples of the signal that appears at the input to the decision circuit. The received signal is sampled at the decision instant t_d, and its sample value I is then compared with a threshold value I_D. The decision circuit produces a '0' at its output if $I < I_D$. While, a '1' is produced if I exceeds the threshold (i.e. if $I > I_D$). In a binary decision system, the probability of making an error is composed of two parts: probability of deciding '1' when a '0' is sent; P_{e1} and probability of deciding '0' when a '1' is sent; P_{e0}. The error probability P_e can be expressed as

$$P_e = P(1) \times P_{e0} + P(0) \times P_{e1}. \qquad \text{(B.1)}$$

Here, $P(0)$ and $P(1)$ are the probabilities that a '0' and '1' is transmitted respectively. Assuming that '0' and '1' are transmitted with equal probability where $P(0) = P(1) = 1/2$, P_e is then given as

$$P_e = \frac{1}{2} P_{e0} + \frac{1}{2} P_{e1}. \tag{B.2}$$

Since the noise on the '0' and '1' is Gaussian, P_{e0} and P_{e1} can be described in Gaussian statistics, which is visually presented in Fig.B.1, as

$$P_{e0} = \frac{1}{\sigma_1 \sqrt{2\pi}} \int_{-\infty}^{I_D} e^{-\left(\frac{(I_1 - I)^2}{2\sigma_1^2}\right)} dI . \tag{B.3}$$

$$P_{e1} = \frac{1}{\sigma_0 \sqrt{2\pi}} \int_{I_D}^{\infty} e^{-\left(\frac{(I - I_0)^2}{2\sigma_0^2}\right)} dI . \tag{B.4}$$

Assuming that

$$x = \frac{I - I_o}{\sigma_0 \sqrt{2}}. \tag{B.5}$$

Taking the derivative of both sides of (B.5)

$$dx = \frac{dI}{\sigma_0 \sqrt{2}}. \tag{B.6}$$

This means that

$$dI = \sigma_0 \sqrt{2}\, dx . \tag{B.7}$$

At a certain decision level I_D, (B.5) becomes

$$x_D = \frac{I_D - I_o}{\sigma_0 \sqrt{2}}. \tag{B.8}$$

Substituting (B.5), (B.7) and (B.8) into (B.4), the P_{e1} is then given as

$$P_{e1} = \frac{1}{\sigma_0 \sqrt{2\pi}} \int_{x_D}^{\infty} e^{-x^2}\, \sigma_0 \sqrt{2}\, dx, \tag{B.9}$$

$$P_{e1} = \frac{1}{\sqrt{\pi}} \int_{\frac{I_D - I_0}{\sigma_0 \sqrt{2}}}^{\infty} e^{-x^2}\, dx . \tag{B.10}$$

Employing the complementary error function $erfc$, expressed as

$$erfc(u) = \frac{2}{\sqrt{\pi}} \int_{u}^{\infty} e^{-x^2}\, dx , \tag{B.11}$$

P_{e1} may be written as

$$P_{e1} = \frac{1}{2} erfc\left(\frac{I_D - I_0}{\sigma_0 \sqrt{2}} \right). \tag{B.12}$$

In a similar fashion, the P_{e0} is given as

$$P_{e0} = \frac{1}{\sqrt{\pi}} \int_{-\infty}^{\frac{I_1 - I_D}{\sigma_1 \sqrt{2}}} e^{-x^2}\, dx = \frac{1}{2} erfc\left(\frac{I_1 - I_D}{\sigma_1 \sqrt{2}} \right). \tag{B.13}$$

Substituting (B.12) and (B.13) into (B.2), P_e is given as

$$P_e = \frac{1}{4}\left(erfc\left(\frac{I_1 - I_D}{\sigma_1 \sqrt{2}} \right) + erfc\left(\frac{I_D - I_0}{\sigma_0 \sqrt{2}} \right) \right). \tag{B.14}$$

In a communication application, the optimum decision level (threshold) is selected so as to minimise the overall probability of error P_e. Since the '0' and '1' are equally probable, the optimum threshold occurs when $P_{e0} = P_{e1}$ which yields

$$\frac{I_1 - I_D}{\sigma_1 \sqrt{2}} = \frac{I_D - I_0}{\sigma_0 \sqrt{2}} . \tag{B.15}$$

$$\frac{I_1 - I_D}{\sigma_1} = \frac{I_D - I_0}{\sigma_0} \equiv Q . \tag{B.16}$$

By solving (B.16), I_D is given as

$$I_D = I_1 - \sigma_1 Q . \tag{B.17}$$

and

$$I_D = I_0 + \sigma_0 Q\,. \tag{B.18}$$

From (B.17) and (B.18), Q can be given as

$$Q = \frac{I_1 - I_0}{\sigma_0 + \sigma_1}. \tag{B.19}$$

The currents I_1 and I_0 can be expressed in terms of the received signal powers and the noise power as

$$I_1 = R \cdot P_1 = R \cdot \left(P_{s1} + P_{bn}\right). \tag{B.20}$$

$$I_0 = R \cdot P_0 = R \cdot \left(P_{s0} + P_{bn}\right). \tag{B.21}$$

Subtracting (B.20) from (B.21) yields

$$I_1 - I_0 = R \cdot \left(P_{s1} - P_{s0}\right). \tag{B.22}$$

Therefore, (B.19) becomes

$$Q = \frac{R \cdot \left(P_{s1} - P_{s0}\right)}{\sigma_0 + \sigma_1}. \tag{B.23}$$

By Substituting (B.16) into (B.14), the P_e with the optimum threshold is given by

$$P_e = \frac{1}{4}\left(erfc\left(\frac{Q}{\sqrt{2}}\right) + erfc\left(\frac{Q}{\sqrt{2}}\right)\right). \tag{B.24}$$

$$P_e = \frac{1}{2} erfc\left(\frac{Q}{\sqrt{2}}\right) \approx \frac{e^{-\left(Q/\sqrt{2}\right)^2}}{Q\sqrt{2\pi}}, \tag{B.25}$$

which indicates that P_e improves as Q increases, for a P_e of 10^{-9}, $Q \approx 6$.

The $Q(x)$ function is defined as

$$Q(x) = \frac{1}{\sqrt{2\pi}} \int_x^{\infty} e^{-\left(u/\sqrt{2}\right)^2} du\,. \tag{B.26}$$

Fig. B.2 shows the variation of P_e with the Q factor.

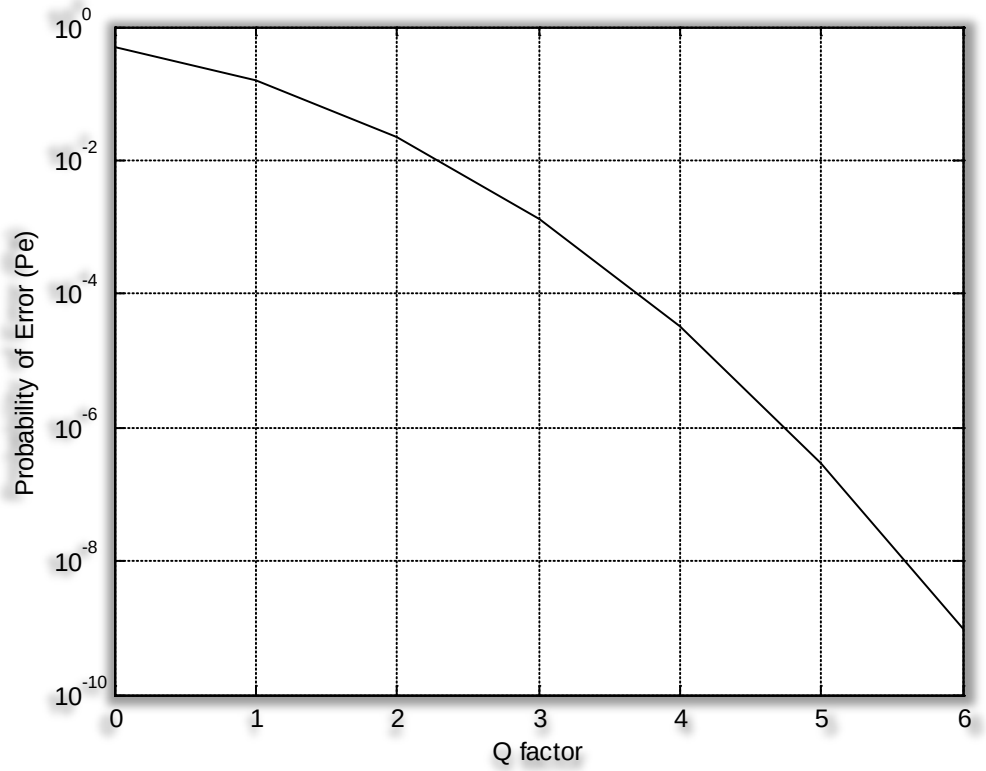

Figure B-2: P_e versus the Q factor